Opening remarks by Academician Zhores Ivanovich Alferov

Fiz. Tverd. Tela (St. Petersburg) **40**, 787–788 (May 1998)

[S1063-7834(98)00105-1]

Today we open the International Symposium, organized in honor of the hundredth anniversary of the birth of one of the most well-known and distinguished scientists in the field of solid-state optics, Professor Evgeniĭ Fedorovich Gross.

I recall how in January of 1953 I attended for the first time a seminar of Professor Gross in the Leningrad Physicotechnical Institute. I was greatly impressed not only by his lecture on the discovery of excitons, but also the very personality of the professor, his emotional manner of presentation and his great love for science.

I think many scientists of our institute, even those who never worked in his laboratory but only met him in seminars and the like, were always under the strong sway of his personality.

The discovery of the exciton was one of the most striking in the physics of condensed media. The exciton was predicted in 1931 by the distinguished theoretical physicist Ya. Frenkel', who gave this quasiparticle the name ''exciton'' to explain the photoreactive absorption of light in solids. Later, in 1951, in a very delicate optical experiment, this quasiparticle was discovered by Professor Gross and his graduate student N. Karryev.

Evgeniĭ Fedorovich was the creator of a scientific school. Today, in this beautiful lecture hall of the House of Scientists of the Russian Academy of Sciences, I see many people (young and not so young) most of whom belong to the scientific school of Professor Gross. The works of the scientists of this school have created a new and important branch of solid-state physics.

For an extended time, we have spoken of the exciton only as a phenomenon of fundamental physics, not having great physical application. But any fundamental discovery always has a practical significance, even if it is not used in devices. Without recourse to excitons we could not explain nor even examine many phenomena. Nowadays the situation is different, and excitons are beginning to play a role in semiconductor devices.

With great pride I can say that many of these discoveries were made by Soviet scientists, including workers of the A. F. Ioffe Physicotechnical Institute.

An important stage in the development of the study of excitons was the discovery of the so-called exciton liquid. Its existence and properties were predicted by Academician L. V. Keldysh and his students. A detailed study of the exciton liquid was undertaken by Professor V. S. Bagaev at the Physical Institute of the Academy of Sciences, Professor A. A. Rogachev and others at the Physicotechnical Institute, and by Corresponding-Member of the Academy of Sciences Ya. E. Pokrovskiĭ and coworkers at the Institute of Radio Electronics.

A section will deal, within the scope of this symposium, with an examination of the properties of quantum dots, the physics of zero-dimensional structures and heterostructures. In these special types of structures, excitons play an important role not only in explaining optical phenomena, but also as quasiparticles ''at work'' in real devices. New semiconductor lasers based on quantum-dot structures would not work without excitons as the working particles. Today, Dr. Grundmann from the Technical University of Berlin will consider the theory of these lasers in his presentation and highlight the important role of excitons in them.

I hope that there will be many interesting presentations and discussions in the course of this symposium.

In the name of the scientists of the Physicotechnical Institute and the St. Petersburg Scientific Center, I welcome all participants of this symposium and hope that it will be useful to you.

I would like to remind our guests that St. Petersburg is one of the most beautiful cities of the world and I hope you will find time to acquaint yourself with it. Best wishes to all.

And now one of the first graduate students of Professor Gross, now Academician, Boris P. Zakharchenya, will tell us about his teacher.

Translated by Paul F. Schippnick

A word about my teacher

B. P. Zakharchenya

Fiz. Tverd. Tela (St. Petersburg) **40**, 789–793 (May 1998)

[S1063-7834(98)00205-6]

VIRTUOSO OF THE OPTICAL EXPERIMENT

Evgeniĭ Fedorovich Gross was born on October 8, 1897 into the family of a metallurgical engineer, specifically the man who ran the Izhorskiĭ Works, a Russian nobleman. This was the largest armaments plant in all of old Russia.

We can say with confidence that Evgeniĭ Gross was an outstanding experimental physicist working in the field of spectroscopy of the condensed state. His faith in the power of optics and spectroscopy as an instrument for penetrating the microscopic structure of matter was in many ways instilled in him him by his teacher Academician Dmitriĭ Sergeevich Rozhdestvenskiĭ and remained with Gross until his death in 1972.

In the field of spectroscopy Gross carried out many brilliant studies, but the high points of his creativity were

—the discovery in 1930 of the fine structure of the Rayleigh line of so-called Brillouin scattering, therewith demonstrating the existence of Debye waves in crystals;

—the discovery of low-frequency spectra in the scattering of light by crystals. In essence this was the observation of new spectral lines appearing in the wings of the Raman lines in the crystallization of liquids. The corresponding frequencies, which have come to be called ''Gross frequencies,'' are associated with intermolecular vibrations;

—the discovery of the spectrum of large-radius excitons in semiconductors—Wannier–Mott excitons. In its significance, this discovery is very close to works for which Nobel prizes are awarded.

I will cite a case and say a little more about one outstanding discovery of Evgeniĭ Fedorovich, which had, alas, a dramatic finale. About it not much is known.

The story goes like this. At the very outset of his scientific career, Evgeniĭ Gross made use of instruments of high resolving power. One of these was the Michelson interferometer. Gross was a master of this instrument and, crossing it with a spectrograph, he commenced a study of the line structure of the radiation from gaseous discharge sources, including those in which Doppler broadening had been eliminated, i.e., the lines were extraordinarily narrow. Employing this technique, Gross observed the hyperfine structure of the lines. Such structure was predicted at this time by Wolfgang Pauli as a result of the interaction of the electron spins with the angular momentum of the nucleus. Having made this outstanding discovery, Gross made an unforgivable mistake by trusting in the authority of one of Rozhdestvenskiĭ's senior collaborators who declared that the structure Gross had discovered was nothing but a result of a trivial self-action of resonance lines in a temperature-inhomogeneous discharge. Gross altered the conditions of the discharge, and the structure disappeared as a result of line broadening.

After publication in 1928 in the journal *Zeitschrift der Physik* of the results of German researchers on the hyperfine splitting of sodium lines in accordance with Pauli's theory, Gross understood what a bad mistake he had made, blindly trusting in the opinion of a higher authority. He outlived his mistake, and always advised us, his students, to take a critical view of all authority, in short—to be dissidents of science.

At the end of the 20's Evgeniĭ Gross took upon himself with great enthusiasm the realization of what in the pre-laser era was a very difficult experiment, namely observing the fine structure of the Rayleigh lines. This experiment was suggested to the young physicist by the distinguished Moscow optical physicists L. Mandel'shtam and G. Landsberg. who tragically let priority for the discovery of inelastic light scattering slip out of their hands in 1928. Now the whole world calls this Raman scattering after the Indian physicist who published his experiments somewhat earlier, even though they were not as vivid a demonstration as that of Landsberg and Mandel'shtam.

An experiment in the 30's on observing the Rayleigh lines was unbelievably difficult, first of all because of the absence of an intense collimated light source and a sensitive photon detector. As his light source Gross had a quartz mercury lamp, more accurately its 2537 Å line, and a photographic plate served as his detector. The scattering object was a quartz crystal, chosen (this, if anything, revealed Gross's perseverance and diligence) from many hundreds of samples. The light power of the setup with the Michelson interferometer was not large; therefore the required exposure time was a hundred hours. During this time Gross never left the setup even once, all the time checking the thermostatic and barostatic control of the Michelson device. The experiment was crowned with success. Gross observed the structure of the Rayleigh line predicted by Leon Brillouin,[1)] but it was more complicated because of the presence of longitudinal and transverse acoustic modes. In the case of quartz, three components were observed in both the Stokes and the anti-Stokes parts. The experiment went beyond the state of the art of its time. Gross published his results in 1930 in the journal *Zeitschrift der Physik* with an expression of deep gratitude to the above-indicated Moscow physicists.

Alas! Gross was able to observe the spectrum and its structure on the photoplate only visually, by the scanning objective method, averaging the grains of the plate in the

darkened region. It was not then possible to record the spectrum on a microphotograph and, therefore, he could not send the result to Leon Brillouin in response to his written request. Gross's discovery waited a full three years for confirmation, when scientists in one of the laboratories of France succeeded in reproducing his experiment. Now it is comparatively simple to observe Mandel'shtam–Brillouin scattering. Laser spectroscopy has simplified the experiment substantially.

I think it appropriate here to tell about this experiment of Gross's since it highlights not only Gross's extraordinary skill as an experimentalist, but also his burning drive to obtain a new result, providing food for further thought.

These qualities were again displayed in the remarkable experiments of Gross and Max Wuchs in observing the low frequencies of the Raman spectra of molecular crystals, about which I have already spoken.

Now let us turn to the exciton part of the research of Gross and his coworkers. This all begins shortly after the end of the Second World War, when Gross was invited by the director of the Physico-technical Institute, Abram Fedorovich Ioffe to organize an optical laboratory in the institute. It is curious that already in the 40's Ioffe understood the significance of optics and spectroscopy for solid state, and especially for semiconductors, with which he himself was actively occupied, foreseeing their remarkable future. At first, Gross continued to occupy himself with light scattering, but soon his interest was diverted by the experimentalists V. Zhuze and S. Ryvkin, who had just discovered that to explain experiments on the kinetics of photoconductivity in crystals of cuprous oxide it was necessary to invoke the idea of an exciton—a quasiparticle carrying energy but not charge, predicted in 1931 by the theoretician Yakov Il'ich Frenkel', also at the institute.

The semiconducting crystal, cuprous oxide, was extremely popular in the 40's. To grow Cu_2O crystals back then, albeit not very high-quality ones, did not require much work. Therefore Gross decided to study its optical absorption spectra in the hopes of finding something associated with the exciton. Fate had a fine gift in store for him. In the first absorption spectrum of a thin ruby-red wafer of cuprous oxide he, together with his graduate student from Turkmenistan, Nuri Karryev, observed a series of narrow absorption lines converging, in accord with a hydrogen-like law, to the limit of continuous absorption corresponding to the fundamental absorption edge or, as we would say today, to the band-to-band transition. At liquid-nitrogen temperature, they observed six or seven lines. The experiment was performed at the beginning of 1951. Gross announced that he observed the absorption spectrum of the quasiparticle, the exciton in an institute seminar. He calculated the excitonic Rydberg and determined to the extent possible the effective masses of the electron and hole.

As is well known, the concept of the exciton was introduced to solid-state physics by the creator of many physical models, Yakov Frenkel'. In the calculation of the exciton states and wave functions, Frenkel' used the Heitler–London approximation, assuming that in the Bloch diagram, familiar to all who work with semiconductors, but based on the Hartree–Fock approximation, there is no place for electron correlations. Later on, Wannier and Mott added exciton states to the familiar Bloch diagram. It was just such a large-radius exciton that Gross had discovered.

Frenkel' excitons or, as they are often called, small-radius excitons, had been discovered a long time earlier, but the experimentalists who had observed them did not realize the connections of the lines they had observed with the exciton. These were Jean Becquerel, who observed narrow lines in crystals of rare-earth salts (the minerals xenotite and tisonite), and Ivan Obreimov, who observed the line spectra of crystals of aromatic hydrocarbons (naphthalene, anthracene, benzene). Roughly three decades after these observations A. Davydov developed a theory of small-radius excitons and formulated the main criterion for recognizing such excitons—the famous Davydov doublet, whose components are polarized relative to the crystal axes. However, the experimentalists persisted in calling the line spectra in the above-indicated crystals spectra of crystalline states. The exciton terminology started to be used only after Gross's discovery.

Closest to the exciton ideology before Gross were those who worked with wide bands at the fundamental absorption edge of alkali-halide crystals discovered by Hilf and Pol. It was in these crystals that exciton migration was first demonstrated at the beginning of the 50's by Apker and Taft.

Having discovered this extraordinarily striking phenomenon and believing in its exciton nature, Gross rushed to publish. However, he encountered serious obstacles in his path. The thing was that just at this time Abram Fedorovich Ioffe had been displaced from his position as director of the Physico-technical Institute by the curator of the nuclear program of the USSR, Lavrentiĭ Beria. A new director had been installed—Anton Komar, the Ukrainian academician. He was under pressure to be especially strict in approving papers for publication since not long before his arrival a cycle of papers on nuclear physics had been published which had been awarded the Stalin prize. The work later turned out to be in error, and the reputation of the institute suffered as a result. On top of that, Komar had been assured by his colleague in the Ukrainian Academy of Sciences, Professor Antonin Prikhod'ko, that the series of lines observed by Gross was nothing but a trivial interference of light in the crystalline wafer. Gross was not just a little disturbed, he was furious: ''They dare to accuse a world-class optical physicist of a primitive error!''

The incompetence of Komar and Prikhod'ko cost Gross dearly. He could not publish his discovery, made at the beginning of 1951, until 1952 in the journal *Doklady Akademii Nauk* (Proceedings of the Academy of Science), publishing there two papers, one after the other. President of the Academy of Science of the USSR A. N. Nesmeyanov helped Gross in this matter. During that time when the papers lay tabled, papers by the Japanese physicists Hayachi and Katsuki appeared. The first was published in 1950 in the Journal of the Physical Society of Japan and arrived in the Soviet Union a year later. No hydrogen-like series was observed in it. An exciton interpretation of the steps (not lines) which were observed at the absorption edge was lacking. In 1951

the same authors published a detailed paper in the journal of the University of Hokkaido, in which they spoke of a hydrogen-like series, admittedly, but much less to the point than Gross. About the exciton, however, not a word. Gross received this paper only after the publication of his own papers with distinct hydrogen-like series and their confident interpretation.

The papers of these Japanese authors were probably examined not too attentively by Professor Rashba who, in his foreword to the book *Excitons* edited by him and published in 1982 by North-Holland Press, ascribed the discovery of the exciton to the Japanese scientists. Gross had already died, but for his many students—Kaplyanskiĭ, Permogorov, Safarov, Novikov, the author of this essay, and others—this was incomprehensible and very unpleasant, not the least because we regard Émmanuil Rashba, like Gross, as a great theoretician.

Still more disagreeable were the numerous attempts by the Strassbourg professor Serge Nikitin somehow to disparage Gross's work and his inarguable priority in the discovery of the new quasiparticle in order, having begun similar research efforts himself, to be able to claim the honor for himself. As a Russian émigré, Nikitin knew well the language and was able to make use of the fact that the journals where Gross published had not been translated into English. Many of Nikitin's papers and reviews, in which it was not hard to divine an effort to plagiarize, disturbed Gross severely. In the archive of Evgeniĭ Fedorovich we have found letters to Nikitin rebuking him in this matter, containing naive efforts to explain that such behavior was at the very least inappropriate.

Gross's main argument in favor of the exciton interpretation of the observed phenomenon was the narrowness of the lines. Such a property of exciton absorption was noted already in the first papers by Frenkel'. The light momentum is small; therefore it creates an exciton with minimum energy in the exciton band. This assertion, appearing in our time as even trivial, was extraordinarily daring in the 30's, when even the existence of quasiparticles in solids was referred to with great hesitation. This argument of Gross's was poorly received even in the 50's. Most of the opponents of the exciton interpretation asserted that most likely this was an impurity without understanding that band-impurity optical transitions cannot give narrow lines as a consequence of the fact that the wave functions of the impurity states occupy a significant region of k space. Such transitions give wide absorption steps.

The argument tied to the narrowness of the lines was poorly received by the participants of the seminars that Gross and I often attended. Striking effects in electric and magnetic fields, proving the huge radius of the exciton orbits, interested them but, as an argument in favor of the existence of a mobile quasiparticle, it was not accepted by the suspicious scientists. They said to us: ''Prove the motion of the exciton, then we will believe.''

The first experiments in this direction were on inversion of the magnetic field, performed in crystals of cadmium sulfide. These included experiments that carefully examined the shape and structure of the luminescence bands in CdS and CdSe, where they demonstrated a Maxwellian distribution of the exciton momenta and, finally, experiments on the spatial dispersion of the excitons, starting with the observation of a quadrupole line in cuprous oxide corresponding to the transition to the first excitonic state.

It is impossible here to list all the discoveries in exciton physics made during a very short time by Gross and his team at the Physico-technical Institute. I love to call this period from the 50's to the 60's, following the terminology of Goethe and Schiller, the period of *Sturm und Drang* in the optics of excitons in semiconductors. It should be noted that cuprous oxide played a distinctive role in these discoveries, this crystal has a valence band and a conduction band that are described by wave functions of the same parity. As a consequence, the absorption coefficient for interband transitions is relatively small, offering the unique possibility of observing up to 13 absorption lines at liquid-helium temperature in the exciton series! Other parameters of the band structure of cuprous oxide also facilitate this. This was Gross's crystal! Looking over its spectrum, located in the visible range, with the help of a simple lens, he exclaimed with great excitement: ''What a wonderful phenomenon! A hydrogen-like series in a crystal! What narrow lines! Boris, what beauty, it is impossible to tear myself away from it! I am convinced this is an exciton!''

Without a doubt, at such moments the triumphant strains of Tannhäuser must have resounded in Gross's soul.

Within a short time, the following phenomena and effects were discovered: a second excitonic series associated with spin-orbit splitting (this before experiments on cyclotron resonance); the diamagnetic exciton shift and the Zeeman effect of exciton lines; the exciton Stark effect and ionization of the exciton in weak fields; diamagnetic excitons (magnetic excitons); the already mentioned polarization of the quadrupole exciton line; in II–VI crystals Gross's students discovered hot excitons; they studied the effect of magnetic field inversion; they discovered the optical analog of the Mössbauer effect; they detected spectra of exciton–impurity complexes and the fine structure of photoconductivity associated with excitonic states; they initiated experiments for creating a high-density exciton gas. I cannot list them all.

It is clear that the discovery of excitons marks the beginning of semiconductor spectroscopy, which, together with the study of electronic states in semiconductors, plays the same role as atomic spectroscopy did in the era of great discoveries in quantum mechanics. About this Abram Fedorovich Ioffe spoke frequently, commenting upon the advances of Gross and his coworkers.

The invention of the laser and the incorporation of its use in laboratory practice led to the discovery of multiexciton complexes and posed the challenge of creating a Bose condensate which, in turn, generated the physics of the electron–hole liquid in semiconductors. Numerous experiments appeared on the optical orientation and alignment of excitons. Finally, brilliant works on exciton physics were made possible by the advent of femtosecond technology.

It is impossible to imagine the spectroscopy of quantum-size structures without a study of exciton states. In this con-

text many subtle phenomena were observed, from quantum beats as a consequence of interference of quantum states to effects of anticrossover of fine structure levels of localized exciton states. I think the discovery of the trion and phenomenon associated with the shake-up process far from completes the giant pyramid of these studies.

In conclusion, I would like to turn to one more side of my teacher, Evgeniĭ Fedorovich Gross, who laid the basis of this pyramid.

Besides his astounding physical intuition, nature bequeathed him with a refined appreciation of music and painting. He was an absolute musical ''addict,'' not missing even one significant musical event in St. Petersburg/Leningrad. I recall his stories of his happy and quite affluent childhood, when his father dressed him in a warm Romanov-era sheepskin coat, seated him in the sleigh, and the troika carried him into St. Petersburg to the Assembly of Nobles (now the Philharmonic Society).

It is difficult for us to imagine that long-ago snowy St. Petersburg, when it was possible to ride on sleighs into the very center of the city. In the concert hall, the beloved Aleksandr Ziloti, conducting his enlightening concerts and lectures, or the eight-year old wunderkind Willi Ferrero, with a huge orchestra obediently playing to the movement of his baton.

Most of all, Gross loved Sergeĭ Prokofiev, and least of all, Tschaĭkovskiĭ and Mendelssohn, considering them to be too mundane and narrow.

Among performers dear to him was Svyatoslav Richter and, of course, the great Glenn Gould, whose concerts in Leningrad Gross considered to be the greatest event of his life.

I could talk for hours about Gross's passion for painting: from the golden-blue Poussin to the abstractions of Kandinskiĭ and the genial colorful discoveries of his student Petrov-Vodkin Chupyatov (he was well represented in Gross's modest collection).

However, I will stop here and ask my young friend, the violinist Boris Kipnis, to remember Gross with the remarkable music of Johann Sebastian Bach.

[1)]Even before Brillouin this structure was predicted by Leonid Mandel'shtam in 1926; therefore we frequently call it Mandel'shtam-Brillouin scattering.

Translated by Paul F. Schippnick

On the validity of Haynes rule for the binding of excitonic complexes in low dimensions

J. Singh

Faculty of Science, Northern Territory University, NT 0909 Darwin, Australia

Fiz. Tverd. Tela (St. Petersburg) **40**, 794–796 (May 1998)

Using a two-dimensional geometrical model and fractional dimension approach, it is found analytically that the ratio of the binding energy of a biexciton to that of an exciton is 0.228 in quantum wells and it is independent of the quantum-well width. This agrees very well with the results in GaAs and ZnSe quantum wells, and CuCl crystals and large quantum dots. It is suggested that, while Haynes rule may be valid for bulk, much higher ratios may be expected in lower dimensions. © *1998 American Institute of Physics.* [S1063-7834(98)00305-0]

1. Much interest has been generated recently in studying excitonic complexes like biexcitons and trions in narrow dimensions, because of their applications in confined quantum optoelectronic devices. In GaAs quantum-well[1,2] and type II superlattices,[3] the binding energy of biexcitons over 2 meV has been observed, whereas in ZnSe quantum well[4] and CuCl single crystals[5–7] much higher binding energies have been measured. The first observation of biexcitons was made by Haynes[8] in crystalline silicon and, on the basis of his previous work on a neutral donor complex,[9] Haynes used the ratio of the binding energy of a biexciton (E_b^{xx}) to that of an exciton (E_b^x) in silicon as 0.1. Ever since this ratio, commonly known as the Hynes Rule, has been assumed to be applicable for all solids, including quantum wells.[10] However, as biexcitons are observed more frequently in confined systems, a desirable question arises if there is a constant ratio for the binding energy of a biexciton to that of an exciton, which can be applied to both bulk and confined systems.

In this paper we have presented a brief account of determining the ratio of the binding energy of quasi-two-dimensional biexcitons to that of an exciton analytically[11] using the fractional dimension approach[12] and compared it with some of the known experimental results on quantum wells. As the Bohr radius of biexcitons is much larger than that of excitons, it may be expected that the effect of confinement will be more pronounced on biexcitons than on excitons. Therefore, while the Haynes rule may be regarded as applicable in bulk crystals, a higher ratio may be expected in lower dimensions.

2. In quantum wells of widths smaller than the biexcitonic diameter, a biexciton is confined into a 2D space. In this situation a planar square geometrical configuration[11] for the electrons and holes involved in the formation of a biexciton can be assumed. Assuming that the quantum well plane is parallel to the xy-plane, the 2D biexciton is free to move only in this plane. Transforming the Hamiltonian of such a geometrical structure into the six relative co-ordinates and a center of mass coordinate, we get the biexciton Hamiltonian as[11]

$$H_{xx}=-\frac{\hbar^2}{2M}\nabla_R^2-\frac{\hbar^2}{2}\left(\frac{2}{\mu_{\rm eh}}\nabla_{\rm eh}^2+\frac{1}{\mu_{\rm ee}}\nabla_{ee}^2+\frac{1}{\mu_{\rm hh}}\nabla_{\rm hh}^2\right)+V, \quad (1)$$

where $M=2(m_{\rm e}^*+m_{\rm h}^*)$, $1/\mu_{\rm eh}=1/m_{\rm e}^*+1/m_{\rm h}^*$, $1/\mu_{\rm ee}=1/m_{\rm e}^*$ and $1/\mu_{\rm hh}=2/m_{\rm h}^*$, $\nabla_{\rm eh}^2$, $\nabla_{\rm ee}^2$ and $\nabla_{\rm hh}^2$ are the Laplacians with respect to the relative co-ordinates between electron and hole, electron and electron, and hole and hole, respectively, and $\nabla_R^2$is that with respect to the center of mass co-ordinate. V is the Coulomb potential of interaction among the electrons and holes of the biexciton. Applying another coordinate transformation to the relative coordinates that ensures a square structure of the 2D biexciton, the Hamiltonian (1) reduces into[11]

$$H_{xx}=-\frac{\hbar^2}{2\mu_{xx}}\nabla_r^2-\frac{e^2}{\varepsilon_{ee}r}, \quad (2)$$

where $\mu_{xx}=\frac{2}{3}\mu_{\rm eh}$, $\varepsilon_{xx}=(\sqrt{2}/(4-\sqrt{2}))\varepsilon$, and ε is the dielectric constant of the material. The kinetic energy operator of the center-of-mass motion is excluded from the Hamiltonian (2). The energy eigenvalue of the Hamiltonian (2) can be obtained by applying the fractional dimension approach [12] in solving the following Schrödinger equation

$$H_{xx}\Psi_{xx,n}(r)=(E_{xx,n}-2E_g)\psi_{xx,n}(r), \quad (3)$$

where $E_{xx,n}$ and $\psi_{xx,n}$ are the energy eigenvalue and eigenfunction of a biexciton in its internal energy state n, respectively, and E_g is the energy gap of the material. We thus obtain

$$E_{xx,n}=2E_g-\frac{E_B'}{(n+((\alpha-3)/2))^2}, \quad \alpha=2, \quad (4)$$

and the corresponding biexciton radius $a_{xx,n}$ as

$$a_{xx,n}=\left(n+\frac{\alpha-3}{2}\right)^2 a_x', \quad (5)$$

where

$$E_B'=\frac{\mu_{xx}}{\varepsilon_{xx}^2 m_e}R_H, \quad (6)$$

and

$$a_x' = \frac{m_e}{\varepsilon_{xx}\mu_{xx}} a_H \tag{7}$$

R_H and a_H are the Rydberg constant and Bohr radius, respectively, and m_e is the free-electron mass.

Using the definition of the biexciton binding energy as $E_b^{xx} = 2E_{x,n} - E_{xx,n}$, where $E_{x,n}$ is the energy eigenvalue of an exciton state, we get the exciton binding energy as

$$E_b^{xx}(n) = \left(\frac{(4/-\sqrt{2})}{3} - 2 \right) E_b^x(n), \tag{8}$$

where $E_b^x(n) = E_g - E_{x,n}$, is the binding energy of a 2D exciton. From (8) one gets the ratio, $E_b^{xx}/E_b^x = 0.228$, which does not depend on the biexciton state principal quantum number n, effective masses of the charge carriers and quantum-well width. The ratio is also more than twice the ratio obtained by Haynes rule.

Using Eq. (5), we also find the ratio of the radius of biexciton to exciton as

$$\frac{a_{xx,n}}{a_{x,n}} = \frac{3(4-\sqrt{2})}{2\sqrt{2}} = 2.74 \tag{9}$$

which is also independent of $n$and, therefore, the ratio is the same for the Bohr radius of biexciton to that of exciton. The ratio (9) suggests that the biexciton Bohr radius can be more than twice as large as the exciton Bohr radius.

3. Using a simple but realistic model strucuture of 2D biexcitons in quantum wells, we have obtained analytically $E_b^{xx}/E_b^x = 0.228$ for 2D biexcitons. The questions now arise (i) Do biexcitons in all quantum well materials have the same ratio? (ii) Although the results derived here are strictly applicable for the two-dimensional case, can this ratio be applied in dimensions lower than 2D (quantum wires, quantum dots etc.)? (iii) Should it really be independent of the quantum-well width? We would like to address these questions below.

Material independence of E_b^{xx}/E_b^x. Biexcitons have been observed in many quantum wells, but they have been studied more systematically only in GaAs quantum wells [2]. In GaAs quantum wells the measured ration is 0.2, and the binding energy of quasi-2D excitons in GaAs quantum wells of width 80 Å is known[2] to be 10 meV which gives a binding energy of 2 meV for biexcitons. In ZnSe single quantum well of width 75 Å[4] the measured binding energy of biexciton is 5 meV and the exciton binding energy is 20–25 meV, which gives a ratio of 0.2–0.25.

In the bulk crystals of CuCl the binding energy of Γ_1 biexciton, the lowest bound state of two Z_3 excitons, has a binding energy of 32 meV[5] and the exciton binding energy is 150–190 meV, which gives a ratio of 0.17–0.21. To the author's knowledge, this is the only example of such a large binding energy of biexcitons in a bulk. The ratio in Eq. (8) is clearly in agreement with the above examples which suggest that the ratio is independent of the material.

However, this is not true for trions (a free charge carrier bound to an exciton), where the ratio E_b^{xx}/E_b^x depends on $\sigma = m_e^r/m_h^*$,[13,14] and hence it is different for different materials. For a negatively charged trion (e–h–e), the binding energy is obtained as

$$E_b^{x^-} = \left[\frac{9(1+\sigma)}{2(3+2\sigma)} - 1 \right] E_b^x, \tag{10}$$

and hence $E_b^{x^-}/E_b^x$ depends on σ. Using Eq. (10) we get a ratio of $E_b^{x^-}$ to the energy of a neutral donor as a function of σ that agrees reasonably well with the variational calculation.[14] Such a difference between E_b^{xx}/E_b^x and $E_b^{x^-}/E_b^x$ may be attributed to the difference in the structure of biexcitons and trions.

Effect of Confinement. As the biexciton Bohr radius is more than twice larger than the exciton Bohr radius [Eq. (9)], one expects that the effect of confinement would be more pronounced on the binding of biexcitons than on excitons. This means that the ratio E_b^{xx}/E_b^x is expected to be larger in narrow dimensions such that it is least in bulk and highest in 1D and 0D. To our knowledge there are only two examples, GaAs and CuCl, which may be used here. In GaAs quantum wires the ratio obtained from a very sophisticated variational calculation[15] suggests that $E_b^{xx}/E_b^x = 0.6$ and it is nearly independent of the length and width of quantum wires. The experimental results[2] in GaAs quantum wells show that $E_b^{xx}/E_b^x = 0.2$ and it is independent of the quantum well width, which is also supported by the ratio obtained in Eq. (8).

In CuCl quantum dots of sizes more than 50 Å, no effect of confinement on biexcitons and excitons is observed.[16] This is because the $1S$ exciton Bohr radius in CuCl is 6.8 Å,[13] and the corresponding biexciton Bohr radius is 15 Å,[16] and the effect of confinement is not found to be significant in quantum dot sizes much bigger than exciton and biexciton Bohr radii.[17] However, more experimental data are needed on the binding energy of excitons and biexcitons as a function of the size of confinement to address the issue any further. Nevertheless, it is interesting to see from the above data[16,18] that the ratio of biexciton to exciton Bohr radii is 2.2 in CuCl, which is comparable with 2.7 obtained in Eq. (9).

I am indebted to Professor T. Itoh for supplying his results on CuCl and to Dr. D. Birkedal for many useful discussions. A part of the work was done at the Mikroelectronik Centret, Danish Technical University, and I would like to thank Professor J. Hvam for the hospitality.

[1] R. C. Miller, D. A. Kleinman, A. C. Gossard, and O. Munteanu, Phys. Rev. B **25**, 6545 (1982).
[2] D. Birkedal, J. Singh, V. G. Lyssenko, J. Erland, and J. M. Hvam, Phys. Rev. Lett. **76**, 672 (1996).
[3] M. Nakayama, K. Suyama, and H. Nishimura, in *Fourth International Meeting Optics of Excitons in Confined Systems*, Cortona, Italy, (28–31 August 1995).
[4] V. Kozlov, P. Kelkar, and A. V. Nurmikko, Phys. Rev. B **53**, 10837 (1996).
[5] R. Shimano and M. Kuwata-Gonokami, Phys. Rev. Lett. **72**, 530 (19994).
[6] K. Saito and N. Nagasawa, Solid State Commun. **94**, 33 (1995).
[7] M. Hasuo and N. Nagasawa, Phys. Rev. Lett. **70**, 1303 (1993).
[8] J. R. Haynes, Phys. Rev. Lett. **17**, 860 (1966).
[9] J. R. Haynes, Phys. Rev. Lett. **4**, 361 (1960).
[10] D. A. Kleinman, Phys. Rev. B **28**, 871 (1983).
[11] J. Singh, D. Birkedal, V. G. Lyssenko, and J. M. Hvam, Phys. Rev. B **53**, 15909 (1996).

[12] X. F. He, Phys. Rev. B **43**, 2063 (1991); H. Mathieu, P. Lefebvre, and P. Christol, Phys. Rev. B **48**, 17308 (1993).
[13] J. Singh, Appl. Opt. (in press).
[14] B. Stebe and A. Ainane, Superlattices Microstruct. **5**, 545 (1989).
[15] F. Madarasz, Phys. Rev. B **49**, 13528 (1994).
[16] K. Yamanaka, K. Edamatsu, and T. Itoh, J. Lumin. DPC'97 (in press).
[17] M. Hasuo, N. Nagasawa, T. Itoh, and A. Mysyrowicz, J. Lumin. **60**, 758 (1994).
[18] Y. Mimura *et al.*, J. Lumin. **66**, 401 (1996).

Published in English in the original Russian journal. Reproduced here with stylistic changes by the Translation Editor.

Anomalous behavior of excitons at light holes in strained (In,Ga)As/GaAs heterostructures

Kh. Moumanis, R. P. Seĭsyan, M. É. Sasin, A. V. Kavokin, and S. I. Kokhanovskiĭ

A. F. Ioffe Physicotechnical Institute, Russian Academy of Sciences, 194021 St. Petersburg, Russia

H. M. Gibbs and G. Khitrova

Optical Sciences Center, University of Arizona, Tucson, Arizona

Fiz. Tverd. Tela (St. Petersburg) **40**, 797–799 (May 1998)

Additional localization of holes due to Coulomb attraction to the electron located in a quantum well is important for light-hole excitons in the heterostructure (In, Ga)As/GaAs. The fine structure of the optical and magneto-optical spectra of these quantum wells is examined in detail with the formation of a ''Coulomb well'' and deformations taken into account. © *1998 American Institute of Physics.* [S1063-7834(98)00405-5]

1. In (In, Ga)As/GaAs heterostructures a ''type-I—type-II'' mixed heterojunction is realized possessing the property that in the InGaAs (ternary solution) layer attractive potentials are present for the electrons and heavy holes and a repulsive potential for the light holes. The nature of the light-hole excitons in these objects is not obvious. Deep in the type-II layer they are spatially indirect; however, maxima are observed in the absorption spectra of (In, Ga)As/GaAs heterostructures for light-hole exciton states whose oscillator strengths are significantly higher than expected for spatially indirect transitions.[1,2] This can be explained by taking into account the possibility of additional localization of the light hole thanks to Coulomb attraction of the latter to the electron spatially confined by the quantum-well potential. This effect leads to the formation of a ''Coulomb well'' for the light hole in the ternary-solution layer, which in turn provides some spatial localization of the light hole within this layer, and the optical transitions turn out to be direct.[3]

In order to observe the fine structure of the spectra associated with the light-hole transitions from states of the ''Coulomb well,'' it is necessary to use high-quality samples characterized by a very small half-width of their spectral lines.

Theoretical calculations of the exciton binding energies in a magnetic field and of the oscillator levels in the ''Coulomb well'' enable us to study the observed behavior of a light-hole exciton. We were the first to successfully isolate the ''Coulomb well'' contribution quantitatively and estimate the height of the ''Coulomb wells'' and the actual energy positions of the LH1 and LH3 levels.

2. We experimentally investigated a set of samples with different parameters, grown by molecular-beam epitaxy. For optical measurements, the substrates were completely removed by chemical etching. To observe effects associated with the influence of the ''Coulomb well,'' we first selected $In_xGa_{1-x}As/GaAs$ heterostructures with low In content $x=0.05-0.08$. The highest-quality samples were obtained at such In concentrations. For samples NMC 21 and NMC 11 with $x=0.045$ and 0.062, respectively, the well width L_z was equal to 90 and 88 Å, and the barrier thickness L_b, to 822 and 758 Å, while the spectral line widths for the HH1E1 transition were 0.8 and 1.1 meV, respectively. Magneto-optical measurements were performed at $T=1.7$ K in a pumped-down helium cryostat with a superconducting solenoid which allowed us to obtain fields up to 7.5 T.

3. The experiments yielded absorption and magneto-oscillation spectra containing numerous maxima corresponding to light-hole and heavy-hole exciton transitions. The optical absorption spectrum of the sample with indium content $x=0.045$, measured before and after substrate removal, is shown in Fig. 1. The spectra of the substrate-free samples exhibit considerably more detail. It is possible to distinguish two absorption levels in the spectra. The first level, corresponding to weaker absorption, corresponds to transitions to an electron level in the InGaAs quantum well, while the stronger spectral features belong to transitions in the GaAs barrier. Absorption in the barriers can be described in terms of exciton–polariton processes overlaid by an effect of weak

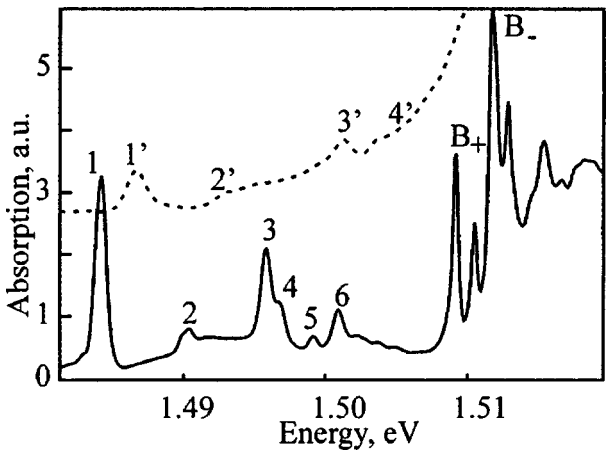

FIG. 1. Absorption spectra of sample NMC21 at 1.7 K with no magnetic field. The dashed line depicts the absorption spectrum of the sample before stripping away the substrate, the solid line—after. The numbers denote the absorption maxima corresponding to transitions between electrons and holes of the well; the letters—transitions in the barrier.

elongation in the layer plane.[4] All peak positions in the free samples are shifted toward lower energies by 2.5–6.6 meV relative to the substrate-bound sample. The shift is different for heavy-hole and light-hole transitions. The longest-wavelength lines, associated with transitions to an electron level in the quantum well, can be divided into two groups: the first two lines are associated with an HH1E1 exciton in the ground state ($1s$) and first excited state ($2s$). The remaining lines can belong only to light-hole exciton states. It is worthy of note that for low In content, according to the energy diagram, other optical transitions in this system are absent. The fan diagram for the positions of the absorption maxima in magnetic fields is shown in Fig. 2. It is clear that one group of lines reveals the typical behavior of diamagnetic excitons in a quantum well,[5] and it can be linked with an HH1E1 exciton.

Most interesting is the behavior of the light-hole exciton lines. Note that a light-hole exciton does not form a natural fan diagram and the positions of the light-hole maxima depend weakly on the magnetic field. In addition, we stress that the second light-hole line also exhibits such a weak field dependence, which contradicts the model for the formation of a magneto-absorption spectrum in an ordinary quasi-$2D$ system proposed in Ref. 5.

4. The difference between the free samples and the substrate-bound samples is seen in the change in the positions of the absorption maxima in Fig. 1. This figure also reveals some deformation of the GaAs barrier layers in the free samples, which can be quantitatively estimated with the aid of the energy shifts δE and the deformation splitting Δ_e relative to a free bulk sample of GaAs. According to Ref. 6, the change in the strain state of the (In, Ga)As layer can be described in terms of the deformation of the barrier e as $\Delta e = e_1 - e_0 = ek$, where e_1 is the resulting deformation, and e_0 is the initial deformation in the (In, Ga)As layer (before substrate removal), and $k = 5.6512/(5.6512 + 0.4x) \approx 1$. This makes it possible to describe the shifts Δ_1 and Δ_2 for HH1E1 and LH1E1, respectively.[7,8]

$$\Delta_1 = -a_x(2-\lambda_x^{100})e - b_x(1+\lambda_x^{100})e,$$

$$\Delta_2 = -a_x(2-\lambda_x^{100})e - b_x(1+\lambda_x^{100}) \times e[1+9b_x(1+\lambda_x^{100})(e_0+e_1)/4\Delta_{0x}], \quad (1)$$

λ_x^{100} is a parameter expressed in terms of the components of the elasticity tensor, and b is the constant of the strain potential.

Heavy-hole exciton transitions dominate in the magneto-absorption spectra. The fan diagrams for these transitions are typical of direct $2D$ exciton transitions in a magnetic field.[5] To regain the ''true'' values of the energies of the transitions between the Landau levels, it is necessary to augment the energies of the exciton transitions obtained from the experimental absorption spectra by the calculated exciton binding energies. A reconstruction of the fan diagram, incorporating experimental data and theoretical calculations, is shown in Fig. 2 by the solid lines. Excluding the system of heavy-hole transitions entering into the diagram, it is possible to confidently distinguish peaks corresponding to light-hole transitions. The theoretical data obtained in Refs. 1 and 2 allow us to calculate the configuration of the Coulomb wells and the oscillator energy levels. The main parameters of such a well depend weakly on the material parameters of the quantum-size layer and its thickness. For samples NMC 21 and NMC 11 the total depth of the Coulomb wells is on the order of $V_0 = 12-17$ meV, where the first LH1 energy level is found at $-12.5-15$ meV relative to the bottom of the ''Coulomb well,'' and the splitting between the first optically active light-hole oscillator levels LH1 and LH3 is equal to $\Delta E_{\rm osc} = 2-5$ meV.

The half-width of the ''Coulomb well'' is around 200 Å, which is substantially greater than the width of the (In,Ga)As layer. Taking mixing of the light-hole states in the well and in the barrier into account, we calculated the exciton binding energies for different Landau levels in different magnetic fields. It turned out to be possible in this way to bring our calculated results into agreement with the experimental data.

We also examined samples with higher indium content x. Figure 3, together with experimental points for the LH1E1 exciton transitions belonging to samples with different x and L_z, plots curves for $E_g(x)$, E_c, and E_{lh} (E_g is the width of the band gap, and E_c and E_{lh} are respectively the levels of the bottom of the conduction band and the top of the light-hole band).

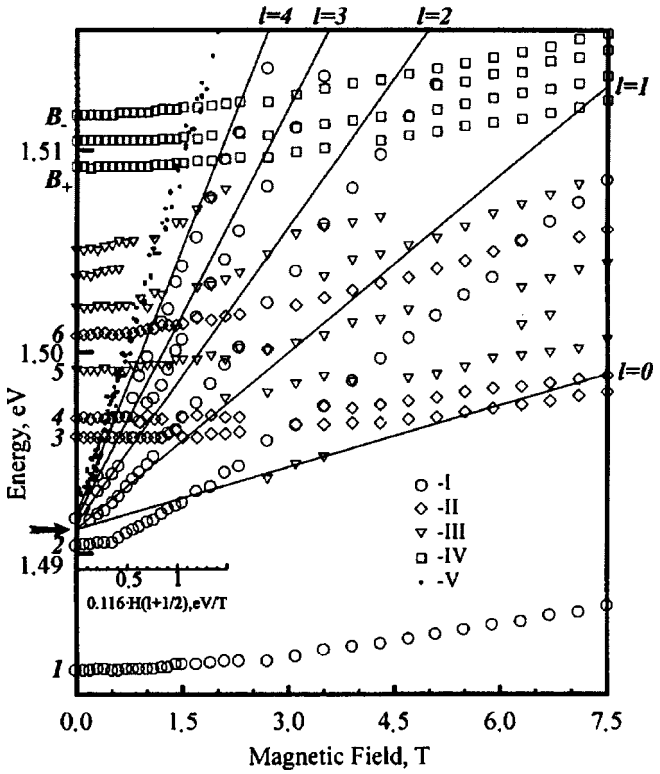

FIG. 2. Fan diagram of sample NMC21, obtained with right-circularly polarized light. Exciton transitions: I — HH1E1, II — LHE1, III — transitions from deeper light-hole ''oscillator'' levels (primarily), IV — transitions in the barrier. The solid lines correspond to transitions between Landau levels of the heavy hole HH1 and the electron E1, l is the number of the Landau level of the electron, the numbers to the left correspond to the numbers in Fig. 1. The arrow indicates the energy of the transition between the HH1 and E1 levels in zero magnetic field.

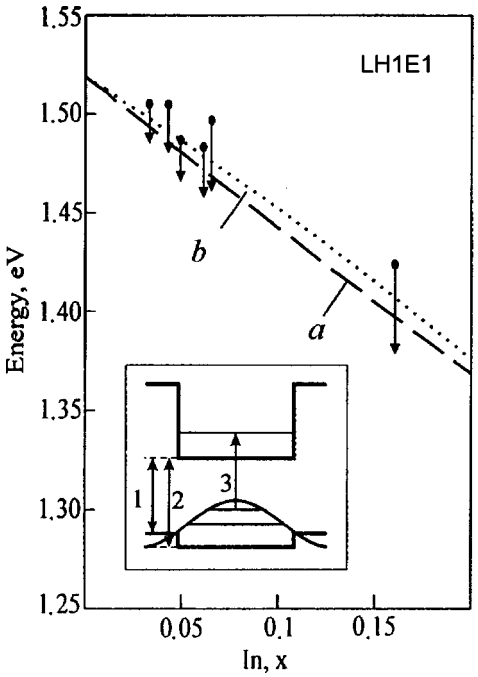

FIG. 3. Energy gap between the bottom of the electron well and the top of the valence band in the barrier (*a*) and between the bottom of the electron well and the top of the light-hole band in (In, Ga)As (*b*) as functions of indium content. Inset: energy diagram of the sample. The central arrow *3* corresponds to transitions in the adopted model.

If we subtract the energies of the first quantum-size levels E1 and HH1 in the quantum wells from the experimental values of the transition energies, we can recover the ''experimental'' $E_g(x)$, E_c, and E_c+E_{lh} for samples with different x. The agreement reached for HH1E1 is very good and the experimental error does not exceed ± 2 meV, while the experimental points for LH1E1 are considerably lower than the corresponding curves for large concentrations ($x>0.05$) and approach them at low indium concentrations ($0<x<0.05$).

This can be explained by the fact that our calculation of the ''Coulomb well'' for low x is not accurate enough because we have neglected the closeness of the electron energy to the barrier. In Fig. 4 we present a calculation of the dependence of the position of the upper oscillator level in the Coulomb well on the indium content x. E_{LH1} is, of course, equal to zero for $x=0$ and reaches an asymptotic value only for $x \gg 0.05$. The experimental points calculated as the difference between the recalculated experimental values (the triangles in Fig. 2) and the dashed curve in Fig. 3 for the energy difference between the bottom of the electron well

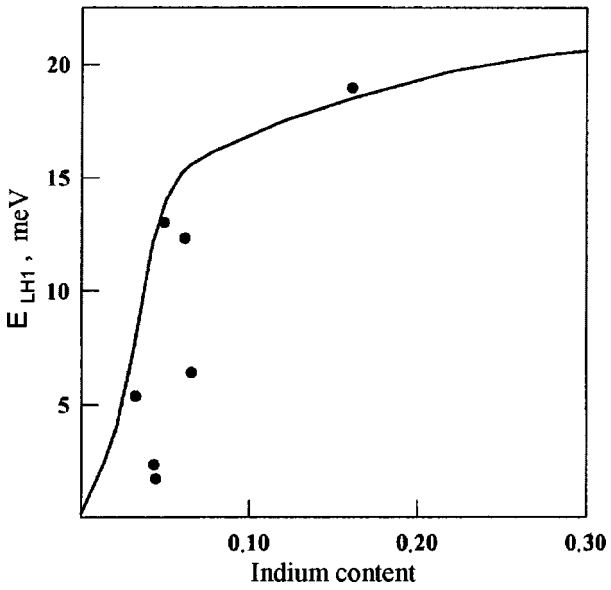

FIG. 4. Position of the oscillator level E_{LH1} relative to the top of the light-hole band in the (In, Ga)As layer as a function of indium content x. Solid curve—theoretical, points—distance between the recalculated experimental data (triangles in Fig. 3) and the dashed curve *b* (also in Fig. 3).

and the top of the light-hole band in the (In, Ga)As layer are in satisfactory agreement with this theoretical dependence, which may be considered as a quantitative confirmation of the ''Coulomb well'' model.

This work was supported by grants No. 1–020/2 and 1–080/4 of the GNTP.

[1] R. P. Seisyan, A. V. Kavokin, S. I. Kokhanovskii, A. I. Nesvizhskii, M. E. Sasin, M. A. Sinitsin, and B. S. Yavich, Semicond. Sci. Technol. **10**, 611 (1995).
[2] A. V. Kavokin, S. I. Kokhanovskiĭ, A. I. Nesvizhskiĭ, M. E. Sasin, R. P. Seĭsvan, A. P. Egorov, A. V. Zhukov, and V. M. Ustinov, Fiz. Tekh. Poluprovodn. **31**, 1109 (1997) [Semiconductors **31**, 950 (1997)].
[3] Al. L. Éfros, Fiz. Tekh. Poluprovodn. **20**, 128 (1986) [*sic*].
[4] G. N. Aliev, N. V. Luk'yanova, R. P. Seisyan, M. R. Vladimirova, V. N. Bessolov, H. Gibbs, and G. Khitrova, Compd. Semicond. **155**, 169 (1996).
[5] A. V. Kavokin, M. A. Kaliteevskii, S. V. Goupalov, J. D. Berger, O. Lyngnes, H. M. Gibbs, G. Khitrova, A. Ribayrol, A. Bellabchara, P. Lefebvre, D. Coquillat, and J. P. Lascaray, Phys. Rev. B **54**, R11078 (1996).
[6] G. N. Aliev, N. V. Luk'yanova, and R. P. Seĭsyan, Fiz. Tverd. Tela **38**, 1067 (1996) [Phys. Solid State **38**, 590 (1996)].
[7] A. V. Kavokin, A. I. Nesvizhskii, and R. P. Seisyan, Fiz. Tekh. Poluprovodn. **27**, 977 (1993) [Semiconductors **27**, 530 (1993)].
[8] S. I. Kokhanovskii, K. Moumanis, M. E. Sasin, and R. P. Seisyan, Nanostructures Physics and Technology (1997), p. 69.

Translated by Paul F. Schippnick

Magnetic polarons in semimagnetic-semiconductor-based heterostructures

K. V. Kavokin, I. A. Merkulov, and D. R. Yakovlev

A. F. Ioffe Physicotechnical Institute, Russian Academy of Sciences, 194021 St. Petersburg, Russia

Fiz. Tverd. Tela (St. Petersburg) **40**, 800–802 (May 1998)

Specific features in the behavior of localized magnetic polarons formed under optical excitation in heterostructures based on semimagnetic semiconductors are considered. These features are due to the strong anisotropy of the hole g factor in low-dimensional systems based on zincblende crystals. The anisotropy is due to the strong spin-orbit coupling in the valence band which, in quantum confinement conditions, results in quadrupole splitting of the hole spin levels. The g factor anisotropy manifests itself in a strong anisotropy of the magnetic and magneto-optical characteristics of localized magnetic polarons. © *1998 American Institute of Physics.* [S1063-7834(98)00505-X]

Theoretical and experimental studies of magnetic polarons date back as far as three decades.[1] Development of semimagnetic semiconductors ($Cd_{1-x}Mn_xTe$, $Hg_{1-x}Mn_xTe$ and so on), whose luminescence at helium temperatures is due to recombination of localized excitons, provided a new impetus to these studies.[2] The fact is that, at not too low concentrations of magnetic impurities ($x \geqslant 0.1$), exchange interaction between localized photoinduced carriers and the surrounding magnetic ions produces a considerable red shift of the luminescence line. The reason for this shift lies in the polarization of the magnetic ions induced by localized carriers, which brings about a decrease of the exchange energy of the system through formation of magnetic polarons (Fig. 1). Optical measurements of photoluminescence spectra, their dynamics, and polarization characteristics permitted one to obtain valuable information on the properties of magnetic-polaron states and stimulated development of their theoretical description.[2]

In the semimagnetic semiconductors under study, the exchange-interaction constant of magnetic ions with carriers in the valence band exceeds by several times that for conduction-band carriers. Therefore, holes play a major role in magnetic-polaron formation in these compounds. Semimagnetic semiconductors have zincblende (or wurtzite) structure, and their valence band is characterized by strong spin–orbit coupling. In cubic crystals, this interaction gives rise to formation of light- and heavy-hole subbands, with the carrier behavior in these subbands described by the Luttinger Hamiltonian[3]. The spins of such carriers change direction in the localization region from point to point, which may result in quantitative and qualitative changes in the properties of the magnetic polaron.[4] The role of hole spin–orbit coupling manifests itself most clearly, however, in magnetic polarons in low-dimension systems (quantum wells, wires, and dots) and wurtzite crystals. Lowering of symmetry gives rise in this case to a strong quadrupole splitting of hole spin levels, which is formally seen in a strong anisotropy of their g factor.[5]

For example, the hole spin projection on the normal to the quantum-well plane (Z axis) at the bottom of the lowest two-dimensional quantum-well (QW) band can assume only two values, $J_Z = \pm 3/2$. A localized hole can in this case be described approximately as a quasi-particle with pseudospin $j = 1/2$ and a strongly anisotropic g factor, $g_{ZZ} = 3$, g_{XX}, $g_{YY} \ll 1$. The g factor is introduced here as a tensor relating the matrix elements of operators of the spin, $\hat{\mathbf{J}}$, and pseudospin, $\hat{\mathbf{j}}$, components, $2\langle \eta | J_\alpha | \eta' \rangle = g_{\alpha,\beta} \langle \eta | \sigma_\beta | \eta' \rangle$, calculated with the wave functions of the spin doublet under study, where $\hat{\sigma}_\beta$ are the Pauli matrices.

The Hamiltonian of exchange interaction of this quasiparticle with surrounding magnetic ions will now depend not only on the angle between the spin of the nth ion, $\mathbf{I}_0$, and the hole pseudospin $\mathbf{j}$, but also on orientation of each of these vectors relative to the principal axes of the g factor tensor (the Z axis for a quantum well):

$$\hat{H}_{\mathrm{ex}} = \frac{\beta}{3} \sum_n (\hat{\mathbf{I}}_n \hat{g} \hat{\mathbf{j}}) |\Psi(\mathbf{R}_n)|^2.$$

Here β is the exchange interaction parameter, and $|\Psi(\mathbf{R}_n)|^2$ is the squared modulus of the hole wave function at this magnetic ion.

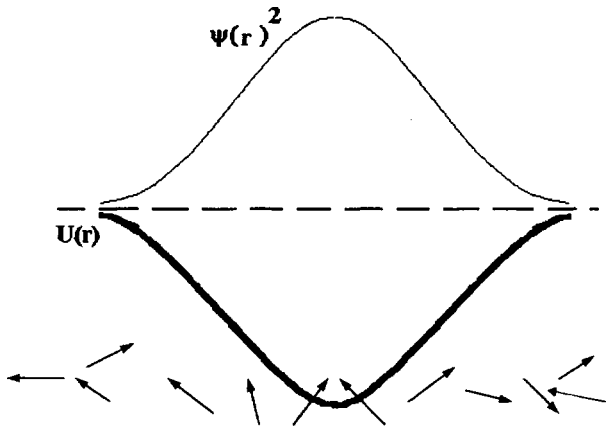

FIG. 1. Exchange energy profile in the carrier localization region before (dotted line) and after (solid line) formation of the magnetic polaron state.

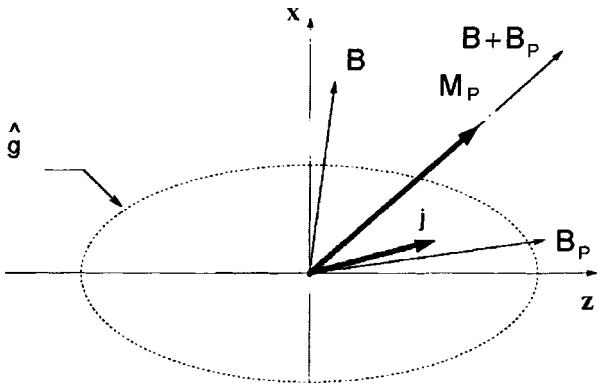

FIG. 2. Spin structure of the magnetic polaron formed by a particle with an anisotropic g factor for arbitrary orientation of external magnetic field. Dotted line: anisotropic g factor ellipsoid ($g_{zz} \gg g_{xx}$). Total spin of magnetic ions making up the polaron, $\mathbf{I}_p$, is directed along the resultant of the external magnetic field $\mathbf{B}$ and the exchange field $\mathbf{B}_p$ produced at these ions by a hole with anisotropic g factor. $\mathbf{I}_p$ and hole pseudospin $\mathbf{j}$ coincide in direction with external magnetic field only when it is parallel to the Z axis.

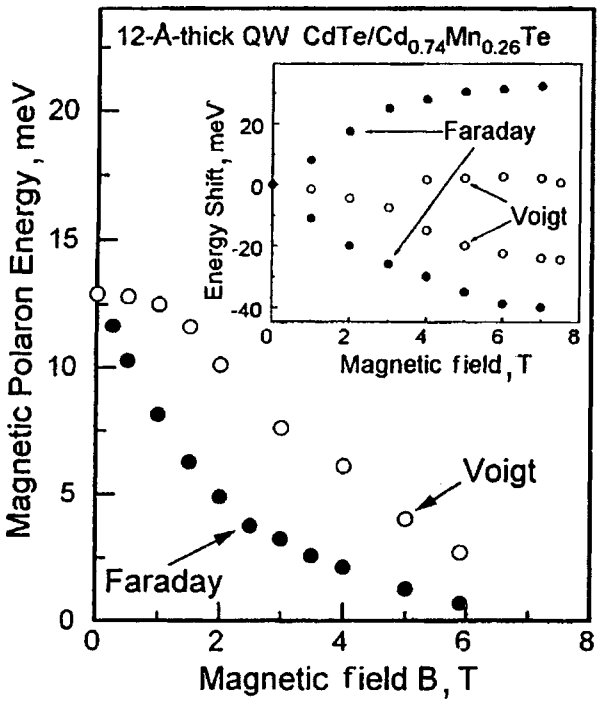

FIG. 3. Anisotropy of depression of the two-dimensional magnetic polaron by an external magnetic field.[6] Inset shows the spin splittings of states of the free exciton formed by a 2D electron and a heavy hole in a magnetic field perpendicular to the quantum-well plane (Faraday geometry) and in an in-plane magnetic field (Voigt geometry).

With the magnetic polaron in steady state, the hole pseudospin $\mathbf{j}$ is oriented along the exchange field of the surrounding magnetic ions, $\mathbf{B}_{ex} \propto \hat{g} \Sigma_n \mathbf{I}_n |\Psi(\mathbf{R}_n)|^2$, and the total magnetic moment of the ions generating this field $\mathbf{M}_p = \mu_B g_{\mathrm{Mn}} \Omega \Sigma_n \mathbf{I}_n |\Psi(\mathbf{R}_n)|^2 \equiv \mu_B g_{\mathrm{Mn}} \Omega \mathbf{I}_p$, along the resultant of the external magnetic field $\mathbf{B}$ and the exchange field of the localized hole $\mathbf{B}_p = (\beta/3\mu_B g_{\mathrm{Mn}}) \Sigma_n \hat{g}\hat{\mathbf{j}} |\Psi(\mathbf{R}_n)|^2$ (see Fig. 2). (Here Ω is the unit-cell volume, and μ_B and g_{Mn} are the Bohr magneton and g factor of magnetic ions, respectively). Thus $\mathbf{j} \| \mathbf{I}_p \| \mathbf{B}$ only when the external magnetic field coincides in direction with one of the principal axes of tensor $\hat{g}$. Moreover, in the case of a strongly anisotropic $\hat{g}$ and of not too strong external magnetic fields, in steady state $\mathbf{j} \| \mathbf{I}_p \| \mathbf{B}$ only if the external magnetic field is directed along the principal axis corresponding to the largest eigenvalue of g.[5] As a result, the characteristics of the magnetic polaron turn out to be strongly dependent on direction of the external magnetic field.

Depression of the magnetic polaron shift for two-dimensional polarons by an external magnetic field was shown, both theoretically and experimentally, to be strongly anisotropic (Fig. 3).[6] In the three-dimensional case, this depression is connected with the polarization of magnetic ions becoming saturated in the applied field. As a result of this saturation, the additional polarization of magnetic ions in the hole exchange field also decreases, and this is what accounts for the eventual disappearance of the polaron. In the case of 2D-hole g factors with the maximum possible anisotropy ($g_{ZZ}=3$, $g_{XX}=g_{YY}=0$) these considerations remain valid if the field $\mathbf{B}$ is along the Z axis. In the case of perpendicular geometry ($\mathbf{B} \perp Z$), the hole pseudospin in a stable, stationary magnetic-polaron state is still directed along the Z axis, the fields $\mathbf{B}$ and $\mathbf{B}_p$ are mutually perpendicular, and the magnetic polaron shift begins to decrease significantly only for $B \geqslant B_p$.

It thus becomes clear that the 2D polaron becomes strongly anisotropic when the magnetic field is applied along the principal axis of the $\hat{g}$ tensor corresponding to the smallest eigenvalue of the latter, and the obvious stationary magnetic polaron state with $\mathbf{j} \| \mathbf{I}_p \| \mathbf{B}$ is unstable. The anisotropy of the hole g factor results in this case in anomalously small value of the magnetic-field-induced linear polarization of the luminescence,[7] as well as in such prominent dynamic effects as the anomalously large number of peaks in optical paramagnetic resonance spectra,[8] oscillations in optically induced Faraday rotation,[9] sign inversion of the Hanle effect in optical-orientation experiments,[10] and dynamic increase of magnetic polaron energy[11]. All these dynamic effects originate from the spin precession of magnetic ions in the total

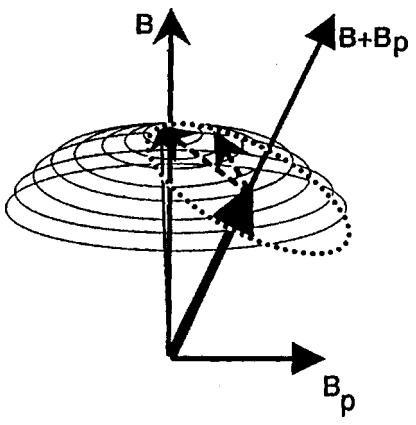

FIG. 4. Precession of the magnetic-ion polatization induced by an external magnetic field in the presence of the exchange field of a photoinduced hole with a strongly anisotropic g factor. It is this precession that accounts for all dynamic effects studied in Refs. 7–11.

field $\mathbf{B}+\mathbf{B}_p$, which is parallel neither to the external magnetic field $\mathbf{B}$ nor to the exchange field $\mathbf{B}_p$ because of the hole g factor being anisotropic (Fig. 4).

Support of the Volkswagen Stiftung and Russian Fund for Fundamental Research (Grants 96-02-16936 and 96-02-1641) is gratefully acknowledged.

[1] P. G. de Gennes, Phys. Rev. **118**, 141 (1960); M. A. Krivoglaz, Usp. Fiz. Nauk **111**, 617 (1973) [Sov. Phys. Usp. **16**, 856 (1973)]; E. L. Nagaev, J. Magn. Magn. Mater. **110**, 39 (1982).
[2] P. A. Wolff, in *Semiconductors and Semimetals*, Vol. 25, edited by J. K. Furdyna and J. Kossut (Academic Press, London, 1988), pp. 413–454.
[3] G. L. Bir and G. E. Pikus, *Symmetry and Strain-Induced Effects in Semiconductors* (Wiley, New York, 1974) [Russian orig., Nauka, Moscow, 1972].
[4] Yu. F. Berkovskaya, É. M. Vakhabova, B. L. Gel'mont, and I. A. Merkulov, Zh. Éksp. Teor. Fiz. **94**, 183 (1988) [Sov. Phys. JETP **67**, 535 (1988)].
[5] I. A. Merkulov and K. V. Kavokin, Phys. Rev. B **52**, 1751 (1995).
[6] D. R. Yakovlev, W. Ossau, A. Waag, R. N. Bicknell-Tassius, G. Landwehr, K. V. Kavokin, A. V. Kavokin, I. N. Uraltsev, and A. Pohlmann, in *Proceedings of the 21st International Conference ''Physics of Semiconductors''* (Beijing, 1992), edited by Ping Jiang and Hou-Zhi Zheng (World Scientific, Singapore, 1992), p. 1136; D. R. Yakovlev and K. V. Kavokin, Comm. Cond. Matter Phys. **18**, 51 (1996).
[7] I. A. Merkulov, D. R. Yakovlev, K. V. Kavokin, G. Mackh, B. Kuhn-Heinrich, W. Ossau, A. Waag, and G. Landwehr, Fiz. Tverd. Tela (St. Petersburg) **39**, 2079 (1997) [Phys. Solid State **39**, 2075 (1997)].
[8] J. Stühler, G. Schaack, M. Dahl, A. Waag, G. Landwehr, K. V. Kavokin, and I. A. Merkulov, Phys. Rev. Lett. **74**, 2567 (1995); K. V. Kavokin and I. A. Merkulov, Phys. Rev. B **55**, R7371 (1997).
[9] S. A. Crooker, J. J. Baumberg, F. Flack, N. Samarth, and D. D. Awschalom, Phys. Rev. Lett. **77**, 2814 (1996).
[10] Yu. G. Kusrayev, A. V. Kudinov, K. V. Kavokin, B. P. Zakharchenya, D. E. Ashenford, and B. Lunn, in *Proceedings of the 23rd International Conference ''Physics of Semiconductors''* (Berlin, 1996), edited by M. Scheffler and R. Zimmermann (World Scientific, Singapore, 1996), p. 2459–2462.
[11] D. R. Yakovlev, K. V. Kavokin, I. A. Merkulov, G. Mackh, W. Ossau, R. Hellmann, E. O. Göbel, A. Waag, and G. Landwehr, Phys. Rev. B **56**, 9782 (1997).

Translated by G. Skrebtsov

Anomalous influence of magnetic field on the indirect exciton in GaAs/AlGaAs double quantum wells

V. V. Krivolapchuk, D. A. Mazurenko, E. S. Moskalenko, N. K. Poletaev, and A. L. Zhmodikov

A. F. Ioffe Physicotechnical Institute, Russian Academy of Sciences, 194021 St. Petersburg, Russia

T. S. Cheng and C. T. Foxon

Nottingham University, NG7 2RD, Great Britain

Fiz. Tverd. Tela (St. Petersburg) **40**, 803–805 (May 1998)

A study is reported of exciton luminescence in GaAs double quantum wells produced in electric and magnetic fields. It has been found that the indirect-exciton line (IX) behaves anomalously, namely, one observes a magnetic-field-induced low-energy shift of the IX line, and the onset of periodic (≈ 5 s) fluctuations in the IX-line intensity. © *1998 American Institute of Physics.* [S1063-7834(98)00605-4]

1. Considerable interest has recently been focused on studying the behavior of carriers in double quantum wells (QW). This interest is stimulated by the possibility of carrier condensation to a superfluid state in such systems.[1–3] Recent experiments indicate very interesting collective phenomena in double QWs initiated by an external magnetic field.[4–6] The present work studies exciton photoluminescence (PL) spectra from slightly asymmetric GaAs double QWs occurring in the presence of a magnetic field perpendicular to the double QW plane.

2. The samples (NU1117) were grown at Nottingham University by molecular-beam epitaxy on 0.4-mm thick (001)GaAs substrates at T=630°C. The samples are three quantum-well pairs with thicknesses (QW/ $Al_{0.33}Ga_{0.67}As$ barrier/QW in nm) of 20.07/3.82/1.95, 10.18/3.82/9.61, and 8.20/3.82/7.63 grown on a 1-μm thick GaAs buffer. The QW pairs are separated by $Al_{0.33}Ga_{0.67}As$ barriers 20 nm thick. A constant dc bias V_{dc} was applied to two indium contacts deposited on the substrate and the sample side with the double QWs (Fig. 1a). The PL was excited and detected through a small (0.2×0.2 mm) hole in the contact on the side of the QWs (Fig. 1a). The sample was illuminated with a cw He–Ne laser ($P<1$ mW, $\lambda = 730.3$ nm), which corresponds to under-barrier excitation, The spectra were measured with a DFS-52 double-grating spectrometer in the photon-counting mode from the sample maintained at $T=4.2$ K.

A magnetic field (up to 5 T) was applied in the growth direction, i.e. parallel to V_{dc}. The polarity of V_{dc} was chosen so as to achieve the indirect mode (Fig. 1b), which corresponds to the lowest energy position of the IX indirect exciton (with the electron localized in the thick, and the hole, in the thin well) relative to the DX direct-exciton transition energy (with both the electron and the hole in the thick well) in PL.

3. The experimental data presented here relate to the behavior of photoexcited carriers in the 10.18/3.82/9.61-nm double QW. The emission spectrum of this QW obtained at $B=0$ and $V_{dc}=-0.4$ V is displayed in Fig. 2a. The spectrum contains the direct-exciton (DX) line at 1.555 eV, the line corresponding to an impurity-bound direct exciton (BDX),[7] the indirect-exciton line IX, and a LIX line. The latter line is produced in recombination of an impurity-bound IX indirect exciton[8]. The positions of the IX and LIX lines are determined by the electric field in the double QWs and depend linearly on V_{dc} within $-0.4<V_{dc}<0$ V. A further decrease of V_{dc} ($V_{dc}<V_0=-0.4$ V) does not practically affect the IX line position and, hence, the electric field in the double QW, while creating a noticeable ($\approx 1\ \mu$A) electric current J through the structure. Application of a magnetic field B changes substantially the behavior of the IX and LIX lines. For comparatively low fields, $B\leqslant 2$ T (see Fig. 2b), these lines shift toward lower energies (this behavior fits into none of the available models describing the magnetic-field dependence of spectral lines in semiconductors and, thus, is anomalous), and only a further increase of the field, i.e. for $B\geqslant 2$ T, makes the IX and LIX lines shift toward higher energies (Fig 2c). At the same time the direct-exciton line DX behaves in the usual way (a diamagnetic shift is observed). Figure 3 shows the shift $\Delta E = E_{IX}(B) - E_{IX}(B=0)$ of the IX line as a function of B for three different values of V_{dc}.

4. Turning now to discussion, it is essential to point out that ΔE increases, while remaining positive, throughout the B range covered only for V_{dc} within a certain interval, $V_0 < V_{dc} < 0$ V (see Fig. 3b and 3c). Note that within this electric-field interval practically no current flows through the structure ($J<0.1\ \mu$A). For $V_{dc}<V_0=-0.4$ V, however, when a noticeable current flows in the structure, magnetic field ($B<2$ T) shifts the IX line toward lower, and for $B>2$ T, toward higher energies (Fig. 3a). The IX shift to lower energies implies creation in the double QW of a larger (compared to the zero B case) electric field, which changes the slope of the energy bands (Fig. 1b). One may thus conclude that magnetic field blocks current flow and in this way favors generation in the double QW of a higher effective

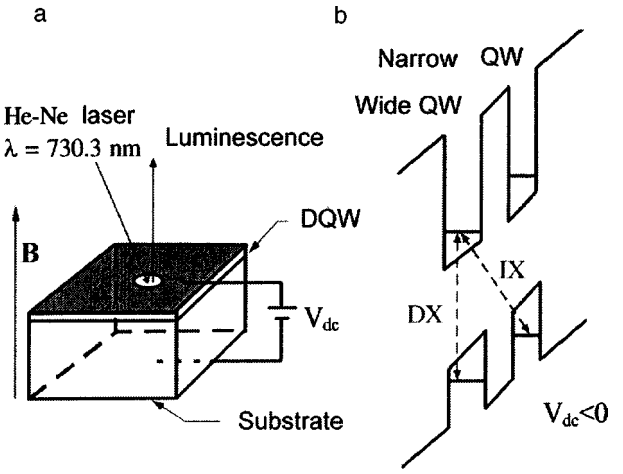

FIG. 1. (a) Schematic representation of experiment and (b) band diagram for indirect mode.

electric field. For $V_{dc} > -0.4$ V, there is practically no current, and magnetic field produces only positive changes in ΔE (Fig. 3b and 3c). A magnetic-field-induced displacement of the IX line toward higher energies was observed earlier and was attributed to diamagnetic shift.[9,10] Diamagnetic shift should be significant for large values of B, $\hbar\omega_c > E_D^{IX}$, where $\hbar\omega_c$ is the cyclotron frequency, and $E_D^{IX} = 3.3$ meV is the IX binding energy[8]. Indeed, ΔE is seen to increase for $B > 2$ T, i.e. for $\hbar\omega_c > 3.5$ meV (Fig. 3).

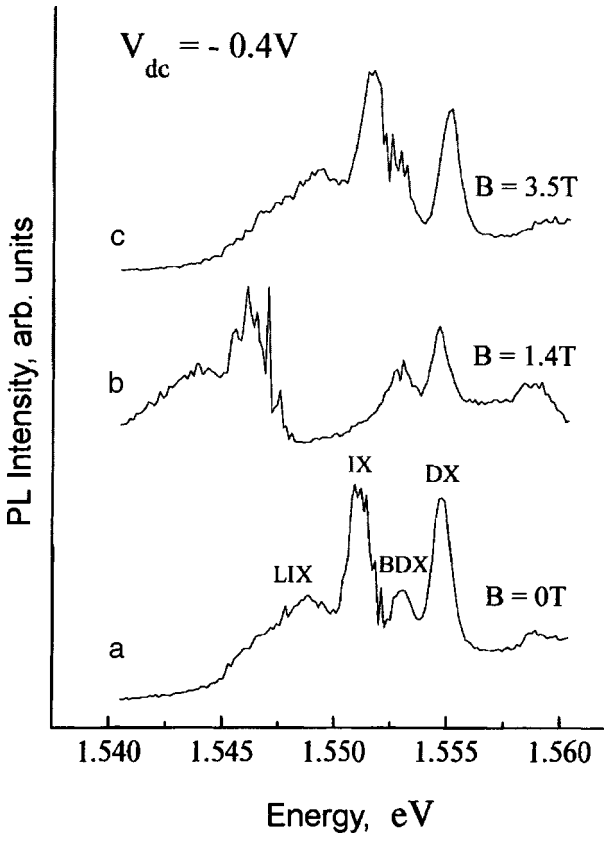

FIG. 2. PL spectra obtained at $V_{dc} = -0.4$ V and B(T): (a) 0, (b) 1.4, and (c) 3.5.

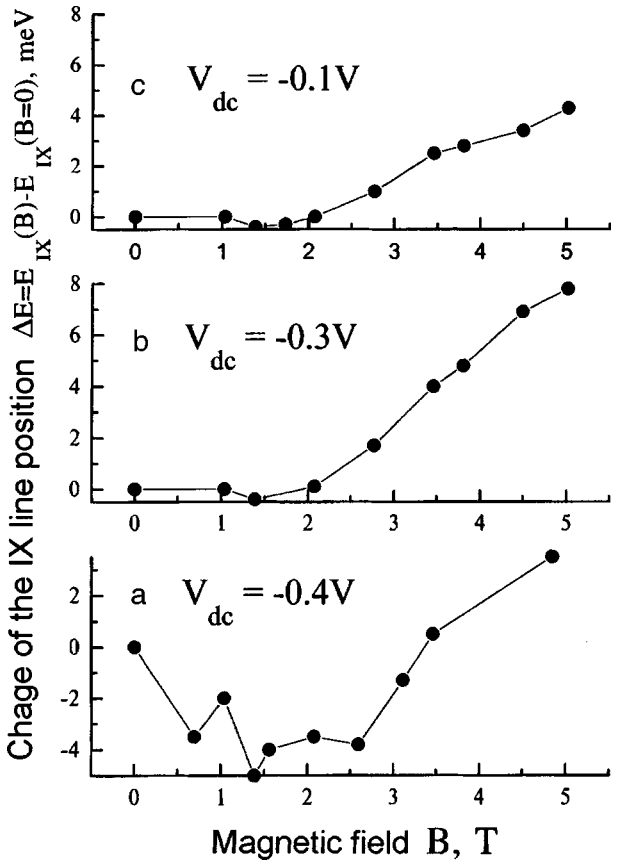

FIG. 3. ΔE-vs-B dependence for different V_{dc}(V): (a) -0.4, (b) -0.3, and (c) -0.1.

One may thus conclude that the shift of the indirect-exciton line IX is caused by two factors: (1) the shift toward higher energies is determined by diamagnetic shift, and (2) the shift to low energies is governed by the change of the electric field in the region of the double QW due to the blocking of J.

Factor (1) should operate for any V_{dc}, provided the condition $\hbar\omega_c > E_D^{IX}$ is met. At the same time factor (2) should manifest itself only in the case where a substantial current flows through the structure at $B = 0$, i.e., for $V_{dc} < V_0$. While the mechanism by which a magnetic field blocks the current remains unclear, experimental data suggest that a significant role is played here both by specific features in the behavior of the electron (exciton) subsystem in double QWs and the behavior of carriers in the AlGaAs layers separating the double QWs.

The experiments aimed at determining the magnetic-field dependence of the current under over-barrier ($\lambda = 632.8$ nm) and under-barrier ($\lambda = 730.3$ nm) excitation showed the character of the blocking to depend on whether electron-hole pairs are created by photoexcitation in the AlGaAs barriers or not. In this connection, one could suggest a mechanism of blocking by which carrier tunneling through the barrier (and, hence, the current) is affected strongly by carrier interaction (trapping, scattering) with impurities localized in the AlGaAs barriers. The efficiency of these processes depends on the in-plane extent of the charge wave functions, namely, the larger is the wave-function extent, the

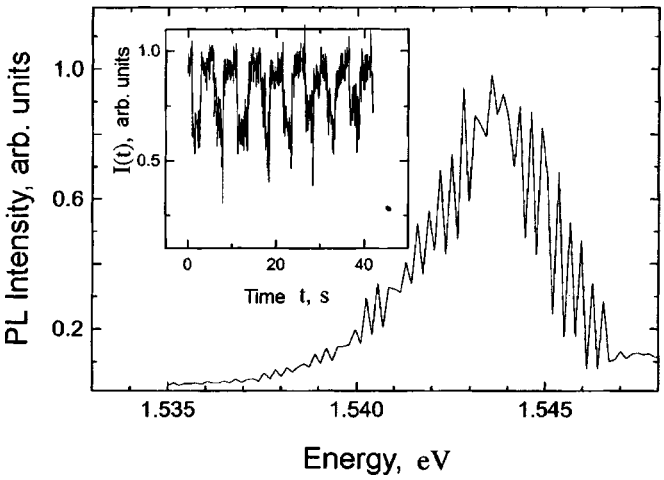

FIG. 4. Spectral profile of the IX line obtained at $V_{dc}=-0.5$ V and $B=2$ T. Inset: $I(t)$ relation measured at $h\nu=1.545$ eV.

higher is the efficiency of carrier trapping by the barrier impurity and the larger is the current. A magnetic field applied in the growth direction localizes carriers in the layer plane with the characteristic localization parameter equal to the magnetic length λ_B, which reduces the probability of carrier passage through the barrier and, hence, reduces the current.

An essential characteristic of the IX line lies in anomalously high fluctuations in the intensity of its spectral profile presented in Fig. 4. Considerable fluctuations in IX PL intensity observed earlier[4,5] in GaAs/AlAs double QWs were attributed to the presence of domains of condensed IX state.

We have measured the temporal variation of the intensity $I(t)$ of a fluctuation in the IX line profile. The $I(t)$ dependence for $h\nu=1.545$ eV is shown in the inset to Fig. 4. We see that $I(t)$ exhibits a distinct amplitude modulation with a period ≈ 5 s. Such a behavior is unusual for radiative characteristics of the electronic (excitonic) transitions in GaAs. It should be noted that the depth of the amplitude modulation does not depend on the width of the spectral interval chosen within the IX profile. There is also no correlation between PL intensity fluctuations in the IX line and fluctuations of the current through the structure. The reason for the onset of low-frequency oscillations and their relation to collective phenomena is unclear and requires further investigation. Note that this phenomenon can be used to develop microelectronic generators (switches) in the Terahertz range.

The authors express their gratitude to A. A. Kaplyanskiĭ, R. A. Suris, O. V. Konstantinov, and V. B. Timofeev for fruitful discussions, and to L. J. Challis for interest in the work.

Support of the Russian Fund for Fundamental Research (Grant 96-02-16952a) and, partially, INTAS (Grant 94-295) is gratefully acknowledged.

[1] Yu. E. Lozovik and V. I. Yudson, Zh. Éksp. Teor. Fiz. **71**, 738 (1976) [Sov. Phys. JETP **44**, 389 (1976)].
[2] I. V. Lerner and Yu. E. Lozovik, Zh. Éksp. Teor. Fiz. **80**, 1488 (1981) [Sov. Phys. JETP **53**, 763 (1981)].
[3] D. Yoshioka and A. H. MacDonald, J. Phys. Soc. Jpn. **59**, 4211 (1990).
[4] L. V. Butov, A. Zrenner, G. Abstreiter, G. Böhm, and G. Weimann, Phys. Rev. Lett. **73**, 304 (1994).
[5] L. V. Butov, A. Zrenner, M. Hagn, G. Abstreiter, G. Bohm, and G. Weimann, Phys. Usp. **166**, 801 (1996).
[6] V. B. Timofeev, A. V. Larionov, P. S. Dorozhkin, M. Bayer, and A. Forchel, JETP Lett. **65**, 877 (1997).
[7] E. S. Moskalenko, A. L. Zhmodikov, A. V. Akimov, A. A. Kaplyanskii, L. J. Challis, T. S. Cheng, and O. H. Hughes, Ann. der Physik **4**, 127 (1995).
[8] D. A. Masurenko, A. V. Akimov, E. S. Moskalenko, A. L. Zhmodikov, A. A. Kaplyanskii, L. J. Challis, T. S. Cheng, and C. T. Foxon, Acta Physica Polonica **90**, 895 (1995).
[9] M. Bayer, V. B. Timofeev, F. Faller, T. Gutbrod, and A. Forchel, Phys. Rev. B **54**, 8799 (1996).
[10] L. V. Butov, A. Zrenner, G. Abstreiter, A. V. Petinova, and K. Eberl, Phys. Rev. B **52**, 12153 (1995).

Translated by G. Skrebtsov

Magnetic excitons in near-surface quantum wells: experiment and theory

V. D. Kulakovskiĭ and L. V. Kulik

Institute of Solid State Physics, Russian Academy of Sciences, 142432 Chernogolovka, Moscow District, Russia

A. L. Yablonskiĭ, A. B. Dzyubenko, N. A. Gippius, and S. G. Tikhodeev

Institute of General Physics, Russian Academy of Sciences, 117942 Moscow, Russia

A. Forchel

University of Würzburg, Würzburg, Germany

Fiz. Tverd. Tela (St. Petersburg) **40**, 806–808 (May 1998)

We have measured the photoluminescence spectra and photoluminescence excitation spectra of magnetic excitons in InGaAs/GaAs near-surface quantum wells in a magnetic field. We have quantitatively investigated the effect of dielectric enhancement of excitons in quantum wells brought about by decreasing the thickness of the barrier layer, both in a magnetic field and without. © *1998 American Institute of Physics.* [S1063-7834(98)00705-9]

Excitons in semiconductor thin films, threads, and dots, surrounded by an insulator or vacuum, are significantly amplified thanks to a decrease in screening of the Coulomb potential in the medium surrounding the semiconductor, which has a lower dielectric constant ε.[1,2] From a formal point of view, this effect is described by allowing for an additional interaction of the electron and hole in the exciton with image charges. This effect, called dielectric enhancement, has been investigated theoretically for various types of structures.[3–5] A change in the binding energy was experimentally observed in semiconductor thin films (CdTe) on a dielectric substrate[6] and in superlattices based on lead iodide in an organic matrix;[7] however, a quantitative study of the effect has not been carried out due to the complex structure of the absorbers. More promising are quantum wells (QW) situated near the boundary with vacuum.[8,9] Such a structure is the simplest realization of a system in which, on the one hand, ε varies strongly in the immediate vicinity of the exciton and, on the other, the distance from the quantum well to the semiconductor–vacuum boundary can be varied in a controlled way.

In the present work we discuss the behavior of an exciton in a near-surface $I_{0.18}Ga_{0.82}As/GaAs$ quantum well with quantum-well thickness $L_{QW}=5$ nm in magnetic fields $B=0-14$ T. The structures were grown by molecular-beam epitaxy with thickness of the surface barrier layer $L_c=20$ nm. Photoluminescence spectra and photoluminescence excitation spectra of the excitons were first recorded for the grown samples. Then, using dry etching, the thickness of the barrier layer L_c was reduced to $10-3$ nm. To avoid forming defects, this was done using low-energy (500 eV) Ar^+ ions and a small angle between the ion beam and the surface of the sample (20°) at a low temperature (≈ 80 K). A tunable Ti-sapphire laser was used to excite photoluminescence.

Figure 1 displays photoluminescence and photoluminescence excitation spectra for a quantum well with $L_c=20$, 5, and 3 nm. Only one line is observed in the photoluminescence spectrum, corresponding to exciton recombination in

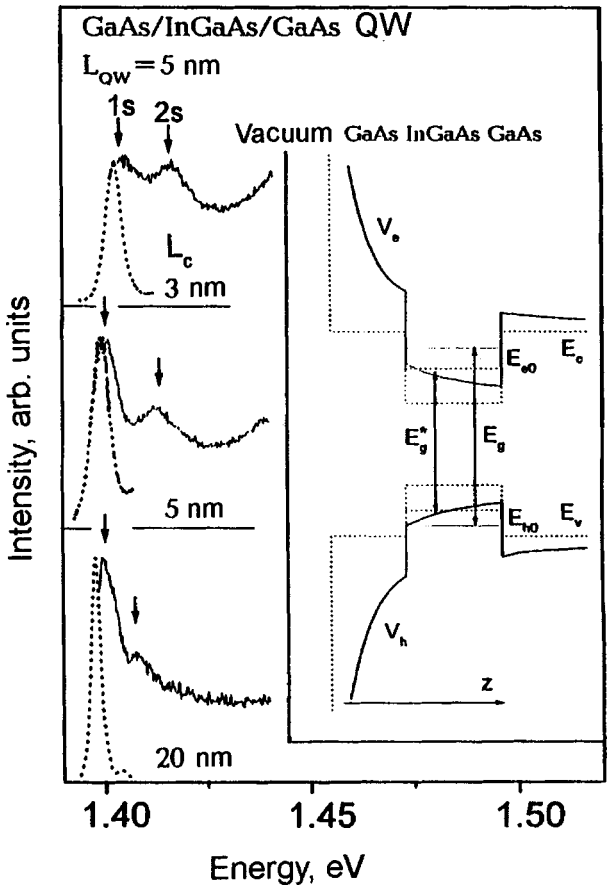

FIG. 1. Photoluminescence and photoluminescence excitation exciton spectra in InGaAs/GaAs near-surface quantum wells for $B=0$ and $L_c=3$, 5, and 20 nm. The inset shows the variation of the localizing potentials and the position of the single-particle levels in a near-surface quantum well with allowance for self-action (solid lines) and without (dashed lines).

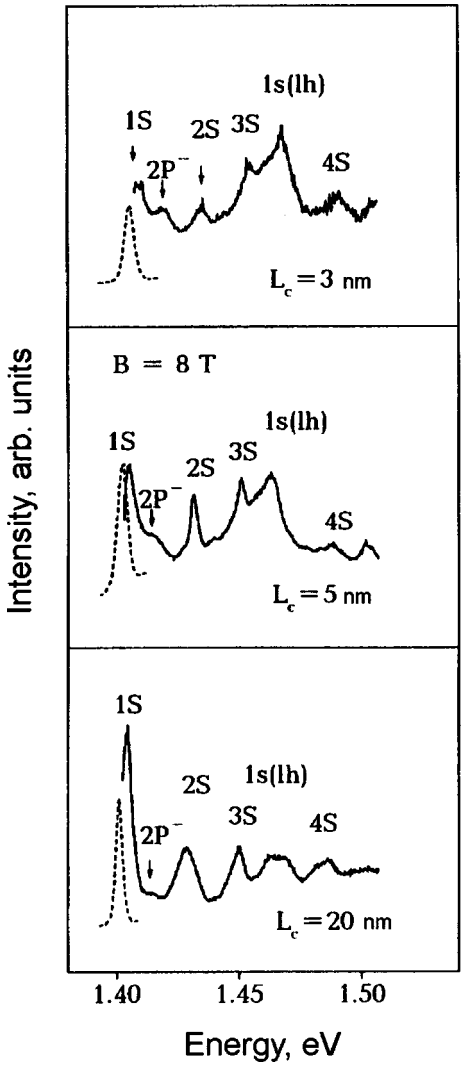

FIG. 2. Effect of a magnetic field on the photoluminescence and photoluminescence excitation exciton spectra in a InGaAs/GaAs near-surface quantum well.

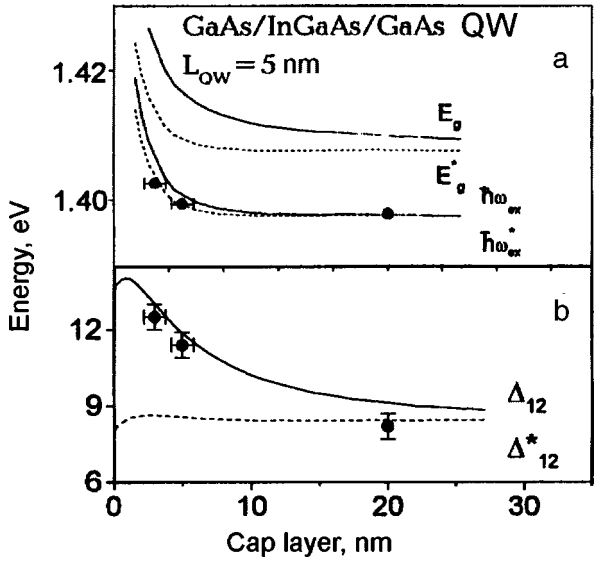

FIG. 3. Position of the bottom of the band and the $1s$ exciton transitions (a), exciton binding energy, and splitting between the $1s$ and $2s$ levels (b) in a InGaAs/GaAs near-surface quantum well as functions of thickness of the cap layer between the well and vacuum: theory with allowance for images (solid lines), without allowance for images (dashed lines), and experiment (points).

the ground ($1s$) state, while two lines are clearly visible in the photoluminescence excitation spectra, corresponding to transitions to the $1s$ and $2s$ states. The Stokes shift of the $1s$ line between the photoluminescence and photoluminescence excitation spectra is around 1.5 meV. The magnitude of the shift and the half-width of the $1s$ line vary only slightly with increase of L_c. As L_c is decreased, both lines are shifted toward higher energies, whereby the magnitude of the $2s$ line shift is substantially larger than that of the $1s$ line. Consequently, as the quantum well approaches the semiconductor–vacuum interface both the exciton transition energy $\hbar\omega_x$ and the exciton binding energy E_{1s} increase.

A magnetic field increases the energy gaps between the exciton states. As a result, additional spectrally resolved lines appear in the photoluminescence excitation spectrum (Fig. 2), corresponding to excitation of excitons in the ''ns'' states with $n=2$, 3, and 4. The energies of all these states grow with increase of L_c, where the magnitude of the effect for the $1s$ and $2s$ states is less than for $B=0$.

Variation of the exciton energies with variation of the barrier thickness is due to two factors: variation of the spatial localization of the exciton and variation of the dielectric constant. The first effect is due to the fact that as L_c is increased, the quantum well approaches the high potential barrier corresponding to the vacuum with a concomitant growth of the contribution to the exciton energies from carrier tunneling through the barrier. The abrupt decrease in ε at the surface also leads to an increase in the transition frequency as a consequence of repulsion of electrons and holes by their corresponding images. In addition, the extra attraction arising here of an electron (hole) to a hole (electron) image leads to a growth of the binding energies of the exciton states. Growth of E_1, partially compensates the dielectric blue shift of the interband transition frequencies as a consequence of the electrical neutrality of the exciton. Obviously, the total magnitude of the effect depends on the radius of the exciton in the quantum-well plane. A magnetic field leads to an additional compression of the exciton states in the quantum-well plane and, consequently, influences the magnitude of the dielectric enhancement of the exciton states.

For a quantitative description of the effect, it is necessary to include the image interaction potentials in the Hamiltonian

$$V_{\text{self}}(z)=\frac{e^2}{2\varepsilon}\left(\frac{\varepsilon-1}{\varepsilon+1}\right)\frac{1}{|2z|}, \tag{1}$$

$$U_{eh,im}(\rho,z_e,z_h)=-\frac{e^2}{\varepsilon}\left(\frac{\varepsilon-1}{\varepsilon+1}\right)\frac{1}{\sqrt{\rho^2+(z_e+z_h)^2}}, \tag{2}$$

which take into account repulsion of a charge by its image and enhancement of attraction between the electron and hole in the exciton due to attraction to the foreign image. The potential $V_{\text{self}}(z)$ leads to a modification of the potentials for the electrons and holes near the semiconductor–vacuum interface as shown in the inset in Fig. 1. The potential $U_{eh,im}$ is

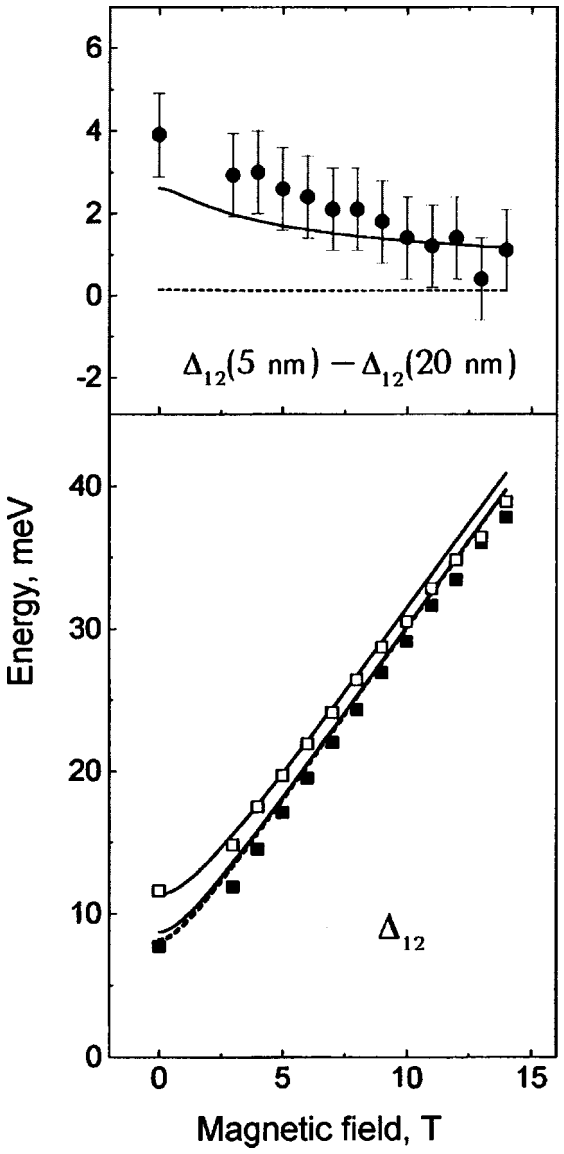

FIG. 4. Magnetic field dependence of the splitting between the $2s$ and $1s$ states [Δ_{12}) for $L_c=5$ nm (empty squares) and 20 nm (dark squares), and the difference $\Delta_{12}(5\ \text{nm})-\Delta_{12}(20\ \text{nm}]$; theory with allowance for images (upper solid curve—for $L_c=5$ nm, lower solid curve—20 nm) and theory without allowance for images (dashed curves).

responsible for dielectric enhancement of the exciton. The problem of finding the eigenfunctions and eigenenergies of the Hamiltonian is solved by numerical diagonalization of the potential matrix in the basis of non-interacting two-particle states of the Hamiltonian taking into account localizing potentials, self-action, and the magnetic field.

Figure 3 plots the dependence of E_g and $\hbar\omega_{1s}$ on L_c for $B=0$. The calculated values are larger for $L_c<8$ nm both as a consequence of the approach of the vacuum potential (dashed curves) and because of interaction with the image charges (difference between the solid and dashed curves). In the case of E_g their contributions are comparable, while the influence of dielectric confinement on the $\hbar\omega_{1s}$ shift is not large by virtue of the electrical neutrality of the excitons. The observed change in $\hbar\omega_{1s}$ (dots) is in qualitative agreement with the calculation; however, the accuracy of the experiment is insufficient to draw any conclusions about the role of dielectric enhancement. For this purpose, it is necessary to analyze the change in the gap between the $1s$ and $2s$ states, Δ_{12}, whose magnitude, as is clear from the calculated results plotted in Fig. 3(b), is hardly influenced by the asymmetry of the potential barrier at the semiconductor–vacuum interface. The dependence $\Delta_{12}(L_c)$ is due to the stronger influence of the image charges on the excited states due to the greater distance between the electron and hole. The experimental values of $\Delta_{12}(L_c)$ are in good agreement with calculation (Fig. 3(b)). The increase in Δ_{12} for $L_c=3$ nm is equal to 4 meV, which corresponds to an increase in E_x by roughly a factor of 1.5.

The effect of a magnetic field on the dielectric enhancement effect is illustrated by Fig. 4, which plots the dependence $\Delta_{12}(B)$ for $L_c=5$ and 20 nm, and also their difference $\Delta_{12}(5\ \text{nm})-\Delta_{12}(20\ \text{nm})$, which should not depend on the magnetic field if the effect of image charges is not taken into account (dashed curve in Fig. 4). The results of calculation of $\Delta_{12}(B)$ (solid curves) are in good agreement with experiment. The difference $\Delta_{12}(5\ \text{nm})-\Delta_{12}(20\ \text{nm})$ decreases with growth of B due to a strong contraction of the $2s$-exciton wave function and is adequately described by the given model. We emphasize that if the effect of the dielectric environment is not taken into account, this difference is equal to zero.

In conclusion, we would like to express our gratitude to Professor L. V. Keldysh and V. B. Timofeev for valuable discussions and T. B. Borzenko and Yu. I. Koval' for ion etching of the samples.

This work was supported by the programs ''Fundamental Spectroscopy'' and ''Atomic Surface Structure'' of the Ministry of Scientific and Technological Programs (experiment) and a grant from the Russian Fund for Fundamental Research (Grant No. 96-17600) (theory).

[1] N. S. Rytova, Dokl. Akad. Nauk SSSR **163**, 1118 (1965) [Sov. Phys. Dokl. **10**, 754 (1965)].
[2] L. V. Keldysh, JETP Lett. **29**, 658 (1979).
[3] D. B. Tran Thoai, R. Zimmermann, M. Grundmann, and D. Bimberg, Phys. Rev. B **42**, 5906 (1990).
[4] E. A. Andryushin and A. P. Silin, Fiz. Tverd. Tela **35**, 1947 (1993) [Phys. Solid State **35**, 971 (1993)].
[5] E. A. Muljarov, S. G. Tikhodeev, N. A. Gippius, and T. Ishihara, Phys. Rev. B **51**, 14370 (1995).
[6] N. A. Babaev, V. C. Babaev, F. V. Garin, A. V. Kochemasov, L. V. Paramonov, N. N. Salashchenko, and V. B. Stopachinskiĭ, JETP Lett. **40**, 92 (1984).
[7] T. Ishihara, J. Lumin. **60&61**, 269 (1994).
[8] L. V. Kulik, V. D. Kulakovskii, M. Bayer, A. Forchel, N. A. Gippius, and S. G. Tikhodeev, Phys. Rev. B **54**, R2335 (1996).
[9] A. L. Yablonskiĭ, A. B. Dzyubenko, S. G. Tikhodeev, L. V. Kulik, and V. D. Kulakovskiĭ, JETP Lett. **64**, 51 (1996).

Translated by Paul F. Schippnick

Exciton dynamics in ZnCdSe/ZnSe quantum-well structures

S. A. Permogorov, A. N. Reznitskiĭ, L. N. Tenishev, A. V. Kornievskiĭ, S. Yu. Verbin, S. V. Ivanov, and S. V. Sorokin

A. F. Ioffe Physicotechnical Institute, Russian Academy of Sciences, 194021 St. Petersburg, Russia

W. von der Osten, H. Stolz, and M. Jütte

Universität GH Paderborn, 33095 Paderborn, Germany

Fiz. Tverd. Tela (St. Petersburg) **40**, 809–810 (May 1998)

Exciton dynamics in ZnCdSe/ZnSe quantum-well structures have been studied from luminescence spectra obtained at $T=2$ K. The energy and phase relaxation times of localized exciton states have been determined from a study of the destruction of exciton optical alignment by an external magnetic field and direct measurements of the polarized-radiation decay kinetics in the picosecond range. The exciton polarization lifetimes measured by two independent techniques are found to be in a good agreement. © *1998 American Institute of Physics.* [S1063-7834(98)00805-3]

The samples studied by us were MBE grown on GaAs substrates as laser structures and represented a set of $Zn_{1-x}Cd_xSe$ quantum wells ($x=0.2$, 7-nm thickness), separated by 6-nm thick ZnSe barriers and sandwiched between thick n and p ZnSe layers.

At helium temperatures, the luminescence spectrum of the ZnCdSe quantum wells consists of one comparatively broad band. This band was shown earlier[1,2] to be a superposition of two overlapping emission bands of different origin (Fig. 1). The shorter wavelength band (LE) is due to radiation of excitons localized at well-thickness or composition fluctuations, whereas the band at lower energies originates from exciton complexes including a defect, presumably of donor type (BE). Both bands are inhomogeneously broadened.

The luminescence produced in the region of the LE band under resonant excitation with linearly polarized light exhibits significant linear polarization $P_{\text{lin}}=(I_{\parallel}-I_{\perp})/(I_{\parallel}+I_{\perp})$. The luminescence spectrum in Fig. 1 was obtained with Ar^+ laser excitation (476.5 nm). The resonant excitation of luminescence is produced in this case as a result of absorption involving emission of one LO phonon. The energy of the excitons excited in this process is 2570 meV and corresponds to the short-wavelength emission-band edge. The spectral dependence of the degree of linear polarization is shown in Fig. 1 by filled circles.

The linear polarization of the radiation results here from optical alignment of the exciton dipole moments under direct excitation while the spectral dependence of the degree of polarization reflects the gradual destruction of this alignment as excitons relax in energy within the inhomogeneously broadened spectrum of localized states by emitting phonons. In accordance with theoretical predictions[3], no optical alignment is observed within the exciton-complex band BE.

Application of an external magnetic field in Faraday geometry results in a decrease in the degree of luminescence linear polarization (Fig. 2), with the P_{lin}-vs-field relation being described by a Lorentzian

$$P_{\text{lin}}=P_0\frac{1}{1+(B/B_{1/2})^2},$$

where

$$B_{1/2}=\frac{h}{g_{ex}\mu T_d}.$$

Here B is the magnetic field strength, μ is the Bohr magneton, h is the Planck constant, $g_{\text{ex}}=3g_h-g_e$ is the exciton g

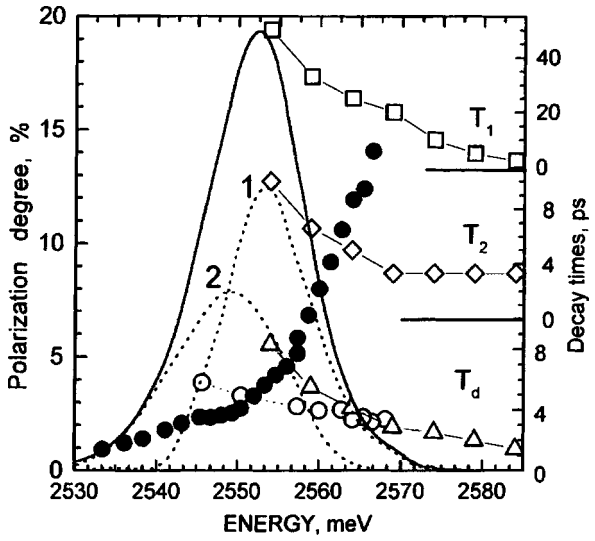

FIG. 1. Exciton luminescence spectrum of ZnCdSe/ZnSe quantum wells obtained at $T=2$ K (solid line) and its deconvolution[1,2] into radiation bands of (*1*) localized and (*2*) bound excitons (dashed lines). Filled circles — spectral dependence of the degree of linear polarization P_{lin} under laser excitation at 476.5 nm. The three right-hand scales relate to total exciton lifetime T_1 (squares), phase relaxation time T_2 (rhombs), and exciton polarization lifetime T_d (triangles). Open circles refer to magneto-optical measurements of T_d.

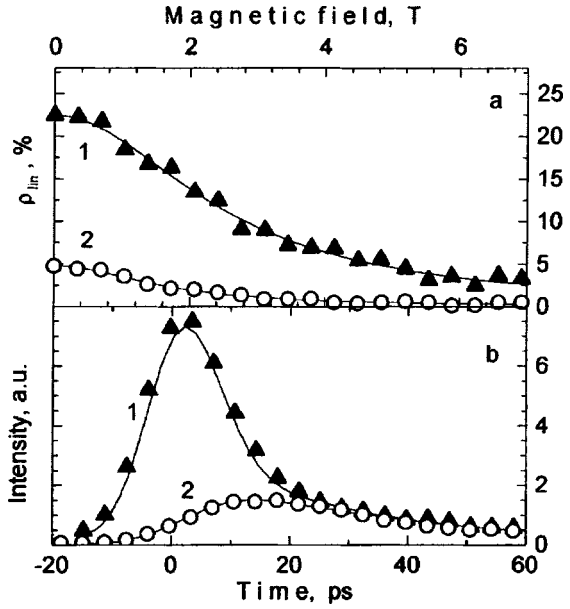

FIG. 2. (a) Degree of linear polarization P_{lin} under excitation conditions used to obtain data in Fig. 1 as a function of external magnetic field, measured at (*1*) 2568 meV and (*2*) 2557 meV. (b) Radiation kinetics under resonant excitation of quantum-well luminescence at 2559 meV measured in polarization (*1*) parallel and (*2*) perpendicular to that of the pump light. Solid curves in panels *a* and *b* are predictions based on theoretical models.

factor, and T_d is the exciton polarization lifetime, which is determined by both the lifetime of the exciton state and carrier spin-relaxation processes in the exciton.

We used the value of the g factor for localized exciton states $g_{\text{ex}}=1.68$ obtained earlier[2] for the same samples from a theoretical analysis of the dependence of the magneto-circular polarization on magnetic field to derive the lifetime of the exciton polarization and its spectral behavior. The results are shown by open circles in the bottom part of Fig. 1.

We readily see that the polarization lifetimes of localized exciton states at the short-wavelength edge of the emission band are of the order of 3 ps. This value is in a good qualitative agreement with observations of a clearly pronounced structure with a period of the LO phonon energy in luminescence excitation spectra of this partof the band[1], a result of the short exciton lifetime restricted by migration of energy to deeper localized states. Only on insignificant increase of T_d is observed, however, with increasing localization energy. This suggests that energy migration is not the only factor affecting the polarization lifetime.

This conjecture received support from direct measurements of the radiation decay kinetics under excitation by a pulsed picosecond-range tunable laser (pulse duration 4 ps at a repetition frequency of 79 MHz). The measurements were performed in polarized light directly at the pump frequency. Shown in the bottom of Fig. 2 are typical results obtained in a study of the radiation kinetics for two polarizations. Using the model proposed in Ref. 4 permits one in this case to extract from the experimental data independently both the total exciton lifetime T_1, which is determined by radiative recombination and energy migration, and the phase relaxation time T_2 dominated by spin relaxation processes in the localized exciton. The spectral dependence of the times T_1 and T_2 obtained in the experiment is displayed in the right-hand part of Fig. 1. Independent determination of T_1 and T_2 provides also a possibility for calculating the total polarization lifetime T_d from $1/T_d=1/T_1+1/T_2$. The values of T_d derived from measured radiation decay kinetics are shown in the lower part of Fig. 1 with triangles.

As evident from Fig. 1, the exciton polarization lifetimes determined by two independent methods agree well with one another in the part of the spectrum where radiation of localized excitons is predominant. A comparison of the spectral behavior of T_1, T_2, and T_d shows that, at the short-wavelength edge of the luminescence band, the T_d times are dominated by the fast energy relaxation of localized excitons. As the localization energy increases, however, the energy relaxation processes slow down, which becomes reflected in a substantial increase of T_1. In these conditions, T_d is increasingly dominated by phase relaxation processes. The phase relaxation time T_2 also grows with localization energy. This may be due to reduced random anisotropy among the localized exciton states.

In the energy region where localized and bound excitons produce comparable radiation intensity, the values of T_d obtained by two different methods disagree. This discrepancy may be caused by the g factor being dependent on exciton localization energy. Besides, the two methods differ in the way used to excite excitons, and therefore the results obtained may correspond to different ensembles of localized states.

Partial support of Russian Fund for Fundamental Research (Grants 96-02-16933 and 97-02-18138) and INTAS (Grant 94-324) is gratefully acknowledged.

[1] S. Permogorov, A. Reznitsky, L. Tenishev, A. Kornievsky, S. Ivanov, S. Sorokin, W. von der Osten, H. Stolz, M. Jütte, and H. Vogelsang, in *Proceedings of the 23rd International Conference ''Physics of Semiconductors''* (Berlin, 1996), p. 2015–2018.
[2] A. Reznitsky, A. Kornievsky, S. Permogorov, L. Tenishev, S. Verbin, S. Ivanov, and S. Sorokin, J. Lumin. **72–74**, 869 (1997).
[3] G. E. Pikus and E. L. Ivchenko, in *Excitons*, edited by E. I. Rashba and M. D. Sturge, *Modern Problems in Condensed Matter Sciences* (North-Holland, Amsterdam, 1982), Vol. 2, Ch. 6, p. 869; Nauka, Moscow, 1985.
[4] H. Stolz, *Time-Resolved Light Scattering from Excitons*, Springer Tracts in Modern Physics, Vol. 130 (Springer, Berlin, 1994).

Translated by G. Skrebtsov

Optical studies of ZnSe/ZnMgSSe-based quantum-well semiconductor heterostructures

A. V. Platonov and V. P. Kochereshko

A. F. Ioffe Physicotechnical Institute, Russian Academy of Sciences, 194021 St. Petersburg, Russia

D. R. Yakovlev

A. F. Ioffe Physicotechnical Institute, Russian Academy of Sciences, 194021 St. Petersburg, Russia; Physicalisches Institut der Universität Würzburg, 97074 Würzburg, Germany

U. Zehnder, W. Ossau, W. Faschinger, and G. Landwehr

Physicalisches Institut der Universität Würzburg, 97074 Würzburg, Germany

Fiz. Tverd. Tela (St. Petersburg) **40**, 811–812 (May 1998)

Results of an optical study of heterostructures based on new compounds, ZnSe/ZnMgSSe, are presented. The possibility of using these compounds to produce high-quality quantum-well structures having strong exciton features in optical spectra is demonstrated. An analysis of reflectance spectra has yielded the exciton parameters: the resonant frequency, oscillator strength, and exciton line damping. The exciton binding energies have been determined from magneto-optical spectra. The samples studied have a high structural perfection and small inhomogeneous width of the excitonic resonances. © *1998 American Institute of Physics.* [S1063-7834(98)00905-8]

The quaternary compounds ZnSeZnMgSSe are promising materials for semiconductor quantum-well optical devices operating in the blue-green spectral region.[1] This is due to the possibility of developing structurally perfect samples which would be lattice matched to GaAs substrate and have a broad gap-width range. The above advantages, as well as the large exciton binding energy (20 meV in ZnSe), make this class of structures potentially interesting also for exciton spectroscopy by permitting detailed investigation of such fine excitonic effects as exciton-polariton quantization,[2] exciton-electron interaction,[3] and so on. This work reports on a measurement of excitonic parameters in ZnSe quantum wells (QW) with ZnMgSSe barriers, which have a low S and Mg concentration.

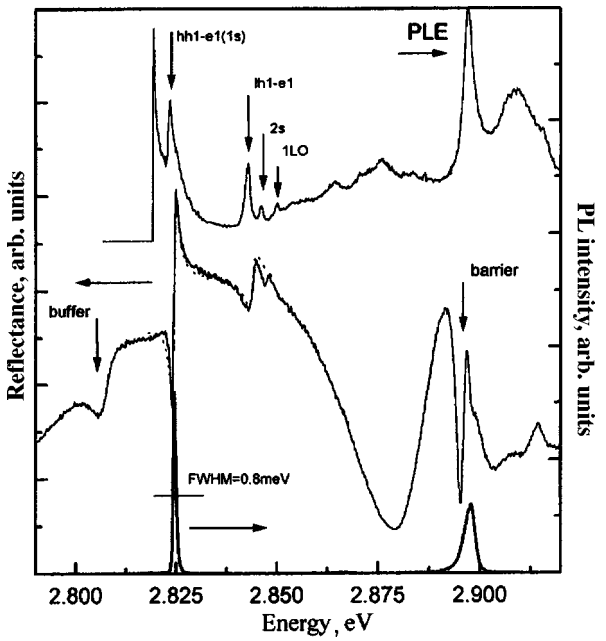

FIG. 1. Reflectance, photoluminescence, and photoluminescence excitation spectra from a 45-Å thick $ZnSe/Zn_{0.95}Mg_{0.05}S_{0.09}Se_{0.91}$ quantum well obtained at 1.6 K. Dotted line — calculated reflectance spectrum in the exciton resonance region.

The samples to be studied were grown by a molecular-beam epitaxy on a (100)GaAs substrate. To improve the interface quality, the II–VI structure was grown on a 200-nm thick GaAs buffer overlaid by a ~10 monolayer-thick ZnSe film. We studied two samples: (1) 45-Å thick ZnSe/$Zn_{0.95}Mg_{0.05}S_{0.09}Se_{0.91}$ quantum well with barrier thickness of 3000 Å, and (2) 20-Å thick $ZnSe/Zn_{0.95}Mg_{0.05}S_{0.1}Se_{0.9}$ quantum well with barrier thickness of 4500 Å.

Photoluminescence (PL) and photoluminescence-excitation (PLE) spectra were obtained with an Ar ion laser operating in the UV range, and a dye (Stilben-3) laser.

Figure 1 plots reflectance, PL, and PLE spectra obtained at 1.6 K from the 45-Å thick QW. The reflectance spectrum exhibits clearly two features due to excitons in the ZnSe buffer and the barrier, as well as three resonances originating from excitons in the QW. These resonances were identified by us as due to the $e1-hh1(1s)$, $e1-lh1(1s)$, and $e1-hh1(2s)$ excitonic transitions, respectively. Note the small

TABLE I. Exciton parameters of ZnMgSSe quantum-well structures.

QW width, Å	Exciton type	$\hbar\omega_0$, eV	$\hbar\Gamma_0$, meV	$\hbar\Gamma$, meV
45	$e1-hh1$	2.825	0.18	0.8
45	$e1-lhl$	2.844	0.08	1.8
20	$e1-hh1$	2.852	0.19	2.2

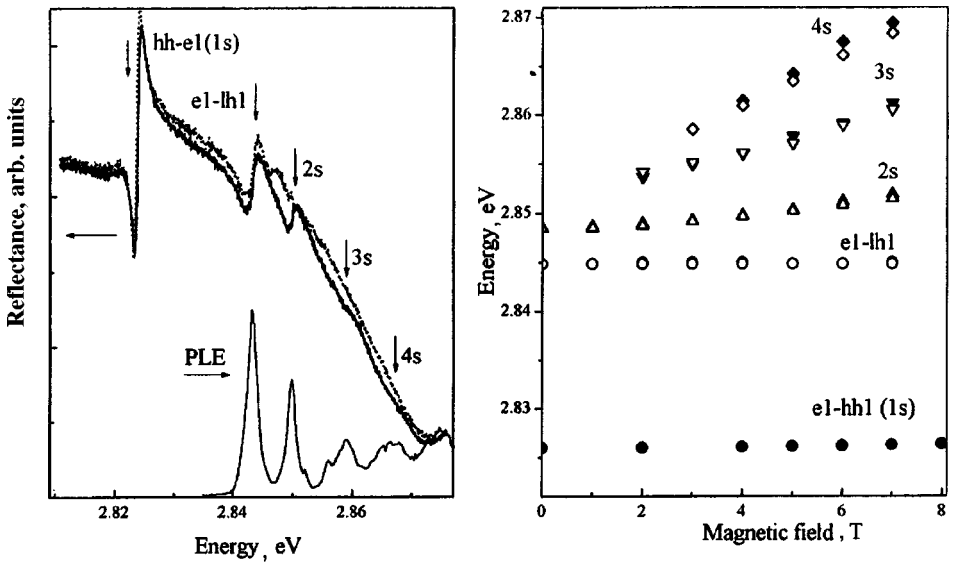

FIG. 2. (a) Reflectance and PL excitation spectra from a 45-Å thick ZnSe/ZnMgSSe quantum well obtained at 1.6 K in a magnetic field of 7 T. Dotted line: reflectance spectrum for zero field. (b) Energies of excitonic transitions in the QW vs magnetic field. Open symbols relate to σ^+ polarization, and filled ones, to σ^- polarization.

inhomogeneous broadening of the excitonic resonances and the absence of the Stokes shift of the PL line relative to the resonance in the reflectance spectrum. For example, the PL line width for the heavy-hole exciton is 0.8 meV, which is a record-low figure for this system at present. Note also the reflectance spectrum in the barrier-exciton region, whose shape corresponds not to a single excitonic resonance but rather to the excitonic polariton in a thin film[2]. The existence of the excitonic polariton is not only derived from the numerical treatment of the reflectance spectrum but follows also from the anti-Stokes shift of the PL line maximum relative to the absorption maximum by the energy equal to the exciton oscillator strength in bulk ZnMgSSe (Ref. 2). The observed width of the exciton PL line includes the inhomogeneous part due to structural imperfections of the sample. The excitonic polariton is also sensitive to inhomogeneous broadening and disappears completely from optical spectra at a certain critical exciton damping for this structure (about 1 meV). The above permits a conclusion of a truly high structural perfection in the sample studied.

Mathematical analysis of the reflectance spectra[4] yielded the excitonic parameters: resonant frequency ω_0, radiative width Γ_0, and exciton damping Γ. The values of the above quantities obtained for the light- and heavy-hole exciton in the 45-Å QW and for the heavy-hole exciton in the 20-Å QW are listed in Table I. The reflectance spectrum in the exciton-resonance region calculated for the 45-Å QW is shown in Fig. 1 by a dotted line.

The 45-Å QW was used in a study of magnetoreflectance and PLE spectra in magnetic fields of up to 8 T, which revealed a strongly pronounced magnetoexciton structure. The spectra obtained at 7 T are shown in Fig. 2a. The spectra exhibit a series of magnetoexciton resonances. Figure 2b displays the magnetic-field dependence of the energies of all observed transitions. Mathematical analysis of these spectra yielded the exciton diamagnetic-shift constant δ_{diam} and the exciton binding energy R.[5] For the ground state, these quantities are $\delta_{\text{diam}}=3.43\ \mu\text{V/T}^2$ and $R=28$. This value of the binding energy is in accord with the observed energy difference between the $1s$ and $2s$ states, which is 23 meV in zero field.

Thus we have performed optical characterization of ZnSe/ZnMgSSe-based QW structures with well thicknesses of 45 and 20 Å. A high perfection of the structures studied has been demonstrated. Radiative and nonradiative damping rates, as well as the binding energy of the exciton have been determined.

Partial support of Deutsche Forschungsgemeinschaft (SFB410), Volkswagen-Stiftung, and Russian Fund for Fundamental Research (Grant 95-02-04061a) is gratefully acknowledged.

*Permanent address: A. F. Ioffe Physicotechnical Institute, Russian Academy of Sciences, 194021 St. Petersburg, Russia.

[1] H. Okuyama, K. Nakano, T. Miyajima, and K. Akimoto, Jpn. J. Appl. Phys. **30**, L1620 (1991).
[2] *Excitons*, edited by E. I. Rashba and M. D. Sturge, *Modern Problems in Condensed Matter Sciences* (North-Holland, Amsterdam, 1982), Vol. 2; Nauka, Moscow, 1985.
[3] K. Kheng, R. T. Cox, V. P. Kochereshko, K. Seminadayar, S. Tatarenko, F. Bassani, and A. Franciosi, Superlattices Microstruct. **15**, 253 (1994).
[4] E. L. Ivchenko, P. S. Kop'ev, V. P. Kochereshko, I. N. Ural'tsev, D. R. Yakovlev, S. V. Ivanov, B. Ya. Mel'tser, and M. A. Kalitievskiĭ, Fiz. Tekh. Poluprovodn. **22**, 784 (1988) [Sov. Phys. Semicond. **22**, 495 (1988)]; E. L. Ivchenko and G. E. Pikus, *Superlattices and Other Heterostructures. Symmetry and Optical Phenomena*, Springer Series in *Solid-State Sciences* (Springer, Berlin, 1995), Vol. 110.
[5] J. Puls, V. V. Rossin, F. Henneberger, and R. Zimmermann, Phys. Rev. B **54**, 4974 (1996).

Translated by G. Skrebtsov

Trions in quantum-well structures with two-dimensional electron gas

D. B. Turchinovich and V. P. Kochereshko

A. F. Ioffe Physicotechnical Institute, Russian Academy of Sciences, 194021 St. Petersburg, Russia

D. R. Yakovlev

A. F. Ioffe Physicotechnical Institute, Russian Academy of Sciences, 194021 St. Petersburg, Russia; Physikalisches Institut der Universität Würzburg, 97074 Würzburg, Germany

W. Ossau and G. Landwehr

Physikalisches Institut der Universität Würzburg, 97074 Würzburg, Germany

T. Wojtowicz, G. Karczewski, and J. Kossut

Institute of Physics, Polish Academy of Sciences, PL02608 Warsaw, Poland

Fiz. Tverd. Tela (St. Petersburg) **40**, 813–815 (May 1998)

A study has been made of bound exciton–electron complexes (trions) and unbound exciton–electron states (combined exciton–cyclotron resonance) from reflectance spectra obtained from modulation-doped CdTe/CdMgTe quantum-well structures. It has been established that the contribution of trions to dielectric permittivity is comparable to that of excitons. An analysis is made of the magnetic-field dependence of the parameters describing the contribution to dielectric permittivity due to exciton-cyclotron-resonance states. © *1998 American Institute of Physics.* [S1063-7834(98)01005-3]

The exciton–electron interaction processes have been considered to be sufficiently well studied until recently. Their analysis reduced to two main mechanisms: (1) destruction by free electrons of the exciton states through k-space filling and screening of the electron–hole Coulomb interaction in the exciton, and (2) enhancement of exciton damping due to exciton–electron scattering. Both these mechanisms lead to destruction of exciton states and suppression of exciton lines in optical spectra. It has recently been found that in the case of a low free-electron density in semiconductor quantum wells (QW) exciton-electron interaction results in the formation of a bound exciton-electron complex (trion).[1,2] Such trion states were observed to exist in II–VI and III–V semiconductor QWs.[2,3] Unbound resonant exciton–electron states, i.e. the exciton cyclotronresonance (ExCR), were detected in the presence of a magnetic field.[4] This work deals with a study of reflectance spectra from modulation-doped $CdTe/Cd_{0.7}Mg_{0.3}Te$ QW structures containing a low-density two-dimensional electron gas.

We studied $CdTe/Cd_{0.7}Mg_{0.3}Te$ heterostructures grown by molecular-beam epitaxy on (100)-oriented GaAs substrates. Structures with a single 80-Å thick CdTe QW were δ doped with iodine at a distance of 100 Å from the QW. The electron density in the QW was 10^9 cm^{-2} in an undoped structure and was as high as 10^{11} cm^{-2} in a doped one.

In the absence of a magnetic field, the reflectance spectra of undoped QW structures contained only one free-exciton line (X) whereas modulation-doped structures exhibit two lines, namely, X, which corresponds to the free exciton, and X^-, due to the trion (Fig. 1). The trion reflectance line is shifted toward long wavelengths by $\sim$3 meV relative to the exciton line. The amplitude of the X^- line grows with electron density in the QW, while that of the exciton line, decreases. In the modulation-doped structure the exciton line is substantially broadened as a result of exciton–electron scattering and screening by free carriers. For high doping levels, the exciton line is not observed at all, and the spectrum is dominated by the X^- line. This implies that the trion state provides the major contribution to the dielectric permittivity of doped QWs.

No changes were observed in the reflectance spectra of the undoped structure as the magnetic field was increased. Fig. 1a and 1b shows reflectance spectra of the modulation-doped quantum-well structure in magnetic fields from zero to 7.5 T obtained in two circular polarizations, σ^+ and σ^-. The σ^+ spectrum exhibits three reflectance lines corresponding, respectively, to the exciton (X), trion (X^-), and exciton–cyclotron resonances (ExCR). Viewed in this polarization, the amplitude of the trion reflectance line falls off with increasing magnetic field to disappear altogether at 4.5 T, whereas that of the exciton line grows. The σ^- spectrum exhibits only the X and X^- lines, and the amplitudes of both resonances increase slightly with magnetic field. The maximum of the ExCR line shifts linearly with increasing magnetic field toward higher energy with a slope close to the electron cyclotron energy. Approximation of this line to zero magnetic field yields the exciton resonance energy. The origin of this exciton–cyclotron resonance line is assigned to the following process: the incident photon creates an exciton with asimultaneous transition of the additional electron between the Landau levels.[4]

All the observed transitions are strongly polarized in a

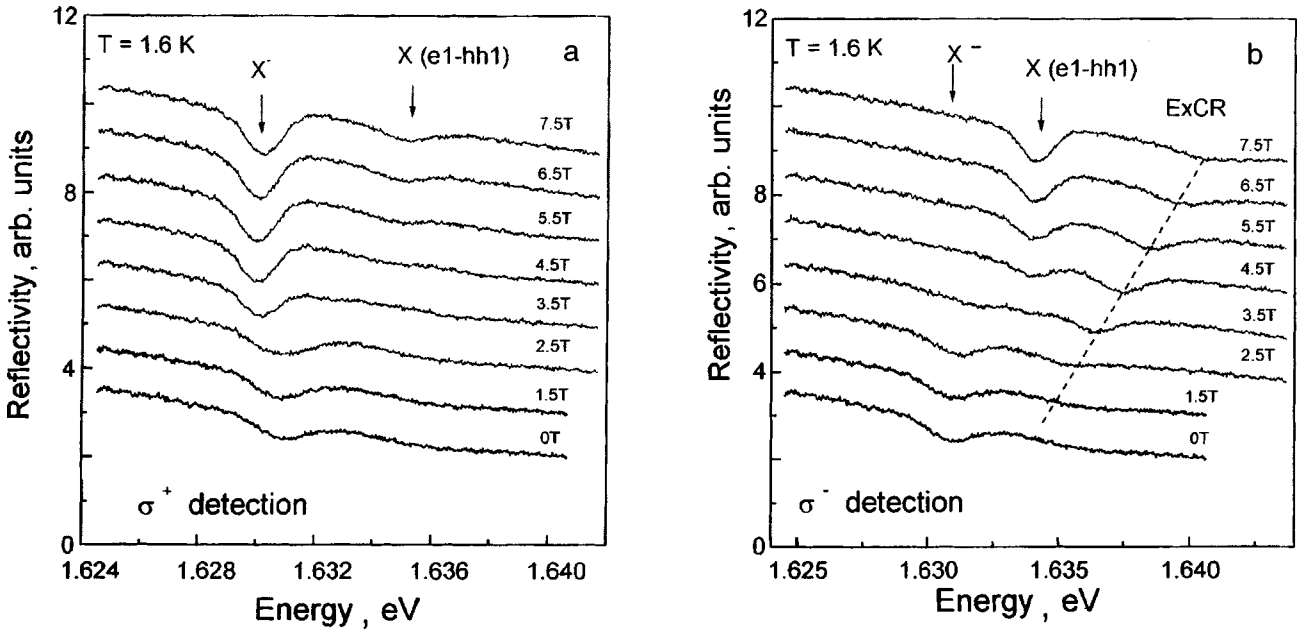

FIG. 1. Reflectance spectra from modulation-doped $CdTe/Cd_{0.7}Mg_{0.3}Te$ structures with 80-Å thick quantum wells containing two-dimensional electron gas with density 10^{11} cm^{-2}, obtained in a magnetic field. (a) Right-handed circular polarization σ^+, (b) left-handed circular polarization σ^-.

magnetic field. The polarization of the trion reflectance line is the result of the trion ground state being a singlet.[1] In a sufficiently strong magnetic field, and at temperatures low enough for all electrons to fall to the lowest Zeeman sublevel, only excitons with a certain angular momentum can form a bound trion state. Indeed, in a strong magnetic field, i.e. when all electrons in the 2D electron gas are oriented along the field, only excitons in which the electron spin is antiparallel to the external field can be excited. The polarization of the exciton reflectance line is opposite to that of the trion.[5] This polarization originates from the exciton damping rates in σ^+ and σ^- polarizations being different. One of the reasons for this lies in that exciton damping in σ^- polarization can increase because binding to form a trion provides a fast relaxation channel for the exciton. The second reason for this exciton polarization may consist in that exciton damping becomes spin dependent in the presence of a magnetic field due to the exchange contribution to exciton–electron scattering. It should be pointed out that, in undoped structures, the exciton reflectance line in a magnetic field is not polarized. The polarization of the ExCR line has the same sign as that of the exciton and is directly related to it.

Figure 2 shows the positions of the exciton, trion, and ExCR reflectance lines as functions of magnetic field. The exciton and trion reflectance lines exhibit a quadratic diamagnetic shift with increasing magnetic field. The ExCR line shifts linearly with increasing magnetic field to shorter wavelengths by an amount close to the electron cyclotron energy with a slope $\propto 1.03$ meV/T.

The observed reflectance spectrum is described by the QW polarizability $\chi_{\alpha\beta}$ (see Ref. 6 for details of the theory proposed by Suris), which can be written in the following form taking into account ExCR:

$$\chi_{\alpha\beta} = \pi (d_\alpha)^* d_\beta |\varphi(0)|^2 \frac{1}{\hbar\omega - E_{\rm ex}(0) - i\Gamma^{\rm exc}} + n_e \left| \int d^2 r \varphi(r) \right|^2 (d_\alpha)^* d_\beta \times \int \frac{d^2 Q}{4\pi} \exp(-Q^2 L_H^2/2) \sum_{n=1}^{\infty} \frac{1}{n!} \left(\frac{Q^2 L_H^2}{2} \right) \times \frac{1}{\hbar\omega - E_{\rm ex}(Q) - n\hbar\omega_{c,e} - i\Gamma^{\rm exc}}, \quad (1)$$

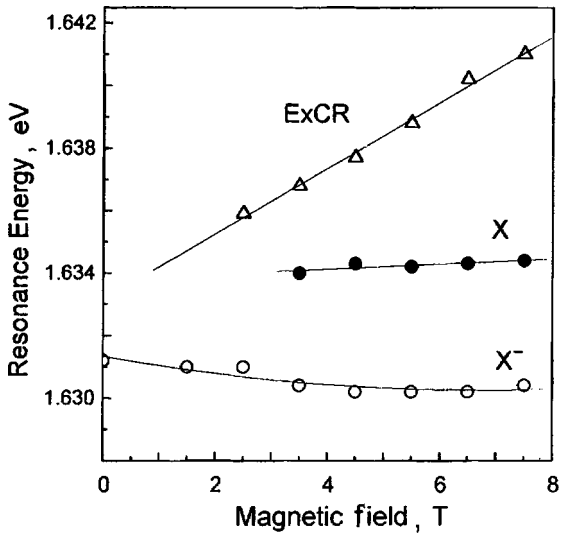

FIG. 2. Magnetic-field dependence of positions of the exciton X, trion X^-, and exciton–cyclotron resonance ExCR lines derived from the spectra of Fig. 1.

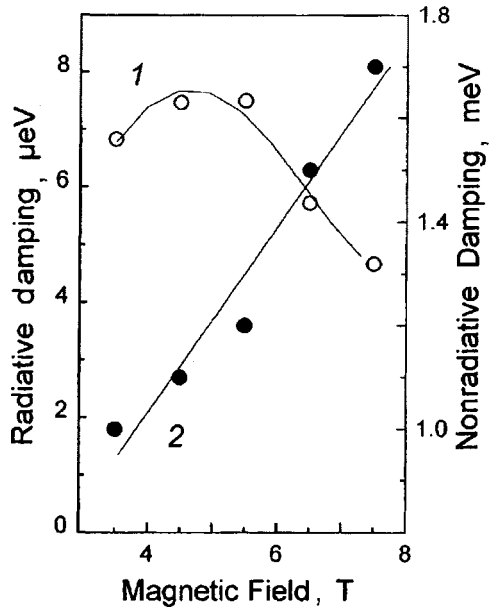

FIG. 3. Magnetic-field dependence of effective parameters (*1*) Γ_0^{ExCR} and (*2*) Γ^{ExCR} for the ExCR line derived from the spectra of Fig. 1.

where $d_{\alpha(\beta)}$ is the interband dipole matrix element of the optical transition, $\varphi(r)$ is the exciton envelope function, E_{ex} and Γ^{exc} are the exciton energy and damping rate, respectively, Q is the in-plane exciton wave vector, L_H is the magnetic length, $\hbar\omega_{c,e}$ is the electron cyclotron energy, and n_e is the two-dimensional electron-gas density.

The first term in Eq. (1) describes the contribution of exciton transitions to the polarizability. The second term, which is proportional to electron density, is the contribution of the exciton and electron resonant states, ExCR. As seen from Eq. (1), the exciton reflectance linewidth is dominated by the damping parameter Γ^{exc}. The term describing ExCR also contains parameter Γ^{exc} [the second term in Eq. (1)]. This is what may account for the polarization of the ExCR reflectance line.

As evident from Eq. (1), the exciton contribution to the reflectance spectrum is described by a Lorentzian. At the same time the ExCR contribution is described by a convolution of a Lorentzian and a Gaussian. It can be shown that this integral is also a Lorentzian with effective parameters: radiative damping Γ_0^{ExCR}, nonradiative damping Γ^{ExCR}, and resonant frequency $\hbar\omega_0^{\mathrm{ExCR}}=\hbar\omega_{c,e}(1+m_e/m_e+m_{hh})$, where m_e and m_{hh} are the electron and hole effective masses, respectively.

To determine these parameters, we fitted the reflectance spectra using the approach[7] describing exciton reflectance in QWs.

The ExCR reflectance linewidth is dominated by effective damping Γ^{ExCR}, which is proportional to magnetic field (1). For magnetic fields large enough that Γ^{ExCR} exceeds the inhomogeneous width of the ExCR line, its width grows linearly with magnetic field (Fig. 3). Note that the exciton reflectance linewidth decreases with increasing magnetic field.

Figure 3 presents also the magnetic-field dependence of the ExCR line amplitude, which is dominated by the effective radiative damping $\hbar\Gamma_0^{\mathrm{ExCR}}$. It increases with magnetic field. The ratio of the first combined exciton–cyclotron resonancepeak intensity to the exciton resonance intensity S_0 can be written

$$\frac{S^{\mathrm{ExCR}}}{S_0}=8n_eL_H^2. \tag{2}$$

Thus the ExCR line amplitude should decrease linearly with increasing magnetic field, which is in agreement with experiment (Fig. 3). Such a decrease in the ExCR reflectance line amplitude contrasts with the usually observed behavior of exciton lines, whose amplitude grows with magnetic field.

Thus we have studied reflectance spectra in a magnetic field from modulation-doped QW structures containing two-dimensional electron gas. The reflectance spectra of these structures exhibited transitions associated with excitation of excitons, trions, and exciton-cyclotron resonance. It has been found that the contribution to dielectric permittivity of the optical transitions associated with trion and ExCR photoexcitation is comparable to that due to exciton transitions. An analysis of the ExCR reflectance profile has permitted us to establish the magnetic-field dependence of the parameters describing the contribution of these processes to reflectance spectra.

Partial support of the Russian Fund for Fundamental Research (Grant 95-02-0406), INTAS (93-3657 Ext), Volkswagen-Stiftung, and ''Nanostructures'' Program of the Russian Ministry of Science is gratefully acknowledged.

*Present address: A. F. Ioffe Physicotechnical Institute, Russian Academy of Sciences, 194021 St. Petersburg, Russia.

[1] K. Kheng, R. T. Cox, Y. Merle d'Aubigné, F. Bassani, K. Saminadayar, and S. Tatarenko, Phys. Rev. Lett. **71**, 1752 (1993).
[2] G. Finkelstein, H. Shtrikman, and I. Bar-Joseph, Phys. Rev. Lett. **74**, 976 (1995); A. J. Shields, M. Pepper, D. A. Ritchie, M. Y. Simmons, and G. A. C. Jones, Phys. Rev. B **51**, 18049 (1995).
[3] G. Finkelstein, H. Shtrikman, and I. Bar-Joseph, Phys. Rev. B **53**, R1709 (1996).
[4] D. R. Yakovlev, V. P. Kochereshko, R. A. Suris, W. Ossau, A. Waag, G. Landwehr, P. C. M. Christianen, and J. C. Maan, in *Proceedings of the 23rd International Conference Physics of Semiconductors* (Berlin, 1996) (World Scientific, Singapore, 1996), p. 2071.
[5] V. P. Kochereshko, D. R. Yakovlev, A. V. Platonov, W. Ossau, A. Waag, G. Landwehr, and R. Cox, in *Proceedings of the 23rd International Conference Physics of Semiconductors* (Berlin, 1996) (World Scientific, Singapore, 1996), p. 1943.
[6] V. P. Kochereshko, D. R. Yakovlev, R. A. Suris, W. Ossau, A. Waag, G. Landwehr, P. C. M. Christianen, and J. C. Maan, Superlatt. Microstruct. (in press); D. R. Yakovlev, V. P. Kochereshko, R. A. Suris, H. Schenk, W. Ossau, A. Waag, G. Landwehr, P. C. M. Christianen, and J. C. Maan, Phys. Rev. Lett. (in press).
[7] E. L. Ivchenko, A. V. Kavokin, V. P. Kochereshko, G. R. Pozina, I. N. Uraltsev, D. R. Yakovlev, R. N. Bicknell-Tassius, A. Waag, and G. Landwehr, Phys. Rev. B **46**, 7713 (1992).

Translated by G. Skrebtsov

Influence of nonequilibrium phonons on exciton luminescence in CdTe/CdMnTe quantum wells

A. V. Shcherbakov, A. V. Akimov, and V. P. Kochereshko

A. F. Ioffe Physicotechnical Institute, Russian Academy of Sciences, 194021 St. Petersburg, Russia

D. R. Yakovlev,* W. Ossau, and G. Landwehr

Physikalisches Institut der Universität Würzburg, 97074 Würzburg, Germany

T. Wojtowicz, G. Karczewski, and J. Kossut

Institute of Physics, Polish Academy of Sciences, 02-668 Warszawa, Poland

Fiz. Tverd. Tela (St. Petersburg) **40**, 816–819 (May 1998)

The luminescence method has been employed for the first time to detect nonequilibrium phonons in CdTe quantum wells with $Cd_{0.6}Mn_{0.4}Te$ barriers. The method makes use of the giant Zeeman splitting of exciton states in CdTe/(Cd,Mn)Te quantum wells and is promising for application in high-sensitivity subterahertz phonon spectrometry. The method can also be useful in revealing the spin-phonon coupling mechanisms in diluted magnetic semiconductors.
 [S1063-7834(98)01105-8]

The luminescence method has for many years been serving as a powerful tool for detection of terahertz acoustic phonons in solids.[1] During the last ten years, it has been successfully used to probe the properties of terahertz phonons and their interaction with electronic excitations in bulk semiconductors and two-dimensional semiconductor structures.[2] These studies were carried out on nonmagnetic semiconductors. Diluted magnetic materials, such as (Cd, Mn)Te, contain a magnetic-ion system which interacts strongly with phonons and carriers.[3–5] The present communication reports on the first experiments in detection of subterahertz acoustic phonons using luminescence of CdTe quantum wells (QW) confined between semimagnetic (Cd, Mn)Te barriers. We obtain qualitative information on the spectral sensitivity of such aphonon detector, which is important for its application in phonon spectrometry. We also show that this method can be used to advantage in studying the mechanisms of spin-phonon interaction in semimagnetic semiconductors. These mechanisms are currently attracting considerable interest in connection with the problem of formation of magnetic polarons.[4,6]

The structure under study contained four CdTe QWs of different thickness (9.0, 4.0, 1.8, and 1.2 nm). The structure was MBE grown on a 0.38-mm thick semi-insulating GaAs substrate. The QWs were separated by 50-nm thick $Cd_{0.6}Mn_{0.4}Te$ barriers. The area with the QWs in the samples was 2.0×1.8 mm. The growth technique used and optical characterization of the samples were reported earlier.[7]

The experiment is illustrated schematically in Fig. 1. The phonon generator h (10-nm thick constantan film), 0.5×0.25 mm in area, was deposited on the end face of the GaAs substrate. The pulse duration was $\Delta t=0.1\ \mu$s, the power density per pulse could be varied up to $P=160$ W/mm^2, and the repetition frequency was 30 kHz. The nonequilibrium phonons injected in this way into the GaAs substrate had a broad spectrum with characteristic energies of a few meV ($10^{11}-10^{12}$ Hz). The phonons traversed GaAs, entered the CdTe/(Cd,Mn)Te structure, and produced changes in the exciton luminescence, which was excited by a 50-mW cw Ar laser (the laser spot diameter on the sample was 0.3 mm). The sample, contained in a liquid-helium cryostat with pumping maintaining a temperature $T=1.8$ K, was placed at the center of a superconducting magnet in Faraday geometry.

One measured luminescence of the 1.8-nm thick QW whose spectrum under stationary excitation (in the absence of nonequilibrium phonons) contains one exciton line, whose spectral position at $T=1.8$ K is strongly dependent on magnetic field B. The exciton luminescence line was observed to shift to longer wavelengths by $\Delta E_B=E_0-E_B$ (E_0,E_B are the exciton transition energies in the absence of and with magnetic field B applied, respectively). This shift is caused by the giant Zeeman splitting of band states and results from

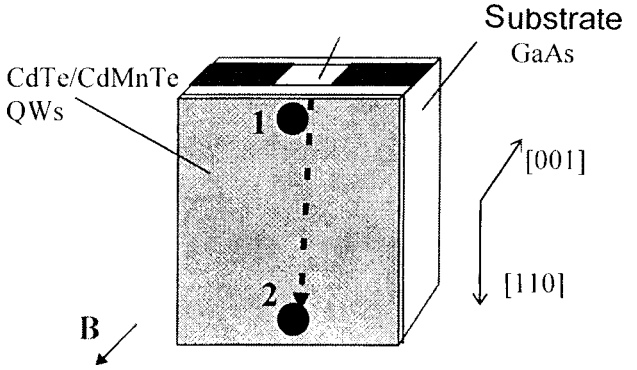

FIG. 1. Schematic representation of the experiment. Filled circles (1 and 2) on CdTe/(Cd,Mn)Te surface identify the locations of phonon excitation. The arrow shows propagation of ballistic phonons from the phonon generator h to point *2*.

the strong exchange interaction of carriers in the CdTe QW and Mn ions localized in the (Cd,Mn)Te barriers.[8] It is known that ΔE_B drops with increasing temperature, which is explained as due to thermal population of higher-lying Zeeman sublevels of the Mn ions and, accordingly, to the decrease of magnetic susceptibility of the carriers confined in the QWs.[9]

The idea underlying the experiments consisted in increasing the Mn ion temperature through interaction with nonequilibrium phonons of the heat pulse, which should reduce δE_B. The dynamic shift of the exciton line, $\delta E_B(t)$, induced by the nonequilibrium phonons was measured at two points located at different distances from the phonon generator (points 1 and 2 in Fig. 1) in different magnetic fields B. The phonon-generator power density P used in the experiment was low enough and corresponded to the largest detectable shift $\delta E_B = 2$ meV in the presence of nonequilibrium phonons. This corresponded to a temperature change in equilibrium conditions $\Delta T \approx 0.5$ K, thus giving grounds to assume that the changes in luminescence intensity, $\delta I_B(t)$, at a fixed wavelength of the detecting monochromator would be directly proportional to $\delta E_B(t)$.

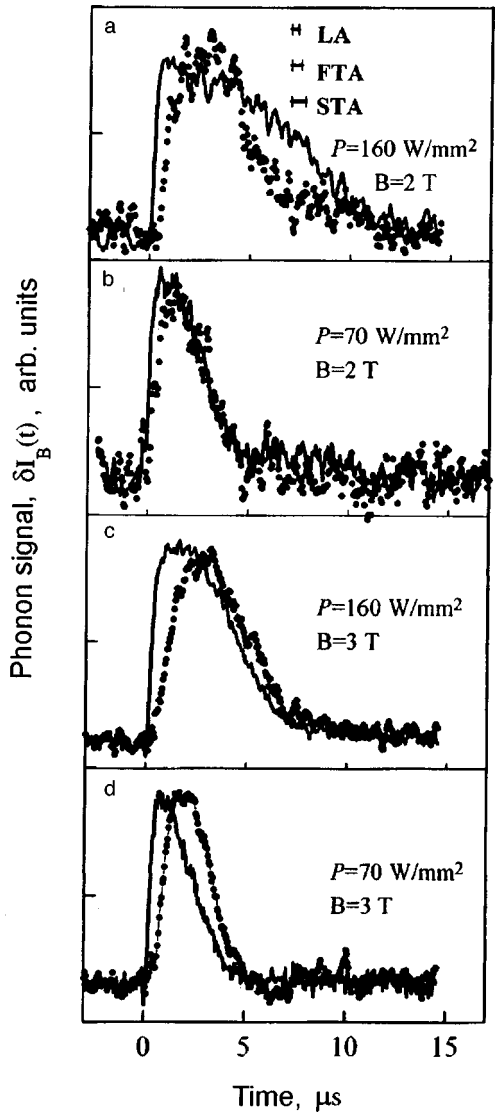

FIG. 2. Normalized evolution of the nonequilibrium-phonon-induced $\delta I_B(t)$ signal measured at points 1 (solid curves) and 2 (circles) for different B and P. Horizontal bars specify the expected ballistic time shift of signals for LA, FTA, and STA phonons (the corresponding sonic velocities $v_j = 5.3$, 3.4, and 2.5 km/s).

Figure 2 presents the time relations $\delta I_B(t)$ measured in the 1.8-nm thick QW for different magnetic fields, phonon generator powers, and positions of the point where the phonon signal was detected (or of the point where the excitons were excited, points 1 and 2 in Fig. 1). The solid lines in Fig. 2 represent the $\delta I_B(t)$ signal measured near the phonon generator (point 1, separated from the center of the phonon generator by $r = 0.24$ mm). The circles in Fig. 2 correspond to the $\delta I_B(t)$ signal measured at point 2 ($r = 1.81$ mm). One observes a distinct shift in time of the leading edge of $\delta I_B(t)$ with increasing r. The magnitude of this shift is in accord with the ballistic time of flight for LA and TA phonons in GaAs (the expected shifts are shown in Fig. 2a with horizontal bars). The results obtained for the trailing edges of the $\delta I_B(t)$ signal for $B = 2$ T and $P = 160$ W/mm^2 (Fig. 2a) appear somewhat unexpected. The $\delta I_B(t)$ signal falls off faster with increasing distance from the phonon generator. This behavior is very unusual compared with the previous experiments with nonequilibrium phonons[1,10]. In the earlier experiments, the detected phonon pulse broadens in time because of phonon scattering in the bulk of the sample. The results displayed in Fig. 2 exclude the ballistic mechanism of phonon detection, and the explanation for the observed relations should be looked for in the spin-phonon interaction in a semimagnetic material. The long trailing edge is observed only at a high power density, $P = 160$ W/mm^2, and disappears at a low power level $P = 70$ W/mm^2 (compare the solid lines in Fig. 2a and 2b).

It is essential that the observed microsecond-scale evolution $\delta I_B(t)$ is substantially longer than the exciton lifetime $\tau_{\text{exc}} \sim 10^{-10}$ s (Ref. 11), as well as the spin-phonon relaxation time $\tau_{\text{sp}} \ll 10^{-7}$ s in $Cd_{1-x}Mn_xTe$ for $x > 0.1$ (Ref. 12). Thus the measured profile of $\delta I_B(t)$ reflects the temporal, spatial, and spectral evolution of the nonequilibrium phonons. We shall first discuss the generation and propagation of acoustic phonons in GaAs. These processes were studied in detail before (see, e.g., Ref. 13). After this we shall consider the spin-phonon coupling mechanisms, which play a major part in the interpretation of our experimental results.

Phonon generation. The phonons are created in a thin metal film heater h. It is assumed[1,10] that phonons generated during a heat pulse have a Planckian distribution in temperature, $T_h \propto P^{1/4}$, which can be calculated by acoustic mismatch theory.[14] In our experiments, $T_h \sim 25$ K for $P = 160$ W/mm^2, which corresponds to a spectral distribution of phonons peaking at $\hbar\omega_m \sim 2kT_h \sim 5$ meV. These phonons have a short mean free path $l(\omega_m) \sim 0.05$ mm, and are confined to a region close to the phonon generator because of elastic scattering.[15,16]

Phonon propagation. The phonon mean free path is strongly frequency dependent ($l \propto \omega^{-4}$), and, therefore, low-energy phonons with $\hbar\omega \leqslant 1$ meV are capable of traversing ballistically (i.e., without scattering) distances of a few mm.

If the phonon detector is sensitive to these low-energy phonons, then the time profiles of signals measured at different distances r from the phonon generator should have a steep leading edge shifted in time by the ballistic time of flight $t_b = r/\nu_j$, where ν_j is the sonic velocity of polarization j (j = LA, FTA, STA). This is indeed observed in the signals measured by us (compare the solid lines and circles in Fig. 2). The trailing edge of a phonon pulse is dominated by the dynamic properties of high-frequency phonons with $\hbar\omega \gg 1$ meV.[16] High-frequency phonons with $\hbar\omega \sim \hbar\omega_m$ are strongly scattered in the bulk of GaAs and reach the detector by diffusion.[15] Thus the relative contribution of high-frequency phonons to the phonon spectrum at point 2 should be substantially smaller than that at point 1 because of the diffusive damping of phonons, as well as a result of their escape to liquid helium from thin samples[17]. Actually, the GaAs substrate acts as a filter for the high-frequency phonons propagating from the phonon generator to point 2.

Spin-phonon interaction. We are turning now to discussing the spectral sensitivity of our luminescence detector. It is determined by the energy spectrum of Mn ions which are heated by nonequilibrium phonons. The Mn ion system in diluted magnetic semiconductors contains paramagnetic spins and clusters consisting of antiferromagnetically interacting spins. The relative contribution of paramagnetic spins and clusters is determined by the Mn content and temperature.[3] The giant Zeeman splitting is determined primarily by paramagnetic spins and, partially, by clusters containing an odd number of Mn ions. The observed phonon signal can be accounted for by interaction with both low- and high-frequency phonons. Low-frequency phonons with $\hbar\omega = g_{\mathrm{Mn}}\mu_B B$ ($g_{\mathrm{Mn}} = 2$ for Mn ions) can initiate *direct* resonant transitions between Zeeman sublevels in Mn ions.[18] For $B = 3$ T, $\hbar\omega = 0.3$ meV, and phonons with such an energy undergo ballistic transport in GaAs.[15] High-frequency phonons can interact with spin clusters, which have a number of excited states with energies of a few meV.[19] This reduces partially the exciton splitting caused by clusters with a nonzero magnetic moment. If the interaction between excited clusters and paramagnetic spins is strong enough, however, the excitation will be transferred from a cluster to an individual spin (*indirect* Urbach process[18]), and the corresponding contribution to the exciton splitting will be determined by paramagnetic spins. It should be pointed out that spin-wave excitation can also contribute to the observed signal through absorption of low-frequency phonons.[20]

The experimental data presented in Fig. 2 indicate that our phonon detector is sensitive to both low- and high-frequency phonons. Indeed, if only high-frequency phonons ($\hbar\omega \sim \hbar\omega_m$) contributed to the observed signal, then $\delta I_B(t)$ would not reflect the ballistic properties of phonons, and the magnitude of $\delta I_B(t)$ at point 2 would be extremely small. A comparison of the values of $\delta I_B(t)$ measured at points 1 and 2 (Fig. 2) reveals a ballistic delay, which is in accord with the behavior of low-frequency phonons. This indicates that our detector is sensitive to low- frequency phonons, and that the $\delta I_B(t)$ signal can be due to direct absorption of $\hbar\omega = g_{\mathrm{Mn}}\mu_B B$ phonons. High-frequency phonons also contribute to $\delta I_B(t)$ at point 1. The signal measured at $B = 2$ T and $P = 160$ W/mm^2 (solid line in Fig. 2a) shows clearly the contribution of the diffusive component to the trailing edge of the $\delta I_B(t)$ signal measured at point 1. The diffusive component disappears at lower power densities, $P = 70$ W/mm^2 (Fig. 2b), when $\hbar\omega_m$ is smaller ($\hbar\omega_m \sim 4$ meV, $T_h \approx 20$ K) than it is for large values of P. Thus high-frequency phonons and, accordingly, interaction with clusters is also essential for the $\delta I_B(t)$ signal. The $\delta I_B(t)$ signal measured at point 2 practically does not contain the diffusive component (Fig. 2), thus confirming that GaAs is a filter for high-frequency phonons.

Interestingly, the role of high-frequency phonons decreases with increasing magnetic field. Indeed, at $B = 3$ T (Fig. 2c) the difference between the values of $\delta I_B(t)$ measured at points 1 and 2 is not so large as that at $B = 2$ T (Fig. 2a). The relative increase in efficiency of direct as compared to indirect processes with increasing B was observed earlier to occur in bulk $Cd_{1-x}Mn_xTe$ for $x \leqslant 0.1$,[12] although in substantially higher fields than the ones used in our experiments. This difference may be due to the significantly higher Mn concentration, as well as to the role of interface Mn ions in our samples, which provide the major contribution to the giant Zeeman splitting of excitons.[21–23]

In conclusion, we propose a new method of luminescence-based detection of nonequilibrium phonons which makes use of the giant Zeeman splitting of exciton states in CdTe quantum wells with barriers of diluted magnetic (Cd,Mn)Te material. This method of phonon detection is sensitive to ballistic phonons and shows promise for high-resolution (< 0.1 meV) phonon spectrometry. This spectrometer would permit one to study acoustic phonons in the spectral region up to $\hbar\omega = g_{\mathrm{Mn}}\mu_B B = 2$ meV and in magnetic fields of up to 20 T, and could serve as a new tool for probing the dynamic vibrational properties of semiconductor nanostructures.

Our sincere gratitude is due to A. A. Kaplyanskiĭ, K. V. Kavokin, and I. A. Merkulov for fruitful discussions.

Support of the Deutsche Forschungsgemeinschaft (Grant SFB 410), Volkswagen Stiftung, Russian Fund for Fundamental Research (Grant 96-02-16952a), and State Committee for Scientific Research of Poland (Grant 8T11B-014-11) is gratefully acknowledged.

*Present address: A. F. Ioffe Physicotechnical Institute, Russian Academy of Sciences, 194021 St. Petersburg, Russia.

[1] W. E. Bron, in *Nonequilibrium Phonons in Nonmetallic Crystals*, Modern Problems in Condensed Matter Sciences, Vol. 16, edited by W. Eisenmenger and A. A. Kaplyanskii (North-Holland, Amsterdam, 1986), 227 pp.

[2] A. V. Akimov, A. A. Kaplyanskii, and E. S. Moskalenko, *Die Kunst of Phonons: Lectures from XXIX Winter School of Theoretical Physics*, edited by T. Paszkiewicz and K. Rapcewicz (Plenum Press, New York, 1994), p. 113; A. V. Akimov, E. S. Moskalenko, L. J. Challis, and A. A. Kaplyanskii, Physica B **219 & 220**, 9 (1996).

[3] J. K. Furdyna, J. Appl. Phys. **64**, R29 (1988).

[4] D. R. Yakovlev and K. V. Kavokin, Comments Condens. Matter Phys. **18**, 51 (1996).

[5] V. D. Kulakovskii, M. G. Tyazhlov, A. I. Filin, D. R. Yakovlev, A. Waag, and G. Landwehr, Phys. Rev. B **54**, R8336 (1996).

[6] T. Dietl, P. Peyla, W. Grieshaber, and Y. Merle d'Aubigné, Phys. Rev. Lett. **74**, 474 (1995).

[7] G. Mackh, W. Ossau, D. R. Yakovlev, G. Landwehr, R. Hellmann, E. O. Göbel, T. Wojtowicz, G. Karczewski, and J. Kossut, Solid State Commun. **96**, 297 (1995).
[8] B. Kuhn-Heinrich, M. Popp, W. Ossau, E. Bangert, A. Waag, and G. Landwehr, Semicond. Sci. Technol. **8**, 1239 (1993).
[9] J. A. Gaj, P. Planel, and G. Fishman, Solid State Commun. **29**, 435 (1979).
[10] R. J. von Gutfeld, in *Physical Acoustics*, Vol. 5, edited by W. P. Mason (Academic, New York, 1958), p. 233.
[11] A. Pohlmann, R. Hellmann, E. O. Göbel, D. R. Yakovlev, W. Ossau, A. Waag, R. N. Bicknell-Tassius, and G. Landwehr, Appl. Phys. Lett. **61**, 2929 (1992).
[12] T. Strutz, A. M. Witowski, and P. Wyder, Phys. Rev. Lett. **68**, 3912 (1992).
[13] Y. B. Levinson, in *Nonequilibrium Phonons in Nonmetallic Crystals*, Modern Problems in Condensed Matter Sciences, Vol. 16 (North-Holland, Amsterdam, 1986), p. 91.
[14] W. Kappus and O. Weis, J. Appl. Phys. **44**, 1947 (1973).
[15] L. J. Challis, B. Salce, N. Butler, M. Sahraoui-Tahar, and W. Ulrici, J. Phys. Condens. Matter **1**, 7277 (1989); M. T. Ramsbey, S. Tamura, and J. P. Wolfe, Phys. Rev. B **46**, 1358 (1992); Z. Xin, F. F. Ouali, L. J. Challis, B. Salce, and T. S. Cheng, Physica B **219 & 220**, 56 (1996).
[16] M. Greenstein, M. A. Tamor, and J. P. Wolfe, Phys. Rev. B **26**, 5604 (1982).
[17] S. A. Basun, S. P. Feofilov, A. A. Kaplyanskii, and W. M. Yen, Phys. Rev. Lett. **67**, 3110 (1991).
[18] A. Abragam and B. Bleaney, in *Electron Paramagnetic Resonance of Transition Ions* (Clarendon, Oxford, 1970).
[19] D. Scalbert, Phys. Status Solidi B **193**, 189 (1996).
[20] I. A. Merkulov, Private communication.
[21] W. J. Ossau and B. Kuhn-Heinrich, Physica B **184**, 422 (1993).
[22] J. A. Gaj, W. Grieshaber, C. Bodin-Deshayes, J. Cibert, G. Feuillet, Y. Merle d'Aubigné, and A. Wasiela, Phys. Rev. B **50**, 5512 (1994).
[23] P. Kossacki, N. T. Khoi, J. A. Gaj, G. Karczewski, T. Wojtowicz, E. Janik, A. Zakrzewski, M. Kutrowski, and J. Kossut, Superlattices Microstruct. **16**, 63 (1994).

Translated by G. Skrebtsov

Molecular layering of 2*D* films and superlattices based on II–VI compounds

R. A. Bisengaliev and B. V. Novikov

Scientific-Research Institute of Physics, St. Petersburg State University, 198904 Petrodvorets, Russia

V. B. Aleskovskiĭ and V. E. Drozd

Scientific-Research Institute of Chemistry, St. Petersburg State University, 198904 Petrodvorets, Russia

D. A. Ageev, V. I. Gubaĭdullin, and A. P. Savchenko

TOO NPKF ''Light,'' 195279 St. Petersburg, Russia

Fiz. Tverd. Tela (St. Petersburg) **40**, 820–821 (May 1998)

The method of molecular layering is used to prepare CdS thin films and CdS/ZnS and CdS/CdSe superlattices. The dependence of the exciton photoluminescence on film thickness is studied, and the role of internal strains is examined. The effect of the excitation intensity on the superlattice photoluminescence spectra is examined, manifested in a shift of the emission maximum toward shorter wavelengths when this intensity is increased. © *1998 American Institute of Physics.* [S1063-7834(98)01205-2]

The method of molecular layering was developed under the direction of Aleskovskiĭ in the middle of the 1960's and has become known abroad under the name ''atomic-layer epitaxy'' (ALE) and occupies a secure position at present as one of the techniques for obtaining superthin uniform semiconductor and insulator films.[1,2]

In their realization of the molecular layering reactions on a substrate surface, the authors of the method proceeded from the following considerations.[1] If chemisorbed groups of atoms are present on the substrate surface, then such a solid body can be represented as an unchanging frame to which functional groups of a known chemical nature are bound. If these functional groups manifest chemical activity relative to any molecules, then it is possible to get them to interact under certain conditions and thereby obtain a new layer of functional groups. The composition of this layer will differ from that of the original and will be predetermined by the composition of the original functional groups and reagent molecules with which the interaction occurred. In general, such functional groups of the substrate may be groups of atoms bound to the substrate not only by strong chemisorption bonds but also by weak bonds even of physical adsorption. If we consider the original solid body in this way, then the first stage of the molecular layering reactions should be formation of a layer of functional groups bound to the substrate. If we pose ourselves the problem to synthesize a prescribed solid body and not just a random hodge-podge of materials, then it is necessary to ensure that the resulting adsorption interactions take place with maximum possible irreversibility. It was shown in Refs. 3 and 4 that the molecular layering method can be successfully applied to synthesize thin films of II–VI compounds using as the reagents metallo-organic compounds and the corresponding hydrides.

In the present work we have performed a synthesis on an novel automated setup according to a preset program at a substrate temperature of 300 °C. The duration of the molecular layering cycle was 1 s and the reagent feed time was 0.02 s. As the reagents we used dimethyl cadmium, diethyl zinc, and hydrogen sulfide and selenide. The layer thickness was measured with the aid of an ellipsometer, and the structure of the films obtained was measured using reflection high-energy electron diffraction. We found that raising the synthesis temperature enhances the quality of the layer structure, and we showed that film growth is epitaxial on mica substrates at 300 °C and the reflections in the electron diffraction patterns become pointlike. On silicon substrates, only a weak orienting effect appeared, and the ordering tendency of the crystalline structure was preserved.

Implementing the indicated method, we grew thin films of CdS, and superlattices of the types CdS/CdSe and CdS/ZnS. In the thin films and the superlattices we examined the photoluminescence, its spectral features, and its dependence on the excitation intensity in the temperature interval 300 -4.2 K. Photoluminescence was excited by a nitrogen laser ($\lambda = 337$ nm) and a mercury lamp using extraction light filters.

CdS thin films. Photoluminescence in thin films was observed at 77 and 4.2 K and consisted of an emission maximum with a half-width of 100–120 meV (Fig. 1a). As the thickness of the thin film was decreased below 150 Å, the maximum shifted toward shorter wavelengths along a curve close to a/d^2, where a is a constant and d is film thickness (Fig. 1b).[5] We associate the photoluminescence maximum in CdS thin films with exciton emission and its shift—with the decrease in thickness and the appearance of a size effect. The relatively large half-width of the maxima is probably due to imperfections in the films, thickness fluctuations, and also strains caused by a difference in the thermal expansion coefficients of the substrate and the laminating material.

Interaction with the substrate can lead to internal strains in the films. We investigated the transmission spectrum of a CdS film ($d \approx 1000$ Å), grown on quartz glass (fused silica)

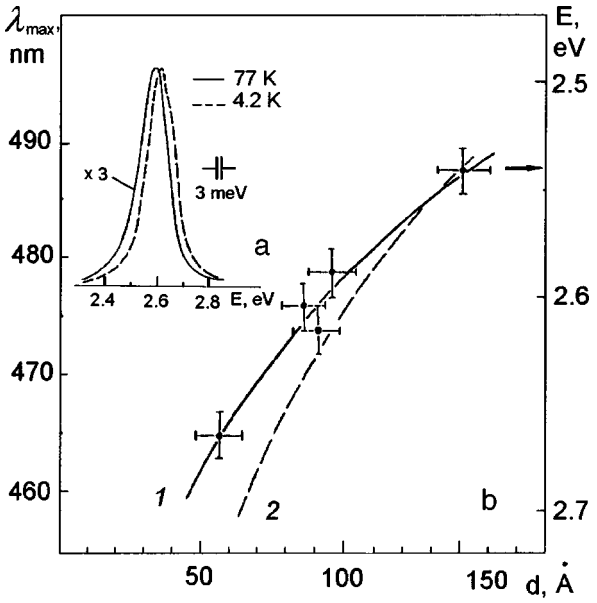

FIG. 1. a) Photoluminescence spectra of CdS thin films at $T=77$ and 4.2 K ($d\approx 95$ Å). b) Dependence of the energy position of the photoluminescence maximum on CdS film thickness at $T=77$ K. *1*—experiment, *2*—theoretical curve ($\sim a/d^2$). The arrow pointing at the energy axis points to the position of the *A* exciton line in a CdS bulk crystal.

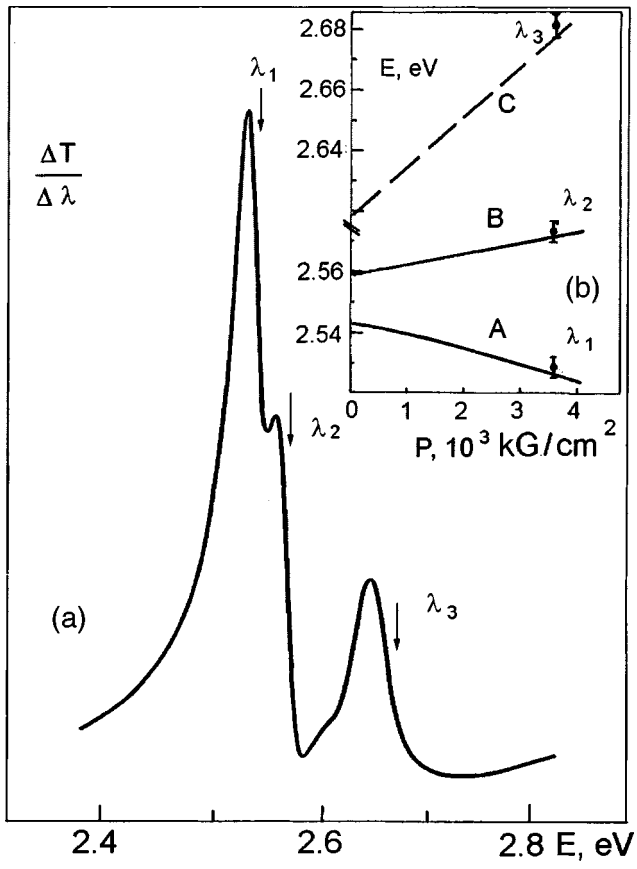

FIG. 2. a) λ-modulation spectrum of a CdS film at $T=77$ K. b) Dependence of the energy position of the exciton lines on strain in the CdS crystal (*A* and *B* excitons are indicated).[6] The points are our data. The dashed line indicates the shift of the *C* line in the film we investigated.

at 300 °C. The spectrum was recorded using the λ-modulation method (Fig. 2a). As can be seen, it has three features ($\lambda_1,\lambda_2,\lambda_3$), which we think are associated with excitation of excitons belonging to the three valence subbands *A*, *B*, and *C*. In the film in question, the energy positions of the excitons differ substantially from their positions in the bulk crystals. As was indicated above, this is due to the large strain caused by the difference in the thermal expansion coefficients of the CdS film and the quartz substrate. Comparison with the data of Ref. 6 shows that the internal strain corresponds to a stress around 3.5×10^3 kg/cm^2 (Fig. 2b).

CdS/ZnS superlattices. We prepared $(CdS)_1/(ZnS)_{52}$ and $(CdS)_{70}/(ZnS)_{52}$ superlattices differing in the width of the quantum well. The spectrum of the sample with the wide quantum well reveals an intense and relatively narrow emission maximum near the absorption edge of bulk CdS (around 2.4 eV). For the narrow quantum well, the maximum is shifted by ~ 0.4 eV toward shorter wavelengths and there is an additional longer-wavelength maximum. This shift is noticeably smaller than the shifts obtained for short-period CdS/ZnS lattices grown by molecular-beam epitaxy on GaAs substrates.[7] For the given structure we were the first to observe a shift of the photoluminescence maximum in a CdS/ZnS superlattice in response to a change in the intensity of the exciting light. We believe that in strained CdS/ZnS samples, a strong internal electric field arises as a result of the piezoelectric effect, which leads to an anomalous Stark shift of the exciton states. This field can be decreased as a result of screening at a high excitation intensity level, which causes the short-wavelength shift.[7] We observed an analogous shift in CdS/CdSe superlattices (grown by us) like the authors of Ref. 8.

[1] V. B. Aleskovskiĭ, *Stoichiometry and Synthesis of Solid Compounds* [in Russian], Nauka, Leningrad, 1976.
[2] T. Suntola, *Atomic Layer Epitaxy* (MSR, North-Holland, Amsterdam, 1989), Vol. 4, No. 7.
[3] V. K. Adamchuk, V. B. Aleskovskiĭ, V. E. Drozd, V. I. Gubaĭdullin, A. V. Fedorov, and A. I. Romanychev, Dokl. Akad. Nauk SSSR **303**, 1390 (1988).
[4] V. B. Aleskovskiĭ, V. E. Drozd, V. I. Gubaĭdullin, and A. I. Romanychev, Dokl. Akad. Nauk SSSR **291**, 136 (1986).
[5] A. D. Yoffe, Adv. Phys. **42**, 173 (1993).
[6] T. Koda and D. W. Langer, Phys. Rev. Lett. **20**, 50 (1968); *Proceedings of the IXth Conference Physics* Semicond., Moscow (1968), p. 242.
[7] G. Brunthaler, M. Lang, A. Forstner *et al.*, J. Cryst. Growth **138**, 559 (1994).
[8] I. V. Bradley, G. P. Cresy, and K. P. O'Donnell, J. Cryst. Growth **159**, 551 (1995).

Translated by Paul F. Schippnick

Appearance of resonant $\Gamma - X$ mixing in gradient GaAs/AlAs short-period superlattices

I. Ya. Gerlovin, Yu. K. Dolgikh, Yu. P. Efimov, I. V. Ignat'ev, and I. A. Nedokus

Scientific-Research Institute of Physics, St. Petersburg State University, 198904 Petrodvorets, Russia

Fiz. Tverd. Tela (St. Petersburg) **40**, 822–823 (May 1998)

We have experimentally investigated the low-temperature (10 K) luminescence and reflection spectra of a gradient GaAs/AlAs superlattice. We have examined the behavior of phonon satellites in the vicinity of the $X-\Gamma$ resonance. Smooth passage through the resonance was achieved by scanning an exciting light beam along the surface of a gradient sample. Based on our experimental results, we have determined the functional dependence of the $\Gamma - X$ mixing potential on the resonance detuning. © *1998 American Institute of Physics.* [S1063-7834(98)01305-7]

The lowest excited states of type-II GaAs/AlAs superlattices are excitons formed by X electrons of the AlAs conduction band and Γ holes of the GaAs valence band. The nonzero value of the oscillator strength of the indirect $X-\Gamma$ exciton is due to adulteration of the X states by Γ states of the GaAs electrons. The $\Gamma - X$ mixing potential depends on the energy difference of the states being mixed together and takes on maximum values in the resonance region.[1]

Experimental data on the near-resonance behavior of the $X-\Gamma$ and $\Gamma-\Gamma$ excitons in GaAs/AlAs short-period superlattices are reported in Refs. 2–6. To obtain a relative shift of the states being mixed, we employed cubic compression of the investigated structures,[2,3] a constant electric field,[4] and a set of superlattices with different heterolayer thicknesses.[5,6] The values of the $\Gamma - X$ mixing potential of 1–5 meV estimated from the experimental results coincided within an order of magnitude with the theoretical estimates.[4,7] However, to compare with theory it is more informative to have not just the value of the mixing potential for one set of values of the parameters of the investigated structures, but but its functional dependence on these parameters. In the present paper we present results of experiments aimed at refining the functional dependence of the oscillator strength of the $X-\Gamma$ exciton transition on the energy gap between the Γ and X electron states.

We studied the variation of the position, shape, and intensity of the exciton lines in the optical spectra of a GaAs/AlAs short-period superlattice near the $X-\Gamma$ resonance. To pass through the resonance we used the dependence of the energies of the X electrons of AlAs and the Γ electrons of GaAs on the thickness of the corresponding layers. The sample was a heterostructure on a semi-insulating GaAs substrate, and the investigated structure (grown on an ÉP-1302 molecular-beam epitaxy setup at the Scientific-Research Institute of Physics, St. Petersburg State University) contained a 50-period GaAs/AlAs superlattice with nominal layer thicknesses of 20 Å(GaAs) and 12 Å(AlAs). A distinguishing feature of the superlattice was the presence of a cross gradient of the GaAs and AlAs layers. Thanks to this gradient, scanning of the exciting light over the surface of the sample was accompanied by a substantial change in the interrelation of the GaAs and AlAs layer thicknesses for an almost constant value of the superlattice period.

We measured the low-temperature (10 K) photoluminescence spectra and the reflection spectra. Luminescence was excited with a He–Ne laser. When recording the reflection spectra we used a halogen-cycle incandescent tungsten lamp.

As the results of our experiments showed, the low-temperature luminescence spectra undergo a dramatic transformation as the laser spot is moved over the sample. The spectrum of the thinner part of the sample contains, in addition to a strong exciton peak, phonon satellites typical of an indirect $X-\Gamma$ transition. In the thickest part of the sample the phonon echoes of the exciton peak disappear, and the peak broadens somewhat, acquiring the typical shape of a $\Gamma-\Gamma$ exciton. Consequently, in this region of the sample the lowest state becomes the GaAs Γ state.

Radiative $X-\Gamma$ recombination with simultaneous emission of a phonon carrying away excess momentum does not require the admixture of GaAs Γ states, i.e., the intensity of the phonon echoes should not change as the $\Gamma - X$ mixing potential is varied. This means that the ratio of intensities of the $X-\Gamma$ exciton peak and the phonon echoes can serve as a measure of variation of the oscillator strength of the purely excitonic transition. Figure 1 plots the dependence of this ratio, measured at different points in the sample, on the magnitude of the energy gap between the Γ and X states, ΔE. The observed dependence is well described by the function

$$I_{\mathrm{ex}}/I_{\mathrm{ph}} \sim \Delta E^{-k}, \quad k = 1.1 \pm 0.1.$$

According to Ref. 1, the oscillator strength of the no-phonon $X-\Gamma$ transition $S_{X-\Gamma}$ is given by

$$S_{X-\Gamma} = |V_{\Gamma X}|^2/\Delta E^2,$$

where $|V_{\Gamma X}|$ is the matrix element of the mixing potential due to overlap of the corresponding wave functions.

As was mentioned above, in the investigated sample a relative change in the GaAs and AlAs layer thicknesses is accompanied by the most insignificant change in the superlattice period normalizing the wave functions. This means that the observed changes in the oscillator strength of the

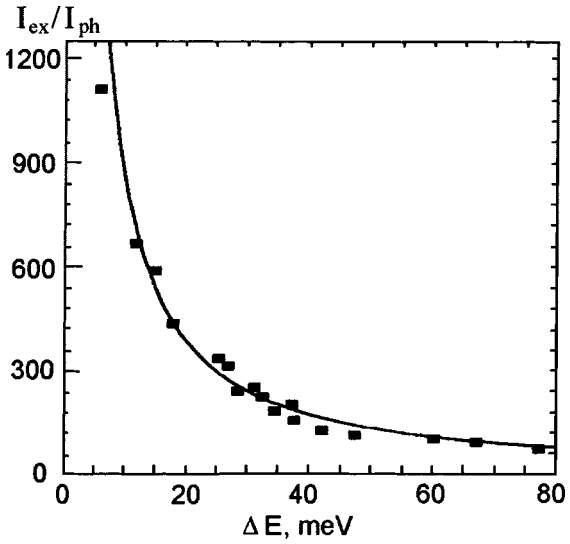

FIG. 1. Dependence of the ratio of the intensity of the $X-\Gamma$ exciton peak to the intensity of the LO phonon echos on the energy difference of the Γ and X exciton peaks.

$X-\Gamma$ transition are almost completely due to the change in the energy gap between the Γ and X electron states. Thus, the experimentally obtained functional dependence of the oscillator strength on the energy gap does not coincide with that predicted by theory.

Apparently the main reason for this disagreement is inhomogeneous broadening of the states being mixed. Such broadening is indicated by the Stokes shift of the $\Gamma-\Gamma$ exciton peak in the reflection and luminescence spectra. To clarify the role of inhomogeneous broadening requires more detailed study.

This work was carried out with the support of the Russian Fund for Fundamental Research (Grants No. 97-02-18163 and 97-02-18339).

[1] M. S. Skolnick, G. W. Smith, I. L. Spain, C. R. Whitehouse, D. C. Helbert, D. M. Whittaker, and L. J. Reed, Phys. Rev. B **39**, 11 191 (1989).
[2] T. Nakayama, F. Minami, and K. Inoue, in *The Physics of Semiconductors*, edited by P. Jiang and H. Z. Zheng (World Scientific, Singapore, 1992), p. 717.
[3] W. R. Tribe, P. C. Klipstein, R. A. Woolley, and J. S. Roberts, Phys. Rev. B **51**, 9735 (1995).
[4] M.-H. Meynadier, R. E. Nahory, J. M. Worlock, M. C. Tamargo, J. L. de Miguel, and M. D. Sturge, Phys. Rev. Lett. **60**, 1338 (1988).
[5] M. Nakayama, K. Imazawa, K. Suyama, I. Tanaka, and H. Nishimura, Phys. Rev. B **49**, 13 564 (1994).
[6] I. L. Aleiner, E. L. Ivchenko, V. P. Kochereshko, G. L. Sandler, P. Lavallard, and R. Planel, Superlattices Microstruct. **13**(2), 237 (1993).
[7] Y. Fu, M. Willander, E. L. Ivchenko, and A. A. Kiselev, Phys. Rev. B **47**, 13 498 (1993).

Translated by Paul F. Schippnick

Toward a theory of light absorption by excitons in quantum-well structures

V. A. Kosobukin

A. F. Ioffe Physicotechnical Institute, Russian Academy of Sciences, 194021 St. Petersburg, Russia

Fiz. Tverd. Tela (St. Petersburg) **40**, 824–826 (May 1998)

A theory of light absorption by excitons in periodic structures with an arbitrary number of quantum wells is constructed. It is shown that the temperature dependence of the frequency-integrated absorption characteristics is due to a competition between the processes of dissipative decay of quasi-two-dimensional excitons and the light–exciton interaction. © *1998 American Institute of Physics.* [S1063-7834(98)01405-1]

The total optical absorption, being temperature-independent for polarization resonances in media without spatial dispersion,[1] falls substantially at low temperatures for spatially dispersed bulk excitons.[2] An analogous temperature behavior was observed recently for the total light absorption by quasi-two-dimensional excitons in GaAs/(Al,Ga)As (Ref. 3) and (In,Ga)As/GaAs (Ref. 4, 5) quantum-well heterostructures. In the present paper we present results of a general theory explaining the temperature dependence of light absorption by excitons in structures with an arbitrary number of quantum wells and period in the absence of exciton spatial dispersion effects.

Consider the propagation of a monochromatic electromagnetic wave with frequency ω along the z axis of a structure formed by $N \leqslant 1$ equispaced quantum wells with period d in a medium with background dielectric constant ε_b. As in Refs. 6 and 7, the resonance contribution of the quasi-two-dimensional excitons to the quantum-well polarization is taken into account in the nonlocal approximation, and tunneling of charge carriers between quantum wells is neglected. The transfer matrix method[7] is used to calculate the reflection R_N and transmission coefficients T_N of the structure, and also the value of Poynting's vector in successive nonabsorbing barrier layers (outside the quantum wells). As characteristics of optical absorption in a structure with N quantum wells, we next consider the following quantities:[1)] 1) the absorptivity of the structure $A_N(\omega)=1-R_N(\omega)-T_N(\omega)$, or probability of absorption of a photon with energy $\hbar\omega$; 2) the absorption coefficient $\alpha_N(\omega)$ (the optical density $D_N(\omega)=\alpha_N(\omega)dN$). Strictly speaking, the absorption coefficient $\alpha(\omega)$ is defined for macroscopically homogeneous media as a characteristic of the properties of a material in which Bouguer's law

$$S(z,\omega)=S(0,\omega)\exp[-\alpha(\omega)z],$$

$$\alpha(\omega)=-S^{-1}(z)[dS(z)/dz] \tag{1}$$

is fulfilled, where $\alpha(\omega)$ does not depend on the coordinate z, along which the flux of electromagnetic energy $S(z,\omega)$ attenuates. For a structure with N quantum wells, in line with Eqs. (1) we define the effective absorption coefficient

$$\alpha_N=-\frac{1}{Nd}\ln\left(\frac{S(Nd)}{S(0)}\right)=-\frac{1}{Nd}\ln\left(\frac{T_N}{1-R_N}\right). \tag{2}$$

It is convenient also to introduce a local absorption coefficient

$$\tilde{\alpha}_n=-(1/d)[(S_n/S_{n-1})-1]=(1/d)(A_1/T_1)\varphi_n, \tag{3}$$

where $A_1/T_1=2\Gamma\Gamma_0/[(\omega-\omega_0)^2+\Gamma^2]$, and S_{n-1} and S_n are the values of Poynting's vector before and after passage of the electromagnetic wave through the nth quantum well ($n=1, 2, \ldots, N$). The quantity $\tilde{\alpha}_n$ in (3) governs the variation of the energy flux due to absorption in the nth quantum well; it is expressed in terms of the exciton excitation frequency ω_0 and its dissipative Γ and radiative Γ_0 decay parameters,[6,7] and the dependence of expression (3) on n is given by the real function $\varphi_n>0$. For an infinite ($N\to\infty$) structure, taking Eq. (3) into account, we obtain Bouguer's law in the form

$$S_{n+m}/S_m=\exp[-\tilde{\alpha}(\omega)dn],$$

$$\tilde{\alpha}=-(1/d)\ln[1-(A_1/T_1)\varphi], \tag{4}$$

where $\tilde{\alpha}(\omega)$ does not depend on either m or n.

We will use the above-defined spectral dependences to examine the following frequency-integrated absorption characteristics:

$$I_N=\frac{1}{2\pi N}\int_{-\infty}^{\infty}\frac{d\omega}{\Gamma_0}A_N(\omega), \tag{5}$$

$$K_N=\frac{1}{2\pi}\int_{-\infty}^{\infty}\frac{d\omega}{\Gamma_0}(\alpha_N d)=-\frac{1}{2\pi N}\int_{-\infty}^{\infty}\frac{d\omega}{\Gamma_0}\ln\left(\frac{T_N}{1-R_N}\right). \tag{6}$$

These integrals become temperature-independent as $N\to\infty$, when Eq. (4) is fulfilled, whereupon $I_N\to 0$ and $K_N\to 1$. Below we will discuss the temperature dependence of the quantities (5) and (6), which is configured by the presence of boundaries (finite N) and peculiarities of exciton re-radiation for small N. The analytical expression (5) for solitary quantum wells ($N=1$) and Bragg structures ($N\gg 1$, $d=\pi/k_0$, where $k_0=\sqrt{\varepsilon_b}(\omega_0/c)$, c is the speed of light) shows that as functions of $x=\Gamma/\Gamma_0$, I_N and K_N grow monotonically from $x=0$ and saturate for $x\gg N$. It follows from a numerical analysis that these conclusions are valid for any N and d.

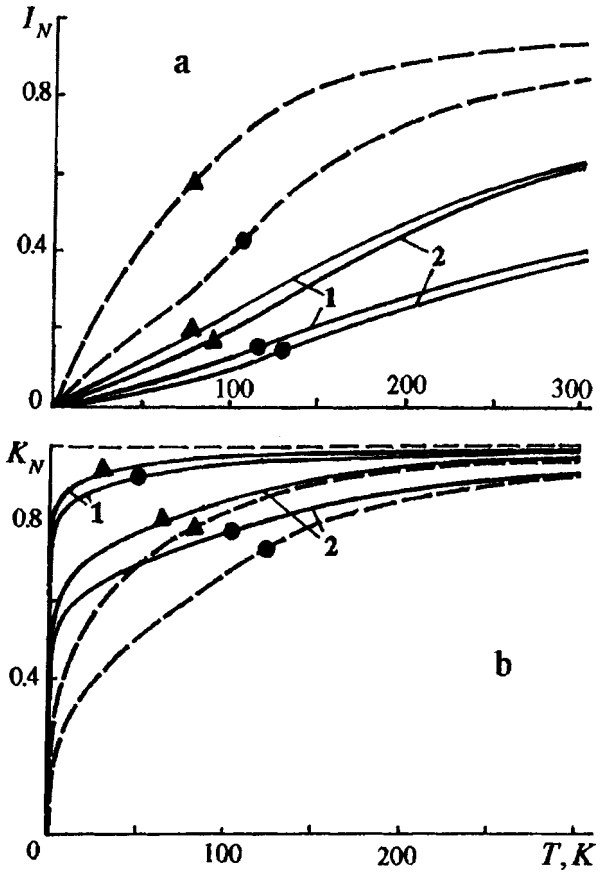

FIG. 1. Temperature dependence of the integrated absorption characteristics I_N (a) and K_N (b) for a heavy-hole exciton 1e−1hh in GaAs/(Al,Ga)As structures with a number of quantum wells $N=1$ (dashed curves) and $N=20$ (solid curves). Curves *1* correspond to $k_0 d=0.4$ ($d\approx 150$ Å), *2*—$k_0 d=3$ ($d\approx 1100$ Å); the filled triangles mark the curves for $\hbar\Gamma_0=0.1$ *meV*, and the filled circles mark the curves for $\hbar\Gamma_0=0.3$ meV. The following parameter values were used: $\hbar\omega_0=1.51$ eV, $\varepsilon_b=12.6$ and $\Gamma=\Gamma_{\rm ph}(T)$, formula (7).

Broadening mechanisms of exciton states in quantum wells, determining in particular the quantity Γ, have been discussed in connection with luminescence spectra.[9] The dependence of the width of the quasi-two-dimensional exciton levels on the temperature T, as for bulk excitons, is governed by the exciton–phonon interaction. The exciton decay mechanism with participation of phonons is universal since theoretically it can be manifested even in heterostructures with ideally planar interfaces and without defects, i.e., when all other possible exciton decay mechanisms are excluded. The phonon contribution to Γ is given by the formula[9]

$$\Gamma_{\rm ph}(T)=C_{\rm ac}T+\Gamma_{\rm op}[\exp(\hbar\Omega_{\rm LO}/k_BT)-1]^{-1}. \qquad (7)$$

For a heavy-hole exciton $1e-1hh$ in GaAs/(Al,Ga)As structures with quantum wells having effective width 200 Å, the parameters in formula (7) are equal to $\hbar C_{\rm ac}=1.5\times 10^{-3}$ meV/K for the acoustic and $\hbar\Gamma_{\rm op}=4$ meV and $\hbar\Omega_{\rm LO}=36$ meV for the optical phonons.[9]

The calculated temperature dependence of the integral magnitudes (5) and (6) for solitary quantum wells and structures is plotted in Fig. 1. In the calculation we used the scaling dependence $\Gamma=\Gamma_{\rm ph}(T)$ from Eq. (7) for any quantum-well width L_z, and the parameter Γ_0 is assumed to depend on L_z (Ref. 10), but not on temperature.[6,7] The curves I_1 in the figure show the upper limit for the corresponding dependences $I_N(T)$ with different N, and the curves K_1 show the lower limit for $K_N(T)$. All the curves shown in the figure are qualitative similar: at first they grow monotonically with temperature and then saturate at temperatures defined by the inequality $\Gamma(T)\gg\Gamma_0$. Physically, this means that for $\Gamma(T)<\Gamma_0$ a polariton mechanism of light propagation is manifested which is associated with re-radiation of excitons of the quantum wells as a consequence of their radiative decay. As the temperature is raised, the dissipative mechanism of exciton decay becomes dominant, which renders polariton effects and radiative decay of excitons, defined by the parameter Γ_0, unimportant.

Analysis based on relations (2) and (3) of the ''microscopic'' picture of the formation of Bouguer's law (4) with increase of N shows the following. The spectral functions $\alpha_N(\omega)$ have a sharp minimum near $\omega=\omega_0$ which is asymmetric for $\Gamma(T)<\Gamma_0$ and approaches a Lorentzian for $\Gamma(T)\gg\Gamma_0$ (in the important frequency region $\alpha_N>\alpha_{N'}$ if $N>N'$). As $N\to\infty$, the quantities $\alpha_N(\omega)$ tend to $\tilde{\alpha}(\omega)$, where the character of this convergence depends substantially on ω and $k_0 d$. Qualitatively, these and similar conclusions pertaining to the two quantities $A_N(\omega)$ and I_N are valid both for short-period ($k_0 d\ll 1$) and for long-period ($k_0 d\leqslant\pi$) structures. In the latter case a quasi-macroscopic description of exciton electrodynamics on the basis of an effective dielectric constant is impossible, i.e., the given theory is in essence microscopic. The theoretical curves shown in the figure of the total exciton absorption in quantum-well structures are in qualitative agreement with the results of experiment.[3–5] Although formally these dependences are the same as for bulk excitons,[2] their physical nature is different: for quantum-well structures we have neglected the effects of spatial dispersion which lie at the basis of the temperature dependence of absorption by bulk excitons. To summarize, we have established that the decrease in the total exciton absorption at low temperatures in quantum-well structures is due to a competition between the processes of dissipative decay of excitons and the light–exciton interaction. In bounded periodic structures radiative decay of quasi-two-dimensional excitons of a quantum well plays a double role: it leads to the formation of the polariton dispersion law via the mechanism of exciton re-radiation and to true radiative decay of excitons, resulting in the escape of an emitted photon from the system. Escape of photons from the system is impossible for $N=\infty$, but for small N it is strongly manifested as a violation of Bouguer's law (3) at low temperatures, where dissipative decay is weak. It may be expected that an account of additional mechanisms of homogeneous and inhomogeneous broadening of exciton levels can lead to an effective increase in the low-temperature part of the total absorption;[5] however, a correct description of this effect is lacking at present.

[1)] These quantities are defined in Ref. 8.

[1] R. Loudon, J. Phys. A **3**, 233 (1970).
[2] A. S. Davydov, *Theory of the Solid State* [in Russian] (Moscow, 1976); N. N. Akhmediev, Zh. Eksp. Teor. Fiz. **79** 4(10), 1534 (1980) [Sov. Phys.

JETP **52**, 773 (1980)]; G. Battaglia, A. Quattropani, and P. Schwendimann, Phys. Rev. B **34**, 8258 (1986); G. N. Aliev, O. S. Koshchug, and R. P. Seĭsyan, Fiz. Tverd. Tela **36**, 373 (1994) [Phys. Solid State **36**, 203 (1994)].
[3] V. A. Kosobukin, R. P. Seisyan, and S. A. Vaganov, Semicond. Sci. Technol. **8**, 1235 (1993).
[4] W. Z. Shen, S. C. Shen, W. G. Tang, S. M. Wang, and T. G. Andersson, J. Appl. Phys. **78**, 1178 (1995).
[5] G. N. Aliev, V. A. Kosobukin, N. V. Luk'yanova, M. M. Moiseeva, R. P. Seisyan, H. Gibbs, and G. Khitrova, Inst. Phys. Conf. Ser. IOP Publishing Ltd (1997), N 155, Ch. 2, p. 165.
[6] E. L. Ivchenko, Fiz. Tverd. Tela **33**, 2388 (1991) [Sov. Phys. Solid State **33**, (1991)].
[7] V. A. Kosobukin, Fiz. Tverd. Tela **34**, 3107 (1992) [Sov. Phys. Solid State **34**, 1662 (1992)]; **37**, 3694 (1995) [Phys. Solid State **37**, 2036 (1995)].
[8] *Physical Encyclopedia* [in Russian], Moscow (1992), Vol. 3.
[9] J. Lee, E. S. Koteles, and M. O. Vassell, Phys. Rev. B **33**, 5512 (1986).
[10] E. L. Ivchenko, V. P. Kochereshko, P. S. Kop'ev, V. A. Kosobukin, I. N. Uraltsev, and D. R. Yakovlev, Solid State Commun. **70**, 529 (1989).

Translated by Paul F. Schippnick

Raman spectroscopy of resonance exciton tunneling in GaAs/AlAs superlattices in electric fields

V. F. Sapega

A. F. Ioffe Physicotechnical Institute, Russian Academy of Sciences, 194021 St. Petersburg, Russia

T. Ruf and M. Cardona

Max Planck Institute of Solid State Physics, Germany

H. T. Grahn and K. Ploog

Paul Drude Institute of Solid State Electronics, Germany

Fiz. Tverd. Tela (St. Petersburg) **40**, 827–829 (May 1998)

Optical-resonance-Raman scattering by acoustic phonons is used to study the effect of an electric field on the state of excitons in GaAs/AlAs superlattices. When the energy of the exciting photon coincides with the energy of an exciton bound to Wannier–Stark states of a heavy hole and electron with $\Delta n = 0, \pm 1$, the acoustic Raman scattering is enhanced. Oscillations in the intensity of the Raman spectrum in the electric field are explained by resonance delocalization of the exciton ground state as it interacts with Wannier–Stark states of neighboring quantum wells or with Wannier–Stark states of a higher electron miniband. © *1998 American Institute of Physics.* [S1063-7834(98)01505-6]

The electric-field induced localization of the wave functions of electronic states in solids (Wannier–Stark localization) has been under active study, both theoretically[1–3] and experimentally. Only with the creation of semiconductor superlattices, however, has it become possible to observe this phenomenon experimentally. Wannier–Stark localization and the so-called Stark ladder of electronic states in an electric field have been studied by photocurrent spectroscopy, photoluminescence excitation,[4] and electroreflection.[5] It has been reported that electric fields do affect the Raman scattering of light by optical phonons[6,7] and effects owing to resonance tunneling have been observed.[8]

In this paper resonance-Raman scattering of light on acoustic phonons is used to study the effect of an electric field on the exciton ground state in a superlattice. (Results from this study have been reported previously.[9,10])

The experiments used the same sample (a GaAs/AlAs superlattice with 60 periods of (70/9) Å) as in the experiments of Schneider *et al.*,[11] and the measurements were made at $T = 15$ K. The pump intensity of the tuneable cw Ti-sapphire laser was $1-2.5$ W/cm^{-2}.

The resonances owing to the Stark levels were determined with a method we have used before for studying Landau levels.[12,13] At each excitation energy, the spectrometer was used as a filter whose transmission passband was shifted into the Stokes region by 6 cm^{-1}. The intensity of the scattered light was measured as a function of the electric field under these conditions. Electro-Raman spectra of this sort are sensitive to all the electronic states satisfying the conditions for an input or output resonance in a Raman scattering process. The advantage of optical scattering by acoustic phonons is that the resonances are studied for small Raman shifts. Thus, it is possible to study individual resonances in great detail. Furthermore, the conditions for a double resonance are almost satisfied for phonons with energies lower than the homogeneous broadening, so that there is a substantial increase in the intensity of the scattered light.[14]

Figure 1 shows some typical electro-Raman spectra measured with different excitation energies relative to the lowest miniband transition. One can distinguish three kinds of resonances in these spectra. The peaks denoted by $n = +1$ in Fig. 1a move to higher fields as the excitation energy E_{ex} is raised. Similar peaks ($n = -1$) are also observed for excitation energies below 1.610 eV. However, they move toward lower energies. Their slopes are $+0.76$ meV/(kV/cm) and -0.94 meV/(kV/cm), respectively. These resonances were interpreted as transitions between Wannier–Stark states of heavy holes and electrons localized in neighboring quantum wells, i.e., transitions with $n = \pm 1$.

The intensity of the continuous Raman spectra is substantially larger in high electric fields. A typical electro-Raman spectrum is shown in Fig. 1b. In this spectrum, one can see distinct drops in intensity (indicated in Fig. 1b by numbers with asterisks) against the background of a broad resonance peak. A comparison with theoretical calculations and the data of Ref. 11 shows that these minima in the electro-Raman spectra occur when an $n = 0$ exciton state is delocalized owing to anticrossing with $n = -6, ..., -2$ Wannier–Stark states (indicated by asterisks) originating from the next, higher miniband. Three of the observed resonances ($n = -2^*, -3^*, -4^*$ in Fig. 1b) coincide with those observed before[11] in photogalvanic experiments with this structure. The interaction of the exciton state ($n = 0$) with the

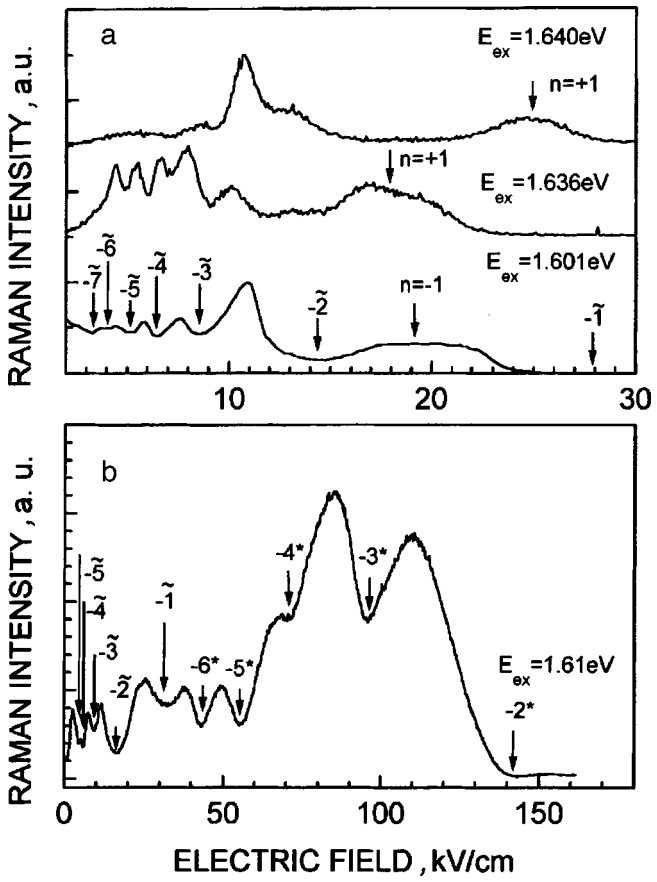

FIG. 1. Electro-Raman spectra of a GaAs/AlAs superlattice for different excitation energies E_{ex}. The peaks denoted by $n=\pm 1$ correspond to resonance-Raman scattering involving transitions between Wannier–Stark states. The oscillations at low fields (minima, denoted by numbers with tildes) are caused by resonance delocalization of an exciton state as it interacts with states in the miniband continuum. The minima at high fields (numbers with asterisks in b) are caused by interactions with Wannier–Stark levels of a higher-lying electron miniband.

Wannier–Stark states of the higher miniband facilitates electron tunnelling between quantum wells. This leads to a reduction in the exciton lifetime in the $n=0$ state. It has been shown[15] that the intensity of the Raman process is related to the dephasing time (lifetime) of the exciton state, which emerges as an intermediate state. Thus, the lower lifetime of the electron in the $n=0$ state causes a reduction in the intensity of the Raman process, which shows up in the spectrum as dips in the intensity of the broad resonance profile.

We now consider the reasons for the oscillations in the intensity of Raman scattering at low fields (indicated by numbers with tildes). The characteristic intensity oscillations in the Raman spectrum in the figure at fields below 15 kV/cm is observed when the excitation energy is either greater than or less than, by 20 meV, the energy between the lowest states of the electron and hole minibands.

It has been shown that in bulk GaAs the exciton state with binding energy $E_{exc}=4.2$ meV is easily ionized, even in rather low electric fields $F=1$ kV/cm.[16] The probability of ionization of an exciton in an external electric field originates in a nonsymmetric reduction in the Coulomb potential and, therefore, increases monotonically as the field F is raised. In a superlattice the situation is obviously more complicated, since the exciton continuum is a miniband consisting of a large number of delocalized wave functions. An electric field splits the continuum state into a discrete set of Wannier–Stark states which are localized in the corresponding quantum wells. These states, however, extend over several periods, so they can interact with similar states localized in other quantum wells. This interaction becomes important when the level energies are close.[17] The interaction of the electron or hole component of the wave functions of excitons localized in different isolated quantum wells leads to resonance tunnelling. These are the resonances which appear as oscillations in the Raman and photoluminescence intensities and they explain the behavior of the low-field electro-Raman spectra shown in the figure. The intensity minima (labelled by numbers with tildes in the figure) are caused by resonance delocalization of an exciton, which has been localized by fluctuations in the widths of the quantum wells, as it interacts with the states of a miniband exciton continuum that has been split by the electric field. This effect has recently been examined theoretically.[18]

In the electro-Raman spectra of the figure there are minima between 3 and 25 kV/cm (numbers with tildes) owing to the interaction of a localized exciton with states that have been localized in the nearest seven quantum wells. The minima $n=-\tilde{1},\ldots,-\tilde{7}$ in an electro-Raman spectrum taken at 1.601 eV were observed at fields of 28, 14.5, 8.5, 6.5, 5.1, 4.0, and 3.2 kV/cm, respectively. Given that the center of the miniband lies at an energy of 1.623 eV and the slopes of the Stark states $n=-1$ and 0 are -0.94 and -0.09 meV/(kV/cm), respectively, we can calculate the location of the resonances using the relation $E=neFd$. The resonances calculated in this way should be observed at fields of 25.9, 12.9, 8.6, 6.5, 5.2, 4.3, and 3.7 kV/cm, in good agreement with the experimental values.

The authors thank D. N. Mirlin and B. P. Zakharchenya for useful discussions and A. Fischer for preparing the samples.

V.F.S. was supported financially by the Volkswagen Foundation (Grant No. 1/70958) and the Max-Planck-Gesellschaft.

[1] G. H. Wannier, *Elements of Solid State Theory*, Cambridge Univ. Press, London (1959); G. H. Wannier, Phys. Rev. **117**, 432 (1960).
[2] R. F. Kazarinov and R. A. Suris, Fiz. Tekh. Poluprovodn. **6**, 148 (1972) [Sov. Phys. Semicond. **6**, 120 (1972)].
[3] J. Bleuse, G. Bastard, and P. Voisin, Phys. Rev. Lett. **60**, 220 (1988).
[4] E. E. Mendez, F. Agulló-Rueda, and J. M. Hong, Phys. Rev. Lett. **60**, 2426 (1988).
[5] P. Voisin, J. Bleuse, C. Bouche, S. Gaillard, C. Alibert, and A. Regreny, Phys. Rev. Lett. **61**, 1639 (1988).
[6] F. Agulló-Rueda, E. E. Mendez, and J. M. Hong, Phys. Rev. B **38**, 12720 (1988).
[7] A. J. Shields, C. Traller-Giner, M. Cardona, H. T. Grahn, K. Ploog, V. A. Haisler, D. A. Tenne, N. T. Moshegov, and A. I. Toropov, Phys. Rev. B **46**, 6990 (1992).
[8] A. J. Shields, M. Cardona, H. T. Grahn, and K. Ploog, Phys. Rev. B **47**, 13922 (1993).
[9] V. F. Sapega, T. Ruf, M. Cardona, H. T. Grahn, and K. Ploog, in *Proceedings of the 23rd International Conference on the Physics of Semiconductors*, edited by M. Scheffler and R. Zimmerman, World Scientific, Singapore (1996), p. 1778.

[10] V. F. Sapega, T. Ruf, M. Cardona, H. T. Grahn, and K. Ploog, Phys. Rev. B **56**, 1041 (1997).
[11] H. Schneider, H. T. Grahn, K. von Klitzing, and K. Ploog, Phys. Rev. Lett. **65**, 2720 (1990).
[12] V. F. Sapega, V. I. Belitsky, T. Ruf, H. D. Fuchs, M. Cardona, and K. Ploog, Phys. Rev. B **46**, 16005 (1992).
[13] G. Goldoni, T. Ruf, V. F. Sapega, A. Fainstein, and M. Cardona, Phys. Rev. B **51**, 14542 (1995).
[14] T. Ruf, V. I. Belitsky, J. Spitzer, V. F. Sapega, M. Cardona, and K. Ploog, Phys. Rev. Lett. **71**, 3035 (1993).
[15] J. E. Zucker, A. Pinczuk, D. S. Chemla, and A. C. Gossard, Phys. Rev. B **35**, 2892 (1987).
[16] D. C. Reynolds and T. C. Collins, in *Excitons*, Academic, N.Y. (1981), p. 1138.
[17] A. M. Fox, D. A. Miller, G. Livescu, J. E. Cunningham, and W. Y. Jan, Phys. Rev. B **44**, 6231 (1991).
[18] M. M. Dignam and J. E. Sipe, Phys. Rev. B **43**, 4097 (1991).
[19] F. Agulló-Rueda, J. A. Brum, E. E. Mendez, and J. M. Hong, Phys. Rev. B **41**, 1676 (1990).

Translated by D. H. McNeill

Exciton spectra of semiconductor superlattices in a parallel magnetic field

N. N. Sibel'din, M. L. Skorikov, and V. A. Tsvetkov

P. N. Lebedev Physics Institute, Russian Academy of Sciences, 117924 Moscow, Russia

Fiz. Tverd. Tela (St. Petersburg) **40**, 830–832 (May 1998)

Low-temperature photoluminescence and photoluminescence excitation spectra of GaAs/AlGaAs semiconductor superlattices having different potential barrier widths ($b=20$, 30, 50, and 200 Å), i.e., degrees of tunnel coupling between quantum wells, are studied in magnetic fields up to 5 T oriented parallel and perpendicular to the layers of the structure. The changes in the qualitative character of the photoluminescence excitation spectra observed in a parallel magnetic field with increasing tunnel transparency of the barrier correspond to a transition from a quasi-two-dimensional to a quasi-three-dimensional electronic spectrum as a miniband develops in the superlattice. In the photoluminescence excitation spectra of the superlattice with $b=50$ Å, as the parallel magnetic field is increased, a new line appears in the violet wing of the spatially indirect exciton excitation line, which is absent in a perpendicular field. A similar line was also observed to arise in the photoluminescence spectra. It is shown that the indirect exciton luminescence line can be suppressed by both parallel and perpendicular magnetic fields. © *1998 American Institute of Physics.* [S1063-7834(98)01605-0]

1. The properties of excitons in symmetric arrays of bound quantum wells and superlattices are of great interest and it is not by chance that they have drawn the interest of researchers in recent years. It is known that there is a transition from a two dimensional to a three dimensional exciton behavior with increasing tunnel transparency of the barriers.[1] The nature of the excitons in these systems depends on the relationship between the exciton binding energy E_{ex} and the total width Δ of the electron and hole minibands. In particular, when $\Delta < E_{ex}$, spatially indirect excitons formed by electrons and holes located in neighboring quantum wells can develop in a superlattice.[2]

The relationship between E_{ex} and Δ in a superlattice can be controlled by acting on the structure with a magnetic field. A magnetic field oriented perpendicular to the plane of the structure increases the binding energy of an exciton without affecting the single-particle superlattice states.

A magnetic field parallel to the layers of the structure changes the one-electron states and the energy spectrum of the superlattice radically.[3] In weak fields, the superlattice acts as a bulk crystal with an anisotropic effective mass: the miniband breaks up into Landau subbands. In fields exceeding $H^*=(\hbar c/ea^2)\cdot(m/M)^{1/2}$ (where m is the effective mass in the plane of a quantum well, $M\cong 2\hbar^2/a^2\Delta$ is the effective mass along the superlattice axis, and a is the superlattice period), the miniband is destroyed and the superlattice breaks up into isolated quantum wells.

2. In this paper we study $GaAs/Al_{0.3}Ga_{0.7}As$ superlattices with quantum well widths $w=80$ Å and barrier widths $b=20$, 30, 50, and 200 Å. Photoluminescence was excited using a tuneable cw Ti-sapphire laser. It was also used to measure the photoluminescence excitation spectra; here the radiation corresponding to the long wavelength wing of the heavy-hole exciton luminescence line was detected. All the measurements were made at a temperature of 2 K.

3. The general features of the photoluminescence excitation spectra of all the samples include intense lines associated with transitions to the ground state of heavy- and light-hole excitons (HH and LH, respectively, in Fig. 1). In most of the spectra, there is also a fairly sharp edge to the continuous spectrum owing to absorption in interband transitions of electrons from heavy-hole bands. As a rule, a transition to the first excited state of an HH-exciton occurs only in a magnetic field.

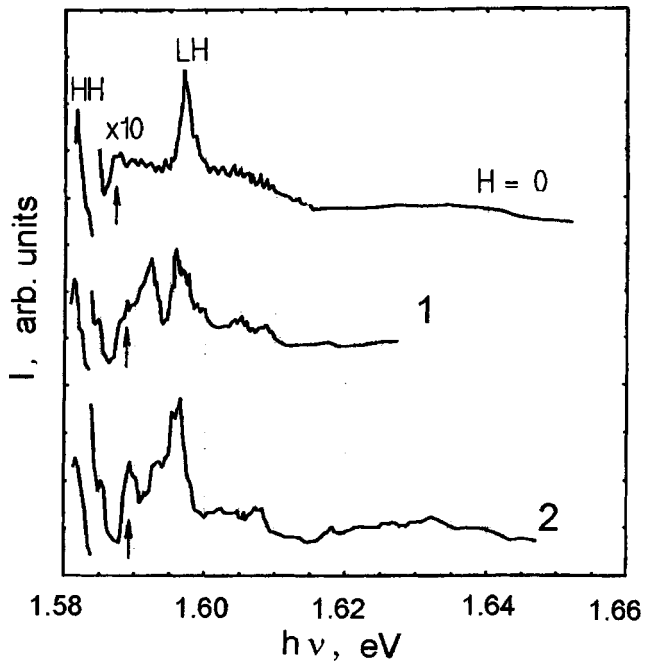

FIG. 1. Photoluminescence excitation spectra of a superlattice with $b=20$ Å in magnetic fields $H=51$ kOe parallel (*1*) and perpendicular (*2*) to the layers. The arrows denote the $2s$ lines of the HH exciton.

A parallel magnetic field has no noticeable effect on the photoluminescence excitation spectrum of the sample with $b=200$ Å, since the quantum wells are isolated from one another owing to the low tunnel transparency in this sample, while the magnetic length $l<w$ over the entire range of magnetic fields. In a field directed along the growth axis of the structure, the photoluminescence excitation spectrum has the customary form corresponding to the spectrum of quasi-two dimensional magnetoexcitons. In this case, at sufficiently high fields, the variation with increasing field in ΔE, the energy separation between the first excited ($2s$) and ground ($1s$) states of the direct HH-exciton (Fig. 2), mainly reflects the change in the splitting between the two lowest Landau levels.

As the barrier thickness is reduced, the influence of a parallel magnetic field on the photoluminescence excitation spectra grows. In the samples with $b=30$ and 20 Å, the excitons are quasi-three-dimensional, as indicated by the qualitatively similar behavior of the photoluminescence excitation spectra in parallel and perpendicular magnetic fields (Fig. 1) and the roughly identical variation in ΔE with increasing field (Fig. 2).

The condition $H>H^*$ is apparently satisfied reliably only for the superlattice with $b=50$ Å within the magnetic field range studied here. (An estimate for $b=20$ Å gives $H^*\approx 7$ *T*.) In this sample, however, the excitons are essentially quasi-two-dimensional, even without a field ($E_{ex}>8$ meV), and the observed changes in the photoluminescence excitation spectra in a parallel field do not yet allow us to judge the further two-dimensionality (destruction of the miniband) of the electron spectrum of this superlattice.

4. Lines associated with spatially indirect (I) HH excitons were observed in the photoluminescence excitation and photoluminescence spectra of the samples with $b=30$ and 50 Å, as well as the direct (D) exciton lines.[2]

In the photoluminescence excitation spectra of the sample with $b=50$ Å, the I exciton line (like the spectrum as a whole) was not displaced noticeably in a magnetic field parallel to the layers, but a new line appears in its high-energy wing, which exceeds the original I line in intensity at

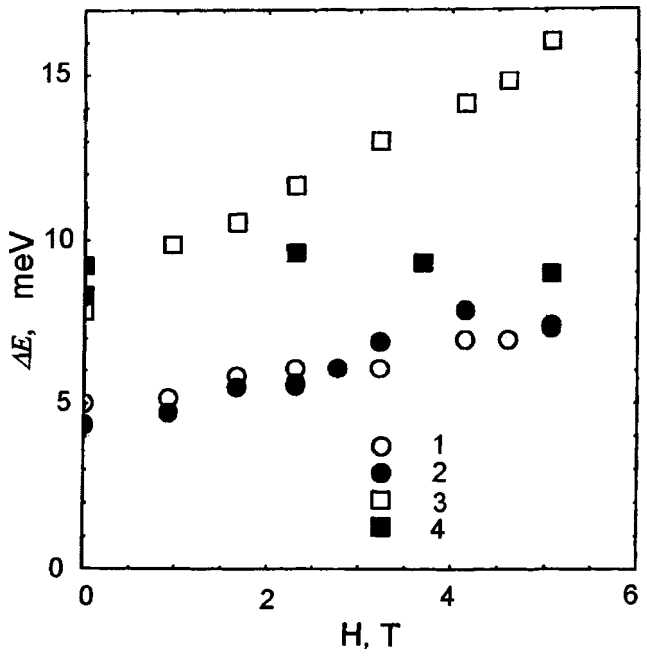

FIG. 2. The energy separation between the first excited and ground states of the direct HH exciton as a function of the magnetic field in samples with $b=20$ (*1,2*) and 200 Å (*3,4*) for field orientations parallel (*2,4*) and perpendicular (*1,3*) to the layers.

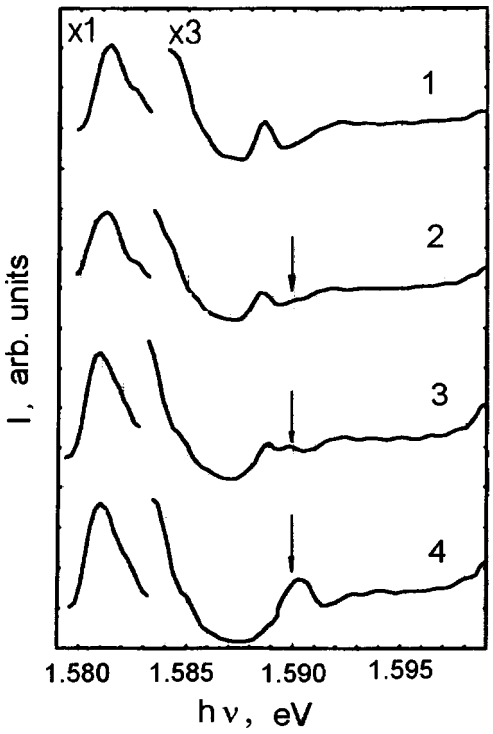

FIG. 3. The appearance of a new line (indicated by an arrow) in the photoluminescence excitation spectrum of a sample with $b=50$ Å as the parallel magnetic field is increased. $H_{\parallel}$(kOe): 0 (*1*), 23 (*2*), 32 (*3*), 51 (*4*).

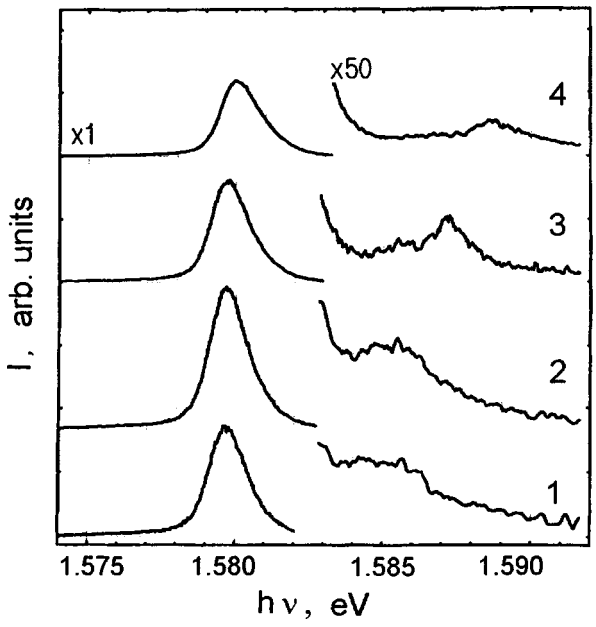

FIG. 4. Luminescence spectra of a superlattice with $b=30$ Å in a parallel magnetic field. $H_{\parallel}$(kOe): 0 (*1*), 9 (*2*), 32 (*3*), 51 (*4*).

high fields (Fig. 3). In a perpendicular field, as its strength increases the I line is shifted to higher energies,[2] but no new line flares up.

In the photoluminescence spectra of this sample taken in parallel and perpendicular fields, the I-exciton line shifts to higher energies, broadens, and falls off in intensity by several times.

In the photoluminescence spectra of the sample with $b=30$ Å, the I-exciton line in zero field is scarcely visible in the short wavelength wing of the main D line. As the strength of the magnetic field parallel to the layers is increased, the I line initially increases in intensity and yet another emission line shows up in its high-energy wing (Fig. 4). With further increases in the field, both these lines fall off in intensity, so that only the shortest wavelength component remains in the spectrum at the highest fields, along with the D line. In a perpendicular field, the analogous phenomena in the photoluminescence spectrum are much less distinct.

This work was supported by the Russian Fund for Fundamental Research (Project No. 96-02-18237) and the Minister of Science of the Russian Federation in the framework of the Programs on the Physics of Solid State Nanostructures (Project No. 97-1050) and Fundamental Spectroscopy (Project No. 2.6).

[1] A. Chomette, B. Labmert, B. Deveaud, F. Clerot, A. Regreny, and G. Bastard, Europhys. Lett. **4**, 461 (1987).
[2] A. I. Tartakovskiĭ, V. B. Timofeev, V. G. Lysenko, D. Birkedal, and J. Hvam, Zh. Éksp. Teor. Fiz. (1997), to be published.
[3] A. M. Berezhkovskiĭ and R. A. Sirius, Zh. Éksp. Teor. Fiz. **86**, 193 (1984) [Sov. Phys. JETP **59**, 109 (1984)].

Translated by D. H. McNeill

Direct and spatially indirect excitons in GaAs/AlGaAs superlattices in strong magnetic fields

V. B. Timofeev, A. I. Tartakovskiĭ, and A. I. Filin

Institute of Solid State Physics, Russian Academy of Sciences, 142432 Chernogolovka, Moscow District, Russia

D. Birkedal and J. Hvam

Microelectronic Center, The Technical University of Denmark, DK 2800 Lyngby, Denmark

Fiz. Tverd. Tela (St. Petersburg) **40**, 833–836 (May 1998)

Luminescence and luminescence excitation spectra are used to study the energy spectrum and binding energies of direct and spatially indirect excitons in GaAs/AlGaAs superlattices having different electron and hole miniband widths in high magnetic fields perpendicular to the heterolayers. The ground state of the indirect excitons formed by electrons and holes which are spatially distributed among neighboring quantum wells is found to lie between the ground $1s$ state of the direct excitons and the threshold of the continuum of dissociated exciton states in the minibands. The indirect excitons have a substantial oscillator strength when the binding energy of the exciton exceeds the scale of the width of the resulting miniband. It is shown that a high magnetic field shifts a system of symmetrically bound quantum wells toward weaker bonding. At high exciton concentrations, spatially indirect excitons are converted into direct excitons through exciton-exciton collisions. © *1998 American Institute of Physics.* [S1063-7834(98)01705-5]

1. Exciton properties are at the center of scientific interest in studies of optical and electronic phenomena in superlattices based on semiconducting heterostructures.[1–10] This interest, in particular, involves spatially indirect excitons, for which the electron and hole are localized in neighboring quantum wells separated by a barrier. This sort of Wannier-Stark localization of the electrons and holes has been discovered and studied[9,10] in sufficiently high electric fields perpendicular to the superlattice layers. Spatially indirect excitons can exist in a superlattice, even without destruction of the inversion symmetry, but their localization within the confines of a superlattice period is of Coulomb origin in this case. A magnetic field (B) perpendicular to the superlattice layers has a significant effect on the exciton states: it increases the splitting between the ground states of the direct and spatially indirect excitons and, thereby, for fixed tunnel coupling in the superlattices, shifts the symmetry of the bound system of quantum wells toward weaker bonding.

In this paper, using GaAs/AlGaAs superlattices as an example, it is shown that indirect excitons are formed in symmetrically bound quantum systems when an inversion center is present. For this purpose, we have studied the energy spectrum of direct and spatially indirect excitons in superlattices as the width of the barrier between the quantum wells is varied. Using a sufficiently strong magnetic field, which enhances the Coulomb bonding in the excitons, made it possible to modify the character of the bonding in superlattices having a fixed barrier size.

In this work we have used superlattices grown on the basis of GaAs/AlGaAs ($x=0.3$) heterostructures by molecular beam epitaxy on an insulating GaAs substrate oriented along the crystallographic [001] direction. Five superlattices were studied with the same GaAs quantum-well thickness, $L_w=80$ Å, but different widths of the AlGaAs barrier between the wells, $L_b=20$, 30, 50, 100, and 200 Å.

2. In the superlattices whose barriers $L_w=50$ Å or less, a new line, $I(1sHH)$, can be seen distinctly in the luminescence excitation spectra between the direct heavy-hole exciton lines $1sHH$ and $2sHH$; it is not associated with the direct exciton spectrum (Figs. 1 and 2). In the superlattices with narrow barriers, this line corresponds to the ground state of a heavy hole exciton with a spatially distributed electron and a hole at a distance corresponding to a single superlattice period. Thus, in this case, we are speaking of a spatially indirect exciton, which is localized in the axial direction within a single superlattice period. Unlike Wannier-Stark localization, in this case the localization is exclusively of Coulomb origin. The indirect exciton state is more weakly bound than the corresponding direct exciton state. The highest oscillator strength of the I exciton occurs in superlattices with an intermediate tunnel bonding. Thus, in an 80/30/80 superlattice (Fig. 2), the oscillator strength of the indirect exciton is about 10% that of a heavy-hole direct exciton. As the barrier width is reduced ($L_b=20$ Å and below), the wave function of the indirect exciton extends ever further in the z-direction and may encompass several superlattice periods. In this limit, the indirect exciton state becomes ever more delocalized and, ultimately, merges with the continuum of dissociated states of the direct excitons.[4] Figure 3 shows how the binding energy of an indirect exciton behaves, as well as its oscillator strength measured relative to a direct exciton, when the bar-

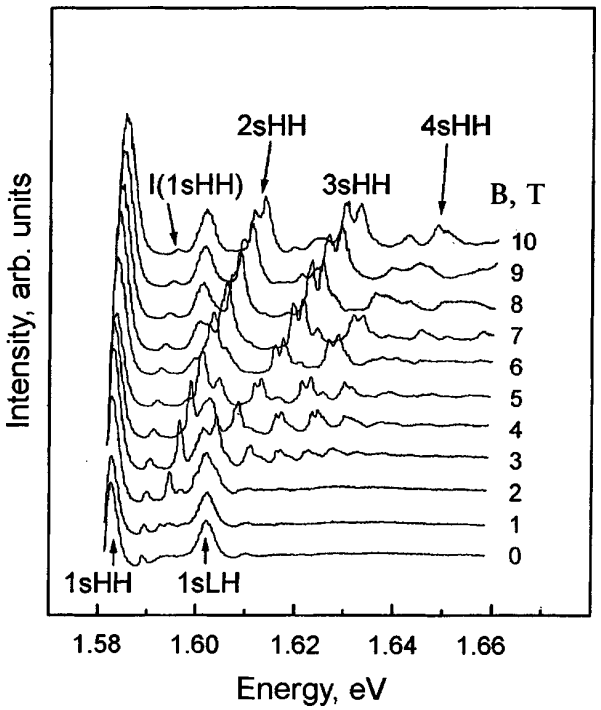

FIG. 1. Luminescence excitation spectra of an 80/50/80 superlattice in a magnetic field.

rier size is changed. It is clear that for superlattices with quantum-well widths $L_w = 80$ Å, the optimal conditions for observing spatially indirect excitons occur for quantum barrier widths of about 30 Å.

Figures 1 and 2 show luminescence excitation spectra for superlattices with barriers $L_b = 50$ and 30 Å, measured in magnetic fields with a step size of 1 T. The strongest lines in these spectra are those of the $1sHH$- and $1sLH$-direct excitons. As the magnetic field increases, these exciton states undergo a diamagnetic shift whose magnitude is greater for a heavy hole exciton, since this state is more weakly bound than the $1sHH$ exciton. As the barrier width is reduced ($L_b = 30$, 20 Å), the diamagnetic shift of the $1sLH$ exciton is essentially zero, since the effect of the superlattice is largest for the exciton states with light holes.

Besides the ground states of the direct excitons, magnetoexcitons corresponding to higher Landau states ($N > 1$) were observed in the luminescence excitation spectra. Only those magnetoexcitons which represent bound states of a electron and hole belonging to the same diamagnetic quantization level are optically active in the spectra (Figs. 1 and 2).

Let us consider the diamagnetic properties of the direct and indirect excitons. The diamagnetic corrections to the energy of the ground state of the spatially indirect exciton are almost a factor of two greater than for the $1sHH$ exciton and much lower than for the $2sHH$ exciton. This correction is roughly 45 μV/T^2 in the 80/50/80 superlattice. Thus, it is evident that the $I(HH)$ exciton has no connection with any excited states of the direct excitons. We conclude that the $I(HH)$ line corresponds to the ground, $1s$ state of an indirect exciton with spatially separated electron and hole in the confines of a single lattice period.

3. Spatially indirect excitons are also observed in the luminescence spectra (Fig. 4). The indirect exciton line, $I(1sHH)$, lines in the spectrum between the spatially direct excitons $D(1sHH)$ and $D(2sHH)$. It is clear that the indirect excitons are not in thermal equilibrium with the direct

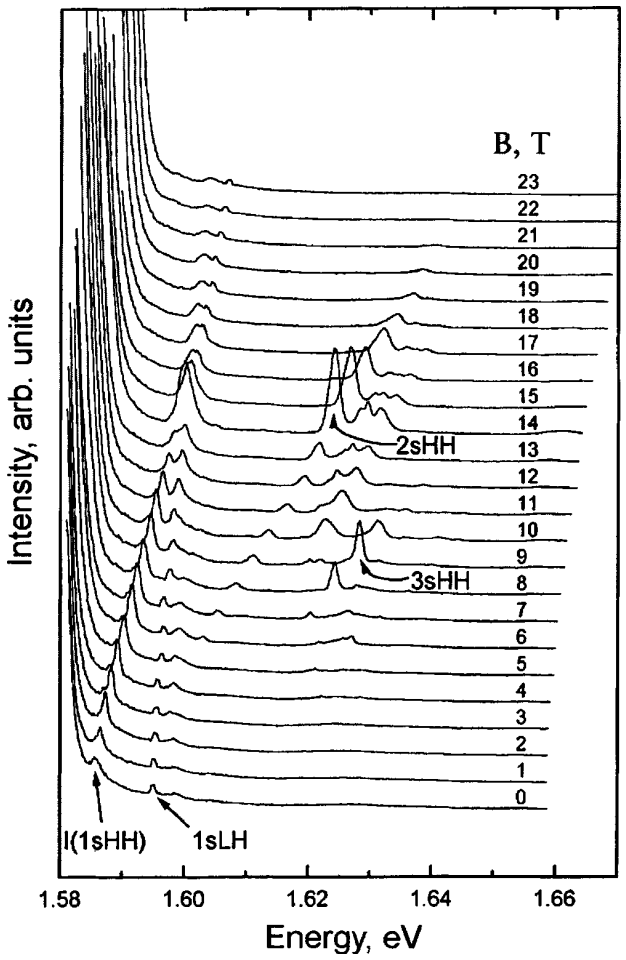

FIG. 2. Luminescence excitation spectra of an 80/30/80 superlattice in a magnetic field for circular polarization σ^+.

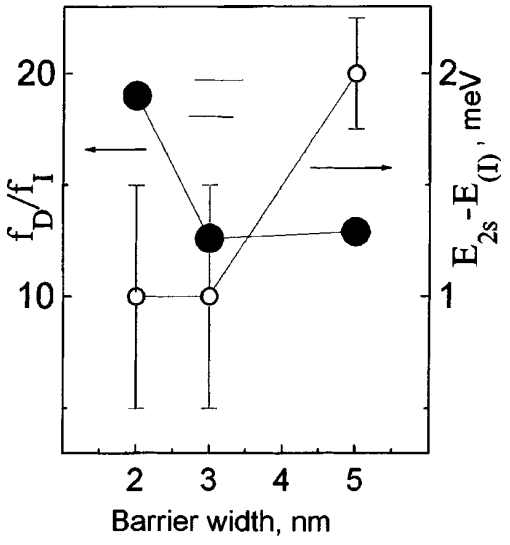

FIG. 3. The behavior of the binding energy and oscillator strength of an indirect exciton as the barrier width in the superlattice is changed.

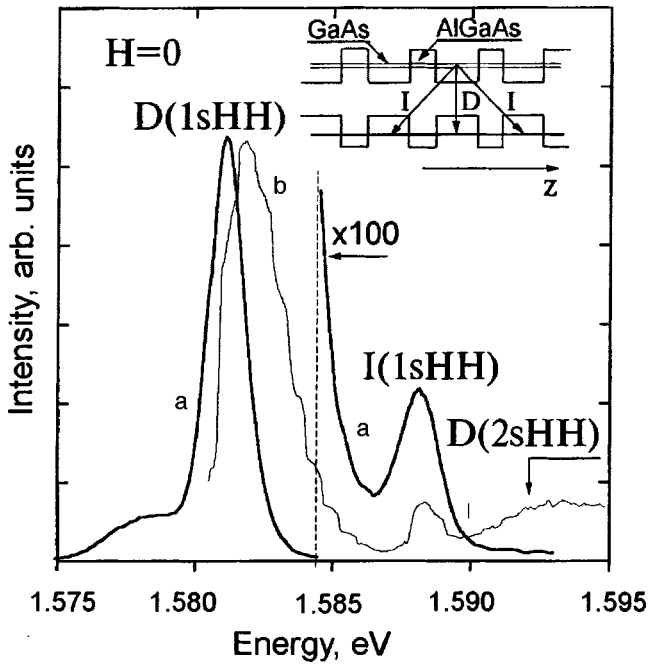

FIG. 4. A photoluminescence spectrum (curve *a*) and a fragment of a photoluminescence excitation spectrum (curve *b*) of heavy hole excitons.

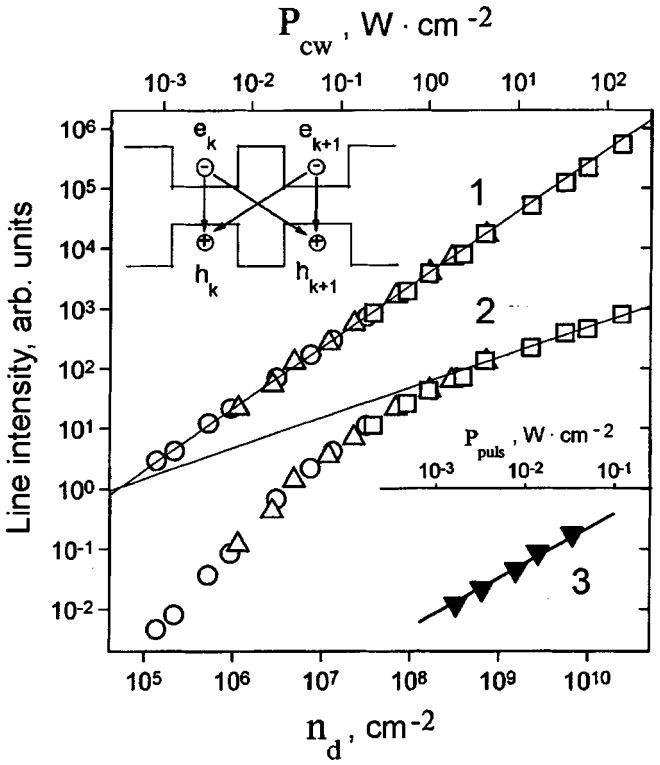

FIG. 5. The intensity of luminescence lines of direct (*1*) and indirect (*2*) excitons as functions of the concentration of direct excitons and (*3*) the behavior of the line intensity of an indirect exciton with pulsed excitation on the same concentration scale. The upper horizontal scale is the power density of the exciting radiation and the lower scale is the concentration of direct excitons. The inset illustrates the scheme for conversion of indirect into direct excitons.

excitons, and the actual population of the indirect exciton states at $T=1.5$ K is many orders of magnitude greater than the thermal equilibrium value. (Under these conditions, there is no excitation of the direct exciton state, $D(2sHH)$, in the photoluminescence spectra.) Such slow relaxation of an indirect exciton into a direct exciton during weak, steady-state pumping is explained by nonresonant tunnelling of an electron through the barrier, which is a slow process. The behavior of the luminescence spectra of the direct (D) and indirect (I) excitons as the power density of cw and pulsed excitation is varied is shown in Fig. 5. Clearly, within the dynamic range studied here, the luminescence intensity of the direct excitons depends linearly on the pump intensity to high accuracy. At the same time, the luminescence of the indirect excitons manifests a clearly nonlinear behavior: a superlinear rise at low excitation levels and a sublinear rise at high levels.

The quenching of the luminescence of the indirect excitons at high pumping levels is explained by inelastic exciton-exciton collision processes. As the concentration of indirect excitons rises, the probability of pairwise collisions between them increases because of a dipole-dipole interaction mechanism with conversion into spatially direct excitons. This process is illustrated schematically in the inset to Fig. 4 and can be written down as follows: $e_k h_{k+1}+e_{k+1}h_k \rightarrow e_k h_k + e_{k+1}h_{k+1}+$photon, where $e_k h_{k+1}$ and $e_{k+1}h_k$ are indirect excitons in the different (k)-th and $(k+1)$-st quantum wells, while $e_k h_k$ and $e_{k+1}h_{k+1}$ are spatially direct excitons. This conversion mechanism does not require tunnelling of an electron or hole under the barrier and is efficient for high densities of indirect excitons.

4. In this paper we have shown that the optimal conditions for observing indirect excitons occur when the Coulomb energy in an exciton exceeds the scale of the electron-hole-miniband width in the superlattice. It is significant that inversion symmetry is not required for observing these states. A strong magnetic field transverse to the heterolayers of the superlattice enhances the Coulomb bonding in the exciton and shifts the system of interacting quantum wells toward weaker bonds.

This work was supported by the Russian Fund for Fundamental Research (Grant 96-02-17535), the Interdepartmental Scientific Program on the Physics of Solid State Nanostructures, and INTAS (Grant 95-IN-RU-576).

[1] H. Chu and Y.-C. Chang, Phys. Rev. B **36**, 2946 (1987).
[2] A. Chomette, B. Lambert, B. Deveaud, F. Clerot, A. Regreny, and G. Bastard, Europhys. Lett. **4**, 461 (1989).
[3] H. Chu and Y.-C. Chang, Phys. Rev. B **39**, 10861 (1989).
[4] D. M. Whittaker, Phys. Rev. B **41**, 3238 (1990).
[5] P. M. Young, H. Ehrenreich, P. M. Hui, and N. F. Johnson, J. Appl. Phys. **74**, 7369 (1993).
[6] B. Deveaud, A. Chomette, F. Clerot, A. Regreny, J. C. Maan, R. Romestain, and G. Bastard, Phys. Rev. B **40**, 5802 (1989).
[7] K. Fujiwara, K. Kawashima, T. Yamamoto, N. Sano, R. Gingolani, H. T. Grahn, and T. Ploog, Phys. Rev. B **49**, 1809 (1994).
[8] K. Fujiwara, Y. Kawashima, T. Yamamoto, and K. Ploog, Solid-State Electron. **37**, 889 (1994).
[9] E. Mendez, F. Agulli-Rueda, and F. Hong, Phys. Rev. Lett. **60**, 3426 (1988).
[10] P. Voisin, J. Bleuse, C. Bouche, S. Gaillard, C. Alibert, and A. Regreny, Phys. Rev. Lett. **61**, 1639 (1988).

Translated by D. H. McNeill

Dynamics of localized excitons in a superlattice grown by molecular-beam epitaxy with submonolayers of CdSe

A. A. Toporov, T. V. Shubina, S. V. Ivanov, S. V. Sorokin, A. V. Lebedev, and P. S. Kop'ev

A. F. Ioffe Physicotechnical Institute, Russian Academy of Sciences, 194021 St. Petersburg, Russia

G. R. Pozina, P. Bergman, and B. Monemar

University of Linköping, S-581 83 Linköping, Sweden

Fiz. Tverd. Tela (St. Petersburg) **40**, 837–838 (May 1998)

The low-temperature photoluminescence spectrum and the recombination dynamics of localized excitons have been studied in a short-period superlattice of CdSe/ZnSe submonolayers. As distinct from structures with isolated submonolayers, which exhibit one narrow photoluminescence peak, the photoluminescence and photoluminescence excitation spectra of a superlattice have two peaks, separated by ~50 meV. The amount of splitting, as well as the temporal characteristics of the damping of the photoluminescence, are interpreted in terms of a model of a disordered superlattice of extended islands, sited randomly in the submonolayers making up the superlattice. © *1998 American Institute of Physics.* [S1063-7834(98)01805-X]

Despite the large number of publications devoted to the fabrication technology and optical properties of quantum-sized heterostructures in the CdSe/ZnSe system,[1] uncertainties about the structural properties of the CdSe/ZnSe interface still evoke a certain amount of disagreement. Based on the narrowness of the photoluminescence line observed in structures with stressed thin layers of CdSe and the anomalous dependence of the line width on the layer thickness (the half width of the peak increases from 5 to 40 meV when the effective thickness of the layer is raised from 0.25 to 2 monolayers), Zhu *et al.*[2] concluded that a spatially uniform layer of ZnCdSe solid solution forms on the interface. An alternative viewpoint assumes that two-dimensional (2D) islands of CdSe are formed in a submonolayer.[3] The narrowness of the photoluminescence line in this case reflects the uniform thickness of the different islands (e.g., exactly 1 monolayer) and their relatively large lateral dimensions. Otherwise, the exciton photoluminescence line would be inhomogeneously broadened owing to fluctuations associated with the size limitation along the growth axis and with a lateral limitation effect in the islands, which are three dimensional quantum dots with a certain size and shape distribution. Inhomogeneous broadening effects of this sort have been observed, for example, in thin ZnS/ZnSe layers, where they produce an exciton photoluminescence line width on the order of 100 meV.[4]

It is difficult to distinguish these two possible submonolayer configurations reliably by only studying the optical characteristics of structures with isolated layers. In fact, the optical properties of uniform layers of ZnCdSe solid solution, as well as of extended 2D islands, are determined primarily by size limitations in the direction of the growth axis, while lateral limitations are unimportant. Thus, the optical spectra will be similar in both cases, with features characteristic of quantum wells. The morphology of the interface, however, may be the decisive factor that determines the properties of the short-period superlattice made up of the submonolayers. For uniform layers of the solid solution, the interaction of electrons in neighboring wells leads to the formation of minibands and, as a consequence, to a shift in the exciton peak toward longer wavelengths, without significant broadening. In the case of randomly positioned planar, extended islands, the disorder determined by the random overlap of the islands in neighboring layers of the superlattice may show up through inhomogeneous spectral broadening and specific localization effects.[5,6]

In this paper, the exciton localization effects are studied in submonolayer CdSe/ZnSe superlattices by cs photoluminescence and photoluminescence excitation spectroscopy, as well as by time resolved photoluminescence spectroscopy. The sample was grown by molecular-beam epitaxy on a substrate of (100) GaAs and included 20 submonolayers of CdSe with a nominal thickness of 0.65 monolayer, separated by 28-Å-thick ZnSe barriers. Samples including single CdSe layers of different thicknesses were also grown. The techniques for growing the samples and calibrating their thicknesses are described in detail elsewhere.[7,8] Photoluminescence spectra with a time resolution on the order of 15 ps were measured using a streak camera after excitation by the frequency doubled output of a mode locked Al_2O_3/Ti laser. Figure 1 shows cw photoluminescence (smooth curve) and photoluminescence excitation (dashed curve) spectra of the sample with a submonolayer superlattice. In distinction from the narrow single-photoluminescence peak observed in the spectra of single layers (not shown here), the photoluminescence and excitation photoluminescence spectra of the submonolayer superlattice reveal two peaks separated by ~50 meV. The general character of these peaks is confirmed by the similarity of their photoluminescence quenching kinetics following excitation by a short pulse. The characteris-

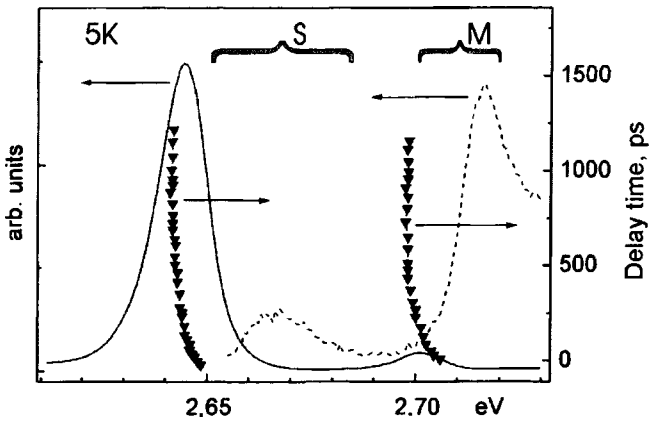

FIG. 1. Cw photoluminescence (smooth curve) and photoluminescence excitation (dashed curve) spectra; the triangles denote the position of the peaks as a function of the detection time delay (scale on the right ordinate).

tic quenching times vary over the line profiles from ~40 ps in the short wavelength wing to ~350 ps in the long wavelength tails, while the energies of the peaks (triangles in the figure) show a shift to longer wavelengths with the detection delay time. This sort of behavior is typical for jump relaxation of localized excitons accompanied by the emission of acoustic phonons.[9,10]

These experimental data cannot be described adequately assuming the formation of uniform solid-solution layers, but they do allow a natural explanation in terms of a disordered superlattice formed by the random positioning of extended planar islands relative to one another. Different local configurations of ''bound'' quantum wells are realized in this kind of superlattice in the direction of the growth axis. A simple estimate for CdSe islands having a thickness of exactly 1 monolayer, in terms of the ''envelopes'' of the functions, neglecting the lateral limitation and the differences in the biding energy of excitons in different configurations, shows that the allowed exciton energies fall into two bands (*S* and *M* bands, indicated by curly brackets in the figure) separated by ~15 meV. The exciton *S* bands correspond to ''strongly bound'' quantum well configurations, separated by a single superlattice barrier, while all the other configurations, which include parts of islands that are essentially isolated from one another, contribute to the *M* band. This description makes it possible to explain all the experimental observations reported above, including the splitting of the exciton band and the characteristic manifestations of the jump relaxation of excitons localized in the random potential from local vertical configurations of extended, planar islands.

Strictly speaking, the good agreement between the proposed model and the experiment only confirms the presence of structural configurational disorder in the sample, while leaving open the question of the exact dimensions of the islands and possible correlations in the positions of the islands in neighboring layers of the superlattice.

This work was supported by the Russian Fund for Fundamental Research and the Program on the Physics of Solid State Nanostructures of the Ministry of Science of the Russian Federation.

[1] K. P. O'Donnell and U. Woggon, Appl. Phys. Lett. **70**, 2765 (1997).
[2] Z. Zhu, H. Yoshihara, K. Takebayashi, and T. Yao, Appl. Phys. Lett. **63**, 1678 (1993).
[3] I. L. Krestnikov, M. V. Maximov, S. V. Ivanov, S. V. Sorokin, S. A. Permogorov, A. N. Reznitsky, A. V. Kornievsky, P. S. Kop'ev, Zh. I. Alferov, N. N. Ledentsov, D. Bimberg, and C. M. Sotomayor Torres, in *Proceedings of the 23rd ICPS (Berlin, 1996). The Physics of Semiconductors*, M. Scheffler and R. Zimmermann (Eds.), World Scientific, Singapore (1996), p. 3187.
[4] T. Yao, M. Fujimoto, S. K. Chang, and H. Tanino, J. Cryst. Growth **111**, 823 (1991).
[5] N. Magnea, J. Cryst. Growth **138**, 550 (1994).
[6] A. Chomette, B. Deveaud, A. Regreny, and G. Bastard, Phys. Rev. Lett. **57**, 1464 (1986).
[7] S. V. Ivanov, S. V. Sorokin, P. S. Kop'ev, J. R. Kim, H. D. Jung, and H. S. Park, J. Cryst. Growth **159**, 16 (1996).
[8] S. Ivanov, S. Sorokin, I. Krestnikov, N. Faleev, B. Ber, I. Sedova, and P. Kop'ev, in *Proceedings of the 8th International Conference on II-VI Compounds*, Grenoble (1997), to be published in J. Cryst. Growth.
[9] L. E. Golub, E. L. Ivchenko, and A. A. Kiselev, J. Opt. Soc. Am. B **13**, 1199 (1996).
[10] U. Neukirch, D. Weckendrup, W. Faschinger, P. Juza, and H. Sitter, J. Cryst. Growth **138**, 849 (1994).

Translated by D. H. McNeill

Carrier statistics in quantum-dot lasers

M. Grundmann, R. Heitz, and D. Bimberg

Institut für Festkörperphysik, Technische Universität Berlin, D-10623 Berlin, Germany

Fiz. Tverd. Tela (St. Petersburg) **40**, 839–842 (May 1998)

The description of quantum-dot ensembles using solely average carrier populations is insufficient. Keeping track of the probablity of all micro states, and solution of the master equations for the transitions between them, allows proper modeling of the phonon bottleneck and laser properties. We predict that a single exciton shows gain and calculate the dependence of threshold current density of the type of capture process. The gain-current relation in quantum-dot lasers is linear. © *1998 American Institute of Physics.* [S1063-7834(98)01905-4]

1. Quantum dots represent a unique electronic system which was recently applied successfully in novel semiconductor lasers [1–4]. The charge carriers populate discrete electronic levels and (at least at sufficiently low temperature) all dots in an ensemble are laterally decoupled from each other. Therefore an event in a quantum dot, e.g., a recombination process, does not depend on the average carrier density (involving all other dots) but only on the particular population of the present dot by electrons and holes.[5] The ensemble has to be averaged over the probability distribution of the different micro states. Different probability distributions of micro states can have the same average carrier population but exhibit different properties like recombination current. In order to illustrate this point with a simple example, we compare two QD ensembles having the same average carrier population: in ensemble I, all electrons are in different dots than the holes: no radiative recombination takes place. In ensemble II, electrons and holes populate the dots in pairs, leading to radiative recombination. We further discuss modeling of the phonon bottleneck effect.

2. Since the epitaxially created self-ordered QDs [6,7] are in a strong confinement regime, it is adequate to model electronic levels in the single-particle picture, i.e., electrons and holes populate single particle levels. Ground-state luminescence is said to originate from the radiative recombination of an electron and a hole in their respective single-particle ground states (exciton). The lifetime of the exciton shall be denoted by τ_X. The Coulomb correlation shall not fundamentally alter that picture. One effect is the shift of recombination energy of the biexciton (two electrons and two holes in their spin-degenerate ground states) with respect to that of the exciton. For InAs/GaAs quantum dots this shift is expected to be small (<2 meV);[8] for II–VI compounds this shift will be larger. The radiative lifetime $\tau_{XX}=\tau_X/2$ (as if two independent exciton decay); shortening of this time by Coulomb interaction is neglected here but could be included in our model.

A micro state represents one particular population of the quantum-dot levels with carriers, e.g., an empty dot (0,0,...), a dot with an electron-hole pair in the ground state (1,0,...), or a dot with an electron-hole pair in the first-excited state (0,1,...). As visualized in Fig. 1, the latter micro state can make two transitions: radiative decay (0,1,...)→(0,0,...) and intersublevel scattering (0,1,...)→(1,0,...). The ensemble state is described by the probability p_n to find a micro-state n in the ensemble of all dots (the total number of dots shall be large), $\Sigma_{\text{all}n}\ p_n=1$. The probability p_n can be also thought of as the time average of the micro states a single dot undergoes during a sufficiently long time interval, i.e., the quantum-dot ensemble is ergodic.

3. The delayed energy relaxation in quantum dots, the so called ''phonon bottleneck'' effect has attracted much attention because of its potentially detrimental impact on performance in high-speed devices. From time resolved experiments with resonance exciton of excited zero-dimensional states of InAs/GaAs self-ordered quantum dots [6,7] intersublevel scattering times of 25–40 ps are found [9]. Ground-state luminescence rise time is similarly fast (40 ps) for nonresonant excitation in the barrier. However, a modeling of such transients requires description with mast equations for the micro states [10]. If a conventional rate equation model (CRE) for the average population of sublevels is used in connection with a short intersublevel scattering time τ_0, the transient of the excited-state luminescence displays a fast and nonexponential decay. The experimental decay of luminescence from the first excited state is exponential as predicted by the master equations for the micro states (MEM) (Fig. 2).

The luminescence of the ground state is composed of photons from excitons and biexcitons. In Fig. 3 we decompose the calculated transient of an initially completely filled ground state into the excitonic and biexciton is parts, which could be experimentally observed if both recombination en-

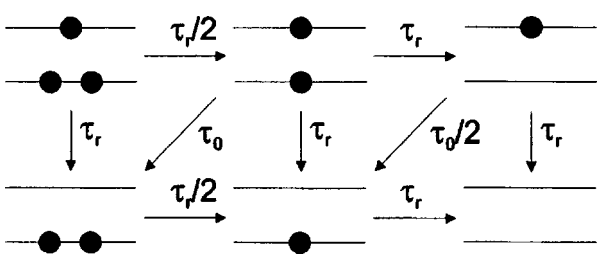

FIG. 1. Scheme of the transitions between microstates. τ is the lifetime for all radiative transitions. τ_0 is the intersublevel scattering time.

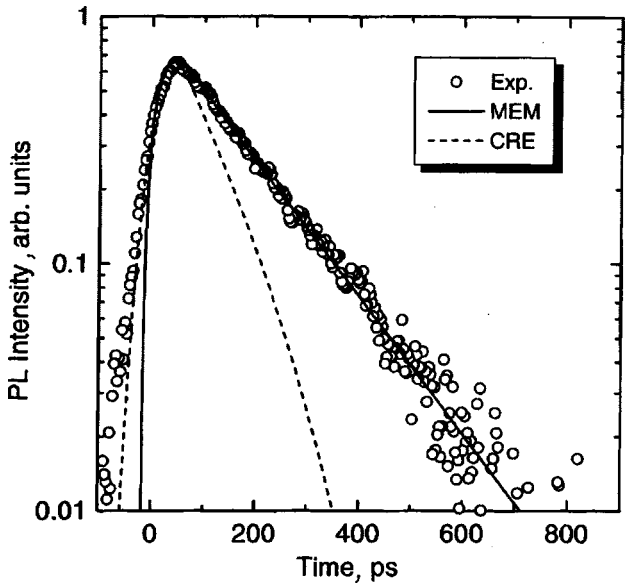

FIG. 2. Experimental decay of the excited-state luminescence from InAs/GaAs self-ordered quantum dots. Lines represent fits with master equations for the micro states (MEM) and conventional rate equations (CRE), both for an inter-sub-level scattering time $\tau_0 = 30$ ps.

ergies are sufficiently separated. The biexciton transient is strictly exponential with a time constant $\tau_{XX} = \tau_X/2$. The excitonic luminescence increases first when excitons start to be created by the $XX \rightarrow X + \gamma$ process; eventually it decays exponentially with the time constant τ_X.

4. The recombination current in a quantum-dot ensemble cannot be described using solely the average electron and hole densities. Throughout the literature, the bulk recombination rate [11] is used for the recombination current which is essentially a bimolecular expression,

$$j = \frac{2eN_D}{\tau_X} f_e f_h, \tag{1}$$

having a maximum of $j = 2eN_D/\tau_X$ for the fully occupied ground state. $0 \leqslant f_{e,h} \leqslant 1$ denotes the average filling of the ground state with electrons and holes. As already indicated in the introduction, the precise distribution of carriers over the dots has to be known to properly obtain the recombination current

$$j_r = \frac{N_X}{\tau_X} + \frac{N_{X-}}{\tau_{X-}} + \frac{N_{X+}}{\tau_{X*}} + \frac{N_{XX}}{\tau_{XX}} = \frac{N_X + N_{X-} + N_{X+} + 2N_{XX}}{\tau_X}, \tag{2}$$

where N_X denotes the number of dots filled with an exciton, N_{X-} and N_{X+} the number of dots with negatively or positively charged excitons and N_{XX} those with biexcitons. The right equality is valid in the strong confinement limit where $\tau_X = \tau_{X-} = \tau_{X+} = 2\tau_{XX}$. If excited states are populated with carriers, additional terms enter Eq. (2). The recombination current is monomolecular as opposed to Eq. (1).

The gain g of a quantum-dot ensemble depends linear on the carrier density [12]. The dependence of total ground-state luminescence intensity and gain on an external injection current (Fig. 4) is also linear (until saturation dominates), while Eq. (1) predicts $g \propto \sqrt{j}$ [dotted line in Fig. 5(a)] In Fig. 4 we

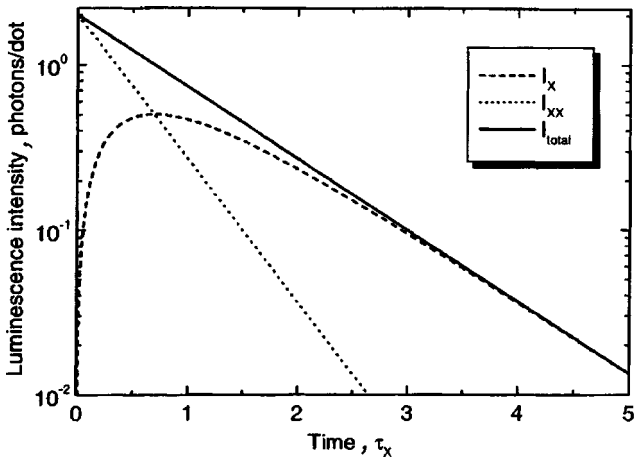

FIG. 3. Calculated luminescence decay of completely filled ground state. Different lines are total intensity and intensity on exciton and biexciton recombination lines ($I_{total} = I_X + I_{XX}$).

assumed for simplicity that no charged dots exist. If exciton and biexciton recombination (and absorption) energy are sufficiently separated (compared to their homogeneous broadening and the inhomogeneous ensemble broadening), gain in the exciton and biexciton recombination energy have to be distinguished. As can be seen in Fig. 4(a), already the exciton offers gain. With increasing current j, excitons are created $\propto j$ and biexcitons $\propto j^2$. At a current of $1e/\tau_X$ per dot, the exciton luminescence reaches its maximum; it decreases

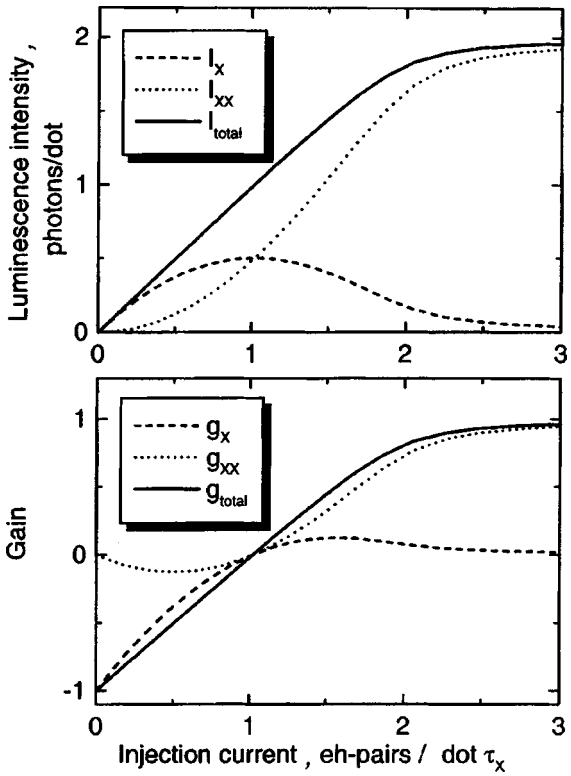

FIG. 4. Total, excitonic and biexcitonic luminescence intensity and gain of the ground state versus external injection current. A capture time from the barrier $\tau_c = \tau_X/100$ and a barrier recombination channel with $\tau_b = \tau_X$ have been assumed.

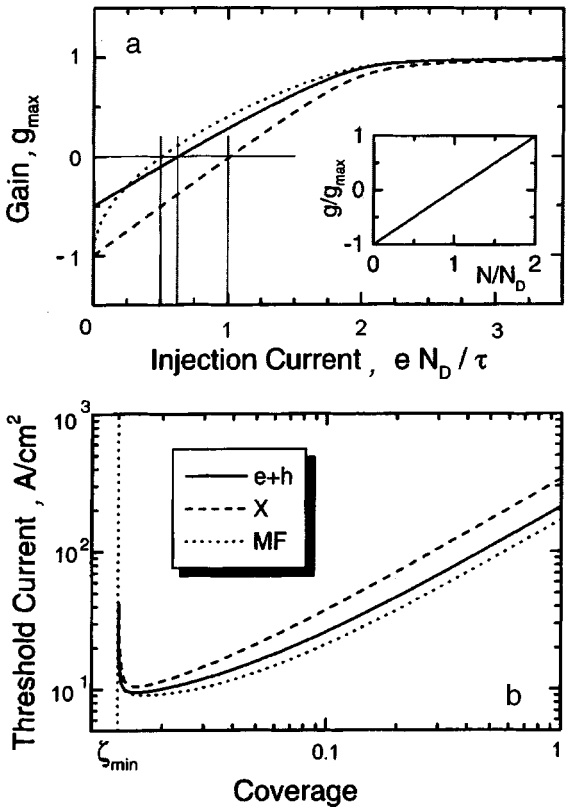

FIG. 5. (a) Gain of a single-layer quantum-dot ensemble as a function of injection current for uncorrelated ($e+h$, solid line) and correlated (X, dashed line) capture of electron and holes. For comparison the result from conventional [Eq. (1)] mean-field theory (MF, dotted line) is shown. The gain is given in units of the maximum gain. The inset shows the relation between gain and carrier density N in the dot ensemble is identical and linear for all models.
(b) Threshold current for both capture models and conventional theory as a function of coverage for a typical dot ensemble and a total loss of $\alpha_{\text{tot}}=10\ \text{cm}^{-1}$ as a function of area coverage.

for larger currents since most dots become filled with biexcitons.

Charged dots contribute gain at a lesser price in recombination current because the extra charge carrier does not radiatively decay but decreases absorption. Consequently the gain-current relation depends on whether or not charged dots exist in the ensemble. This depends on the capture mechanism as shown in Fig. 5. The limiting cases of completely correlated and uncorrelated electron-hole capture are considered. In the first case excitons are captured and only neutral dots exist, causing the higher threshold current. In self-organized quantum dots, capture occurs directly from the barrier as well as via the two-dimensional wetting layer in which excitons can form before capture. If not pure exciton capture is present, we expect the capture of electrons and holes to be correlated because charged dots represent a more attractive site for the opposite charge.

A typical ensemble of self-organized InGaAs/GaAs quantum dots [1] was assumed with $\tau=1$ ns, inhomogeneous broadening $\sigma_E=20$ meV, a vertical optical confinement factor $\Gamma_z=0.7\%$ and a total loss (including the loss at mirrors) of $\alpha_{\text{tot}}=10\ \text{cm}^{-1}$; ζ describes the area filling factor with dots. For small $\zeta\leqslant 1.3\%$ the maximum gain is insufficient to evoke lasing on the ground state. The threshold (for ground-state lasing) goes smoothly to infinity, for $\zeta\to 1.3\%$, because a recombination channel in the barrier had been included in the model (see caption of Fig. 3). For large coverage, when the threshold current density is close to the transparency current density, the two capture scenarios differ by almost a factor of two. For small coverage, when the gain has to be close to maximum, the difference becomes smaller. The conventional approach [Eq. (1)] yields a falsely small threshold in any case. We note that the presence of charge carriers at zero injection (due to doping) decreases the threshold [12,13].

5. Fundamental properties of quantum dot lasers are insufficiently described by using solely average carrier densities. A detailed analysis based on bookkeeping of the micro states is required and has been worked out by us. Time-resolved experiments involving intersublevel scattering can be properly modeled. New properties of quantum-dot lasers result, i.e., linear gain-current relation and excitonic gain. The threshold current density is higher for excitonic capture as compared to uncorrelated electron-hole capture.

Parts of this work are funded by Deutsche Forschungsgemeinschaft in the framework of Sfb 296, INTAS and Volkswagenstiftung.

[1] N. Kirstaedter, N. N. Ledentsov, M. Grundmann, D. Bimberg, V. M. Ustinov, S. S. Ruvimov, M. V. Maximov, P. S. Kop'ev, Zh. I. Alferov, U. Richter, P. Werner, U. Gösele, and J. Heydenreich, Electron. Lett. **30**, 1416 (1994).
[2] D. Bimberg, N. Kirstaedter, N. N. Ledentsov, Zh. I. Alferov, P. S. Kop'ev, and V. M. Ustinov, IEEE J. Sel. Top. Quantum Electron. **3**, 1 (1997).
[3] K. Kamath, P. Bhattacharya, T. Sosnowski, and T. Norris, Electron. Lett. **32**, 1374 (1996).
[4] J. A. Lott, N. N. Ledentsov, V. M. Ustinov, A. Yu. Egorov, A. E. Zhukov, P. S. Kop'ev, Zh. I. Alferov, and D. Bimberg, Electron. Lett. **33**, 1150 (1997).
[5] M. Grundmann and D. Bimberg, Phys. Rev. B **55**, 9740 (1997).
[6] M. Grundmann, J. Christen, N. N. Ledentsov, J. Böhrer, D. Bimberg, S. S. Ruvimov, P. Werver, U. Richter, U. Gösele, J. Heydenreich, V. M. Ustinov, A.Yu. Egorov, A. E. Zhukov, P. S. Kop'ev, and Zh. I. Alferov, Phys. Rev. Lett. **74**, 4043 (1995).
[7] N. N. Ledentsov, M. Grundmann, N. Kirstaedter, O. Schmidt, R. Heitz, J. Böhrer, D. Bimberg, V. M. Ustinov, V. A. Shchukin, A.Yu. Egorov, A. E. Zhukov, S. Zaitsev, P. S. Kop'ev, Zh. I. Alferov, S. S. Ruvimov, P. Werner, U. Gösele, and J. Heydenreich, Solid-State Electron. **40**, 785 (1996).
[8] Ph. Lelong and G. Bastard, Solid State Commun. **98**, 819 (1996).
[9] R. Heitz, M. Veit, A. Kalburge, Q. Xie, M. Grundmann, P. Chen, N. N. Ledentsov, A. Hoffmann, A. Madhukar, D. Bimberg, V. M. Ustinov, P. S. Kop'ev, and Zh. I. Alferov, Proc. MSS-8 (1997).
[10] M. Grundmann, R. Heitz, D. Bimberg, J. H. H. Sandmann, and J. Feldmann, Phys. Status Solidi B **203**, 121 (1997).
[11] W. van Roosbroeck and W. Shockley, Phys. Rev. **94**, 1558 (1954).
[12] K. J. Vahala, IEEE J. Quantum Electron. **QE-24**, 523 (1988).
[13] M. Grundmann and D. Bimberg, Jpn. J. Appl. Phys. **36**, 4181 (1997).

Published in English in the original Russian journal. Reproduced here with stylistic changes by the Translation Editor.

Excitonic waveguiding and lasing in wide bandgap semiconductor

N. N. Ledentsov

A. F. Ioffe Physicotechnical Institute of the Russian Academy of Science, 194021 St. Petersburg, Russia; Institut für Festkörperphysik, Technische Universität Berlin, 10623 Berlin, Germany

Fiz. Tverd. Tela (St. Petersburg) **40**, 843–845 (May 1998)

New type of structures for optoelectronics, we refer to as excitonic waveguides, are proposed and realized. Oppositely to conventional waveguides and double-heterostructure lasers, no significant difference in the average refractive index between the cladding and the active layers is necessary, and these regions can be fabricated from the same matrix material (homojunction laser). In this approach: (i) the waveguiding effect has a resonant nature and appears on the low-energy side of the strong exciton absorption peak in agreement with the Kramers–Kronig transformation; (ii) the absorption peak is induced by nanoscale island-like insertions of narrow-gap material in a wide bandgap matrix (quantum dots), preventing free-carrier screening of excitons and, simultaneously, allowing lasing resonant to the spectral range of the enhanced refractive index. © *1998 American Institute of Physics.* [S1063-7834(98)02005-X]

Currently the structure of semiconductor lasers is defined by the double-heterostructure concept.[1]. Using thick layers of a wider bandgap material having a lower refractive index is assumed to be necessary. However, this wider bandgap material, lattice matched to the active layer, does not always exist, or, if it exists, does not necessarily provide sufficient conductivity. The interest in using a wider range of materials and an ultimate shift towards blue and UV spectral region requires a search for alternative approaches for efficient waveguiding. An attractive idea is to use resonant waveguiding, which originates of the low energy side of the absorption peak due to a Kramers–Kronig equation which relates the absorption with the dielectric susceptibility.

Exciton absorption can be considered as a possible candidate to realize excitonic waveguiding.[2] In conventional III-V bulk or quantum wells (QWs), however, excitons are effectively screened at exciton densities well below threshold. To the contrary, high exciton binding energies and oscillator strengths, and high densities required to screen exciton in II–VI and III–N materials (around 10^9 cm^{-3}) make these excitons stable. However, exciton-induced lasing, resonant to the range of strongly enhanced refractive index, can be hardy realized[2] by free excitons with finite k values dominant at high excitation densities and observation temperatures cannot recombine radiatively, as it was demonstrated first by Gross *et al.* [3] and an additional particle (LO-phonon) is required for lasing.

On the other hand, excitons in quantum dots (QDs) cannot be screened, and also provide exciton or biexciton luminescence and gain resonant to the waveguiding region at any lattice temperature. As large QDs trap carriers more effectively and, at finite temperature, there always exists recapture of thermally excited carriers from smaller dots by larger ones, gain initially appears on the low-energy side of the QD exciton resonance and, unless the main QD absorption peak remains, the waveguiding effect remains. The crucial point to produce excitonic waveguides is thus related to a possibility of creating arrays of uniform QDs either isolated or electronically-coupled and providing a lateral confinement of the order of the exciton diameter. Recently, ultrathin submonolayer[4] or monolayer (ML)[5] insertions were proposed to be used in excitonic waveguides. These insertions are shown to form dense array of nanoscale 2D islands which can efficiently localize excitons. The structures composed of stacked ultrathin insertions result both in lifting of the k-selection rule and in strong increase in the exciton oscillator strength, providing a new possibility for lasing and

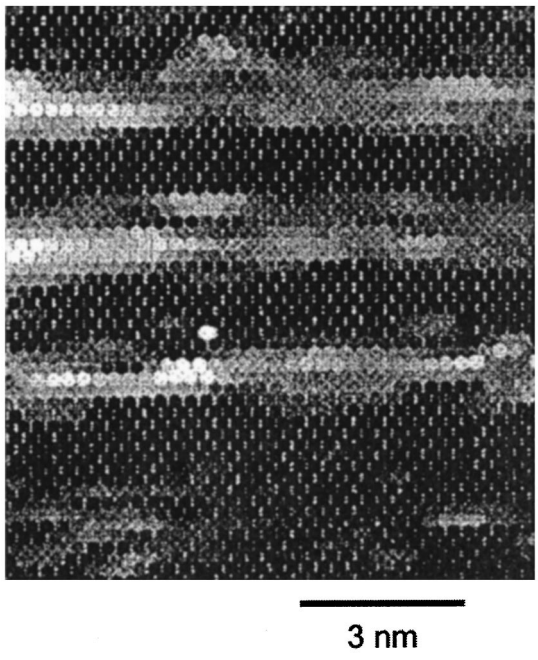

FIG. 1. Local lattice-parameter image of the structure with CdSe insertions in a ZnSe matrix.

waveguiding.[6–9] At the same time we underscore that different approaches can be used for QD fabrication.[10]

The cross-sectional local lattice-parameter image of the stack composed of 1 ML CdSe insertion separated by 3 nm-thick ZnSe layers is presented in Fig. 1. White color corresponds to CdSe lattice parameter in the growth direction, while the black spots indicate the ZnSe lattice parameter in the growth direction. As it can be clearly seen, the CdSe deposition results in islands having a lateral size of about 4 nm. The average thickness of the CdSe insertion in the island area obtained from numerical analysis of the local lattice-parameter image is about 1.6 ML and significantly exceeds the average thickness of the deposit.

Photoluminescence, optical reflection, and lasing spectra of the structure with 30 stacks of CdSe insertions grown on top of a thick ZnSSe layer and covered by ZnSSe cap are shown in Fig. 2. The important result which follows from Fig. 2 is an extremely pronounced modulation of the optical reflection spectra at the SL heavy-hole exciton energy, which indicates the high exciton-oscillator strength and, hence, effective refractive-index modulation in the active region. Increase in the exciton-oscillator strength in the array of QDs with respect to that for QWs has been demonstrated in Ref. 11. To describe the exciton peculiarity in optical reflection spectrum we use the model of resonant modulation of dielectric susceptibility[12]

$$\varepsilon(\omega)=\varepsilon_b\left(1+\frac{\omega_{LT}}{\omega_0-\omega-i\Gamma}\right), \tag{1}$$

where ε_b—dielectric constant without exciton resonance; $\hbar\omega_0,\hbar\omega_{LT},\hbar\Gamma$—exciton resonant, longitudinal-transverse splitting and damping energies, respectively. Fitting of the calculated optical reflection spectrum to the experimental one gives the following values: $\hbar\omega_0=2.701$ eV, $\hbar\omega_{LT}=1.9$ meV and $\hbar\Gamma=3.5$ meV. The region of the exciton-induced enhancement of the refractive index and, thus, of the exciton-induced waveguiding is placed on the low-energy side from the exciton resonant energy.[2] The anti-waveguiding region is, consequently, placed on the high-energy side of this energy. As it follows from Fig. 2, the lasing spectrum recorded in the waveguide geometry is 16 meV Stokes shifted with respect to the surface photoluminescence peak and the exciton resonance energy in the optical reflection spectrum. The refractive index enhancement at lasing wavelength is estimated to be of 0.15. This value is comparable with the refractive index enhancement provided by thick (Zn,Mg)(S,Se) cladding layers.

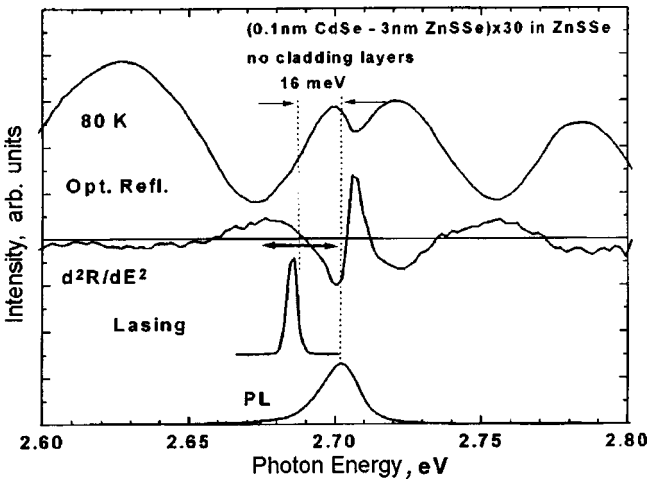

FIG. 2. Photoluminescence, lasing, and optical reflectance spectra of the excitonic waveguide structure.

$ZnS_{0.06}Se_{0.94}$–$Zn_{0.8}Cd_{0.2}Se$ quantum-well-laser structures with comparable cavity lengths lase at energies $\sim\hbar\omega_{LO}$ (30 meV) below the exciton transition revealed by photoluminescence and optical reflection spectra, in agreement with the exciton- LO phonon lasing model [13,14]. At room temperature this shift increases to about 100 meV [2].

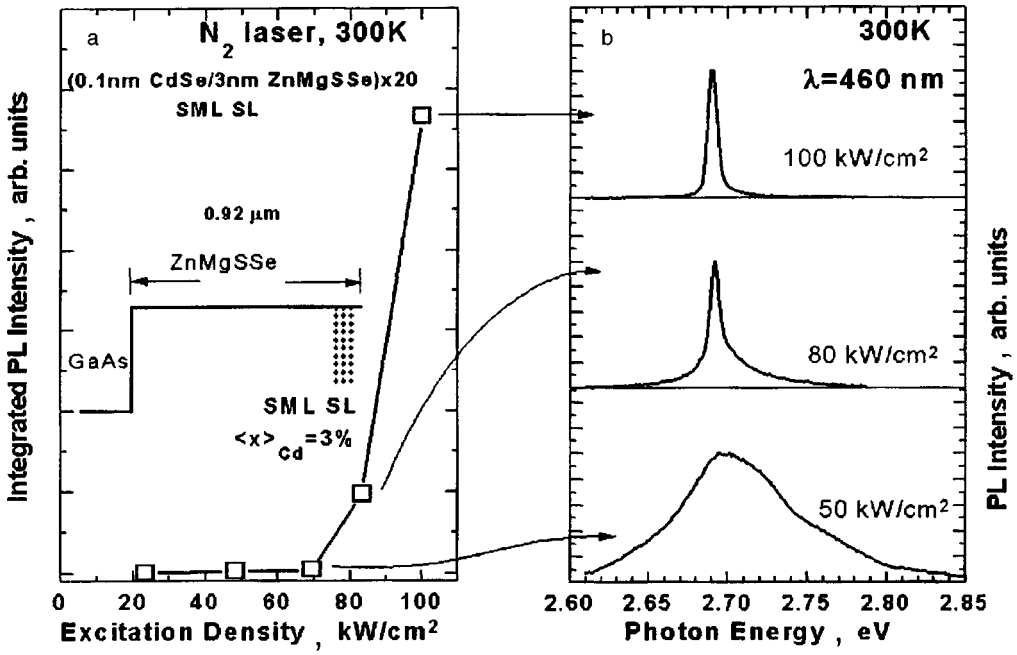

FIG. 3. Dependence of integrated PL intensity versus excitation density (a) and luminescence spectra (b) of the excitonic waveguide structure.

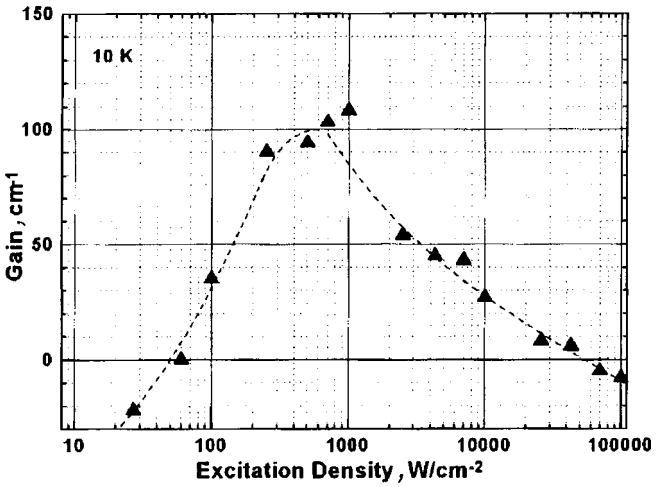

FIG. 4. Gain vs excitation density in the structure with excitonic waveguide.

For ultrathin CdSe insertions, exciton localization makes the interaction with another particle (LO-phonon, or another exciton) unnecessary, allowing the lasing to occur without additional many-body interactions directly in the region of the exciton-induced waveguiding.

For CdSe insertions in a (Zn,Mg)(S,Se) matrix we were able to realize entirely exciton-induced waveguiding and lasing up to 300 K ($\lambda = 460$ nm) without using wider bandgap cladding layers (Fig. 3). The upper limit estimated for internal losses is comparable to that in structures with optimized cladding layers and is below 18 cm^{-1}. As a highly absorbing GaAs substrate is used, and the active layer is separated by only ~ 0.9 μm from the substrate, the efficient confinement of the optical mode in the excitonic waveguide is, thus, proven. Lasing has been realized also in structures with only 0.4-μm-thick buffer layers and in very diluted arrays of QDs with 8 nm thick spacers.

Gain studies under pulsed excitation using a variable stripe length method demonstrate fast saturation of the absorption at the low energy side of exciton luminescence with excitation density (P_{exc}) and a development of a gain peak at energies ~ 3–4 meV below the exciton resonance energy in the optical reflection spectrum. Further growth in P_{exc} results in monotonic increase in gain up to values of 100 cm^{-1}. For further excitation density increase the most of QD excitons convert to biexcitons, and the excitonic gain decreases (Fig. 4). At the same time biexcitonic gain being Stokes-shifted by 7–10 meV develops and dominates the spectrum at high-excitation densities.

To conclude, excitonic waveguides represent a unique system with high device potential, particularly in wide-gap materials. The recent progress became possible due to application of self-organized growth of quantum dots in III–V and II–VI materials systems.

The work is carried out in cooperation with S. V. Ivanov, I. L. Krestnikov, M. V. Maximov, A. V. Sakharov, S. V. Sorokin, P. S. Kop'ev, Zh. I. Alferov, D. Gerthsen, A. Hoffmann, M. Straβburg, A. Rosenauer and D. Bimberg.

This work is supported by the Russian Fund for Fundamental Research (Grant No. 96-02-17911, 97-02-18138, 97-02-18269), and by the INTAS. The author is grateful to the Alexander von Humboldt Foundation.

[1] Zh. I. Alferov, Fiz. Tekh. Poluprovodn. **1**, 436 (1967) [Sov. Phys. Semicond. **1**, 358 (1967)].
[2] Zh. I. Alferov, S. V. Ivanov, P. S. Kop'ev, A. V. Lebedev, N. N. Ledentsov, M. V. Maximov, I. V. Sedova, T. V. Shubina, and A. A. Toropov, Superlattices Microstruct. **15**, 65 (1994).
[3] E. Gross, S. Permogorov, and A. Razbirin, J. Phys. Chem. Solids **27**, 1647 (1966).
[4] N. N. Ledentsov, I. L. Krestnikov, M. V. Maximov, S. V. Ivanov, S. L. Sorokin, P. S Kop'ev, Zh. I. Alferov, D. Bimberg, and C. M. Sotomayor Torres, Appl. Phys. Lett. **69**, 1343 (1996).
[5] N. N. Ledentsov, I. L. Krestnikov, M. V. Maximov, S. V. Ivanov, S. L. Sorokin, P. S. Kop'ev, Zh. I. Alferov, D. Bimberg, and C. M. Sotomayor Torres, Appl. Phys. Lett. **70**(5) (1996).
[6] I. L. Krestnikov, M. V. Maximov, S. V. Ivanov, N. N. Ledentsov, S. V. Sorokin, A. F. Tsatsul'nikov, O. G. Lyublinskaya, B. V. Volovik, P. S. Kop'ev, and C. M. Sotomayor Torres, Fiz. Tekh. Poluprovodn. **31**, 166 (1997) [Semiconductors **31**, 164 (1997)].
[7] I. L. Krestnikov, M. V. Maximov, S. V. Ivanov, S. L. Sorokin, S. A. Permogorov, A. N. Reznitsky, A. V. Kornievski, N. N. Ledentsov, D. Bimberg, and C. M. Sotomayor Torres, in *Proceedings of the 23rd International Conference on the Physics of Semiconductors (Berlin, Germany, July 21–26, 1996)*, edited by M. Scheffler and R. Zimmermann (World Scientific, Singapore, 1996), Vol. 1, p. 3187.
[8] I. L. Krestnikov, N. N. Ledentsov, M. V. Maximov, A. V. Sakharov, S. V. Ivanov, S. V. Sorokin, L. N. Tenishev, P. S. Kop'ev, and Zh. I. Alferov, Pis'ma v Zh. Tekhn. Fiz. **23**(1), 33 (1997) [Tech. Phys. Lett. **23**, 23 (1997)].
[9] A. V. Sakharov, S. V. Ivanov, S. V. Sorokin, B. V. Volovik, I. L. Krestnikov, P. S. Kop'ev, N. N. Ledentsov, Pis'ma v Zh. Tekhn. Fiz. **23**, 28 (1997).
[10] N. N. Ledentsov, M. Grundmann, N. Kirstaedter, O. Schmidt, R. Heitz, J. Böhrer, D. Bimberg, V. M. Ustinov, V. A. Shchukin, P. S. Kop'ev, Zn. I. Alferov, S. S. Ruvimov, A. O. Kosogov, P. Werner, U. Richter, U. Gösele, and J. Heydenreich, in *Proc. MSS7 (Madrid, 1995)*, Solid-State Electron. **40**, 785 (1996).
[11] M. V. Belousov, N. N. Ledentsov, M. V. Maximov, P. D. Wang, I. N. Yassievich, N. N. Faleev, I. A. Kozin, V. M. Ustinov, P. S. Kop'ev, and C. M. Sotomayor Torres, Phys. Rev. B **51**, 14346 (1995).
[12] E. L. Ivchenko, A. V. Kavokin, V. P. Kochereshko, P. S. Kop'ev, and N. N. Ledentsov, Superlattices Microstruct. **12**, 317 (1929).
[13] C. Benoit a la Guillaume, J. M. Denber, and F. Salvan, Phys. Rev. **177**, 567 (1969).
[14] J. Ding, M. Hagerott, P. Kelkar, A. V. Nurmikko, D. C. Grillo, L. He, J. Han, and R. L. Gunshor, Phys. Rev. B **50**, 5758 (1994).

Published in English in the original Russian journal. Reproduced here with stylistic changes by the Translation Editor.

Excitonic effects in diluted magnetic semiconductor nanostructures

Yasuo Oka

RISM, Tohoku University, Katahira 2-1-1, Aoba-ku, Sendai 980-77, Japan
CREST, JST, Kawaguchi, 332, Japan

Fiz. Tverd. Tela (St. Petersburg) **40**, 846–848 (May 1998)

Excitonic properties and the dynamics are reported in quantum dots (QDs) and quantum wells (QW) of diluted magnetic semiconductors. Transient spectroscopies of photoluminescence and nonlinear-optical absorption and emission have been made on these quantum nanostructures. The $Cd_{1-x}Mn_xSe$ QDs show the excitonic magnetic polaron effect with an increased binding energy. The quantum wells of the $Cd_{1-x}Mn_xTe$/ZnTe system display fast energy and dephasing relaxations of the free and localized excitons as well as the tunneling process of carriers and excitons in the QWs depending on the barrier widths. The observed dynamics and the enhanced excitonic effects are the inherent properties of the diluted magnetic nanostructures. © *1998 American Institute of Physics.* [S1063-7834(98)02105-4]

1. INTRODUCTION

Nanometer-scale confinements of the band electrons in semiconducting materials provide varieties of quantum phenomena such as low-dimensional electronic states, increased exciton binding energies and dynamics of carriers in the systems. Diluted magnetic semiconductors (DMSs), which involve magnetic ions in the cation sites, show marked magneto-optical properties due to the exchange interaction of the band electrons (holes) with the magnetic ions. Therefore, nanostructure DMSs are expected to show particular magneto-optical effects owing to the confinement of both the electronic and magnetic states. In this paper, we report properties of the quantum dots (QDs) of $Cd_{1-x}Mn_xSe$ and the quantum wells (QWs) of the $Cd_{1-x}Mn_xTe$ and ZnTe layers and show the dynamics of low-dimensional excitons in the confined magnetic nanostructures[1–7].

2. EXPERIMENTAL

$Cd_{1-x}Mn_xSe$ QDs in SiO_2 matrices were fabricated by rf-sputtering and subsequent heat treatments. Diameters were fabricated of the QDs range from 20 to 400 Å, and the Mn concentration x is 0.05–0.2. Multiquantum wells (MQWs) and asymmetric quantum wells (ADQWs) of $Cd_{1-x}Mn_xTe$/ZnTe ($x=0-0.2$) were prepared by the hot-wall epitaxy method. Excitonic properties and the dynamics have been studied by the transient spectroscopies of photoluminescence, degenerate four-wave mixing (DFWM) and pump-probe differential absorptions, where the optical excitations were made by a mode-locked Ti-sapphire laser and amplification system.

3. EXCITONIC EFFECTS IN DMS QUANTUM DOTS

Microcrystals of $Cd_{1-x}Mn_xSe$ grown in SiO_2 amorphous matrices show a lattice image as displayed in Fig. 1, where the microcrystal of 150 Å diameter $Cd_{1-x}Mn_xSe$ in the SiO_2 matrix appears with the lattice fringe of the wurtzite structure.[1,3] The crystal structure is the same as that of the bulk crystal and the lattice constant is 4.3 Å. The absorption spectra of the $Cd_{1-x}Mn_xSe$ microcrystals show humps of the band-edge absorption in the 2.0–2.5 eV region, which are the evidence of the exciton absorption in the $Cd_{1-x}Mn_xSe$ microcrystals. The average diameter D of the microcrystals in the samples is determined by x-ray diffraction.

The microcrystal-size dependence of the exciton energy measured from the absorption edge agrees with the calculation of the exciton confinement energy, which indicates that these $Cd_{1-x}Mn_xSe$ microcrystals can be described by the QDs for the excitonic state. Transient characteristics of the luminescence in $Cd_{1-x}Mn_xSe$ QDs (the average diameter is 220 Å) is shown in Fig. 2, where the exciton luminescence at 0 T decays with the decay time-constant of 100 ps in the higher-energy region at 2.03 eV, while in the lower-energy region around 1.94 eV the decay is much slower. At 5 T the exciton luminescence decays with a faster decay-time constant.[4] The lifetime of the QD excitons deduced from the luminescence decay is distributed in the range of 100 ps to 1 ns. The variation is caused by the difference in the exciton lifetime in the size-distributed QDs. In a magnetic field of 5 T, the exciton lifetime decreases markedly due to the increase of the radiative recombination rate. The decrease in the exciton lifetime by the magnetic field also showed evidence of an exchange interaction of the exciton with the Mn ions in the QDs, since this decrease is caused by the level crossing of the singlet and triplet exciton states in a magnetic field.

The exciton average energy in the QDs, which is given by the gravity center of the time-resolved luminescence spectra, decreases by 40 meV at 0 T for the increase of time with the time constant of 900 ps. At 5 T, the increased radiative recombination rate induces a fast decay of the exciton luminescence. The observed variation of the exciton luminescence displays the formation process and the radiative decay of the excitonic magnetic polaron in the QDs.

The magneto-luminescence of the $Cd_{1-x}Mn_xSe$ QDs for

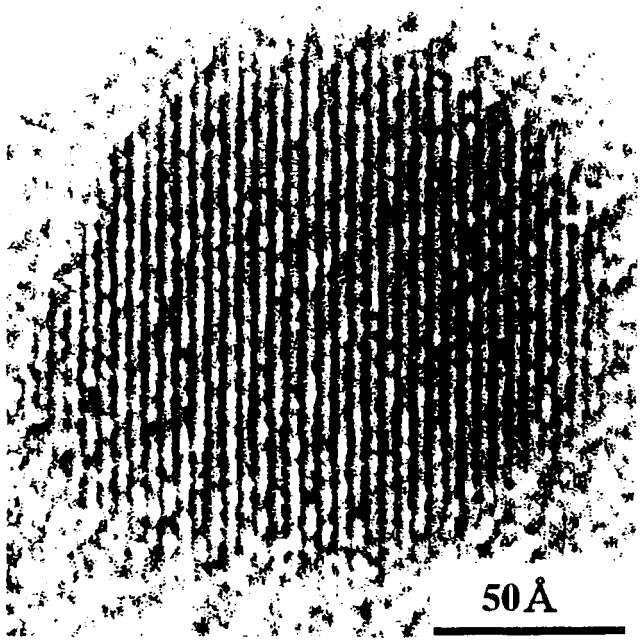

FIG. 1. Lattice image of the $Cd_{1-x}Mn_xSe(x=0.15)$ QD grown in the SiO_2 amorphous matrix.

the selective energy excitation in the exciton absorption region shows decrease of the Stokes-shift energy ΔE of the luminescence with increasing the magnetic field. ΔE varies from 80 meV to 53 meV with increasing H from 0 T to 7 T for a fixed excitation energy of $E_{exc}=1.905$ eV. The Stokes shift ΔE in the selective excitation is related to the magnetic polaron formation energy. The formation energy of the excitonic magnetic polaron is suppressed by the presence of strong magnetic fields, since the external magnetic field aligns the Mn spins along the field direction. Therefore the reduction of the Stokes shift due to the magnetic field corresponds to the binding energy of the excitonic magnetic polaron. The existence of the excitonic magnetic polaron in the DMS QD of 160 Å diameter is confirmed in the present work with the magnetic polaron binding energy of 27 meV. Recently the magnetic polaron binding energy of the exciton state in DMS QDs has been calculated [8]. The fairly good agreement between the experimental results of $Cd_{1-x}Mn_xSe$ QDs with the calculation indicates marked increase of the exchange interaction in the QDs due to the confinement effect.

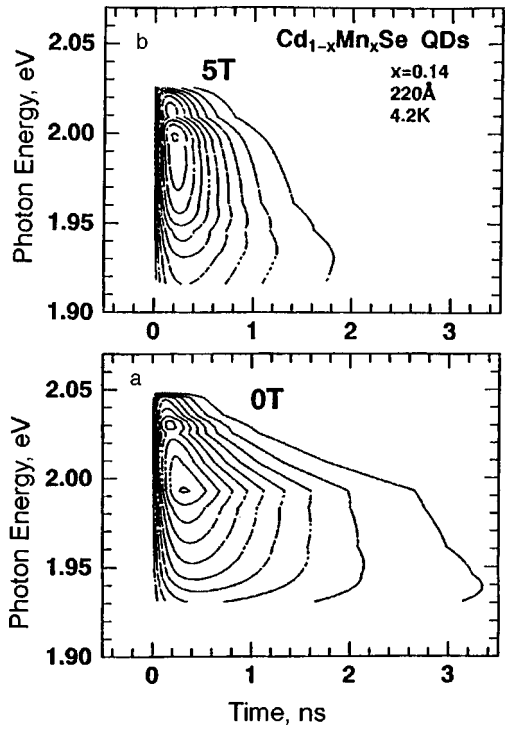

FIG. 2. Transient exciton luminescence in the $Cd_{1-x}Mn_xSe$ QDs at 0 and 5 T.

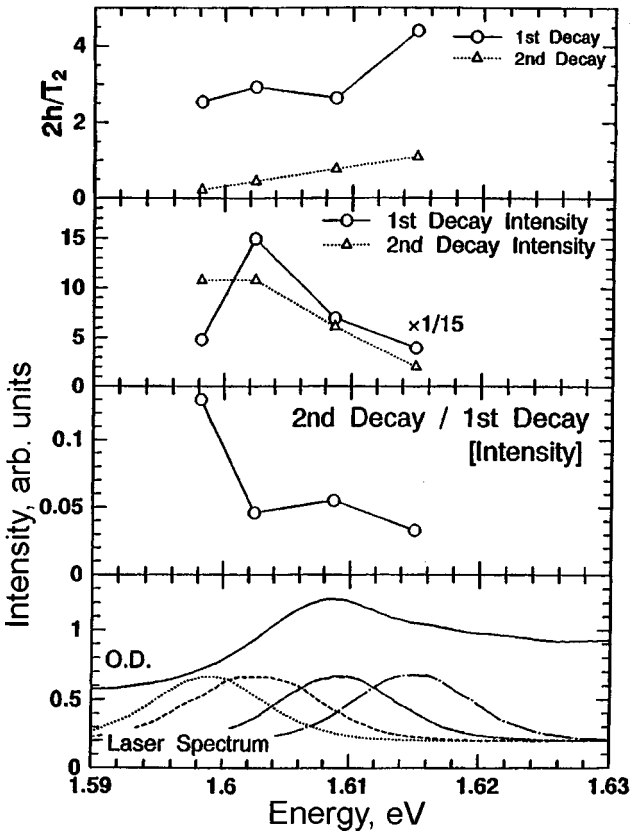

FIG. 3. DFWM signal intensities in the CdTe/ZnTe MQWs, which show resonant behavior of DFWM signals at the QW exciton energy.

4. EXCITONIC EFFECTS IN DMS QUANTUM WELLS

The DMS QWs are studied by the transient nonlinear optical spectroscopies [6,7]. The DFWM measurements have been made on the $Cd_{1-x}Mn_xTe/ZnTe$ QWs. In the $Cd_{1-x}Mn_xTe$ MQWs (the well width $L_x=124$ Å, the barrier width $L_b=8$ Å, the periods $P=35$) at the resonance excitation on the exciton state, a double-exponential-decay signal is observed, where the fast decay component corresponds to the dephasing time $T_2=450$ fs. This fast dephasing is caused by the free exciton in the QWs, which is confirmed by the resonance behavior of the component at the exciton absorption peak as shown in Fig. 3. The slow decay component can be attributed to the dephasing process of the localized excitons, where the slow decay of 6.4 ps partly involves the

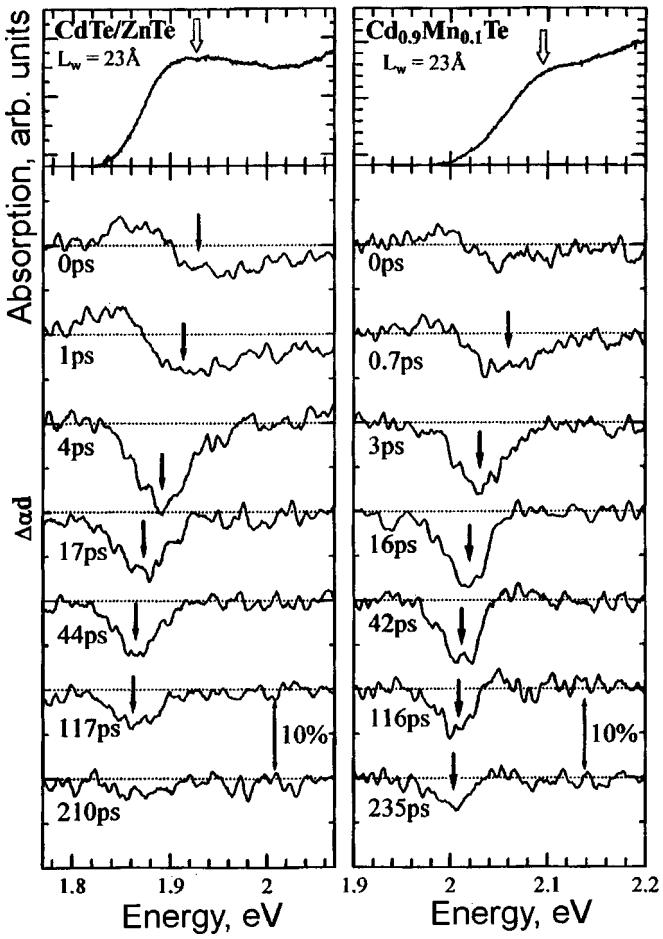

FIG. 4. Pump-probe differential absorption spectra in the $Cd_{1-x}Mn_xTe$/ZnTe MQWs ($x=0$ and 0.1).

longitudinal relaxation rate of the free exciton to the localized state in the QW. The observed short T_2 of the QW exciton is independent of the lattice temperature, indicating a less affection of acoustic and optical phonon relaxations. The fast dephasing of the exciton in the $Cd_{1-x}Mn_xTe$/ZnTe QW system is caused by the relaxation due to the lattice inhomogeneity involved in the strained QWs because the free exciton is much affected by the inhomogeneous relaxation of the lattice. Present experimental results display the dynamics and the dephasing process of the excitons in the strained quantum wells.

The pump-probe differential absorption spectra of the $Cd_{1-x}Mn_xTe$/ZnTe MQWs ($x=0$and 0.1) with $L_w=23$ Å are displayed in Fig. 4. The exciton absorption in these MQWs locates at 1.92 and 2.10 eV. In the $Cd_{0.9}Mn_{0.1}Te$/ZnTe MQWs the absorption saturation peak shows a fast low-energy shift of 70 meV within 10 ps and also shows a subsequent gradual low-energy shift of 20 meV until 235 ps after the pump excitation. On the other hand, the CdTe/ZnTe MQWs exhibits the gradual low energy shift of 60 meV until 210 ps after the pumping. The dominant fast-energy-relaxation of the exciton in the $Cd_{0.9}Mn_{0.1}Te$/ZnTe MQWs indicates the formation process of the excitonic magnetic polarons in the two-dimensional QWs, while the gradual energy relaxations seen in both of the MQWs are due to the localization process of the excitons in the inhomogeneous MQWs. Exciton luminescence peaks are shifted by 60–100 meV to the lower-energy side from the exciton absorption peak in the steady state, where the large Stokes shift of the exciton luminescence indicates the existence of the fluctuation of the well thickness in the MQWs.

The result of the pump-probe differential absorption in the $Cd_{1-x}Mn_xTe$/ZnTe ADQWs (the narrow well width $L_{NW}=10$ Å, the wide well width $L_{WW}=20$ Å) shows, in the case of $L_b=300$ Å that the saturation of absorption in *NW* and *WW* decays with a same time constant of 160 ps, where the tunneling time on *NW* exciton is the order of 10^6 ps. In the ADQW of $L_b=75$ Å, the saturation of absorption of *NW* decays faster than that of *WW*, which is interpreted by the fast tunneling time (1 ps) of the electrons from *NW* to *WW*. Numerical analysis of the pump-probe absorption spectra shows the tunneling process of electrons and holes through the barrier in the ADQW of $L_b>38$ Å

In summary, ultrafast spectroscopies on the QDs and QWs of MDSs in magnetic fields have clarified the energy and phase relaxations and the tunneling processes of the excitons and carriers. The magneto-optical properties of the DMS nanostructures are significantly affected by both the confinement effect and the exchange interaction.

The author is grateful to H. Okamoto, I. Souma, T. Sato, M. Takahashi, K. Yanata, K. Egaws, and K. Matsui for their helpful collaborations. This work is partly supported by the Ministry of Education, Science, and Culture, Japan and also by CREST, the Japan Science and Technology Corporation.

[1] Y. Oka and K. Yanata, J. Lumin. **70**, 35 (1996).
[2] Y. Oka, H. Okamoto, S. Takano, K. Egawa, K. Matsui, K. Yanata, and M. Takahashi, J. Surf. Analys. **3**, 524 (1997).
[3] K. Yanata, K. Suzuki, and Y. Oka, J. Appl. Phys. **73**, 4596 (1993).
[4] K. Yanata and Y. Oka, Superlat. Microstruct. **15**, 233 (1994).
[5] K. Yanata and Y. Oka, Physics of Semiconductors (World Scientific, 1996), p. 1477.
[6] H. Okamoto, T. Hisatsugu, M. Takahashi, and Y. Oka, *ibid.*, p. 2239.
[7] Y. Oka, K. Matsui, S. Takano, T. Hisatsugu, H. Okamoto, and M. Takahashi, *High Magnetic Fields in the Physics of Semiconductors* (World Scientific, 1997), p. 705.
[8] A. K. Bhattacharjee and C. Benoit a la Guillaume, Phys. Rev. B **51**, 9912 (1995); *Physics of Semiconductors* (World Scientific, 1996), p. 1469; Phys. Rev. B **55**, 10613 (1997).

Published in English in the original Russian journal. Reproduced here with stylistic changes by the Translation Editor.

Structural characterization of self-organized nanostructures

S. Ruvimov, Z. Liliental-Weber, and J. Washburn

Lawrence Berkeley National Laboratory, Berkeley, CA 94720, USA

N. N. Ledentsov, V. M. Ustinov, V. A. Shchukin, P. S. Kop'ev, and Zh. I. Alferov

A. F. Ioffe Institute, 194021 St. Petersburg, Russia

D. Bimberg

Technische Universität Berlin, D-10623 Berlin, Germany

Fiz. Tverd. Tela (St. Petersburg) **40**, 849–851 (May 1998)

Self-organized nano-objects fabricated in different semiconductor systems are currently at the focus of scientific interest because of their unique electronic properties. Transmission electron microscopy and high-resolution electron microscopy have been used to study the InAs quantum dots grown by molecular-beam epitaxy (*MBE*) on GaAs and InP substrates. Optimal imaging conditions for visualization of quantum dots were established. Size, shape, and stability of the equilibrium island arrays were analyzed with respect to the growth conditions. Both decrease and increase of the As pressure compared to the optimal value were shown to destroy the regular arrangement of the islands. Energy benefit due to the strain relaxation in the InAs islands is likely to be the driving force for their formation. © *1998 American Institute of Physics.* [S1063-7834(98)02205-9]

Further progress in opto- and microelectronics currently involves quantum effects in semiconductor heterostructures of reduced dimensionality: quantum wires and quantum dots (QDs). Quantum objects uniform in size and in shape can be fabricated in a way compatible with advanced semiconductor technology by utilizing self-organization phenomena during crystal growth,[1–12] alloy decomposition[13–15] and surface faceting.[16,17] The Stranski–Krastanow epitaxial growth of highly mismatched, semiconductor systems (Si/Ge,[2] InAs/GaAs,[4,6,7] GaSb/GaAs,[11] ZnSe/ZnS,[12] etc.) has been shown to result in the formation of coherent strained nm-scale islands that allow attainment of a high level of quantum confinement.[4–7] Vertical coupling of quantum dots in superlattices has been found to decrease the radiative lifetime and to result in injection lasing at low current densities.[18] The understanding of these phenomena is dependent on the employment of atomic-level electron microscopic techniques such as high-resolution transmission-electron microscopy (HREM)[6,7] and scanning tunneling microscopy (STM).[4] These techniques are complementary: STM is efficient for surface characterization and morphology evaluation during growth while HREM is used to characterize atomic structure of quantum objects. Due to the small sizes of quantum objects and the strain effects, their HREM visualization requires special imaging conditions. Here we review results on structural evaluation of self-organized nano-objects fabricated in different semiconductor systems.

Scattering in size and shape for the quantum dots reported by different groups makes it of interest to study the equilibrium geometry of small islands grown in the Stranski–Krastanow mode. A typical HREM image of an InAs quantum dot is shown in Fig. 1. Pyramid-like InAs islands with 14 nm base length and 7 nm height are embedded in the GaAs active layer which is located between two cladding superlattices of (2 nm $Al_{0.3}Ga_{0.7}As$/2 nm GaAs)$_{10}$. Strain-induced contrast significantly influences the image, but the pyramidal shape of the island is still visible. A plan-view image of this heterostructure (not shown) demonstrates ordering of the islands in both shape and size.[7]

Because the strain-induced contrast strongly affects the dot image on TEM micrographs, optimization of imaging conditions is required to visualize the true shape and size of the quantum dot. Molecular dynamics calculations have been applied to model the atomic displacement field of the InAs island and the GaAs matrix. The calculations were carried out using the CERIUS program package (Molecular Dynam-

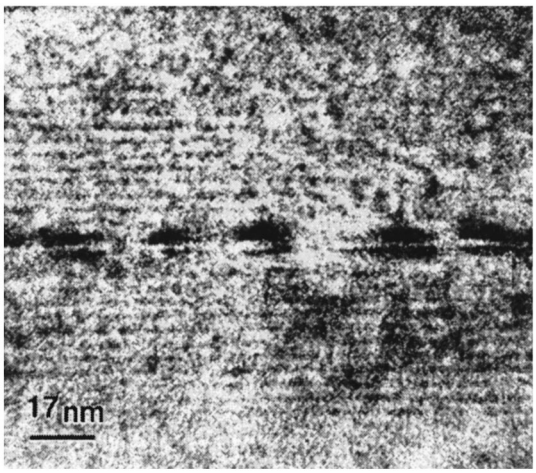

FIG. 1. InAs quantum dots in GaAs: HREM cross-section (a) and plan-view (b) TEM micrographs.

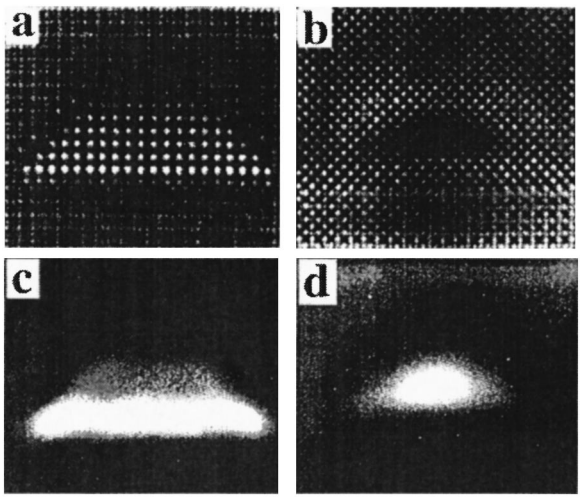

FIG. 2. Simulated cross-sectional HREM (a,b) and corresponding bright-field (c,d) images of unrelaxed (a,c) and relaxed (b,d) InAs island.

ics Inc., Cambridge) detailed elsewhere.[19] A pyramid-like InAs island has a base length $a=6$ nm because the total number of atoms in the model was limited to 2×10^4. The atomic displacement field has then been used for simulations of HREM images at different foil thicknesses and defoci.[19] Figure 2 shows the calculated HREM image and corresponding calculated bright-field images of unrelaxed (a,c) and relaxed (b,d) InAs islands. An increase of foil thickness significantly affects the image due to strain-induced contrast so that the true size and shape of the island is poorly resolved at foil thickness larger than 2a. The island contrast is most clearly seen at certain defoci (60–70 nm for JEOL 4000EX microscope), where the chemical contrast difference is most pronounced.[19] Detuning from these optimal imaging conditions results in the over- or underestimation of the QD size. Strain affects conventional TEM image of QDs even more strongly. Contrast on calculated bright-field images taken at symmetrical Laue orientation [e.g., in Fig. 2d] depends on the foil thickness, but is independent of defocus. Even for a thin foil, the shape of the dot is difficult to resolve. However, the size of the dot can be determined if the thickness of the foil is not larger than 2a. Similar results were found for plan view imaging.[19]

Formation of InAs dots on InP substrates differs from that on GaAs and significantly depends on the material of the matrix. Figure 3 shows typical TEM images for InAs/InGaAs and InAs/InAlAs systems grown on (001) InP substrates. The InGaAs and InAlAs ternary alloys had the same lattice parameters as the InP substrate. The characteristic lateral sizes of InAs quantum dots were 50–70 nm for InAs/InGaAs and InAs/InAlAs systems, respectively. The dot heights were in the range of 2.5–3 nm in both cases. Besides the InAs dots, strain modulation contrast due to spinodal decomposition of ternary alloys was observed along ⟨110⟩ directions. Similar composition modulations have been reported for other systems [13,14]. The InAs dots in Fig. 3 are more rounded and more shallow for the InAs/InGaAs system compared with that of the InAs/InAlAs.

In contrast, each island in the InAs/GaAs system has a square base and they are locally arranged in a two dimensional square lattice with main axes along ⟨100⟩ crystallographic directions.[6,7] The square base of the islands can be understood by taking into account the elastic anisotropy of

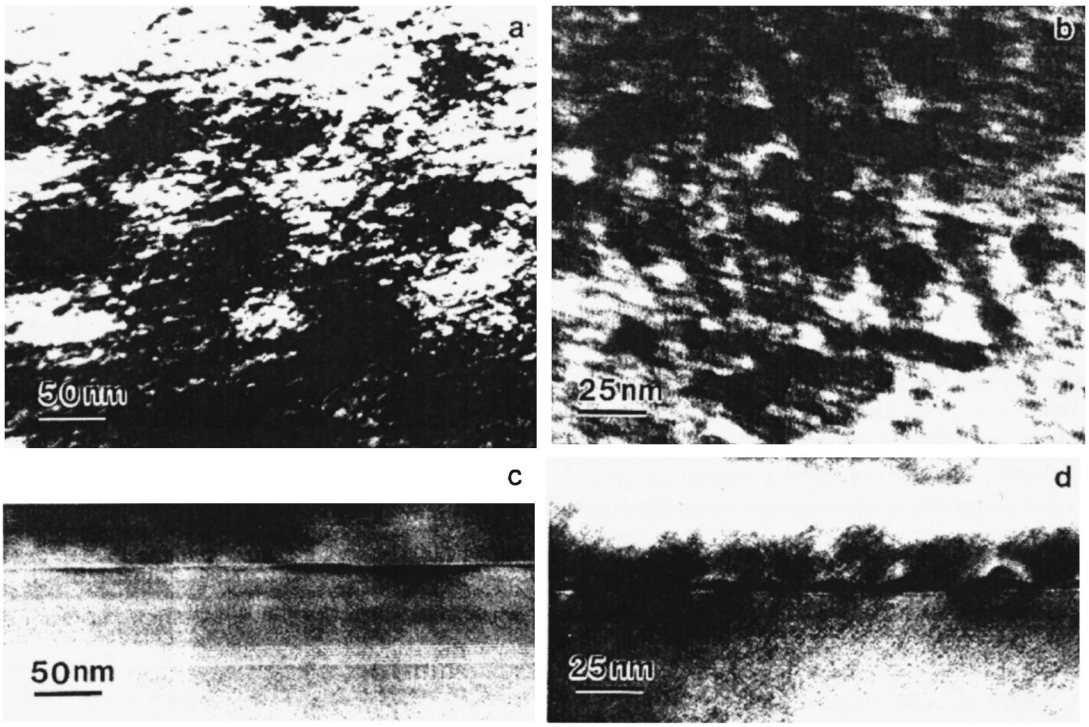

FIG. 3. Plan-view (a,b) and cross-sectional (c,d) bright-field TEM images of InAs dots for InAs/InGaAs (a,c) and InAs/InAlAs (b,d) systems grown on (001) InP substrates.

cubic GaAs with the minimum stiffness along ⟨100⟩ and ⟨010⟩ crystallographic directions. The repulsive interaction of islands of high density due to the strained substrate results in their ordering into the two dimensional square lattice. The uniform quantum dot array can result in minimal possible free energy of the system.[20] Thus, the characteristic size of the island is energetically favorable.

According to our calculations,[20] the total energy of the system has a minimum for a particular dot size which depends on material parameters. This agrees well with observations of the effect of growth interruption and variation in As pressure on dot sizes and their distribution (not shown). Growth interruption for 40 s after 2.5 ML InAs is deposited is enough to let the dot reach the equilibrium size that was typical for 4 ML InAs deposition without growth interruption. Both decrease and increase of the As-pressure compared to the optimal value were shown to destroy the regular arrangement of the islands. An increase of the substrate temperature from 480 to 520 °C at optimal arsenic pressure results in an increase of the lateral size of the dot to ~180 Å and in a strong decrease of dot density (down to $\sim 1.5-2.0 \times 10^{10}$ cm^{-2}). The dot lateral shape (well-defined square) is not affected. Large clusters appear locally. The PL peak position shifts slightly (~30–50 meV) towards higher energy with respect to the Pl line for 480 °C growth, indicating that the increase of the lateral size is compensated by the reduction of the dot height and the facet angle. Since the stability of the equilibrium dot array strongly depends on the face surface energy this result is expected because changes in growth parameters influence the surface energy of the InAs layer. MBE growth at optimal conditions is a near-equilibrium process [21]. However, kinetics plays an important role when the process is not equilibrium, and results in macroscopic surface structures (~1000 Å) under both low and high arsenic pressures.

In conclusion, self-organization phenomenon are promising for the fabrication of nanostructures in semiconductor epitaxial systems for optoelectronics applications. TEM and HREM appear to be key techniques for structural characterization of nano-objects.

This study was supported by the Office of Energy Research, U. S. Department of Energy under Contract No. DE-AC03-76F00098. The use of the facilities of the National Center of Electron Microscopy is greatly appreciated.

[1] L. Goldstein, F. Glas, J. Y. Marzin, M. N. Chavasse, and J. Le Roux, Appl. Phys. Lett. **47**, 1099 (1985).
[2] Y.-W. Mo, D. E. Savage, B. S. Swartzentruber, and M. G. Lagally, Phys. Rev. Lett. **65**, 1020 (1990).
[3] J. Tersoff and R. M. Tromp, Phys. Rev. Lett. **70**, 2782 (1993).
[4] D. Leonard, M. Krishnamurthy, C. M. Reaves, S. P. Denbaars, and P. M. Petroff, Appl. Phys. Lett. **63**, 3203 (1993).
[5] J. M. Moison, F. Houzay, F. Barthe, L. Leprince, E. Andre, and O. Vatel, Appl. Phys. Lett. **64**, 196 (1994).
[6] N. N. Ledentsov, M. Grundmann, N. Kirstaedter, J. Christen *et al.*, in *Proceedings of the 22nd International Conference ''Physics of Semiconductors''*, Vancouver, Canada (1994), Vol. 3, p. 1855.
[7] S. Ruvimov, P. Werner, K. Scheerschmidt, U. Richter *et al.*, Phys. Rev. B **51**, 14766 (1995).
[8] R. Nötzel, J. Temmyo, and T. Tamamura, Nature **369**, 131 (1994).
[9] V. Bressler-Hill, A. Lorke, S. Varma, P. M. Petroff, and W. H. Weinberg, Phys. Rev. B **50**, 8479 (1994).
[10] P. D. Wang, N. N. Ledentsov, C. M. Sotomayor Torres, P. S. Kop'ev, and V. M. Ustinov, Appl. Phys. Lett. **64**, 1526 (1994).
[11] E. R. Glawer, B. R. Bennett, V. V. Shanabrook, and R. Magno, Appl. Phys. Lett. (1997) (in press).
[12] M. C. Harris Liao, H. Chang, Y. F. Chen, J. W. Hsu, J. M. Lin, and W. C. Chen, Appl. Phys. Lett. **70**, 2256 (1997).
[13] F. Glas, C. Gors, and P. Henoc, Philos. Mag. B **62**, 373 (1990).
[14] L. H. Kuo, L. H. Salmanka-Riba, B. J. Wu, J. M. De Puydt, J. M. Haugen, H. Cheng, S. Juha, and M. A. Haase, Appl. Phys. Lett. **65**, 1230 (1994).
[15] A.-L. Barabasi, Appl. Phys. Lett. **70**, 764 (1997).
[16] R. Nötzel, N. N. Ledentsov, L. Däweritz, M. Hohenstein, and K. Ploog, Phys. Rev. Lett. **67**, 3812 (1991).
[17] V. I. Marchenko, Sov. Phys. JETP **54**, 605 (1981).
[18] N. N. Ledentsov, V. A. Shchukin, M. Grundmann, N. Kirstaedter *et al.*, Phys. Rev. B **54**, 8743 (1996).
[19] S. Ruvimov and K. Scheerschmidt, Phys. Status Solidi A **150**, 471 (1995).
[20] V. A. Shchukin, N. N. Ledentsov, P. S. Kop'ev, and D. Bimberg, Phys. Rev. Lett. **75**, 2968 (1995).
[21] J. Tersoff, M. D. Johnson, and B. G. Orr, Phys. Rev. Lett. **78**, 282 (1997).

Published in English in the original Russian journal. Reproduced here with stylistic changes by the Translation Editor.

Study of the phase composition of AgI microcrystals by exciton spectroscopy and differential scanning calorimetry

I. Kh. Akopyan, B. V. Novikov, and S. A. Soboleva

Physics Scientific-Research Institute, St. Petersburg State University, 198904 Petrodvorets, Russia

Fiz. Tverd. Tela (St. Petersburg) **40**, 852–854 (May 1998)

Differential absorption spectra of $RbAg_4I_5$ have been measured in the exciton absorption region of AgI within the temperature range 27–250 °C. In the same temperature range, the temperature behavior of the heat capacity of $RbAg_4I_5$, Rb_2AgI_3, and KAg_4I_5 have been obtained by differential scanning calorimetry. An analysis of the results suggests that, in AgI microcrystals less than r_{cr} in size, the upper boundary for stability of the low-temperature β modification is higher by several tens of degrees. © *1998 American Institute of Physics.* [S1063-7834(98)02305-3]

The dependence of structural phase transitions occurring in small particles on their size is of considerable interest both from the scientific and practical standpoints. Experiment indicates that a decrease in the size of particles may be accompanied by a change in their structure, as well as in a change of the boundaries separating the existence regions of different phases. For example, AgI aerosol particles may have, depending on size, different structure (hexagonal for $r<20$ nm and cubic for $r>30$ nm).[1] The transition of $BaTiO_3$ to cubic symmetry as the particle size was reduced to 49 nm[2] has been reported as well as the high-temperature tetragonal phase of ZrO_2 becoming stable up to room temperature if the particles were small enough.[3]

The present work studies the phase composition of finely dispersed silver iodide present in ternary superionic compounds ($RbAg_4I_5$, Rb_2AgI_3, KAg_4I_5) by exciton spectroscopy and differential scanning calorimetry.

It is known that, in bulk samples, the low-temperature hexagonal β modification of silver iodide transforms to the superionic cubic α phase at $T_{co}\approx 147$ °C. It was also shown[4] that this transformation entails pronounced changes in the exciton spectrum of AgI, in particular, a significant shift of the exciton structure toward lower energies by 0.26 eV.

Studies of the optical properties of single-crystal $RbAg_4I_5$ revealed, in the reflectance and luminescence spectra of most samples, a structure belonging to silver iodide.[5] The presence of AgI in MAg_4I_5 compounds (M=Rb, K, NH_4) results both from the their thermal instability[6] and from deviations from stoichiometry in the course of crystal growth, with the origin of silver iodide in the starting crystal affecting the dimensions and structure of the inclusions.

A study of the temperature dependence of wavelength-modulated transmission spectra of comparatively freshly grown $RbAg_4I_5$ single crystals (as a rule, they are transparent, slightly yellowish in color) made in the spectral region of the AgI exciton structure showed its strong shift toward longer wavelengths, which is characteristic of the $\beta\rightarrow\alpha$ transition, to be observed at ~200 °C, i.e., considerably above T_{co} (Fig. 1). Spectra obtained around T_{co} shift smoothly toward longer wavelengths with increasing temperature.

The increase of the phase-transition temperature in silver iodide present in a finely-dispersed form in $RbAg_4I_5$ crystals is supported by calorimetric measurements. Curves 2 and 3 in Fig. 2 display the temperature behavior of the heat capacity, which show the exciton structure in absorption spectra to shift sharply at 200 °C. Besides the effect of thermal origin in the region of the melting temperature of $RbAg_4I_5$ ($T_m=232$ °C),[7] the $C_p(T)$ curves exhibit an endothermal peak

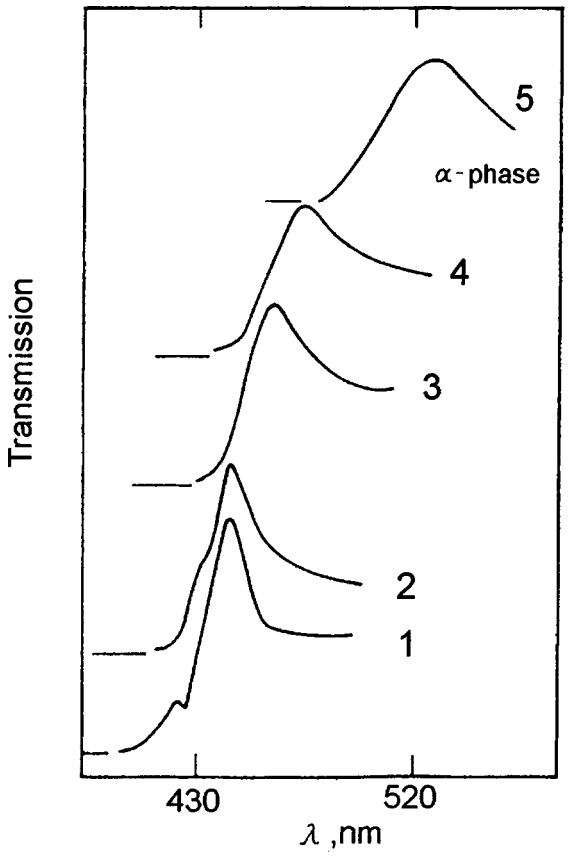

FIG. 1. Wavelength-modulated transmission spectra of a $RbAg_4I_5$ crystal taken at different temperatures. T(°C): *1*—27, *2*—70, *3*—170, *4*—195, *5*— 200.

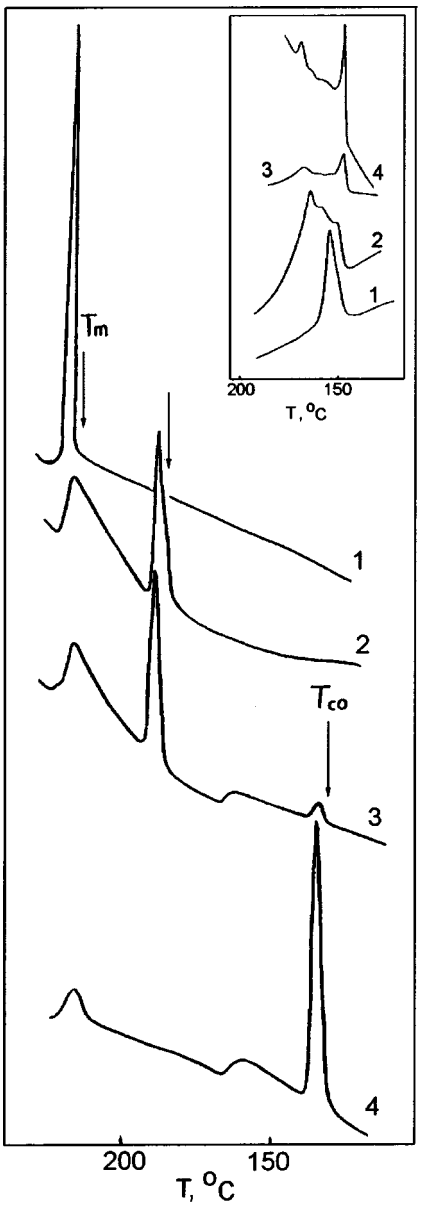

FIG. 2. Temperature dependence of the heat capacity of $RbAg_4I_5$ crystals. 1— melt-grown single crystal, 2 and 3—single crystals grown from acetone solution, 4—single crystal grown from acetone solution and subjected to prolonged storage. Inset: heat capacity of $RbAg_4I_5$ powder (1—with excess of AgI, 2—stoichiometric composition), 3—Ag_2HgI_4 crystal, and 4—powder $CdHgI_4$.

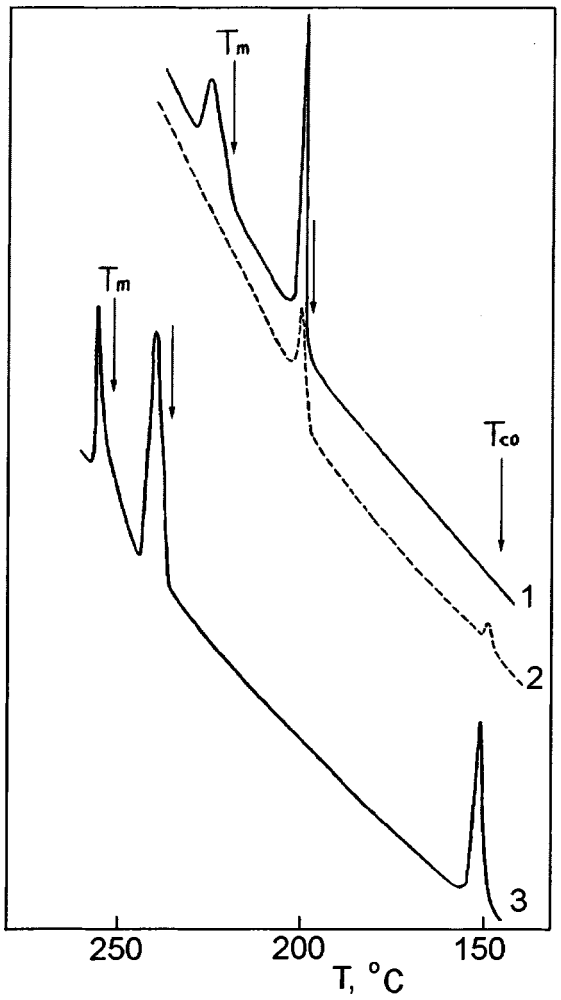

FIG. 3. Temperature dependence of the heat capacity of (1) single-crystal $RbAg_4I_5$, (2) single-crystal Rb_2AgI_3, and (3) polycrystalline KAg_4I_5.

at 200 °C. One observes also sometimes a very weak maximum around 147 °C.

As the storage time of $RbAg_4I_5$ crystals increases, the maximum at 147 °C associated with the phase transition in bulk crystals grows, and the thermal effects at 200 °C and around the melting point of the ternary crystal become weaker. This is accompanied by a very strong increase in the luminescence of silver iodide in the emission spectra of $RbAg_4I_5$. Curve 4 in Fig. 2 illustrates the temperature behavior of the heat capacity of a $RbAg_4I_5$ crystal stored for several months in humid air. One immediately notices the following points: (1) an increase of AgI microcrystals in size does not entail a gradual shift of the phase transition temperature toward T_{co}, and (2) the transition temperature observed in these microcrystals practically coincides with the eutectic temperature of the RbI–AgI system ($T_e = 199$ °C, Ref. 7).

Figure 3 presents temperature dependences of the heat capacity of single-crystal $RbAg_4I_5$ and Rb_2AgI_3, as well as that for a polycrystalline KAg_4I_5 sample. The coincidences between the phase-transition temperatures in $RbAg_4I_5$ and Rb_2AgI_3 (curves 1 and 2), on the one hand, and of the transition temperature in KAg_4I_5 (curve 3) with the eutectic point of the KI–AgI system ($T_e = 239$ °C, Ref. 7), on the other, suggest that it is at T_e that finely dispersed AgI microcrystals undergo a phase transition to the α modification.

The features in the temperature dependences of heat capacity observed around 150–165 °C (curves 3 and 4 in Fig. 2) were discussed[8] for the AgI–HgI_2 system and assumed to be due to phase transitions occurring in small silver iodide microcrystals dispersed in the matrix of the ternary compound Ag_2HgI_4. There are reports of a slight temperature increase in the superionic transition in AgI due to the small size of particles and, as a consequence, a more uniform structure.[9] Note that the thermal effects observed in this tem-

perature region are characteristic of AgI inclusions in various matrices (inset in Fig. 2).

One can thus assume that the small size of AgI inclusions in matrices of ternary crystals is responsible for the increase of the transition temperature (up to 168 °C) to the α phase. As the size of the inclusions drops, however, below a certain critical level, the boundary of stability of the low-temperature β modification is found to increase up to the eutectic point of the system, where the silver iodide microcrystals grow to transfer to the superionic α phase. The absence of noticeable size-quantization effects in the exciton spectra of the AgI phase suggests that the critical size is not less than four exciton Bohr radii.

Support of the Russian Fund for Fundamental Research (Grant 96-02-18710) is gratefully acknowledged.

[1] N. A. Kakutkina, *Author's Abstract of Candidate Thesis* (Novosibirsk, 1980).
[2] S. Schlag and H. F. Eicke, Solid State Commun. **91**, 883 (1994).
[3] G. Ya. Akimov, V. M. Timchenko, and I. V. Gorelik, Fiz. Tverd. Tela (St. Petersburg) **36**, 3582 (1994) [Phys. Solid State **36**, 1906 (1994)].
[4] I. Kh. Akopyan, V. N. Bondarev, D. N. Gromov, A. B. Kuklov, and B. V. Novikov, Fiz. Tverd. Tela (Leningrad) **29**, 2263 (1987) [Sov. Phys. Solid State **29**, 1305 (1987)].
[5] I. Kh. Akopyan, T. A. Vorob'eva, D. N. Gromov, and B. V. Novikov, Fiz. Tverd. Tela (Leningrad) **32**, 1038 (1990) [Sov. Phys. Solid State **32**, 610 (1990)].
[6] L. E. Topol and B. B. Owens, J. Phys. Chem. **72**, 2106 (1968).
[7] D. A. Gallagher and M. V. Klein, Phys. Rev. B **19**, 4282 (1979).
[8] I. Kh. Akopyan, S. A. Soboleva, and B. V. Novikov, Fiz. Tverd. Tela (St. Petersburg) **36**, 2495 (1994) [Phys. Solid State **36**, 1357 (1994)].
[9] J. E. Maskasky, Phys. Rev. B **43**, 5769 (1991).

Translated by G. Skrebtsov

Effect of substrate misorientation on quantum-dot size distribution in the InAs/GaAs system

D. G. Vasil'ev, V. P. Evtikhiev, V. E. Tokranov, I. V. Kudryashov, and V. P. Kochereshko

A. F. Ioffe Physicotechnical Institute, Russian Academy of Sciences, 194021 St. Petersburg, Russia

Fiz. Tverd. Tela (St. Petersburg) **40**, 855–857 (May 1998)

A study is reported of the effect of (001)GaAs substrate misorientation in the [010] direction on the distribution of MBE-grown self-assembled InAs/GaAs quantum dots in size and position in the GaAs matrix. Temperature-induced narrowing of the exciton photoluminescence line of a quantum-dot ensemble caused by redistribution of photoexcited carriers among dots of different size has been observed. © *1998 American Institute of Physics.* [S1063-7834(98)02405-8]

The fast progress witnessed to occur in microelectronics has been shifting the interest of researchers to the region of ever smaller nanoobjects, from semiconductor quantum wells to quantum wires to quantum dots. Production of ensembles of dots with the highest possible uniformity is a major problem in this area. The use of dots in heterolasers requires the possibility of controlled fabrication of ensembles with a given dot density. These problems can be solved by using self-organization effects[1]. This approach permits one to obtain ensembles of dots uniform in size to within $\pm 10\%$.[2] Attempts at increasing the dot density on ideal (001)substrates gives rise, however, to coalescence of adjacent dots. Dislocation growth in such dots results in a drop of their photoluminescence (PL) efficiency. This places a severe limit on the maximum possible density of luminescent quantum dots in the InAs/GaAs system.

A method of growing uniform quantum-dot ensembles in InAs/GaAs on [010]-misoriented substrates has recently been developed.[3] The steps forming on such surfaces are along the [110] and $[\bar{1}10]$ directions. Intersection of such steps can produce a network ofisolated terrace fragments consisting of alternating broadenings and narrowings bounded on all sides by steps, with the quantum dots grown on such surfaces being located primarily in the broadened parts of a terrace (Fig. 1). This provides a possibility of making dot production a controlled process and permits one to form dot ensembles with a sufficiently high density and uniformity.

The self-assembled quantum dots used in this work were grown by molecular-beam epitaxy (MBE) in the InAs/GaAs system on GaAs substrates with misorientation angles of 1, 2, 4, and 6°. To achieve the maximum possible dot density, the effective thickness of the InAs layer was chosen to be 2.3 monolayers.

Increasing the misorientation angle results in an increase of terrace density (2 nm^{-1} for 1°, 2.7 nm^{-1} for 2°, and 4 nm^{-1} for 6°) and, accordingly, in a decrease of their size. The terrace width was 500, 360, 300, and 250 Å for 1, 2, 4, and 6° misorientation angle, respectively. While the corners of broadened terrace fragments are energetically preferred locations for dot growth, dots can form at other sites on a terrace as well. We studied PL spectra of an ensemble of quantum dots as a function of substrate misorientation angle within the 6–200-K temperature interval. The spectra were excited with a He–Ne laser operating at a power density of 1 W/cm^2.

Figure 2a shows PL spectra obtained at 6 K from a quantum-dot structure on a substrate misoriented by 1°. Two inhomogeneously broadened PL profiles stand out in the spectrum. Each of these profiles is a Gaussian with a width ~ 80 meV. The maxima of the profiles are displaced with respect to one another by ~ 100 meV. The inhomogeneous broadening of each of the observed PL peaks is due to a quantum-dot spread in size. Straightforward evaluation of this spread as $\delta E/E \approx 2\delta R/R$ (where E is the quantization energy and R is the dot size) shows the quantum dot ensembles thus obtained to be highly uniform, with a spread $\delta R/R \approx \pm 8\%$.

The presence of two PL peaks implies the existence in the sample of two quantum-dot ensembles with different average sizes. The average size of dots in these ensembles dif-

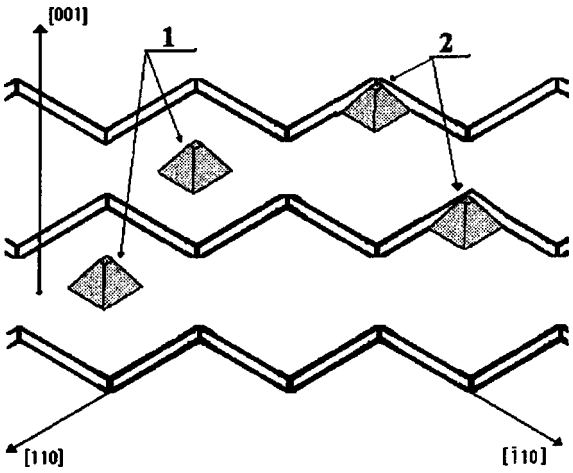

FIG. 1. Schematic diagram of a quantum-dot structure (filled pyramids) in the InAs/GaAs system. Positions 1 and 2 indicate two possible locations of dots on terraces of a misoriented substrate.

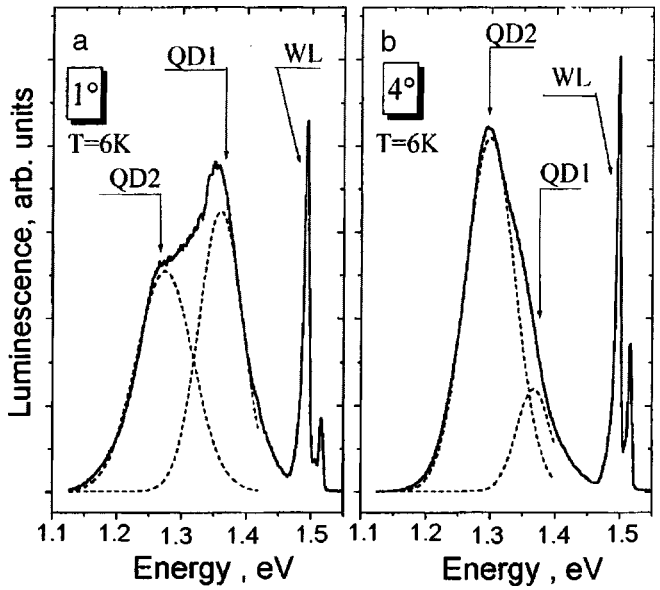

FIG. 2. Photoluminescence spectra of the structures under study obtained at $T=6$ K. (a) spectrum from a sample with 1° misorientation, (b) sample misorientation angle 4°. QD1 and QD2 are two Gaussian distributions (dashed lines) used to approximate the quantum-dot photoluminescence lines. The peak denoted WL identifies emission from the wetting layer.

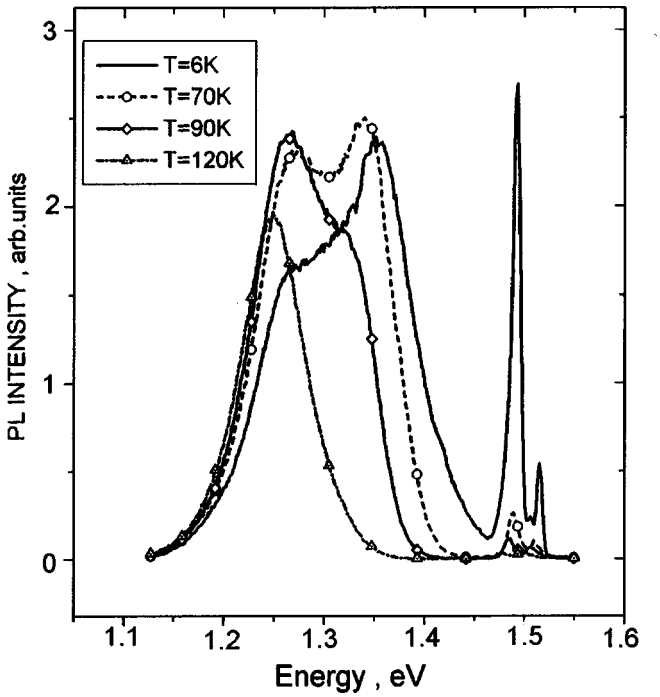

FIG. 3. Photoluminescence spectra of a structure with 1° misorientation obtained at different temperatures.

fers by ~15%. We relate one of the ensembles to dots growing at corners of the broadened terrace fragments (position 2 in Fig. 1). Such dots should have a larger average size compared to those that grew at terrace centers because of a partial strain relaxation in InAs dots bordering on another terrace. The other quantum-dot ensemble combines dots that grew spontaneously on flat parts of the terraces (position 1 in Fig. 1). Such dots should be, on average, smaller than the ones in position 2. Accordingly, the PL maximum of the first ensemble lies at longer wavelengths compared to that of the second ensemble. As the substrate misorientation angle increases, the terrace density increases, and the average terrace size decreases, so that the fraction of the quantum dots in the first ensemble should increase. Figure 2b presents a PL spectrum obtained at $T=6$ K from a quantum-dot structure on a substrate misoriented by 4°. The redistribution of PL intensity between the two quantum-dot ensembles suggests an increase in the relative number of dots growing at terrace corners.

Quantum-dot PL spectra were observed to undergo strong changes with increasing temperature (Fig. 3). An increase in temperature results in a long-wavelength shift of the quantum-dot PL spectrum which exceeds by far the temperature-induced shift of the InAs and GaAs bands (Fig. 3). Besides the shift of the spectrum, the PL lines are observed to become more narrow with increasing temperature. At $T=200$ K, the PL spectra in all the samples studied became similar, with one maximum ~70 meV wide in the region of ~1.2 eV.

This modification of the PL spectrum can be explained as due to a redistribution of photoexcited carriers among the dots.[4] At low temperatures, nonresonant photoexcitation populates uniformly all dots. If the carrier tunneling time between dots exceeds the electron–hole radiative recombination time in a dot, the spectrum will contain radiation from dots of all sizes.

The probability of carrier tunneling between dots grows with temperature. As a result, it is increasingly deeper dots that will be populated, and it is there that radiative recombination will occur. This will tend to shift the PL line toward longer wavelengths. The existence of this temperature-induced redistribution of photoexcitation indicates a high density of quantum dots whose average separation, as follows from tunneling-length calculations, should not exceed 150 Å.

The PL linewidth is determined by the interplay between the probabilities of radiative recombination and of carrier transition to a deeper dot. Because the dot distribution in size is limited, the PL line will become narrower with increasing temperature.

Thus low-temperature PL spectra of InAs/GaAs quantum-dot ensemblesgrown on misoriented substrates suggest the existence of dot ensembles with two characteristic sizes differing by 15%. The spread of dots in size within each ensemble did not exceed ±8%. Photoexcited carriers were observed to undergo redistribution with increasing temperature toward populating larger dots.

The authors are grateful to A. V. Platonov for assistance in carrying out the experiments.

Partial support of the Russian Fund for Fundamental Research (Grant 95-02-06038) and of the ''Nanostructures'' Program of the Russian Ministry of Science is gratefully acknowledged.

[1] D. Leonard, K. Pond, and P. M. Petroff, Phys. Rev. B **50**, 11687 (1994).
[2] J.-Y. Marzin, J.-M. Gérard, A. Izraël, D. Barrier, and G. Bastard, Phys. Rev. Lett. **73**, 716 (1994).

[3] A. B. Komissarov, V. P. Evtikhiev, A. K. Kryganovskii, A. N. Titkov, M. Ichida, and A. Nakamura, in *Proceedings of the 23rd International Conference Compound Semiconductors* (St. Petersburg, Russia, 1996), edited by M. Shur and R. Suris, Inst. Phys. Conf. Ser. No. **155**, p. 351.
[4] A. Patane, M. Grassi Alessi, F. Intonti, A. Polimeni, M. Capizzi, F. Martelli, M. Geddo, A. Bosacchi, and S. Franchi, *Proc. OECS-5* (Göttingen, 1997), edited by R. G. Ulbrich.
[5] A. V. Estichiev, V. E. Tokranov, A. K. Kryzhanovskiĭ, A. M. Boĭko, R. A. Suris, A. N. Titkov, A. Nakamura, and M. Ichida, F.T.P., 5 (1998).

Translated by G. Skrebtsov

Optical orientation and alignment of excitons in quantum dots

R. I. Dzhioev, B. P. Zakharchenya, E. L. Ivchenko, V. L. Korenev, Yu. G. Kusraev, N. N. Ledentsov, V. M. Ustinov, A. E. Zhukov, and A. F. Tsatsul'nikov

A. F. Ioffe Physicotechnical Institute, Russian Academy of Sciences, 194021 St. Petersburg, Russia

Fiz. Tverd. Tela (St. Petersburg) **40**, 858–861 (May 1998)

Optical orientation and alignment of excitons in InAlAs quantum dots in the AlGaAs matrix have been studied both theoretically and experimentally. Experiments performed in a longitudinal magnetic field (Faraday geometry) reveal transformation of optical orientation to alignment and alignment to orientation, which is caused by exchange splitting of the dipole-active exciton doublet and allowed by the quantum-dot low symmetry. A comparison of theory with experiment made with inclusion of the anisotropy of exciton generation and recombination along the $[1\bar{1}0]$ and $[110]$ axes permits one to determine the character of dipole distribution in direction for resonant optical transitions in the self-organized quantum-dot ensemble studied.
 [S1063-7834(98)02505-2]

Even in semiconductors having a simple band structure, the energy levels of excitons are degenerate, if one includes electron and hole spin states. In particular, the heavy-hole exciton ground level $e1-hh1(1s)$ in zincblende quantum dots is fourfold degenerate and has an angular momentum projection $M=s+j=\pm 1,\pm 2$, where the electron spin $s=\pm 1/2$ and the hole angular momentum $j=\pm 3/2$. Exchange interaction splits this level into a radiative doublet $|\pm 1\rangle$ and two closely lying, optically inactive singlets. Exciton localization at an anisotropic island or in an anisotropic quantum dot lowers the symmetry of the system, so that the radiative doublet splits into two sublevels polarized linearly in two orthogonal directions, whose orientation is determined by the form of the localizing potential.[1] Studies of photoluminescence spectra of excitons trapped in GaAs/AlGaAs(001) quantum dots performed in optical near-field regime showed the $e1-hh1(1s)$doublet to undergo exchange splitting into two components polarized along $[110]$ and $[1\bar{1}0]$.[2] In GaAs/AlGaAs(001) type-II superlattices, a similar splitting caused by exciton localization at an interface and the low symmetry C_{2v} of a single interface[3] was studied by polarized photoluminescence[4,5]. It was shown that observation of the optical-orientation–optical-alignment or alignment–orientation transformation in a magnetic field $\mathbf{B}\|z$, i.e., observation of linear (circular) polarization of photoluminescence under circularly (linearly) polarized excitation permits reliable determination of the splitting and of the direction of polarization of optically active sublevels, while not resolving the fine spectral structure. This work studies the fine structure of localized excitons in a self-assembled quantum-dot system InAlAs/AlGaAs.

The structures were grown by molecular-beam epitaxy in a RIBER 32P setup with a solid-state source As_4 on (100)GaAs semi-insulating substrates. The quantum-dot ensemble was produced by self-organized growth at 485 °C of a 1.6-nm thick $In_xAl_{1-x}As$ layer ($x=0.45$).[6] The remainder of the structure was grown at 700 °C in an arsenic-rich environment. The active region in the sample consists of three rows of quantum dots separated by 5-nm-thick $Al_{0.3}Ga_{0.7}As$ layers. It is bounded on the side of the substrate and of the surface by 50-period $Al_{0.45}Ga_{0.55}As$(2 nm)/GaAs(1 nm) superlattices followed by $Al_xGa_{1-x}As$ ($x=0.45-0.6$) and $Al_{0.6}Ga_{0.4}As$ layers 0.15 and 0.1 μm thick, respectively. The transition from two-dimensional uniform to three-dimensional nonuniform regime of InAlAs growth was monitored from changes in the RHEED pattern from the surface of the growing film.

The sample was placed in a liquid-helium cryostat. The helium was pumped out to a temperature $T=2$ K. The measurements were made under quasi-resonant photoexcitation (Kr^+ laser, $\lambda_{ex}=6764$ Å). The laser beam was directed at a small angle to the growth axis z, along which recombination radiation was detected in reflection geometry. The magnetic field parallel to the z axis was generated by a superconducting coil. The luminescence polarization was analyzed in Faraday geometry. We used a modulation technique, in which either the polarizer is fixed, and the analyzer position is modulated, or the analyzer is fixed, and the sample is excited by light with alternating sign of circular or linear polarization at the 26.61-kHz photoelastic-modulator frequency.[5] In the first case one measured the degrees of polarization

$$P_c^\alpha=\frac{I_{\sigma_+}^\alpha-I_{\sigma_-}^\alpha}{I_{\sigma_+}^\alpha+I_{\sigma_-}^\alpha},\quad P_l^\alpha=\frac{I_{1\bar{1}0}^\alpha-I_{110}^\alpha}{I_{1\bar{1}0}^\alpha+I_{110}^\alpha},\quad P_{l'}^\alpha=\frac{I_{100}^\alpha-I_{010}^\alpha}{I_{100}^\alpha+I_{010}^\alpha},\tag{1}$$

and in the second, the effective degrees of polarization

$$\rho_\alpha^c=\frac{I_\alpha^{\sigma_+}-I_\alpha^{\sigma_-}}{I_\alpha^{\sigma_+}+I_\alpha^{\sigma_-}},\quad \rho_\alpha^l=\frac{I_\alpha^{1\bar{1}0}-I_\alpha^{110}}{I_\alpha^{1\bar{1}0}+I_\alpha^{110}},\quad \rho_\alpha^{l'}=\frac{I_\alpha^{100}-I_\alpha^{010}}{I_\alpha^{100}+I_\alpha^{010}}.\tag{2}$$

Here symbol I_β^α stands for the intensity of recombination radiation in the (α,β) polarizer and analyzer configuration,

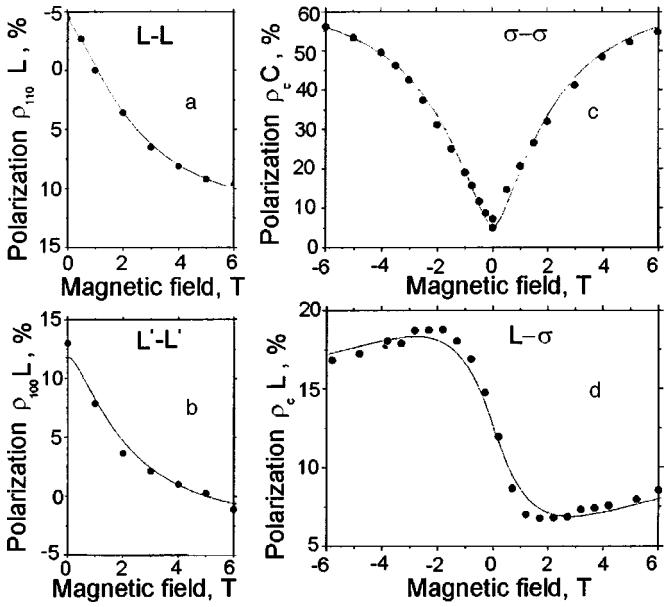

FIG. 1. Optical alignment of excitons along (a) $[1\bar{1}0]$ and [110] axes and (b) [100] and [010] axes; (c) optical orientation of excitons; (d) transformation of optical alignment along the $[1\bar{1}0]$ and [110] axes to orientation. Solid lines show the results of calculation using Eqs. (5), (6), and (11) and distribution (12).

and index α or β assumes one of six values: linear polarization along the [100], [010], $[1\bar{1}0]$, [110] axes or circular polarization σ_+, σ_-.

An emission spectrum obtained under quasi-resonant excitation ($\hbar\omega = 1.832$ eV) contains peaks separated from the pump line by the optical-phonon energy in GaAs (35 meV) and AlAs (48 meV), as well as a weakly pronounced structure[7,8]. The experimental data presented below relate to the phonon peak distant from the laser line by 35 meV. Similar results were obtained also for the other phonon line.

Figure 1 shows the dependence of the degree of luminescence polarization on longitudinal magnetic field. Panels *a* and *b* illustrate exciton alignment along the $[1\bar{1}0]/[110]$ and [100]/[010] axes, respectively. Measurements of the effective degree of linear polarization of the luminescence (i.e., of the exciton alignment) were performed under linearly polarized excitation, with the electric vector of light alternating in direction from parallel to the $[1\bar{1}0]$ axis to perpendicular to it (or from [100] to [010]) at a frequency of 26.61 kHz, and a linear polarizer transmitting along $[1\bar{1}0]$ or [100] was inserted into the luminescence detection channel. The degree of effective circular polarization of excitons (exciton orientation) was measured under excitation with circularly polarized light changing the sign of polarization with the same frequency (26.61 kHz), with a quarter-wave phase plate and a linear polarizer (analyzer of circular polarization) placed into the luminescence channel.

As seen from Fig. 1a, optical alignment of excitons along the $[1\bar{1}0]/[110]$ axes is not destroyed below 12.5%. Additional experiments showed this to be due to the luminescence intensity being modulated by the pump polarization modulation. The intensity modulation, in its turn, is caused by a difference between the absorption coefficients for light polarized along $[1\bar{1}0]$ and [110] (linear dichroism) and does not depend on the field B. When measuring the linear dichroism in absorption, excitation was produced in the same way as in the exciton alignment experiments, and a depolarizer was introduced in the luminescence detection channel to eliminate the polarizing action of the diffraction gratings and mirrors in the spectrometer.

Optical alignment of excitons is observed with the pump light polarized both along [110] and along [100] (see Fig. 1a and 1b). In a longitudinal magnetic field, linear polarization is depressed in the same characteristic field range in which one observes growth of circular polarization (Fig. 1c). Note that the depression of alignment along [110] is determined by the difference between the linear polarizations in zero and a strong magnetic field, because the effective linear polarization $\rho^{l}_{1\bar{1}0}$ is superposed upon by intensity modulation. When excited along the [100] and [010] axes, the linear dichroism is insignificant.

As already mentioned, anisotropic exchange interaction combined with the Zeeman effect in the exciton results in the optical orientation becoming connected with alignment. This effect is illustrated by Fig. 1d; indeed, exciton-spin orientation in the quantum-dot structure under study placed in a longitudinal magnetic field is connected with alignment of oscillating dipole moments in the $[1\bar{1}0]$, [110] system. It should be stressed that, when excited with circularly polarized light in a magnetic field, no linearly polarized component appeared in the [100], [010] system, just as the reverse effect of transformation of linear polarization along the [100], [010] axes also did not respond to circular polarization.

The quantum dots studied here had the shape of a pyramid (possibly,truncated), whose height is parallel to $z \| [001]$, and the rectangular base is oriented along the [100] and [010] axes.[6,9] To analyze the optical orientation and alignment of excitons, one can conveniently consider the $|\pm 1\rangle$ doublet as a pair of states of the pseudospin $S = 1/2$. Then the Hamiltonian describing doublet splitting in a longitudinal magnetic field $\mathbf{B} \| z$ can be written

$$\mathcal{H} = \frac{\hbar}{2}(\Omega_1\sigma_1 + \Omega_2\sigma_2 + \Omega_\parallel\sigma_3), \tag{3}$$

where $\hbar\Omega_\parallel = g_\parallel\mu_0 B$, $g_\parallel$ is the longitudinal g factor of the exciton, μ_0 is the Bohr magneton, σ_i are Pauli matrices along axes 1,2,3 of the effective space where the pseudospin rotates, and $\hbar\Omega_1$ and $\hbar\Omega_2$ are two linearly-independent exchange-splitting parameters of the radiative doublet. Square-based quantum dots have point-group symmetry C_{2v} for which $\Omega_1 = 0, \Omega_2 \neq 0$, so that, with no magnetic field applied, the doublet components are polarized along $x \| [1\bar{1}0]$ and $y \| [110]$. In the general case of a rectangular base, local symmetry is lowered down to C_2, and Ω_1 is nonzero. Clearly enough, this quantity has opposite signs for quantum dots with bases extended along [100] and [010]. Note that for $\Omega_2 = \Omega_\parallel = 0$ and $\Omega_1 \neq 0$ the components of the doublet would be polarized along the axes $x' \| [100]$ and $y' \| [010]$ turned through 45° with respect to the x,y axes.

Neglecting the anisotropy in exciton generation and recombination, the average values of the pseudospin projections S_j $(j=1,2,3)$ are connected with the degree of polarization of emitted light, or Stokes parameters, through simple relations

$$P_{l'}=2S_1, \quad P_l=2S_2, \quad P_c=2S_3. \tag{4}$$

Similar expressions relate the incident polarization $P^0_{l'}, P^0_l, P^0_c$ to the direction of pseudospin $\mathbf{S}^0$ at the instant of exciton generation, provided the excitation does not entail partial loss of polarization. According to Eq. (3), the pseudospin precesses about vector $\mathbf{\Omega}=(\Omega_1,\Omega_2,\Omega_\parallel)$ with a frequency $|\mathbf{\Omega}|$. If this frequency exceeds significantly the reciprocal exciton lifetime τ^{-1}, and the spin relaxation time $\tau_s \gg \tau$, the average pseudospin vector $\mathbf{S}$ can be found by projecting vector $\mathbf{S}^0$ on the direction of $\mathbf{\Omega}$, i.e. $\mathbf{S}=\mathbf{\Omega}(\mathbf{\Omega}\cdot\mathbf{S}^0)/|\mathbf{\Omega}|^2$. We finally obtain a relation connecting the polarizations of the photoluminescence and of the incident light:

$$P_i=\Lambda_{ij}P^0_j (i,j=l',l,c), \tag{5}$$

$$\|\Lambda_{ij}\|=\frac{1}{\Omega_1^2+\Omega_2^2+\Omega_\parallel^2}\begin{bmatrix}\Omega_1^2 & \Omega_1\Omega_2 & \Omega_1\Omega_\parallel\\ \Omega_1\Omega_2 & \Omega_2^2 & \Omega_2\Omega_\parallel\\ \Omega_1\Omega_\parallel & \Omega_2\Omega_\parallel & \Omega_\parallel^2\end{bmatrix}. \tag{6}$$

Note that neglecting the effects of level anticrossover and absorption dichroism the polarization P_i^α coincides with the quantities ρ_α^i introduced in Eq. (2).

To take into account the anisotropy of generation and recombination along $[1\bar{1}0]$ and $[110]$, introduce the concentration of zero-dimensional excitons N_0 and vector $\mathbf{N}$ whose projections are connected through $N_l=2N_0S_l$ $(l=1,2,3)$ with the average pseudospin projections. In the case of steady-state excitation, the rate equations for the quantities N_0 and $\mathbf{N}$ can be written in the form

$$\frac{\mathbf{N}}{\tau}+\frac{N_0}{T}\mathbf{o}_2+\mathbf{\Omega}\times\mathbf{N}=\dot{\mathbf{N}}, \quad \frac{N}{\tau}+\frac{N_2}{T}=\dot{N}_0, \tag{7}$$

where

$$\frac{1}{\tau}=\frac{1}{2}\left(\frac{1}{\tau_{1\bar{1}0}}+\frac{1}{\tau_{110}}\right), \quad \frac{1}{T}=\frac{1}{2}\left(\frac{1}{\tau_{1\bar{1}0}}-\frac{1}{\tau_{110}}\right), \tag{8}$$

$\tau_{1\bar{1}0}, \tau_{110}$ are the exciton lifetimes in states $|1\bar{1}0\rangle$ and $|110\rangle$, and $\mathbf{o}_2$ is the unit vector in the direction of axis 2. The relation between the generation rates $\dot{N}_0, \dot{\mathbf{N}}$ and the incident polarization, as well as between $N_0, \mathbf{N}$ and the characteristics of secondary radiation can be written

$$\dot{N}_0=AI_0(1+aP^0_l), \quad \dot{N}_j=AI_0(\zeta_jP^0_j+b\,\delta_{j2}), \tag{9}$$

$$I=B(N_0+cN_2), \quad IP_j=B(N_j+cN_0\delta_{j2}). \tag{10}$$

Here the components I_0, I are intensities of the primary and secondary radiation, respectively, components P_1, P_2, P_3 are identified with $P_{l'}, P_l, P_c$, $\delta_{jj'}$ is the Kronecker symbol, coefficients $\zeta_j \leqslant 1$ account for polarization losses in the course of nonresonant or quasi-resonant excitation, parameter a characterizes the relative difference between generation rates of the total exciton number under excitation with light polarized along the $[1\bar{1}0]$ and $[110]$ axes, parameter b describes selectivity of generation of the $|1\bar{1}0\rangle$ and $|110\rangle$ states under unpolarized or circularly polarized excitation, and parameter c describes the anisotropy of radiative recombination. It is assumed that the values of $a, b,$ and c are small compared to one. An analysis of solutions to Eqs. (7) shows that experimental data can be fit satisfactorily for $|b-d| \ll |c|$, where $d \equiv T/\tau=(\tau_{110}-\tau_{1\bar{1}0})/(\tau_{110}+\tau_{1\bar{1}0})$. Then in first order in the small parameters $|\Lambda_{ij}\zeta_j|, |a|, |b| \ll 1$ we obtain

$$P_j^\alpha=\zeta_j(P_j^\alpha)_{a=b=0}+c\,\delta_{j2}, \quad \rho_\alpha^j=(P_j^\alpha)_{a=b=0}+a\,\delta_{j2}, \tag{11}$$

where $(P_j^\alpha)_{a=b=0}$ is the polarization calculated neglecting anisotropy and for $\zeta_j=1$. Within the two-level model, intensity I does not depend on magnetic field.

Experimentally, one analyzes light emitted by a large number ofquantum dots and, therefore, $\Lambda_{\alpha\beta}$ has to be averaged over the distribution of Ω_1 and Ω_2, to which fluctuations in quantum dot shape and local strains contribute. The apparent contradiction of experimental results, namely, (1) optical alignment of excitons irrespective of direction of the pump-light linear polarization and (2) the orientation-alignment transformation in a longitudinal field which implies that the $[110]$ and $[1\bar{1}0]$ axes are nonequivalent, can be explained satisfactorily by assuming that positive and negative values of Ω_1 are equally probable, i.e. that $\langle\Omega_1\rangle=0$, while the mean $\langle\Omega_2\rangle$ is nonzero. When calculating the polarization of radiation we assumed the exchange splitting parameters to have a Gaussian distribution:

$$P(B_1,B_2)=\frac{1}{2\pi b_1b_2}\exp\left(-\frac{B_1^2}{b_1^2}\right)\exp\left[-\frac{(B_2-\langle B_2\rangle)^2}{b_2^2}\right], \tag{12}$$

where $B_1=\hbar\Omega_1/(\mu_B g_\parallel)$, $B_2=\hbar\Omega_2/(\mu_B g_\parallel)$, and took into account that the average value of Ω_1 is zero.

By the parameters a and c characterizing the linear dichroism for absorption and emission, respectively, one should understand their values averaged over the quantum-dot ensemble. The solid lines in Fig. 1 were obtained theoretically by averaging expressions (11) with the use of the distribution function (12) for $\langle B_2\rangle=1.2$ kG, $b_2=b_1=1.8$ kG, $P^0_c=63\%$, $P^0_l=P^0_{l'}=33\%$. The values of P^0_j are not equal to one because of the polarization losses involved in quasi-resonant exciton excitation. The linear dichroism in absorption, a, with respect to the $\langle 110\rangle$ axes is 12.5%. There is also an indication of a linear dichroism along the $\langle 100\rangle$ axes (see Fig. 1b). This effect is, however, small and may be associated with the $[100]$ axis being not parallel to the plane of the pump light polarization. Therefore when processing the data in Fig. 1b the theoretical curve was shifted by 2.5%. The recombination anisotropy parameter was derived from the linear polarization along the $1\bar{1}0/110$ axes under unpolarized excitation and was found to be $c=6\%$.

Thus in contrast to GaAs/AlGaAs quantum-well structures[2] and GaAs/AlAs type-II superlattices[5], the major axes ofanisotropic exchange splitting for excitons in InAlAs/AlGaAs quantum dots are not fixed along the $[110]$ and $[1\bar{1}0]$ directions and are characterized by two linearly independent parameters Ω_1 and Ω_2. If the rectangular bases do

not have any preferred orientation in the (001) plane, the mean $\langle \Omega_1 \rangle = 0$, and the average value of the square of Ω_1 is nonzero.

E. L. I. acknowledges gratefully partial support of the Volkswagen Stiftung and of the Russian Fund for Fundamental Research (Grant 95-02-06038), and N. N. L., V. M. U., A. E. Zh., and A. F. Ts., that of the Russian Fund for Fundamental Research (Grant 96-02-17824), INTAS-RFRF (Grant 95-618), and Volkswagen Stiftung.

[1] S. V. Goupalov, E. L. Ivchenko, and A. V. Kavokin, in *Proceedings of the International Symposium ''Nanostructures: Physics and Technology''* (St. Petersburg, Russia, 1996), p. 322.
[2] D. Gammon, E. S. Snow, B. V. Shanabrook, D. C. Katzer, and D. Park, Phys. Rev. Lett. **76**, 3005 (1996).
[3] I. L. Aleĭner and E. L. Ivchenko, JETP Lett. **55**, 692 (1992); E. L. Ivchenko, A. Yu. Kaminski, and U. Rössler, Phys. Rev. B **54**, 5852 (1996).
[4] E. L. Ivchenko, V. P. Kochereshko, A. Yu. Naumov, I. N. Ural'tsev, and P. Lavallard, Superlattices Microstruct. **10**, 497 (1991).
[5] R. I. Dzhioev, H. M. Gibbs, E. L. Ivchenko, G. Khitrova, V. L. Korenev, M. N. Tkachuk, and B. P. Zakharchenya, Phys. Rev. B **56**, 13405 (1997).
[6] A. F. Tsatsul'nikov, A. Yu. Egorov, A. E. Zhukov, A. R. Kovsh, V. M. Ustinov, N. N. Ledentsov, M. V. Maksimov, A. V. Sakharov, A. A. Suvorova, P. S. Kop'ev, Zh. I. Alferov, and D. Bimberg, Fiz. Tekh. Poluprovodn. **31**, 109 (1997) [Semiconductors **31**, 88 (1997)].
[7] N. N. Ledentsov, M. Grundmann, N. Kirstaedter, J. Christen, R. Heitz, J. Böhrer, F. Heinrichsdorff, D. Bimberg, S. S. Ruvimov, P. Werner, U. Richter, U. Gösele, J. Heydenreich, V. M. Ustinov, A. Yu. Egorov, M. V. Maximov, P. S. Kop'ev, and Zh. I. Alferov, in *Proceedings of the 22nd International Conference Phys. Semicond.* (Vancouver, Canada, 1994), p. 1855; R. Heitz, M. Grundmann, N. N. Ledentsov, L. Eckey, M. Veit, D. Bimberg, V. M. Ustinov, A. Yu. Egorov, A. E. Zhukov, P. S. Kop'ev, and Zh. I. Alferov, Appl. Phys. Lett. **68**, 361 (1996).
[8] S. Raymond, S. Fafard, S. Charbonneau, R. Leon, D. Leonard, P. M. Petroff, and J. L. Merz, Phys. Rev. B **52**, 17238 (1995).
[9] M. Grundmann, O. Stier, and D. Bimberg, Phys. Rev. B **51**, 11969 (1995).

Translated by G. Skrebtsov

Effect of spin–orbit splitting on electron–hole transitions in microscopic CdS and CdTe crystals

A. A. Lipovskiĭ and E. V. Kolobkova

St. Petersburg State Technical University, 195251 St. Petersburg, Russia

V. D. Petrikov

A. F. Ioffe Physicotechnical Institute, Russian Academy of Sciences, 194021 St. Petersburg, Russia

Fiz. Tverd. Tela (St. Petersburg) **40**, 862–864 (May 1998)

The effect of the Luttinger parameters and finite spin–orbit splitting on the location of the lowest-lying size quantization levels of holes in spherical microscopic crystallites having cubic symmetry is examined for the case of type II–VI semiconductors using a model with a multigap hamiltonian. It is shown that, under conditions of severe size limitation, the controlling factor in the inversion of the s and p states if the relationship of the Luttinger parameters. The theory is compared with experiment for microscopic CdS and CdTe crystals. © *1998 American Institute of Physics.* [S1063-7834(98)02605-7]

The symmetry of the lowest-lying hole state in the valence band of microscopic crystals of type II–VI semiconductors has, thus far, only been established unambiguously for the case of cadmium selenide. Because of size quantization of the hole levels, in this case the lowest hole state has the symmetry of an s state ($1S_{3/2}$), while the next is a p state ($1P_{3/2}$).[1,2] Here there is an allowed transition from the lowest electron s level ($1S_e$) to the hole s level so that luminescence at the absorption edge of microscopic cadmium selenide crystals is observed.[1,2] At the same time, an inversion of the lowest hole s and p states has been noted in microscopic crystals of cadmium sulfide and telluride.[3–5] Such inversion should lead to the transition between the lowest electron and hole levels (the $s-p$ transition) forbidden by the selection rules, so that luminescence at the absorption edge should not be observed in microscopic crystals of these semiconductors. However, the question of the existence of an $s-p$ inversion in microscopic crystals of CdS and CdTe remains open, especially since edge luminescence has been detected for microscopic crystals cadmium sulfide and telluride in a number of experiments.[6–9] The purpose of the present paper is to study the dependence of the location of the lowest hole levels in microscopic crystals of II–VI semiconductors on the magnitude of the spin–orbit splitting, Δ_{SO}, and on the ratio of the Luttinger parameters, $\mu = 2\gamma_2/\gamma_1$, which describes the degree of mixing of the light and heavy subbands of the valence band.[10]

We have used in the analysis a multiband Hamiltonian model of the valence band in the effective mass approximation,[3] which makes it possible to find analytic solutions for spherical boundary conditions, while taking finite spin–orbit splitting Δ_{SO} into account.[1,3] These solutions also work well for the hexagonal microscopic crystals of CdSe when strong size quantization is present (the radius of the microscopic crystals is smaller than the exciton Bohr radius), since in this case the size quantization energy exceeds the splitting of the crystal field associated with the hexagonal symmetry.[2] The theory assumes conservation of the total hole angular momentum $F=L+J$, where L is the orbital angular momentum and J is the hole spin operator. The resulting hole energy levels are denoted by nQ_F, where n is the number of the energy level of the given symmetry and $Q=S,P,\ldots$ is the smallest orbital angular momentum included in the hole wave function. The lowest hole states are $1S_{3/2}$ and $1P_{3/2}$.[1–4]

Our calculations made it possible to determine the range of spin–orbit splitting and degrees of mixing of the light and heavy subbands over which $s-p$ inversion is possible. Figure 1 is a diagram in the μ,Δ_{SO} plane which illustrates the dependence of the type of lowest hole level in microscopic semiconductor crystals on μ and Δ_{SO} for (a) $\gamma_1=1.09$ (corresponding to γ_1 for microscopic CdS crystals[4]), (b) $\gamma_1=2.04$ (corresponding to CdSe[2]), and (c) $\gamma_1=4.7$ (corresponding to CdTe[5]). Using other published values of γ_1 for these semiconductors does not change the form of the diagrams qualitatively. Near $\mu=0.75$, the lowest levels are so close to one another that in the case $\gamma_1=4.7$ of a rather weak interaction with a very widely split band ($\Delta_{SO}\sim 9$ eV!), an inversion of the s and p levels would occur in small sized (~ 2 nm) microscopic crystals. Thus, the inversion of states is mainly determined by the degree of mixing of the light and heavy subbands, μ, rather than by the spin–orbit interaction, although an inversion of the s and p levels cannot occur without the influence of the latter. In the figure the asterisks denote the values of μ and Δ_{SO} for CdSe, CdS, and CdTe.[2–5,11] It can be seen that in CdSe the lowest hole state is always an s state, while for CdTe it is a p state. For CdS, the magnitude of μ is not adequately determined and it may happen that as the size of the microscopic crystals is reduced, an inversion from the s to the p state takes place.

We have made an experimental study of the structure of optical transitions in microscopic crystals of CdS and CdTe.

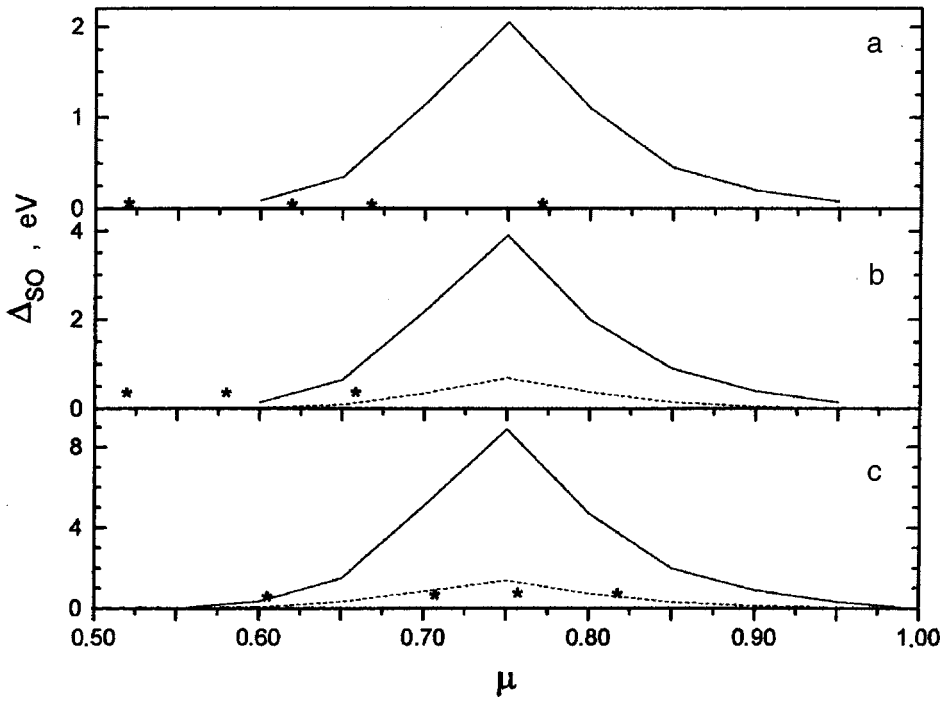

FIG. 1. A state diagram for the lowest hole level in microscopic crystals with radii of 2 nm (smooth curves) and 5 nm (dashed curves). Values of the parameters $\{\mu,\Delta_{SO}\}$ lying above the curve correspond to the s state, and below the curve, to the p state of the lowest level for $\gamma_1=1.09$ (a), 2.04 (b), and 4.7 (c). The asterisks denote published values of the parameters $\{\mu,\Delta_{SO}\}$ for cadmium sulfide (a), selenide (b), and telluride (c).

The microscopic crystals which we studied were formed in a specially developed matrix of phosphate glass of the system $P_2O_5-Na_2O-ZnO-AlF_3-Ga_2O_3$. The crystallite radius was varied from ~ 2 nm to the exciton Bohr radius. The crystallites had a narrow size distribution.[12] As a result, we observed at room temperature up to 7 transitions in the CdTe optical absorption spectra and up to 6 in those for CdS. (The locations of the transitions were determined from the second derivative of the absorption spectra.) It should be noted that the small amount of spin–orbit splitting in CdS leads to strong mixing of the hole states within a narrow energy interval and that, unlike microscopic CdSe and CdTe crystals, in this case the system of observed optical transitions (within an interval of ~ 1 eV) is caused by transitions to the higher electronic levels $1P_e$ and $1D_e$. The experimentally determined transition energies were compared with the calculated values and this allowed us to estimate the ratio μ of the Luttinger parameters. We found μ for CdTe to be $\mu\sim 0.6$ and for CdS, also $\mu\sim 0.6$. Thus, our data agree with published values of μ.[4,11]

Since the energies of the s and p states of the microscopic crystals are then close (see Fig. 1a and 1c), the $s-p$-inversion problem must be examined more rigorously. For example, in the existing model, the Coulomb interaction is treated as an effect which determines a correction to the optical transition energy and its effect on the mixing of states[10] is neglected. At the same time, the result of such mixing may be, for example, the absence of an inversion between close low hole states in CdTe crystallites. This appears to be confirmed by our and others'[9] observation of luminescence at the edge of the absorption band of microscopic CdTe crystals with sizes of 2–5 nm. Final conclusions about the luminescence of small-size CdS crystallites can be reached only after further study of high quality samples, since passivation of surface defects of microscopic CdS crystals produces luminescence of the bound exciton.[6,7]

We have shown in this way that the main factor controlling the $s-p$-inversion in microscopic crystals of type II–VI semiconductors is not the magnitude of the spin–orbit splitting, but the degree of mixing of the subbands of light and heavy holes in the valence band. Estimates of the ratios of the Luttinger parameters based on experiments with microscopic crystals of cadmium sulfide and telluride are consistent with the expected values, which confirms the validity of the computational procedure we have used. It was pointed out that the question of $s-p$-inversion requires a more rigorous model because of the closeness of the lowest hole levels.

[1] A. I. Ekimov, F. Hache, M. C. Schanne-Klein, D. Ricard, C. Flytzanis, I. A. Kudryavtsev, T. V. Yazeva, and A. V. Rodina, J. Opt. Soc. Am. B **10**, 100 (1993).
[2] D. J. Norris and M. G. Bawendi, Phys. Rev. B **53**, 16338 (1996).
[3] G. B. Grigoryan, É. M. Kazaryan, Al. L. Éfros, and T. V. Yazeva, Fiz. Tverd. Tela **32**, 1772 (1990) [Sov. Phys. Solid State **32**, 1031 (1990)].
[4] T. Richard, P. Lefebvre, and H. Mathiue, Phys. Rev. B **53**, 7287 (1996).
[5] P. Lefebvre, T. Richard, H. Mathiue, and J. Allegre, Solid State Commun. **98**, 303 (1996).
[6] Y. Wang, A. Suna, J. McHugh, E. F. Hilinski, P. A. Lucas, and R. D. Johnson, J. Chem. Phys. **92**, 6927 (1990).
[7] K. Misawa, H. Yao, T. Hayashi, and T. Kobayashi, J. Chem. Phys. **94**, 4131 (1991).
[8] T. Sekikawa, H. Yao, T. Hayashi, and T. Kobayashi, Solid State Commun. **83**, 969 (1992).
[9] T. Rajh, O. I. Micic, and A. J. Nozik, J. Phys. Chem. **97**, 11999 (1993).
[10] Y. Z. Hu, S. W. Koch, and N. Peyhambarian, J. Lumin. **70**, 185 (1996).
[11] C. R. M. de Oliveira, A. M. de Paula, F. O. Plentz Filho, J. Madeiros Neto, L. C. Barbosa, O. L. Alves, E. A. Menezes, J. M. M. Rios, H. L. Fragnito, C. H. Brito Cruz, and C. L. Cesar, Appl. Phys. Lett. **66**, 439 (1995).
[12] A. A. Lipovskii, E. V. Kolobkova, and V. D. Petrikov, Proc. SPIE **2967**, 30 (1996).

Translated by D. H. McNeill

Manifestation of near-surface localized excitons in spectra of diffuse reflection of light

J. Madrigal-Melchor, F. Pérez-Rodríguez, and A. Silva-Castillo

Instituto de Física, Universidad Autónoma de Puebla, Apdo. Postal J-48, Pue. 72570 Puebla, México

H. Azucena-Coyotécatl

Facultad de Ciencias Físico-Matemáticas, Universidad Autónoma de Puebla, Apdo. Postal 1152, Pue. 72000 Puebla, México

Fiz. Tverd. Tela (St. Petersburg) **40**, 865–866 (May 1998)

The interaction of excitons with rough surfaces and its effect on light scattering spectra were investigated theoretically. We have employed a model for the excitonic surface potential based upon the generalized Morse potential, taking into account its random fluctuations produced by the surface roughness. Applying first-order perturbation theory, we calculate the cross section of light scattering from a rough GaAs surface and analyze its frequency dependence in the presence of an extrinsic surface-potential well with excitonic bound states. © *1998 American Institute of Physics.* [S1063-7834(98)02705-1]

At present there is a great interest in the study of optical properties of spatially dispersive media such as excitonic crystals.[1] In these materials the interaction of excitons with the surface play an important role in determining the lineshape of their optical spectra (reflectivity, transmissivity, etc.). In the case of high-quality crystals the exciton-surface interaction is well described by a repulsive surface potential.[1] However, surface treatments (heating, intense illumination, electron and ion bombardment, doping, and electric-field application) modify the concentration of impurity ions in the transition layer and, consequently, the form of the surface potential. The extrinsic contribution to the surface potential may be attractive, unlike intrinsic potentials. The generation of excitonic bound state within an extrinsic potential well produces resonances (peaks and dips) in the optical spectra. Their resonance structure is very sensitive to the polarization of the incident light.[2,3] The resonances associated to transverse polaritonic modes appear in both *s*- and *p*-polarization geometries, whereas the longitudinal resonances, due to quantized polarization waves,[3] are present only in the latter geometry.

In this paper we present theoretical results for spectra of light scattering from random rough surfaces of GaAs crystals, having near-surface localized excitons. We will show that there spectra give useful information about the behavior of excitons near treated surfaces.

We solved analytically the system of equations that describes the exciton-polariton fields inside the semiconductor. It is composed of the Maxwell equations coupled to the equation for the excitonic polarization.[1] In the calculation we considered a surface potential $U(\mathbf{r})$given by

$$U(\mathbf{r})=U_1e^{-z/a}+U_2e^{-2z/a}+\zeta(\mathbf{r}_\parallel)(U_1e^{-z/a}+2U_2e^{-2z/a})/a. \quad (1)$$

This model holds when the surface is sufficiently smooth and its roughness is very small such that $\delta \ll a \ll L$ (δ is the mean-square deviation of the surface from its average plane $z=0$, a is the characteristic size of the transition layer, L is the correlation length of the surface profile function $\zeta(\mathbf{r}_\parallel)$, which is assumed to be a stationary, Gaussian stochastic process). Under these conditions, the exciton interacts, locally, with a flat surface and, therefore, the potential fluctuations are strongly correlated with the surface profile. The first two terms on the right-hand side of Eq. (1) represent the surface potential for an ideal flat surface,which is modeled here by the generalized Morze potential.[3] The terms proportional to $\zeta(\mathbf{r}_\parallel)$ in (1) describe the small (in $\delta/a \ll 1$) fluctuations of the surface potential.

The amplitudes of the electromagnetic fields, both inside the semiconductor ($z>\zeta(\mathbf{r}_\parallel)$) and in vacuum ($z<\zeta(\mathbf{r}_\parallel)$), are found by employing usual Maxwell boundary conditions together with the condition that the excitonic polarization vanishes at $z=\zeta(\mathbf{r}_\parallel)$. Applying first-order perturbation theory, we calculate the dimensionless cross section $d\sigma/d\Omega$, defined as the ratio of the intensity of light scattered into direction (θ,ϕ) (θ is the scattering angle, measured from the normal of the average surface, and ϕ is the azimuthal angle) to the intensity of the incident light.

The light scattering spectra in Figs. 1 and 2 were calculated for GaAs near exciton resonance frequency $\hbar\omega_T = 1.515$ eV. The rough-surface parameters, used here, are $\delta = 15$ Å, $L = 5000$ Å. Figs. 1a and 2a correspond to the case of a high-quality GaAs crystal with an intrinsic (exponential) potential ($U_1 = 0.5$ meV, $U_2 = 0$, $a = 130$ Å). The curves (2) in Figs. 1 and 2 were obtained for a surface potential well ($U_1 = -2.718$ meV, $U_2 = 3.694$ meV, $a = 550$ Å), having three excitonic bound states at the frequencies $\hbar\omega_{T1} = 1.51465$ eV, $\hbar\omega_{T2} = 1.51485$ eV, $\hbar\omega_{T3} = 1.51497$ eV. The near-surface localized excitons produce transverse resonances (broad peaks) in the frequency dependence of $d\sigma/d\Omega$ close to their eigenvalues ω_{Tn} ($n=1,2,3$). These peaks coalesce and form a huge maximum below the exciton resonance frequency ω_T in the spectrum $d\sigma(\omega)/d\Omega$ (see Figs. 1b and 2b). In the case of *p*-polarized incident light, besides transverse modes, quantized polarization waves[3] are

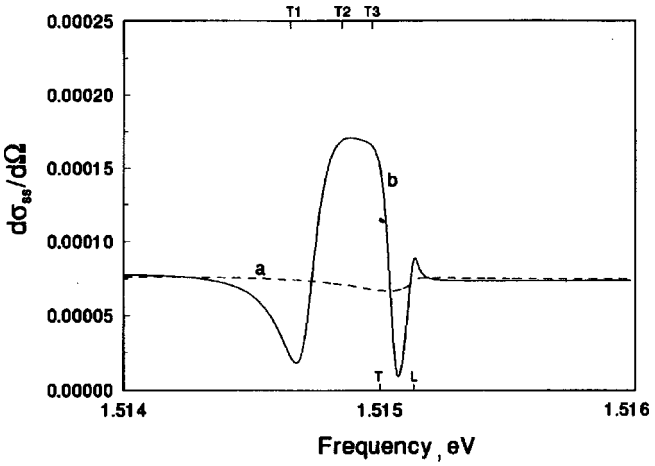

FIG. 1. Frequency dependence of the dimensionless cross section of light scattering from a rough GaAs surface. The incident light is *s*-polarized with an angle of incidence $\theta_0=40°$, and the scattered light is *s*-polarized in the plane of incidence ($\phi=0$) with $\theta=10°$. Curves (a) and (b) were calculated for an exponential potential and an extrinsic surface potential well, respectively.

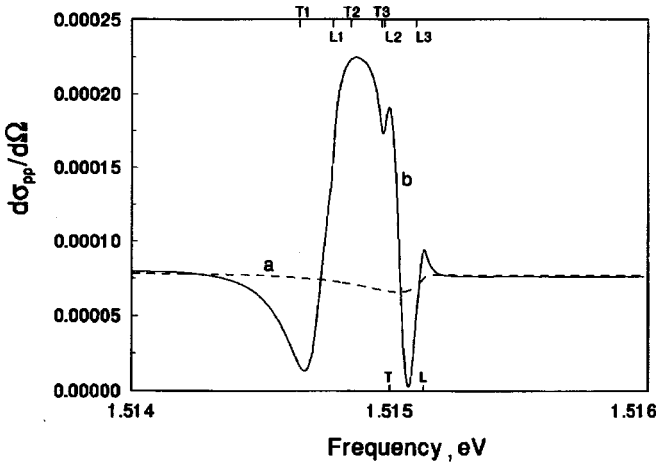

FIG. 2. The same as in Fig. 1, but both the incident light and the scattered light are *p*-polarized.

excited at frequencies $\omega_{Ln}=\omega_{Tn}+\omega_{LT}$ (ω_{LT} is the frequency value of the longitudinal-transverse splitting). These longitudinal modes give rise to new resonances in the spectrum $d\sigma(\omega)/d\Omega$ that interfere with the transverse ones. As is seen in Fig. 2b, the longitudinal resonances manifest themselves as dips in the spectrum of light scattering for GaAs. It is noteworthy that this manifestation is similar to that observed in reflectivity spectra.[3] This fact can be explained as a consequence of the assumed strong correlation between the potential fluctuations and the surface roughness.

In conclusion, the spectra of diffuse reflection can be useful to characterize the state of the surface transition layer and defect near-surface localized excitons.

The present work was partially supported by the Consejo Nacional de Ciencia y Tecnología.

[1] P. Halevi, in *Spatial Dispersion in Solids and Plasmas*, edited by P. Halevi, Vol. 1, *Electromagnetic Waves—Recent Developments in Research,* Chap. 6 (Elsevier, Amsterdam, 1992) (and references therein).
[2] A. S. Batyrev, N. V. Karasenko, and A. V. Sel'kin, Fiz. Tverd. Tela. **35**, 11, 3099 (1993) [Phys. Solid State **35**, 1525 (1993)].
[3] F. Pérez-Rodríguez and P. Halevi, Phys. Rev. B **53**, 10086 (1996).

Published in English in the original Russian journal. Reproduced here with stylistic changes by the Translation Editor.

Polariton reflectance spectra from thin ZnS_xSe_{1-x} layers

G. V. Astakhov, V. P. Kochereshko, and A. V. Platonov

A. F. Ioffe Physicotechnical Institute, Russian Academy of Sciences, 194021 St. Petersburg, Russia

D. R. Yakovlev, W. Ossau, W. Faschinger, and G. Landwehr

Physikalisches Institut der Universität Würzburg, 97074 Würzburg, Germany

Fiz. Tverd. Tela (St. Petersburg) **40**, 867–868 (May 1998)

A study of reflectance spectra from thin ZnS_xSe_{1-x} solid-solution layers in the region of excitonic resonances is reported. It has been found that an increase in sulfur concentration in the layers increases the inhomogeneous broadening of the quantized polariton lines. It has been established that the inhomogeneous line broadening in a reflectance spectrum depends on the magnitude of exciton-photon mixing; it is small in the long-wavelength region where the photon component of the polariton is large, and large at short wavelengths where the mechanical component dominates. © *1998 American Institute of Physics.* [S1063-7834(98)02805-6]

A large number of studies of exciton polaritons in thin semiconductor layers, quantum wells, and microcavities have recently been published.[1–3] The renewed interest in polariton-related phenomena stems from the explosive progress in the technology of fabricating semiconductor microcavities and observing the strong exciton-photon mixing in them. Of particular interest in this connection are II–VI semiconducting compounds, such as ZnS and ZnSe, which can be used to produce blue-green heterolasers.[3]

This work reports a study of the effect of fluctuations in the solid-solution composition x in thin ZnS_xSe_{1-x} layers on quantized polariton spectra.

The samples under study were ZnS_xSe_{1-x} layers about 250 nm thick with a cubic structure and sulfur composition within $0<x<0.12$, which were grown by molecular-beam epitaxy on (001)GaAs substrate. All the spectra presented in this work were measured at 1.6 K.

Figure 1 displays reflectance spectra for three samples with different sulfur concentrations ($x=0.12$, 0.07, and 0) obtained in the heavy-hole exciton-resonance region. Because of the lattice misfit between GaAs and ZnSe, the layers under study were strained. This lifts degeneracy in the valence band and splits the light- and heavy-hole states (in our case, by ~15 meV). This study deals only with heavy-hole excitons. The arrows in the figures identify the features associated with quantization of the exciton as a whole in a ZnS_xSe_{1-x} layer (minima in this particular case). The strongest polariton structure (four features) is observed in the binary compound ZnSe. An increase in sulfur concentration results in a broadening of the observed quantized polariton lines and a decrease of their number in the reflectance spectrum. In the $ZnS_{0.12}Se_{0.88}$ sample one sees already only one feature in the reflectance spectrum. We believe that an increase in sulfur concentration leads to increasing composition fluctuations in the solid solution, which, in its turn, gives rise to inhomogeneous broadening of the polariton quantized lines.

Based on Refs. 4 and 5, one can calculate a complex reflectance spectrum having a clearly pronounced polariton structure using the following parameters: exciton resonant frequency ω_0, nonradiative damping Γ, longitudinal-transverse exciton splitting $\hbar\omega_{LT}$, exciton translational mass M_{ex}, and sample thickness d. Figure 2 presents an experimental (solid line) and a theoretical (dashed line) reflectance spectrum from the ZnSe structure (the parameters of the calculation are specified in the figure caption). A good agreement of the measured with calculated spectrum was ob-

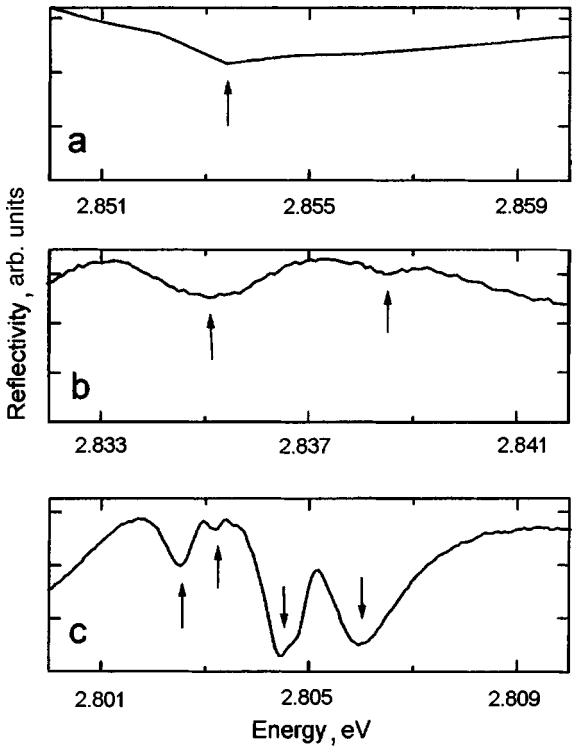

FIG. 1. Light reflectance spectra in the $e1-hh1$ exciton resonance region from ~250-nm thick layers of (a) $ZnS_{0.12}Se_{0.88}$, (b) $ZnS_{0.07}Se_{0.93}$, and (c) ZnSe.

tained. This shows that in the case of pure ZnSe (i.e., if the effect of inhomogeneous broadening can be neglected) the reflectance spectrum in the excitonic resonance region can be described in terms of an effective damping ($\hbar\Gamma = 0.25$ meV) which does not depend on energy. To explain the physical origin of the polariton structure, the inset to Fig. 2 shows schematically polariton dispersion curves. The presence of alternating maxima and minima in the reflectance spectra is due to interference of the exciton polaritons from branches 1 and 2.[6] The condition for an extremum (a minimum in our case) to appear corresponds to the interference condition

$$Kd = \frac{\omega}{c} nd = \pi\left(N + \frac{1}{2}\right), \tag{1}$$

where K is the polariton wave vector, d is the layer thickness, n is the refractive index, and N is an integer.

Shown in Fig. 3 is a reflectance spectrum obtained from a $ZnS_{0.07}Se_{0.93}$ structure (Line 1). Line 2 corresponds to a calculated reflectance spectrum with a damping $\hbar\Gamma = 2.2$ meV. The theoretical curve fits the experiment well only in the high-energy region of the polariton structure, and describes it poorly at low energies. By contrast, line 3, corresponding to a damping $\hbar\Gamma = 0.8$ meV, exhibits a good fit in the low-energy region while disagreeing with experiment at high energies.

We believe that the effect of inhomogeneous broadening is different for different polariton quantized levels and increases with increasing contribution of the mechanical exciton to the mixed exciton-photon mode (the polariton). As seen from the inset to Fig. 2, an increase in the number of the quantized polariton level corresponds to moving away from the anti-crossover of the photon and exciton modes and to a decrease in exciton-photon mixing.[7] Accordingly, levels with a higher energy (a larger number) are associated with a larger contribution of the mechanical exciton to the polariton mode and, hence, with a larger inhomogeneous broadening.

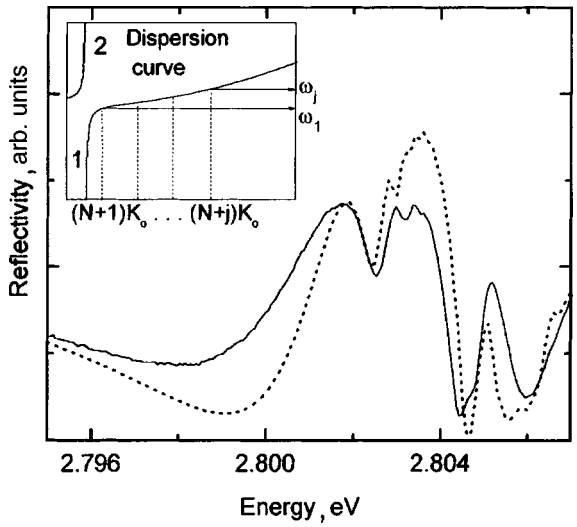

FIG. 2. Experimental (solid line) and calculated (dashed line) reflectance spectra from a ZnSe layer. The parameters used in the calculation: $\hbar\Gamma = 0.25$ meV, $\hbar\omega_0 = 2.803$ eV, $\hbar\omega_{LT} = 1.3$ meV, $M_{ex} = 0.65m_0$, $d = 250$ nm.

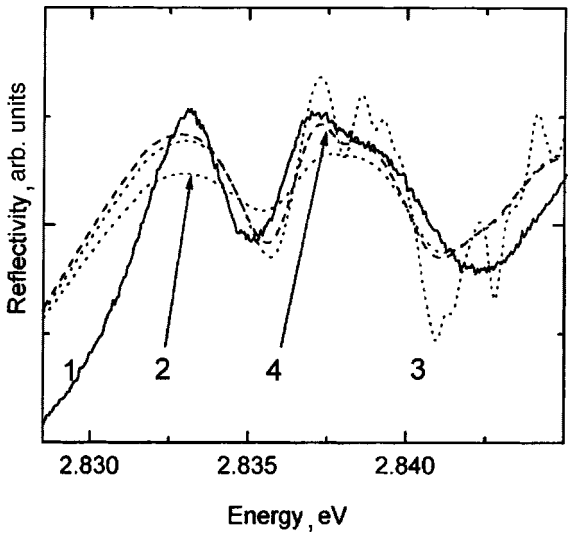

FIG. 3. Experimental (line 1) and calculated (lines 2–4) reflectance spectra from a $ZnS_{0.07}Se_{0.93}$ layer. The parameters used in the calculation: 2 — $\hbar\Gamma = 2.2$ meV, 3 — $\hbar\Gamma = 0.8$ meV, 4 — $\hbar\Gamma_{low} = 0.95$ meV, $\hbar\Gamma_{high} = 1.45$ meV. The other parameters are: $\hbar\omega_0 = 2.839$ eV, $\hbar\omega_{LT} = 1.8$ meV, $M_{ex} = 0.65m_0$, $d = 267$ nm.

To describe the reflectance spectrum from the $ZnS_{0.07}Se_{0.93}$ structure, one has to introduce the dependence of effective damping Γ on energy. Line 4 in Fig. 3 is a reflectance spectrum calculated for the case of Γ increasing linearly with decreasing wavelength: $\hbar\Gamma_{low} = 0.95$ meV in the low-energy part of the polariton spectrum, i.e. around the first feature, and $\hbar\Gamma_{high} = 1.45$ meV at high energies, in the region of the second feature in the polariton spectrum (Fig. 1b). We see that line 4 fits best the reflectance spectrum obtained.

Support of INTAS 93-3657 Ext, Volkswagen Stiftung, Russian Fund for Fundamental Research (Grant 96-02-17929), and ''Nanostructures'' Program of the Ministry of Science of Russia is gratefully acknowledged.

*Permanent address: A. F. Ioffe Physicotechnical Institute, Russian Academy of Sciences, 194021 St. Petersburg,Russia.

[1] A. D'Andrea and R. Del Sole, Phys. Rev. B **41**, 1413 (1990).
[2] N. Tomassini, A. D'Andrea, R. Del Sole, H. Tuffigo-Ulmer, and R. T. Cox, Phys. Rev. B **51**, 5005 (1995).
[3] J. Ding, H. Jeon, T. Ishihara, M. Hagerott, A. V. Nurmikko, H. Huo, N. Samarth, and J. Furdyna, Phys. Rev. Lett. **69**, 1707 (1992).
[4] Y. Chen, A. Tredicucci, and F. Bassani, Phys. Rev. B **52**, 1800 (1995).
[5] M. R. Vladimirova, A. V. Kavokin, and M. A. Kaliteevski, Phys. Rev. B **54**, 14566 (1996).
[6] V. A. Kiselev, B. S. Razbirin, and I. N. Ural'tsev, JETP Lett. **18**, 296 (1973).
[7] V. A. Kiselev, I. V. Makarenko, B. S. Razbirin, and I. N. Ural'tsev, Fiz. Tverd. Tela (Leningrad) **19**, 2348 (1977) [Sov. Phys. Solid State **19**, 1374 (1977)].

Translated by G. Skrebtsov

Thickness dependence of exciton absorption in pure GaAs crystals at the ''prequantum'' limit

G. N. Aliev

Kh. I. Amirkhanov Physics Institute, Russian Academy of Sciences, 367000 Makhachkala, Russia

N. V. Luk'yanova and R. P. Seĭsyan

A. F. Ioffe Physicotechnical Institute, Russian Academy of Sciences, 194021 St. Petersburg, Russia

Fiz. Tverd. Tela (St. Petersburg) **40**, 869–871 (May 1998)

The optical absorption of GaAs crystals with thicknesses $d=0.4-4.4$ μm is measured in the exciton-polariton resonance region at a temperature of 1.7 K. As the thickness is reduced, both a broadening of the exciton line and increased absorption with a negligible Stark shift are observed. The way the absorption spectra vary with crystal thickness is examined in terms of a competition between two regions for light-exciton interactions in the crystal: in the field of surface charges and electric-field free. © *1998 American Institute of Physics.* [S1063-7834(98)02905-0]

With thicknesses $a_x \leqslant d \leqslant l^*$, where a_x is the exciton Bohr radius and l^* is the polariton mean free path, thin films of semiconducting crystals can have optical properties at photon energies $h\nu \leqslant E_g$ which differ strongly from those of thicker ''bulk'' crystals. Here the optical phenomena also differ substantially from processes taking place in semiconducting heterostructures with layers of ''quantum'' thickness. In this regard, there is some interest in a separate study of the light absorption in this range of small thickness, immediately adjacent to the quantum-sized $2D$ structures. In the following, we shall refer to this range as ''prequantum.'' The purpose of this paper is to study the features of exciton optical absorption by semiconducting crystals of gallium arsenide with ''prequantum'' thicknesses.

1. SAMPLES AND EXPERIMENTAL TECHNIQUE

We have studied samples of high-quality pure GaAs ($n<5\times10^{14}$ cm^{-3}, $\mu_{77}=(1-1.5)\times10^5$ cm^2/V·s) with ''prequantum'' thicknesses (0.4–4.4 μm) cut from a thicker epitaxial layer. To measure the transmission spectra the substrate was etched chemically and the thickness of the epitaxial layers was reduced from 10 μm to the required size. Relatively uniform segments were selected for the measurements by masking. The technique for packaging and experimenting with the samples in free form without any kind of fastening or gluing has been described elsewhere.[1,2] The problem in analyzing the spectra obtained this way was to determine the sample thickness. Previously, for this purpose, we observed the end of the sample in an electron microscope. In this case, however, it would be difficult to compare the segments of the sample where the measurements were made with those parts where the thickness had been determined. Thus, we used the known absorption coefficient α for GaAs at the onset of the continuum. Then the thickness d of the crystal in the test section could be estimated as $d=D/\alpha^*$, where D is the optical density at $E=1.525$ eV and $\alpha^*=8\times10^3$ cm^{-1}.[3] The optical measurements were made while the sample was immersed in liquid helium which was pumped to a temperature of 1.7 K.

2. EXPERIMENTAL RESULTS

We obtained optical absorption spectra of a series of GaAs samples with thicknesses of 0.4 to 4.4 μm. With decreasing thickness in the range 4.4–2.0 μm, the absorption spectra essentially did not change and corresponded to those observed earlier (the half width of the line $H\approx0.3-0.5$ meV, a distinct exciton series $n_0=1,2,(3)$, a quasicontinuum, continuum, and exciton-impurity complex[4,5]). As the thickness is lowered down to 1 μm, simultaneous increases in the half width of the line and its amplitude were observed, which were then replaced by a drop in amplitude against the background of a continued increase in the half width (Fig. 1). Here the lines of the excited state and the exciton–impurity complex became indistinguishable.

In some of the ''prequantum'' samples with smaller thicknesses, it was possible to observe the effects of interference of the polariton waves, as well as quantization of the exciton as a whole. These features have shown up most clearly in samples with (In,Ga)As/GaAs quantum wells with a widened GaAs-barrier.[6] In studies of the optical absorption spectrum in GaAs barriers with $L_b=82.2$ and 75.8 nm, besides a series of narrow lines in the neighborhood of the discrete exciton spectrum of GaAs, it was possible to observe up to ten weak peaks in the continuum region. A transport matrix method has been used to calculate[6] the spectrum for these samples theoretically, including polariton interference and exciton quantization, and good agreement with the experimental spectrum was obtained—for a certain choice of the translational masses and ''exciton'' thickness of the crystal and ''dead'' layers.

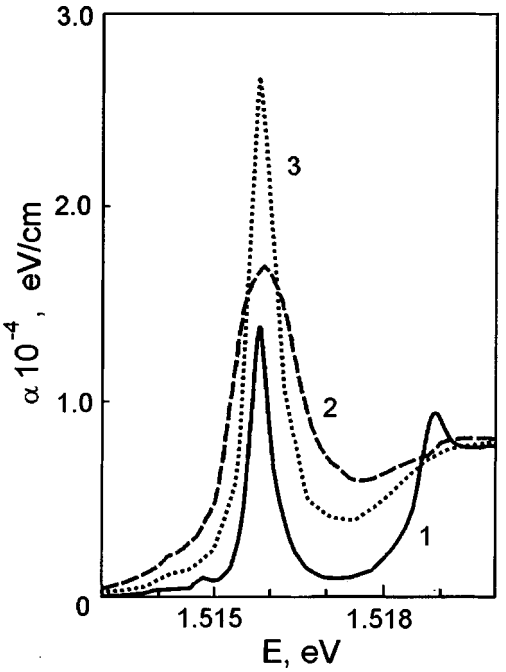

FIG. 1. Absorption spectra of GaAs samples with different thicknesses in the neighborhood of the exciton resonance, $T=1.7$ K, thickness d (μm): 3.2 (*1*), 0.4 (*2*), 1 (*3*).

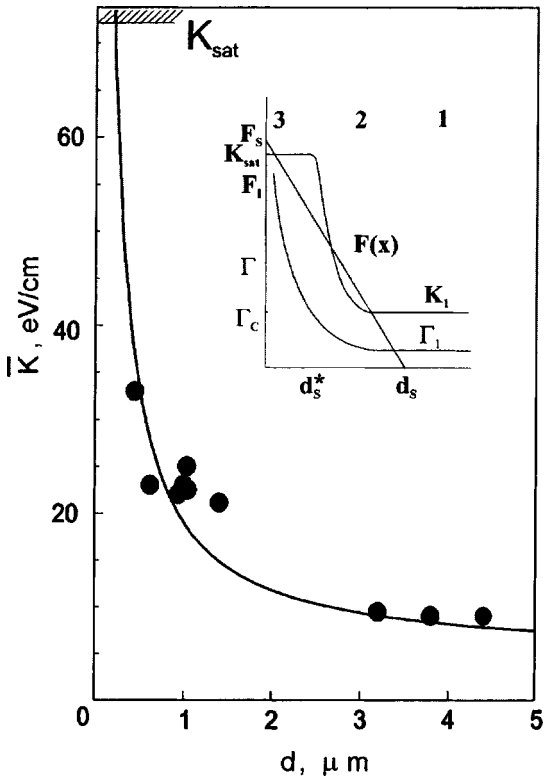

FIG. 2. The integrated absorption $\bar{K}$ of the ground exciton state of GaAs as a function of the crystal thickness d. The smooth curve is fit according to Eq. (1), with $K_1=5$ eV/cm, $K_s=74$ eV/cm, and $d_s^*=0.11$ μm. The points denote experimental data. Inset: the electric field distribution, dissipative damping, and integrated absorption according to Eq. (2) as functions of depth in the sample (model).

3. DISCUSSION OF RESULTS

During the course of the experiment we obtained a result that was strange at first sight: the optical absorption coefficient, which is usually a constant of the material, depended on the thickness in the region of the discrete exciton spectrum. An attempt to explain this fact can be made by noting the presence of an inhomogeneous electric field F near the sample surface (inset to Fig. 2) generated by the surface charge Q_s. The absorption coefficient is nonuniform over the cross section of the sample and the characteristic which we obtain is its effective value $\bar{\alpha}$.

If we assume that the conditions at the boundaries are unchanged as the sample thickness is reduced, there is a reduction in the size of the average region where an exciton is not subjected to an electric field. Changes in the exciton spectrum of such samples may be related to a change in the fraction of the crystal lying in the field of the surface charge. In the surface regions with $F(x)>F_I$, where $F_I=R/ea_x$ (e is the electronic charge and R is the exciton binding energy), an exciton is ionized; in the region where the field is smaller than F_I, it causes an inhomogeneous Stark shift of the line and broadens it. In this case, the absorption coefficient depends on the thickness as[1]

$$\bar{\alpha}(\omega)=\alpha(\omega)(1-2\,\delta\alpha_1(\omega)d_s/\alpha(\omega)d),$$

where $\delta\alpha_1$ is the surface absorption coefficient averaged over the layer, d_s, in which an exciton is acted on by the electric field. This dependence is hyperbolic and, by choosing the frequency, a rising or falling result can be obtained. At the exciton resonance frequency, however, because of electric field effects the amplitude of the absorption can only fall off with a broadening corresponding to the oscillator strength, which obviously contradicts the experimentally observed growth in the absorption as the thickness is reduced to $d\sim 1$ μm.

For further processing of the experimental data, we analyzed the integral absorption $K=\hbar\int\alpha d\omega$ as a response function. In general, it is proportional to the oscillator strength and is insensitive to a frequency shift of the line, as well as to its inhomogeneous broadening. It turned out that the area under the profile of the exciton ground state $n_0=1$ increased continuously over the entire range of variation (reduction) in the thickness, from 4.4 to 0.4 μm. $K(d)$ is plotted in Fig. 2. Clearly, for thicknesses $d>2$ μm, the integrated absorption coefficient approaches a constant value $\sim 5-8$ eV/cm and increases to 33 eV/cm when the thickness is reduced from 2 to 0.4 μm.

This behavior of the integrated absorption coefficient may be evidence of exciton-polariton processes. Since an exciton polariton with spatial dispersion ''absorbs'' light only to the extent of the real dissipative damping, one might think that in the central region of a sample of ''prequantum'' thickness, there would be almost no dissipative processes at 1.7 K. Such an effect has been observed in similar samples of GaAs during studies of the temperature characteristics of the integrated absorption coefficient.[7,8] Up to a critical temperature corresponding to a critical damping Γ_c, K was observed to rise, followed by saturation at $T>T_c$. The magnitude of the integrated absorption in the saturation region, K_{sat}, was determined by the oscillator strength of the state

and proportional to the longitudinal-transverse splitting energy, Δ_{LT}: $K_{\rm sat}=\pi/c\,\omega_0\Delta_{LT}\sqrt{\varepsilon_b}$, where ε_b is the background dielectric permittivity, which is determined by the effective dissipative damping until saturation. For GaAs the calculated value of $K_{\rm sat}=70$ eV/cm. Based on the preceding discussions, the integrated absorption coefficient of a thin sample in the neighborhood of the exciton resonance can be determined as follows:

$$\overline{K}(d)=K_1+2\frac{d_s^*}{d}K_s\left(1-\frac{K_1}{K_s}\right), \tag{1}$$

where K_s is the average integrated absorption coefficient of the surface regions and K_1 is the integrated absorption of the inner region of the sample. A curve constructed using Eq. (1) is shown in Fig. 2, where the fit parameters were chosen to be $K_1\approx 5$ eV/cm, $K_s\approx 74$ eV/cm, and $d_s^*\approx 0.11$ μm. The experimental points clearly lie well on the curve. It is noteworthy that we obtained a value of K_s that is almost the same as the calculated value of $K_{\rm sat}$, while the ratio $K_s/\overline{K}\approx 7$ for samples with $d\geqslant 2$ μm is consistent with the results from an earlier paper[7] on the thermal broadening of the exciton line.

We can, therefore, assume that in the interior region, where the excitons are not subject to the influence of an electric field, the polariton damping parameter Γ is smaller than the spatial dispersion owing to the losses, $\Gamma_c=2\hbar\omega_0\sqrt{2\varepsilon_b\Delta_{LT}/Mc^2}$. ($M$ is the translational electron mass.) In the surface layers the damping parameter increases rapidly as the field rises from the inner boundary of the space charge region to the surface according to $\Gamma\approx\Gamma_1+AR/f\exp(-4/3f)$, where $f=F/F_I$, Γ_1 is the damping parameter in the absence of a field, and A is a numerical factor. Of course, because of the presence of inhomogeneous line broadening and because the absorption coefficient has been calculated incorrectly as a parameter in the Bouguer law in the neighborhood of the exciton–polariton resonance, the observed linewidth is not quantitatively equal to Γ_1. It can be calculated using a calculation[9] of the integral absorption as the inverse logarithm of the transmission in a correct solution of the theoretical problem of the optical transmission of a uniform plane parallel slab in the neighborhood of the exciton–polariton resonance:

$$K=\frac{2}{\pi}\left(\arctan(d/\sqrt{1-g^2})+g\sqrt{1-g^2}\right)K_{\rm sat}, \tag{2}$$

where $g=(\Gamma/\Gamma_1)\leqslant 1$. According to Eq. (2), the integral absorption K varies almost linearly with increasing damping Γ for $\Gamma<\Gamma_c$ and saturates for $\Gamma\geqslant\Gamma_c$ (inset to Fig. 2). Figure 2 also implies that for $g\ll 1$ the dissipative damping is given by $\Gamma=(\pi K/4K_{\rm sat})\Gamma_c$. Substituting our data and the estimate for K_1 in these equations, we obtain $\Gamma_1\approx 0.02$ meV, while $\Gamma_c\approx 0.24$ meV. The inset to Fig. 2 illustrates the variation in Γ and K over the cross section of the sample. Since the transition from Γ_1 to Γ_c and, therefore, from K_1 and $K_{\rm sat}$ takes place within a relatively narrow region of the crystal, our dividing the sample up into three layers and applying the equations in Ref. 9 derived for a uniform sample, to this highly nonuniform case, appear to be justified.

This experimental study has shown that exciton–polariton processes play an important role in the transport of light through thin slabs of highly-perfected semiconducting crystals whose thickness is ''prequantum,'' with $a_x\leqslant d\leqslant l^*$. Our analysis shows that, in our relatively ''pure'' GaAs crystals at low temperatures, the true dissipative damping is $\Gamma=0.02$ meV for the measured linewidth of 0.3–0.5 meV. Polariton processes manifest themselves through a substantial (by many times) increase in the transparency of the sample in the neighborhood of exciton–polariton resonances compared to exciton absorption without spatial dispersion. This happens right up to $\Gamma\geqslant\Gamma_c$, where Γ is the true dissipative damping. Throughout this interval, the transparency of a ''prequantum'' sample is greater than in the saturation region characterized by spatial dispersion losses. The condition $\Gamma\geqslant\Gamma_c$ is achieved in our experiments because of the effect of an electric field as the sample thickness is reduced to $d\leqslant 2d_s^*$, where d_s^* is the corresponding part of the space- charge layer. In the earlier experiments,[7,8] it was then achieved because of temperature.

This work was supported by State Scientific-Technical Program Grants 1-020/2 and 1-080/4.

[1] R. P. Seĭsyan, *The Spectroscopy of Diamagnetic Excitons* [in Russian], Nauka, Moscow (1984), 282 pp.
[2] G. N. Aliev, N. V. Luk'yanova, and R. P. Seĭsyan, Fiz. Tverd. Tela **38**, 1067 (1996) [Semiconductors **38**, 590 (1996)].
[3] M. D. Sturge, in *Excitons*, E. I. Rashba and M. D. Sturge (Eds.), North-Holland, Amsterdam (1982), p. 9.
[4] D. D. Sell, Phys. Rev. **86**, 3750 (1972).
[5] C. Weisbuch, in *Semiconductors and Semimetals*, B. Dingle (Ed.), Academic Press (1987), Vol. 24, p. 1.
[6] G. N. Aliev, N. V. Luk'yanova, R. P. Seisyan, R. Vladimirova, H. Gibbs, and C. Khitrova, Phys. Status Solidi A **164**, 193 (1997).
[7] V. A. Kosobukin, R. P. Seisyan, and S. A. Vaganov, Semicond. Sci. Technol. **8**, 1235 (1993).
[8] G. N. Aliev, O. S. Coschug-Toates, V. A. Kosobukin, R. P. Seisyan, and S. A. Vaganov, Proc. SPIE, J. Singh (Ed.), Vol. 2362, p. 561.
[9] N. N. Akmediev, Zh. Eksp. Teor. Fiz. **4**, 1534 (1980) [*sic*].

Translated by D. H. McNeill

Optics of excitons in systems with sharp heteroboundaries. Approximation of a strongly localized exciton wave function

G. F. Glinskiĭ and K. O. Kravchenko

St. Petersburg State Electrotechnical University, 197376 St. Petersburg, Russia

Fiz. Tverd. Tela (St. Petersburg) **40**, 872–874 (May 1998)

Optical reflection spectra from a $Ga_{0.7}Al_{0.3}As/GaAs$ heteroboundary are calculated using the approximation of a strongly localized exciton wave function. The calculation is based on electron Γ_6 and hole Γ_8 **kp**-Hamiltonians with position-dependent parameters. © *1998 American Institute of Physics.* [S1063-7834(98)03005-6]

It has been shown[1] that the use of the **kp** Hamiltonian derived for a bulk material is inadmissible for investigating systems with heteroboundaries. When a heteroboundaries are present, the effective **kp** Hamiltonian in the x representation for an arbitrary degenerate band contains position-dependent parameters and can be written in the form

$$H_{mm'}(\mathbf{x})=[E+\Delta E\,\theta(z)]\delta_{mm'}-\frac{\hbar^2}{2m_0}\frac{\partial}{\partial x_i}\times[M^{ij}_{mm'}(z)]\frac{\partial}{\partial x_j}+\Delta U_{mm'}\delta(z), \quad (1)$$

where ΔE is the band gap, $\theta(z)$ is the step function, $M^{ij}_{mm'}(z)$ are position dependent parameters which determine the matrix elements of the Hamiltonian, and $\Delta U_{mm'}$ are corrections which characterize the short-range part of the heteroboundary potential. In particular, for A_3B_5 semiconductors, the Γ_6 band **kp**-Hamiltonian will be characterized by two position-dependent parameters α_1 and α_2. Of these, the first $\alpha_1(z)=m_0/m_e(z)$ determines the effective electron mass in band Γ_6, while the second $\alpha_2(z)$ is caused by the presence of a heteroboundary and vanishes in the bulk material:

$$H^{\Gamma_6}=I^e(\hat{\mathbf{k}}\alpha_1\hat{\mathbf{k}})+i(\sigma_x[\hat{k}_y\alpha_2\hat{k}_z]+\sigma_y[\hat{k}_z\alpha_2\hat{k}_x]+\sigma_z[\hat{k}_x\alpha_2\hat{k}_y]), \quad (2)$$

where I^e is the 2×2 unit matrix, the σ_i are the Pauli matrices, $\hat{k}_j=-i\partial/\partial x_j$, $(\hat{\mathbf{k}}a\hat{\mathbf{k}})=\hat{k}_xa\hat{k}_x+\hat{k}_ya\hat{k}_y+\hat{k}_za\hat{k}_z$, and $[\hat{k}_ia\hat{k}_j]=\hat{k}_ia\hat{k}_j-\hat{k}_ja\hat{k}_i$.

The Hamiltonian of the Γ_8 band in the presence of a heteroboundary will be characterized by the three Luttinger parameters γ_1, γ_2, and γ_3, as well as the additional parameters γ_4 and γ_5 (a refinement of the data obtained previously[2]):

$$\begin{aligned}H^{\Gamma_8}=&I^h(\hat{\mathbf{k}}\gamma_1\hat{\mathbf{k}})-(1/3)[(2J_z^2-J_x^2-J_y^2)(2\hat{k}_z\gamma_2\hat{k}_z-\hat{k}_x\gamma_2\hat{k}_x-\hat{k}_y\gamma_2\hat{k}_y)+3(J_x^2-J_y^2)(\hat{k}_x\gamma_2\hat{k}_x-\hat{k}_y\gamma_2\hat{k}_y)]-4[\{J_yJ_z\}\\&\times\{\hat{k}_y\gamma_3\hat{k}_z\}+\{J_xJ_z\}\{\hat{k}_x\gamma_3\hat{k}_z\}+\{J_xJ_y\}\{\hat{k}_x\gamma_3\hat{k}_y\}]\\&+i2(J_x[\hat{k}_y\gamma_4\hat{k}_z]+J_y[\hat{k}_z\gamma_4\hat{k}_x]+J_z[\hat{k}_x\gamma_4\hat{k}_y])\\&+i8(J_x^3[\hat{k}_y\gamma_5\hat{k}_z]+J_y^3[\hat{k}_z\gamma_5\hat{k}_x]+J_z^3[\hat{k}_x\gamma_5\hat{k}_y]),\end{aligned} \quad (3)$$

where I^h is the 4×4 unit matrix, J_i are the matrices for angular momentum 3/2, $\{J_iJ_j\}=(1/2)(J_iJ_j+J_jJ_i)$, and $\{\hat{k}_ia\hat{k}_j\}=(1/2)(\hat{k}_ia\hat{k}_j+\hat{k}_ja\hat{k}_i)$.

The additional parameter γ_4 can be determined approximately if we neglect the **kp** interaction of the Γ^{ν}_{15} valence band with the Γ_{25} bands. In this case, $\gamma_4=-(1/3)(1+\gamma_1-2\gamma_2-3\gamma_3)$. The parameters α_2 and γ_5 show up only when the spin-orbit splitting of the intermediate states is taken into account and are given by

$$\alpha_2=-\frac{\Delta_{\rm co}}{3E_g+2\Delta_{\rm co}}\left(\frac{m_0}{m_e}-1\right),$$

$$\gamma_5=\frac{1}{18}(1+\gamma_1-2\gamma_2)\frac{\Delta'_{\rm co}}{E'_g+\Delta'_{\rm co}},$$

where E_g and $\Delta_{\rm co}$ are, respectively, the $\Gamma^c_6-\Gamma^{\nu}_8$ energy gap and the spin-orbit splitting of the Γ^{ν}_{15} valence band, and E'_g and $\Delta'_{\rm co}$ are, respectively, the $\Gamma^c_7-\Gamma^{\nu}_8$ energy gap and the spin-orbit splitting of the Γ^c_{15} conduction band. In calculating α_2, we included only the **kp** interaction of the Γ^c_1 conduction band with the Γ^{ν}_{15} valence bad, and in calculating γ_5, the interaction of the Γ^{ν}_{15} valence band with the nearest conduction band, Γ^c_{15}. From the condition that the Hamiltonian (1) be hermitian and using Eqs. (2) and (3), it is possible to derive the following boundary conditions for the electron wave function in the Γ_6 band and the hole wave function in the Γ_8 band at a [001] interface:

$$\begin{aligned}&\psi^{\rm e,h}(+0)=\psi^{\rm e,h}(-0),\\&(\hat{A}^{\rm e,h}_z\psi^{\rm e,h})|_{z=+0}-(\hat{A}^{\rm e,h}_z\psi^{\rm e,h})|_{z=-0}-B^{\rm e,h}_z\psi^{\rm e,h}(0),\\&\hat{A}^h_z=\gamma_1I^h\hat{k}_z-(1/3)\gamma_2[(2J_z^2-J_x^2-J_y^2)2\hat{k}_z]\\&\quad-2\gamma_3[\{J_yJ_z\}\hat{k}_y+\{J_xJ_z\}\hat{k}_x]+i2\gamma_4[-J_x\hat{k}_y+J_y\hat{k}_x]\\&\quad+i8\gamma_5[-J_x^3\hat{k}_y+J_y^3\hat{k}_x],\\&\hat{A}^{\rm e}_z=\alpha_1I^{\rm e}\hat{k}_z+i\alpha_2[-\sigma_x\hat{k}_y+\sigma_y\hat{k}_x],\quad B^{\rm e}_z=(i/a_0)nI^{\rm e},\\&B^{\rm h}_z=(i/a_0)[m_1I^{\rm h}+m_2(2J_z^2-J_x^2-J_y^2)+m_3\{J_xJ_y\}],\end{aligned} \quad (4)$$

where n and $m_{1,2,3}$ are constants which determine the matrix $\Delta U_{mm'}$. In particular, m_3 mixes the states of light and heavy holes at the heteroboundary.[3]

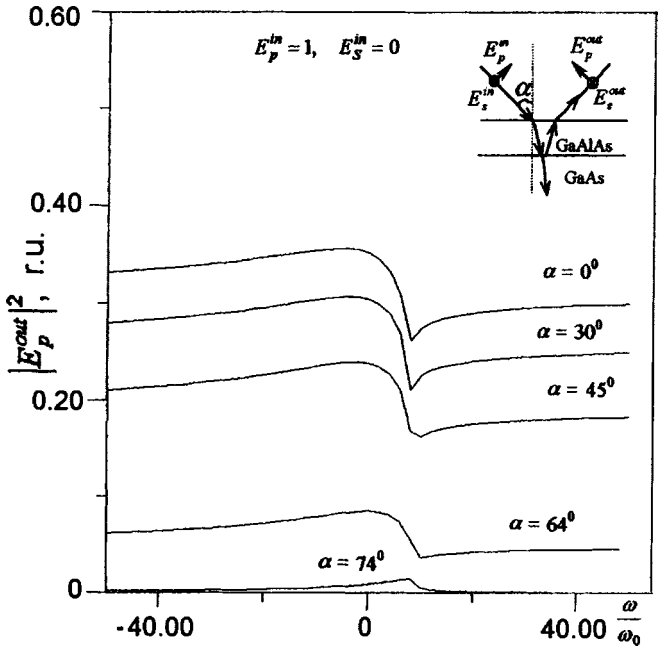

FIG. 1. Intensity of p-polarized reflected light, E_p^{out} for different angles of incidence near the exciton resonance for $E_p^{\text{in}}=1$ and $E_s^{\text{in}}=0$. $\omega_0=(E_{gx}^{\text{GaAs}}/\hbar)(E_{gx}^{\text{GaAs}}/2m_0c^2)(m_0/M_{ex}^{\text{GaAs}})$.

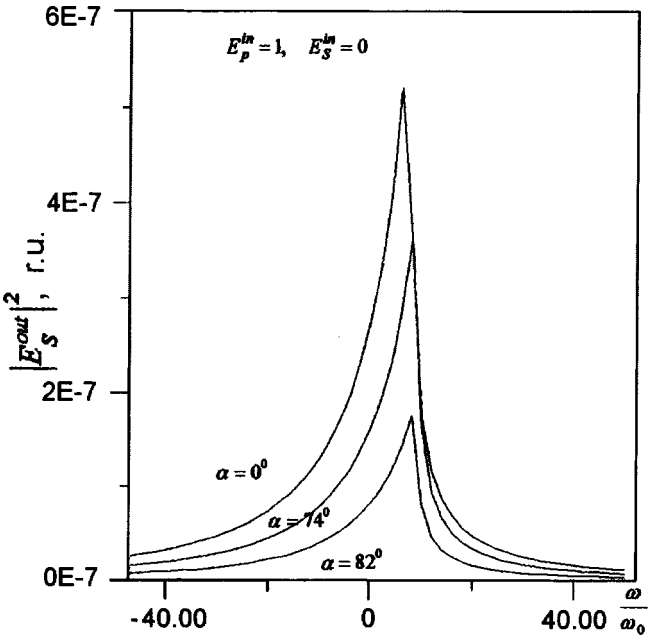

FIG. 2. Intensity of s-polarized reflected light, E_s^{out} for different angles of incidence near the exciton resonance for $E_p^{\text{in}}=1$ and $E_s^{\text{in}}=0$. $\omega_0=(E_{gx}^{\text{GaAs}}/\hbar)(E_{gx}^{\text{GaAs}}/2m_0c^2)(m_0/M_{ex}^{\text{GaAs}})$.

When a heteroboundary is present, the exciton Hamiltonian has the form

$$\hat{H}_{\text{ex}}(\mathbf{x}_e,\mathbf{x}_h)=H_{cc'}(\mathbf{x}_e)\delta_{vv'}+H_{vv'}(\mathbf{x}_h)\delta_{cc'}+U_{\text{Coul}}(\mathbf{x}_e-\mathbf{x}_h)\delta_{vv'}\delta_{cc'}, \tag{5}$$

where $H_{cc',\nu\nu'}(\mathbf{x}_{e,h})$ are determined by Eq. (1) and U_{Coul} is the Coulomb interaction operator.

As for the position dependence $M_{mm'}^{ij}(z)$, it is more convenient not to transform to the center-of-mass system in the Hamiltonian (5), but to consider, for this purpose, the Hamilton function

$$H=\langle\psi|\hat{H}_{\text{ex}}|\psi\rangle=\sum_{cvc'v'}\int d\mathbf{x}_c\int d\mathbf{x}_h\{\psi_{cv}^*(\mathbf{x}_e,\mathbf{x}_h)\times\hat{H}_{\text{ex}}(\mathbf{x}_e,\mathbf{x}_h)\psi_{c'v'}(\mathbf{x}_e,\mathbf{x}_h)\}. \tag{6}$$

This makes it possible to preserve the invariance of the tensor equations automatically and, also, to facilitate taking averages over the relative coordinates of the electron and hole.

Even in the absence of band degeneracy, a heteroboundary does not permit separation of the translational and relative motion of an electron-hole pair. This can, however, be accomplished approximately with the position dependent parameters of the transformation $\gamma_{e,h}(Z)$,

$$\begin{cases}\mathbf{x}_e=\mathbf{R}+\gamma_e(Z)\mathbf{r},\\ \mathbf{x}_h=\mathbf{R}-\gamma_h(Z)\mathbf{r},\end{cases}\quad \gamma_e(Z)+\gamma_h(Z)=1. \tag{7}$$

The parameters $\gamma_{e,h}(Z)$ can be determined if we separate the diagonal parts $M^{e,h}(Z\pm\gamma_{e,h}(Z)z)\delta_{mm'}\delta_{ij}$ in the matrices $M_{mm'}^{i,j;e,h}(Z\pm\gamma_{e,h}(Z)z)$ and expand them in a power series in z, limiting ourselves to the first terms of the expansion and requiring cancellation of cross terms of the form $\partial\psi^*/\partial\mathbf{R}\cdots\partial\psi/\partial\mathbf{r}$ in Eq. (6). Here the exciton wave function is conveniently sought in the form of the expansion

$$\psi_{cv}(\mathbf{R},\mathbf{r})=\sum_p\varphi_p(Z,\mathbf{r})\Phi_{\text{exp}}(\mathbf{R}),$$

where $\varphi_p(Z,\mathbf{r})$ is the solution of the auxiliary parametric problem

$$\left\{-\frac{\hbar^2}{2m_0}[M_e(Z)+M_h(Z)]\frac{\partial^2}{\partial\mathbf{r}^2}+U_{\text{Coul}}(\mathbf{r})\right\}\varphi_p(Z,\mathbf{r})=E\varphi_p(Z,\mathbf{r}).$$

In this case, we shall have ($J(\mathbf{R},\mathbf{r})$ is the Jacobian of the transformation (7))

$$H=\langle\psi|\hat{H}_{\text{ex}}|\psi\rangle=\sum_{cvc'v'pp'}\int\int\{\Phi_{\text{exp}}^*(\mathbf{R})\varphi_p^*(Z,\mathbf{r})\times\hat{H}_{\text{ex}}(\mathbf{R},\mathbf{r})\varphi_{p'}(Z,\mathbf{r})\Phi_{c'v'p'}(\mathbf{R})\}\times J(\mathbf{R},\mathbf{r})d\mathbf{r}d\mathbf{R}.$$

In first-order perturbation theory for the Hamiltonian of the translational motion of the $1S$ state of the exciton, this yields

$$\hat{H}_{1S}(\mathbf{R})=\int\varphi_{1S}^*(Z,\mathbf{r})\hat{H}_{\text{ex}}(\mathbf{R},\mathbf{r})\varphi_{1S}(Z,\mathbf{r})J(\mathbf{R},\mathbf{r})d\mathbf{r}. \tag{8}$$

Here all the abrupt functions $M_{e,h}(\mathbf{x}_{e,h})$, $\theta_{e,h}(\mathbf{x}_{e,h})$, and $\delta(\mathbf{x}_{e,h})$, after the averaging (8), are smoothed out over a scale length on the order of the exciton Bohr radius a_B. In the optical range, where $K_{\text{ex}}\ll 1$, however, this smoothing can be neglected. In this case, the problem with the hamiltonian (8) reduces to a boundary value problem.

Using Eq. (8) for the exciton hamiltonian and the boundary conditions derived from Eq. (4), we have calculated the

optical reflection spectra from a $Ga_{0.7}Al_{0.3}As/GaAs$ heteroboundary for normally and obliquely incident light near the $\Gamma_6 \otimes \Gamma_8$-exciton resonance of GaAs. In calculating these spectra, we have used the polariton theory developed previously.[4–6] The results of these calculations are shown in Figs. 1 and 2. It can be seen that even at the Brewster angle $\alpha \approx 74°$, in the neighborhood of the exciton resonance ($\omega = 0$) the reflection coefficient is nonzero. In addition, mixing of light and heavy hole states at the heteroboundary, even for normally incident light, causes the appearance of forbidden modes in the reflected light at intensities $\approx 10^{-7}$ times that of the incident light.

[1] G. F. Glinskii and K. O. Kravchenko, in *Proceedings of the International Symposium ''Nanostructures-97: Physics and Technology''*, St. Petersburg (1997).
[2] B. A. Foreman, Phys. Rev. B **48**, 4964 (1993).
[3] E. L. Ivchenko, A. Yu. Kaminski, and U. Rössler, Phys. Rev. B **54**, 5852 (1996).
[4] Z. G. Koinov and G. F. Glinskii, J. Phys. A **21**, 3431 (1988).
[5] G. F. Glinskii and Z. G. Koinov, Phys. Status Solidi B **155**, 501 (1989).
[6] Z. G. Koinov and G. F. Glinskii, Phys. Status Solidi B **155**, 513 (1989).

Translated by D. H. McNeill

Photoreflection and photoconduction spectra of CdS crystals: excitons in the electric fields of surface states

R. A. Bisengaliev, É. D. Batyrev, and B. V. Novikov

Scientific-research Institute of Physics, St. Petersburg State University, 198904 Petrodvorets, Russia

A. V. Sel'kin

A. F. Ioffe Physicotechnical Institute, Russian Academy of Sciences, 194021 St. Petersburg, Russia

Fiz. Tverd. Tela (St. Petersburg) **40**, 875–876 (May 1998)

The exciton photoreflection spectra of CdS crystals are studied. It is found that the form of the exciton photoreflection spectrum is determined by a Stark shift of the exciton energy in the electric field of surface states. The dependences of the exciton photoreflection spectrum on temperature on the intensity and wavelength of the modulating radiation, and on the processes by which the photoreflection signal relaxes is determined. An energy scheme is proposed for the surface states which explains the observed effects of photoinduced changes in the surface field. A correlation is established between the exciton photoreflection spectrum and the form of the fine structure in the photoconductivity. © *1998 American Institute of Physics.* [S1063-7834(98)03105-0]

Exciton photoreflection spectra of CdS crystals have been studied by a number of authors. It has been proposed that the photomodulation of the reflection is related to screening of the surface field[1] or to screening of excitons.[2] Risch[3] has related photoreflection to a change in the surface field and in the conditions for recombination on the crystal surface.

In this paper, as in Ref. 3, it is found that CdS crystals obtained by different methods can be divided into two groups in terms of the form of their exciton photoreflection spectra: *A* and *B* (Figs. 1 and 2). A spectrum of type *A* has the form of an inverse dispersion profile and a spectrum of type *B* has the form of a direct dispersion profile. The modulated light sources used in the exciton photoreflection spectral studies were a nitrogen laser ($\lambda = 337$ nm), mercury lamps, and incandescent lamps in combination with a monochromator to isolate a narrow spectral interval from their continuous spectrum. Single quasimonochromatic pulses of the modulated light with a duty factor and duration of several seconds were used.

A type *A* exciton photoreflection spectrum corresponds to a photoinduced shift in the reflection profile to longer wavelengths and a type *B* spectrum, to a shift to shorter wavelengths (positive and negative Stark shifts ΔE in the exciton resonance). A shift to longer wavelengths is caused by an enhancement in the surface field (filling of the surface states) and a shift to shorter wavelengths, by an attenuation of this field (emptying of surface states). The magnitude of the shift is basically determined by the intensity of the modulating radiation. The amplitude of the exciton photoreflection spectrum and the shift $|\Delta E|$ decrease as the crystal temperature is lowered from 77 K to 4.2 K (especially strongly for type *B* crystals), which signifies a reduction in the strength of the induced component of the surface field.

ΔE was measured from the shift in the inflection point in the reflection profile. For several samples $|\Delta E|$ was as high as 2 meV (Figs. 1 and 2). This method of measuring ΔE is justified by comparing the experimental spectra with theoretical ones, calculated using a model of an exciton Stark effect in the surface field of a Schottky barrier.[4] Qualitative agreement between the experimental and theoretical spectra is attained if it is assumed that the excess donor concentration in these samples is of order 10^{16} cm^{-3}, while the surface deflection of the bands varies over 0.1–0.2 eV.

The temporal relaxation of the photoreflection signal in type *A* crystals is characterized by fast ($\tau < 0.1$ s) and slow ($\tau > 5$ s) components, and in type *B* crystals mainly by the fast component (Fig. 1a and 1b). The fast component may be related to Coulomb capture of holes at surface states, while the slow component is related to thermal ejection of electrons from relatively shallow surface states into the conduction band. As the temperature is lowered, this component becomes weaker.

In our studies of the dependence of the exciton photoreflection spectrum on the wavelength of the modulated light, it was somewhat surprising that a photoreflection signal is also observed in the vicinity of the exciton resonance when the energy E_{MO} of the modulated light photons was substantially lower than the band gap E_g. Figure 2 shows plots of the rise ΔR in the reflection coefficient R in the spectral neighborhood of the maximum in R as a function of the modulated light photon energy for both types of crystal. The variation in ΔR is clearly qualitatively different for crystals of type *A* and *B*.

Changing the wavelength of the modulated light in the transparency region of the crystal leads to a change in the amplitude and sign of the exciton photoreflection spectrum signal which corresponds to a transition from type *A* to type *B* or *vice versa*. For type *A* crystals, this kind of transition is

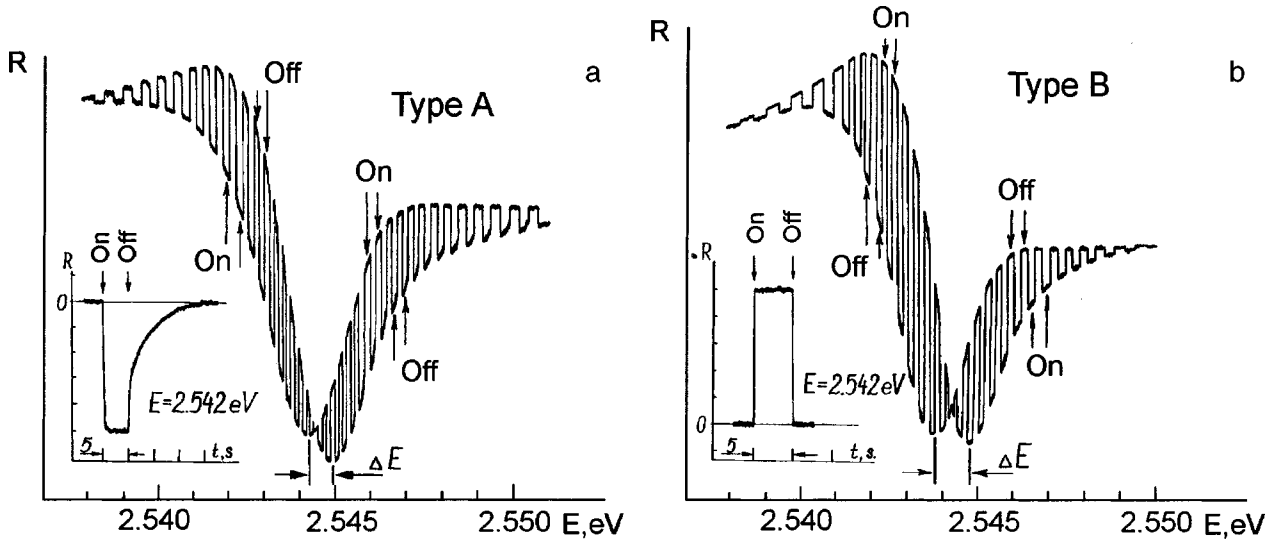

FIG. 1. Reflection spectrum and the shape of the relaxation pulses in type *A* (a) and *B* (b) CdS crystals at $T=77$ K with $\mathbf{E}\perp C$.

observed at an energy $E_{t1}=E_g-0.58$ eV ($\lambda=625$ nm), and for type *B* crystals, at $E_{t2}=E_g-0.10$ eV ($\lambda=503$ nm).

We assume that the filling of the surface states predominates in type *A* crystals when $E_{MI}>E_{t1}$, while, when $E_{MO}<E_{t1}$, the emptying of these states predominates leading to an increase or decrease in the surface field, respectively. In type *B* crystals, there is initially a strong bending of the bands (a strong surface field). This is related to the high concentration of surface states and to a greater (than in type *A*) filling of these states by electrons. In this case, capture of holes by the surface states predominates and, as a consequence, there is a reduction in the surface field. When, on the other hand, the modulated light photon has an energy close to the energy of the unfilled surface states ($E_g-0.05$ eV, $E_g-0.4$ eV), filling of the surface states predominates and there is a growth in the surface field. With the change in the type of exciton photoreflection spectrum there is a change in the type of relaxation processes. In the transition region, the shape of the relaxation pulses may be complicated and caused by different relative contributions of the fast and slow processes (Fig. 2). For these calculations we have used photo-emf measurements of the energy location of the surface states for a prismatic CdS surface at a temperature of 300 K.[5]

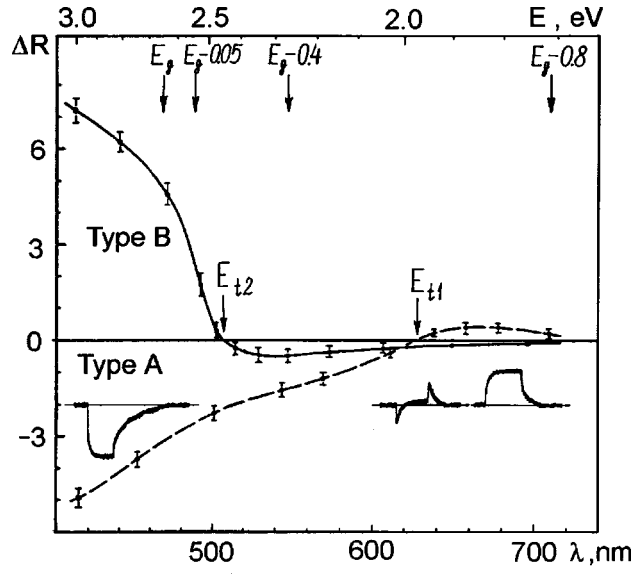

FIG. 2. Change in the amplitude and shape of pulses at the peak photoreflection signal as the energy of the modulated light is varied at $T=77$ K with $\mathbf{E}\perp C$ for type *A* and *B* CdS crystals.

The fine structure in the photoconductivity of CdS crystals also manifests two characteristic types of spectra (groups *1* and *2*).[6] It has been reported[3] that there is a direct correspondence between type *A* and *B* exciton photoreflection spectra and crystals of groups *1* and *2*. In our work we have found that the correlation is more complicated. Some crystals with a type *A* exciton photoreflection spectrum have a type 2 photoconductivity spectrum. However, under IR light the photoconductivity spectrum of these crystals has the structure of group 1. We attribute this to charge exchange of the surface states and to the complicated bending of the bands at the surface of these crystals. These questions will be examined in detailed in a separate article.

This work was supported by the Russian Fund for Fundamental Research (Grant No. 97-02-18322).

[1] E. Y. Wang and W. A. Albers, J. Phys. Lett. A **27**, 347 (1968).
[2] W. Stossel, K. Colbow *et al.*, J. Phys. **348**, 1675 (1970).
[3] L. Risch, Phys. Status Solidi B **88**, 3 (1978); Phys. Status Solidi A **49**, 177 (1978).
[4] A. B. Novikov, B. V. Novikov, G. Roppisher, A. V. Sel'kin, N. Stein, and R. B. Yuferev, JETP Lett. **64**, 42 (1996).
[5] J. Lagowski, C. L. Balestra *et al.*, Surf. Sci. **29**, 213 (1972).
[6] E. F. Gross and B. V. Novikov, J. Phys. Chem. Solids **22**, 87 (1961).

Translated by D. H. McNeill

A series of free exciton lines in zinc diarsenide

V. A. Morozova, V. S. Vavilov, O. G. Koshelev, and M. V. Chukichev

M. V. Lomonosov Moscow State University, 119899 Moscow, Russia

S. F. Marenkin

Institute of General and Inorganic Chemistry, Russian Academy of Sciences, 117907 Moscow, Russia

Fiz. Tverd. Tela (St. Petersburg) **40**, 877–878 (May 1998)

A structure corresponding to the $n=1$, 2, and 3 free-exciton states is observed in the optical transmission spectra of zinc diarsenide at 5 K. The band gap for $E\perp C$ at temperatures of 5–300 K and the exciton binding energy (17.5 eV) are determined. © *1998 American Institute of Physics.* [S1063-7834(98)03205-5]

Series of exciton levels are usually observed in relatively wide-gap semiconductors with $\varepsilon_g \geqslant 1.5$ eV.[1] Among the anisotropic II–V semiconductors, series of this type have been observed in the optical transmission and reflection spectra of ZnP_2 ($\varepsilon_g > 1.5$ eV).[2,3] For the narrower-gap semiconductor $ZnAs_2$ ($\varepsilon_g \approx 1$ eV), which crystallizes in a monoclinic system, a structure corresponding to free-exciton states with $n=1$ and 2 has been observed in reflection spectra for $\mathbf{E}\|\mathbf{C}$ and in optical transmission spectra for $\mathbf{E}\perp\mathbf{C}$ and 4.2 K (**E** is the electric field vector of the electromagnetic field of the light wave and **C** is the crystal axis) and this has yielded an estimate $G=12$ meV for the exciton binding energy.[3] In the reflection spectra, the state with $n=2$ showed up weakly and was only observed at 4.2 K. In the optical transmission spectra, the $n=1$ and 2 exciton peaks were detected only at 4.2 K,[3] apparently owing to a high level of impurity absorption ($\sim 2\ \mathrm{cm}^{-1}$). With more perfect single crystals, the $n=1$ state has been observed in optical transmission spectra ($\mathbf{E}\perp\mathbf{C}$) at temperatures of 78–300 K.[4]

Because of advances in the techniques for growing single crystals of $ZnAs_2$,[5] the level of impurity absorption has been reduced to $6\times 10^{-2}\ \mathrm{cm}^{-1}$.[5] This paper is devoted to a study of the optical transmission spectra of structurally perfect single crystals of $ZnAs_2$ for the purpose of observing the series of free-exciton levels.

These studies were made at temperatures of 5–300 K in polarized light using an IKS-21 monochromator. Control measurements at 78 and 300 K were made on an IFS-113v (Bruker) monochromator with a spectral resolution of better than $1\ \mathrm{cm}^{-1}$. Optical transmission spectra, $T_{tr}(h\nu)$, were measured on samples with different thicknesses cut perpendicular to the principal axes of the crystal. These spectra reflect a spectral variation in the absorption coefficient, since the reflectivity over the range $h\nu = 0.8-1.1$ eV is essentially invariant, in accordance with published data.[2]

Figure 1 shows optical transmission spectra of a sample with $d=250$ μm at temperatures of 300 K (curve *1*), 78 K (*2*), and 5 K (*3*) for the $\mathbf{E}\perp\mathbf{C}$ polarization. It is clear that at 5 K we have observed a series of three narrow lines, which converge at higher $h\nu$ and correspond to the free-exciton states with $n=1,2,3$. As the temperature is raised, the exciton peaks broaden and are shifted to lower energies, while the energy separation between the peaks remains unchanged. The $n=3$ line is smeared out by 10 K, while the $n=2$ line is observed up to 110 K, and the $n=1$ line is observed right up to room temperature. The binding energy of the exciton was determined in a hydrogen-like approximation using the standard formula $\varepsilon_n = \varepsilon_g - G/n^2$ (where the ε_n are the energies of the exciton states). Using the experimentally observed values of ε_1 and ε_2 and of ε_2 and ε_3, respectively, we obtained $G(1,2)=16.8\pm 0.1$ meV and $G(2,3)=17.5\pm 0.2$ meV. Because of the influence of the electron–hole exchange interaction on the $n=1$ state, this value of $G(1,2)$ may be low.[1] Given this fact, the agreement between $G(1,2)$ and $G(2,3)$ is satisfactory. Thus, in $ZnAs_2$ the $n=1$, 2, and 3 states are well described by the characteristic formula for three-dimensional Wannier–Mott excitons with a binding energy $G=17.5\pm 0.2$ meV.

G was also estimated in accordance with a hydrogen-like model with the formula $G=13.6\mu/mk^2$ eV. Here μ is the reduced mass of the exciton, $\mu^{-1}=m_e^{-1}+m_h^{-1}$, where $m_e=0.345m$ and $m_h=2.450m$ are the effective masses of an electron and hole, m is the free-electron mass, and $k=15$ is the dielectric permittivity.[6] The calculation gives $G\cong 18$ meV, in good agreement with the value determined above.

The experiment shows that the intensity of the optical transitions from the valence band to the conduction band for $\mathbf{E}\perp\mathbf{C}$ is one or two orders of magnitude smaller than for dipole allowed transitions. The low absorption intensity may be related either to a forbidden or a partially allowed character of the direct transition. But, according to Elliott's theory,[7] for forbidden transitions the $n=1$ exciton state is not realized. Assuming that the first line in the series originates in the state with $n=2$, we obtain an anomalously high value of $G=91$ meV; that is, the first line in the optical transmission spectra corresponds to the state with $n=1$, rather than $n=2$. Most likely, in $ZnAs_2$ a partially allowed transition takes place in the $\mathbf{E}\perp\mathbf{C}$ polarization. However, the possibility that this transition is forbidden is also not excluded. Thus, some calculations[8] have confirmed the possi-

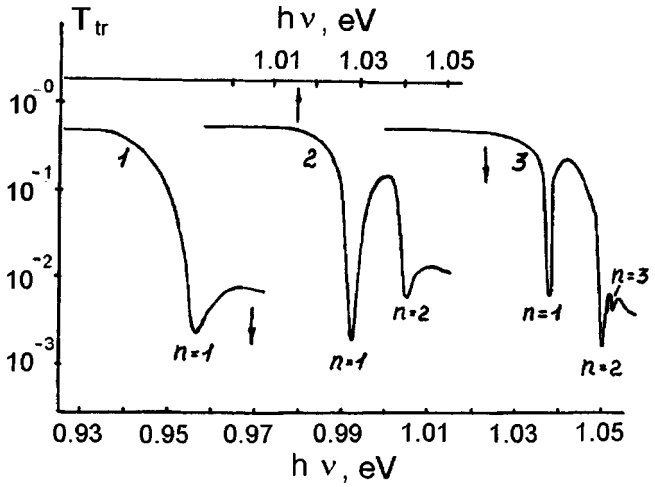

FIG. 1. Optical transmission spectra for $\mathbf{E}\perp\mathbf{C}$ at 300 K (*1*), 78 K (*2*), and 5 K (*3*).

bility of experimentally observing the $n=1$ state for indirect forbidden transitions in TlBr and TlCl.

Knowing the energy of the $n=1$ exciton state (ε_1) over 5–300 K and G, it is easy to determine $\varepsilon_g^{\perp}$ and its thermal displacement coefficient $\beta^{\perp}$. At temperatures of 300, 78, and 5 K, we obtain $\varepsilon_g^{\perp}=0.973$, 1.046, and 1.055 eV, respectively, with an accuracy of 4×10^{-4} eV and $\beta^{\perp}=(-3.3\pm0.1)10^{-4}$ eV/K over 60–300 K.

Because of the intense absorption it was not possible to detect exciton peaks in the optical transmission spectra for $\mathbf{E}\|\mathbf{C}$.

We thank A. I. Belogorokhov and L. I. Belogorokhova for performing the measurements on an IFS-113v spectrograph.

[1] R. P. Seĭsyan, *Spectroscopy of Diamagnetic Excitons* [in Russian], Nauka, Moscow (1984).
[2] N. N. Syrbu, *Optoelectronic Properties of Group II–V Compounds* [in Russian], Stiintsa, Kishiniev (1983).
[3] V. V. Sobolev and A. I. Kozlov, Phys. Status Solidi B **126**, k59 (1984).
[4] V. A. Morozova, D. I. Pishchikov, S. M. Loseva, O. G. Koshelev, and S. F. Marenkin, Fiz. Tekh. Poluprovodn. **25**, 1664 (1991) [Sov. Phys. Semicond. **25**, 1005 (1991)].
[5] S. F. Marenkin, A. M. Raukhman, D. I. Pishchikov, and V. B. Lazarev, Izv. RAN. Neorgan. Materialy **28**, 1813 (1992).
[6] Ya. A. Ugaĭ and T. A. Zyubina, Izv. RAN. Neorgan. Materialy **2**, 9 (1996).
[7] R. I. Elliott, Phys. Rev. **108**, 1384 (1957).
[8] J. Nakahara, K. Kobayashi, and A. Fujii, J. Phys. Soc. Jpn. **37**, 1312 (1974).

Translated by D. H. McNeill

Excitons in the preionization electric field of a Schottky barrier

A. B. Novikov, B. V. Novikov, H. Röppischer, A. V. Sel'kin, N. Stein, R. B. Yuferev, and Yu. A. Bumaĭ

Scientific-Research Institute of Physics, St. Petersburg State University, 198904 St. Petrovorets, Russia

Fiz. Tverd. Tela (St. Petersburg) **40**, 879–880 (May 1998)

The low-temperature ($T=80$ K) exciton reflectance spectra of CdS crystals in the electric field of a Schottky barrier are investigated. An anomalous Stark shift of a hydrogenic exciton state is detected in the preionization limit. An analysis of the spectra within the theory of a nonlocal dielectric response in a spatially inhomogeneous medium reveals the character of the subbarrier electric field distribution. © *1998 American Institute of Physics.* [S1063-7834(98)03305-X]

The ground exciton state of a crystal is known to undergo Stark displacement and broadening under the action of an electric field.[1] In the case of weak fields, the free-exciton line undergoes a shift toward longer wavelengths, which is quadratic with respect to the field. However, when the value of the electric field strength E is not small in comparison to the critical value E_1, which corresponds to the condition for the complete ionization of excitons, a significant deviation from the quadratic displacement law, including reversal of the sign of the shift and strong broadening of the exciton state, should be expected (in analogy to the behavior of a hydrogenic atom in a strong electric field[2]).

In the present work we studied experimentally the optical reflectance spectra (Fig. 1) of CdS crystals with a thin semitransparent gold coating, under which a Schottky barrier was formed, in the region of the A- and B-exciton resonances. When a reverse bias was applied to the barrier, we were able to record all the stages of variation of the reflectance spectra as the subbarrier field was increased until the resonant spectral features were completely obliterated.

To describe quantitatively the experimental data obtained, the spectra were calculated (on the basis of the approach described in Ref. 3) including the spatial dispersion effects and the inhomogeneous distribution of the electric field in the Schottky barrier, in which the Stark shift $\Delta\omega_0$ and the Stark broadening $\Delta\Gamma$ of the exciton state depend on the distance Z to the surface. The local values of $\Delta\omega_0$ and $\Delta\Gamma$ as functions of the reduced electric field E/E_1 were calculated on the basis of table data.[2,4]

Correspondence between the experimental and calculated values of the ''ionizing'' voltages is achieved, if it is assumed that the concentration of excess ionized donors

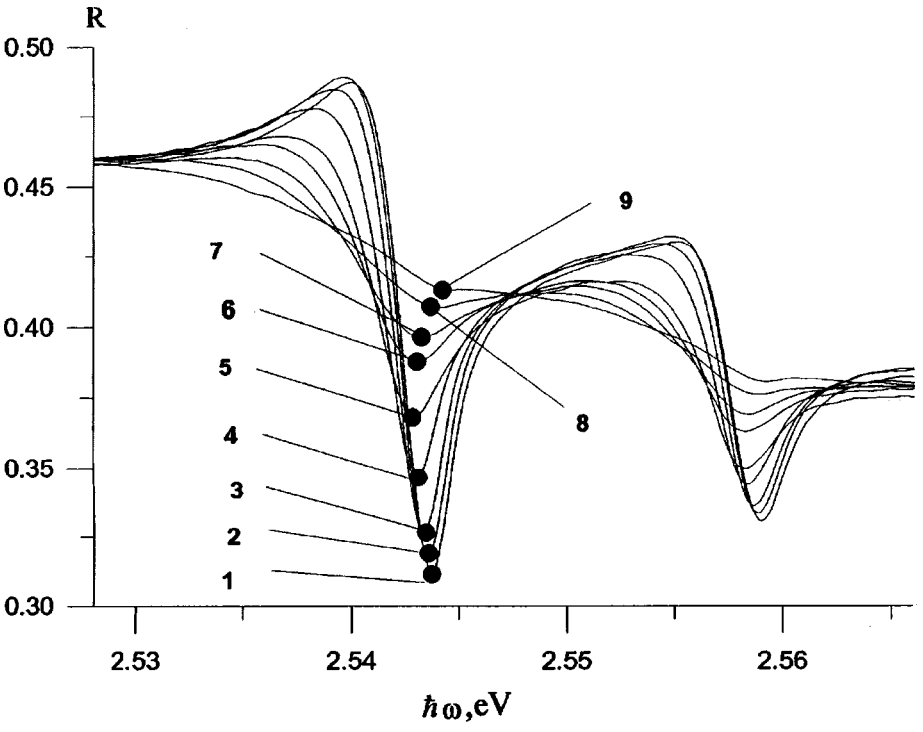

FIG. 1. Reflectance spectra of a CdS crystal ($T=80$ K) in the region of the A- and B-exciton resonances for the constant components of the voltage on the Schottky barrier $U=0$, 0.1, 0.2, 0.3, 0.4, 0.5, 0.6, 0.7, and 0.8 V (curves *1–9*, respectively) and a modulating component equal to 0.05 V.

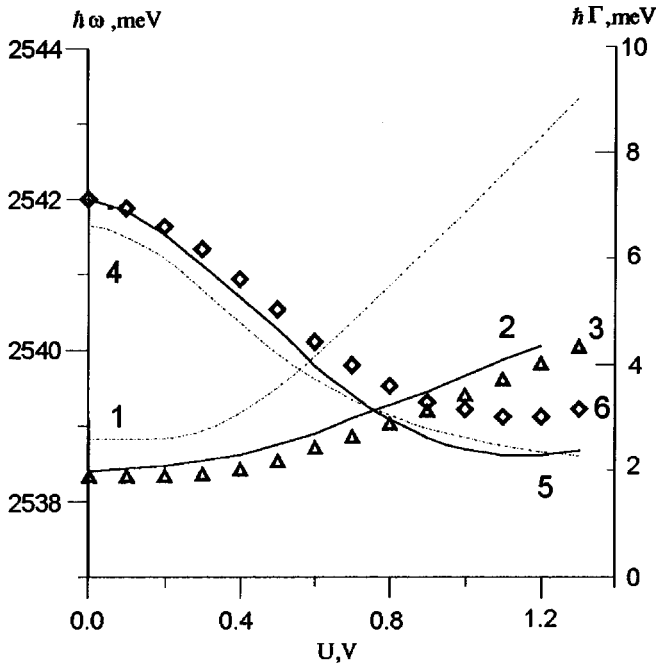

FIG. 2. Exciton resonant frequency [curves *4* and *5* and rhombuses (*6*)] and total broadening [curves *1* and *2* and triangles(*3*)] as functions of the applied barrier voltage U for the $A_{n=1}$ state in CdS.

$\Delta N = N_D - N_A$ is significantly smaller near the surface than in the remaining volume of the crystal. The sharp decrease in ΔN near the surface is apparently caused by the implantation of compensating acceptors in the near-surface layer of the crystal during deposition of the gold film.

The simplest model which reflects the fundamental aspect of the situation just described corresponds to a stepped representation of the coordinate dependence of ΔN with a smaller value in a near-surface layer of a certain thickness W_1 than in the remaining volume of the crystal. We performed theoretical calculations of the reflectance spectra within such a model with variation of the parameters W_1 and ΔN. The best correspondence between the theoretical spectra and the experimental data was attained for $\Delta N = 4 \times 10^{14}$ cm^{-3} in the region $Z < W_1$ and $\Delta N = 4 \times 10^{15}$ cm^{-3} in the region $Z > W_1$ ($W_1 = 110$ nm, the Z axis is directed into the sample, and the $Z = 0$ plane corresponds to the Au–film/crystal interface).

Thus, the thickness W_1 of the near-surface region (where there is a practically uniform electric field because of the small values of ΔN) turned out to be of the order of the exciton mean free path, i.e., the experimental situation is close to the case of the behavior of excitons in a uniform electric field, including the preionization decay limit. This permits utilization of the standard Aspnes procedure,[5] which is usually employed in the treatment of reflectance spectra for the purpose of determining the resonance parameters.

In Fig. 2 curve *6* depicts the Stark shift of the resonant frequency ω_0 of the $A_{n=1}$ exciton in CdS, which was obtained from an analysis of experimental reflectance spectra using the Aspnes procedure. The corresponding total broadening Γ (which was also determined within this procedure) is depicted by curve *3*. Solid curves *2* and *5* are the results of an Aspnes treatment of the theoretical reflectance spectra calculated for different values of the voltage U on the barrier. The curves depicted in Fig. 2 are compared with the calculations of the Stark shift (curve *4*) and the total broadening (curve *1*) in the region of an almost uniform field E at the point $Z = W_1$ (on the boundary between weak and strong compensation of the donor impurity).

The Stark shifts of the exciton resonance determined by the three methods (curves *4*, *5*, and *6*) agree well with one another, confirming the correctness of the proposed theoretical model. The experimental data which we obtained clearly point out the anomalous character of the Stark effect on the exciton state, i.e., the significant deviation of the shift of the exciton resonance in a strong electric field from the quadratic law with respect to the field, in good agreement with the theoretical conclusions in Ref. 2 regarding the behavior of hydrogenic states in electric fields.

As for the dependence of the broadening Γ on the applied voltage U, there is an appreciable difference between the values of Γ in the region of a uniform field (curve *1*) and the values obtained as a result of the treatment of the spectra according to Aspnes (curves *2* and *3*). In fact, the value of Γ measured according to the method in Ref. 5 in a case where it depends strongly on Z is only an effective parameter and, for the most part, is determined by the portions of the spectrum on the wings of the reflectance contours, where the absorption of light is small and the region of the crystal $Z > W_1$ with relatively small values of $\Gamma(Z)$ makes a significant contribution to shaping the reflected wave.

This work was carried out with financial support from the Russian Fund for Fundamental Research (Grant No. 97-02-18322).

[1] A. G. Aronov and A. S. Ioselevich, ''Excitons in semiconductor alloys,'' in *Excitons*, E. I. Rashba and M. D. Sturge (Eds.), North-Holland, Amsterdam (1982), pp. 319–348; Nauka, Moscow (1985), p. 193.
[2] R. J. Damburg and V. V. Kolosov, J. Phys. B **9**, 3358 (1976).
[3] A. V. Sel'kin, Vestn. S. Peterb. Univ., Ser. 4: Fiz. Khim. (2(11)), 87 (1996).
[4] V. A. Kiselev, B. V. Novikov, and A. E. Cherednichenko, *Exciton Spectroscopy of the Near-Surface Region of Semiconductors* [in Russian], Izd. LGU, Leningrad (1987).
[5] D. E. Aspnes, in *Handbook on Semiconductors*, T. S. Moss (Ed.), North-Holland, New York (1980), Vol. 2, p. 109.

Translated by P. Shelnitz

Structure of the free exciton luminescence band of heteroepitaxial ZnSe/GaAs layers

Yu. P. Rakovich, A. L. Gurskiĭ, A. S. Smal', A. A. Gladyshchuk, Kh. Khamadi, G. P. Yablonskiĭ, and M. Khoĭken

Brest Polytechnical Institute, 224000 Brest, Belarus

Fiz. Tverd. Tela (St. Petersburg) **40**, 881–883 (May 1998)

The exciton reflectance and photoluminescence spectra of epitaxial ZnSe/GaAs layers with a thickness of 2–4 μm are investigated in the temperature range 10–120 K. It is shown that one of the causes of the formation of the doublet structure of the $A_{n=1}$ photoluminescence band is interference of the exciton radiation at the boundaries of the near-surface dead layer. © *1998 American Institute of Physics.* [S1063-7834(98)03405-4]

The fine structure in the free-exciton photoluminescence (PL) spectra of ZnSe/GaAs is observed even when the thickness h of the ZnSe layer exceeds the critical value for the relaxation of elastic stresses, $d_{cr}=1$ μm.[1] In samples with $h \ll d_{cr}$ the loads caused by the lattice mismatch between the layer and the substrate lead to splitting of the valence band of ZnSe and to the formation of a fine structure in both the exciton reflectance and PL spectra.[2] The formation of a fine structure in the PL spectra of thick ZnSe layers has been attributed to the influence of the stresses arising when the samples are cooled from the growth temperature due to the difference between the coefficients of thermal expansion of ZnSe and GaAs[3] or polariton effects.[4,5] However, these opinions do not provide an explanation for the temperature behavior of the spectral positions of the fine-structure components, their anomalously small width, and the absence of a fine structure in the exciton reflectance spectra.

In the present work we investigated the temperature variation of the exciton reflectance and PL contours of epitaxial ZnSe/GaAs layers with a thickness $h>1$ μm to elucidate the mechanism of the formation of the fine structure in the PL spectra.

1. EXPERIMENTAL TECHNIQUES AND SAMPLES

Samples of ZnSe with a resistivity of $10^{10}-10^{11}\Omega\cdot$cm were grown by metalorganic vapor phase epitaxy (MOVPE) on GaAs(110) substrates at 330–480 °C.[6] The PL was excited by a He–Cd laser ($\lambda_{exc}=325.0$ nm, and the excitation intensity $I_{exc}\sim 0.02-10$ W/cm^2). The spectral resolution of the recording instrument was no less than 0.3 meV.

2. DISCUSSION

The PL spectra recorded at $T=10$ K display a pronounced line at 2.799–2.800 eV with a full width at half-maximum ~ 3 meV (Fig. 1). As the temperature is increased, a doublet structure appears on its short-wavelength wing, and the spectral distance between its components increases slightly. At the same time, the corresponding reflectance spectra do not exhibit any fine structure. At all temperatures the spectral position of the dip in the PL spectrum corresponds exactly to the exciton resonance energy determined from a comparison of the experimentally measured exciton reflectance spectra with a calculation based on the dead-layer model.[7,8] These features of the formation of the fine structure in the PL spectra with maintenance of the shape of the exciton reflectance spectrum cannot be attributed to the influence of thermoelastic stresses or polariton effects, since the fine structure is retained up to 150 K. A similar structure was previously observed in the PL spectra of II–VI single crystals,[9–18] which were calculated using a model of the diffusion of excitons with consideration of the self-absorption of their luminescence.[9,19,20] However, agreement with experiment was achieved only for extremely large values of the diffusion length L_D (several microns[9]). Our calculations of the PL spectra of ZnSe/GaAs using this model[18] gave $L_D \sim 8-10$ μm, which exceeds the thickness of the ZnSe layer (4 μm).

More reliable results were obtained when the interference of the free-exciton radiation at the boundaries of the near-surface dead layer is taken into account. In this model the reflectance of an exciton impinging on the surface of the layer from inside was calculated by a method similar to the method in Ref. 7 and was then used to calculate the PL spectrum.[18,21] Figure 2 presents the results of a calculation of the spectrum measured at $T=45$ K with the diffusion coefficient $D=0.03$ cm^2/s and the exciton lifetime $\tau=150-200$ ps, which gives $L_D=0.67-0.77$ μm for the diffusion length and is in good agreement with the results of other investigators for ZnSe/GaAs: $\tau=100-150$ ps. However, the thickness of the dead layer d_{eff} significantly exceeds the value obtained from the corresponding exciton reflectance spectrum: $d_{eff}=29$ and 7 nm, respectively.

Since d_{eff} depends on the electric field at the surface,[10] the most probable reason for such a disparity might be the increase in the surface charge under the action of laser radiation when PL is excited, for example, by the trapping of photogenerated charge carriers in surface centers or the adsorption of oxygen.[18] To test this hypothesis, we measured exciton reflectance spectra at $T=80$ K with laser illumination of the sample surface. It was found that dramatic transformation of the exciton reflectance spectrum (to the point of complete inversion of the contour) is observed under the effect of illumination. It is due to alteration of the dead layer ($d_{eff}=47$ nm with illumination and $d_{eff}=4$ nm in the dark) and disappears after the laser is switched off. The value of

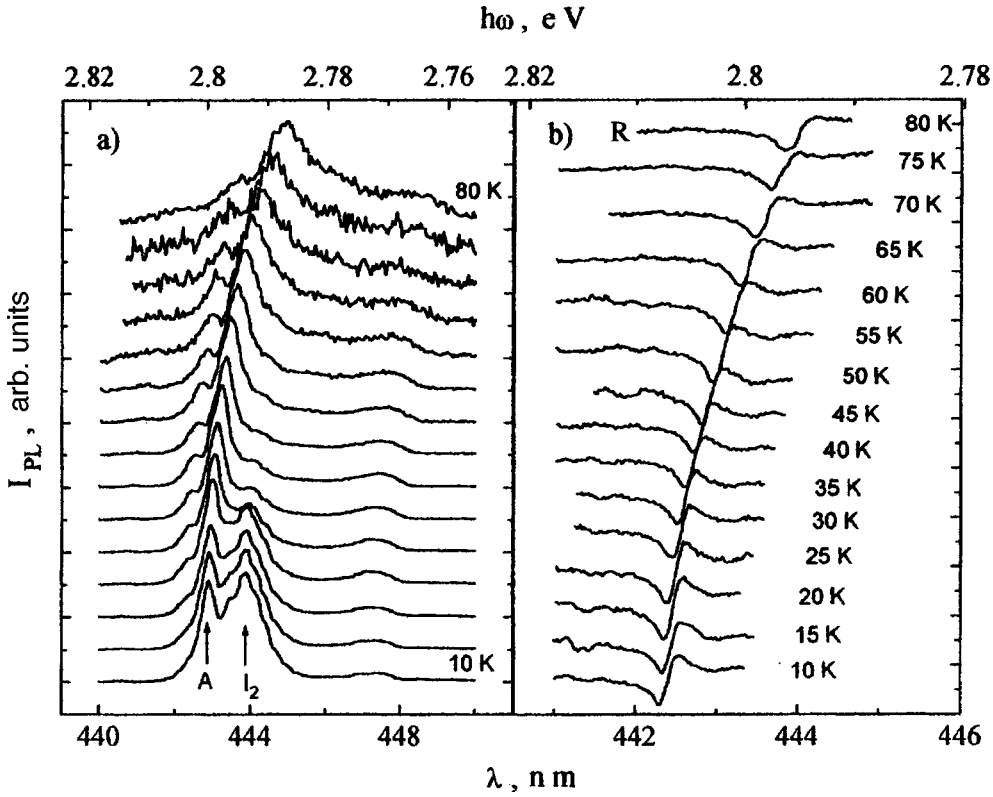

FIG. 1. Photoluminescence (a) and reflectance (b) spectra of an epitaxial ZnSe layer of thickness $h=4\ \mu$m with variation of the temperature.

d_{eff} permits an approximate estimation of the surface field F_s and the corresponding density of charged states n_s.[10] When PL is excited by an He–Cd laser with $I_{\text{exc}}=0.1$ cm^2/W at $T=80$ K and the exciton field-ionization threshold $F_{\text{cr}} \approx 50$ kV/cm,[23,24] we obtain $F_s \approx F_{\text{cr}}$ and $n_s \approx 2 \times 10^{11}$ cm^{-2}.

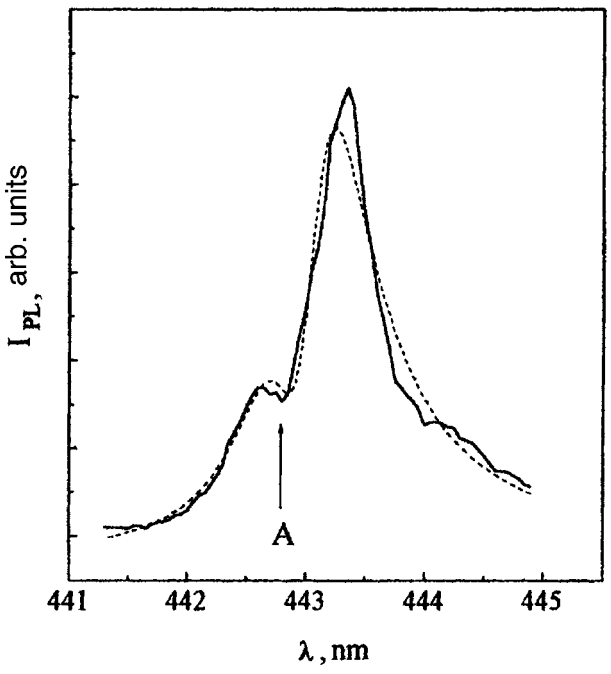

FIG. 2. Experimental (solid curve) and calculated (dashed curve) free exciton photoluminescence spectra of ZnSe/GaAs at $T=45$ K.

[1] H. Mitsuhashi, I. Mitsuishi, and M. Mizuta, Jpn. J. Appl. Phys. **24**, L578 (1985).
[2] J. Gutowski, N. Presser, and G. Kudlek, Phys. Status Solidi A **120**, 11 (1988).
[3] G. Kudlek, J. Gutowski, and J. Lumin. **52**, 55 (1992).
[4] G.-J. Yi, L. Radomsky, and G. F. Neumark, J. Cryst. Growth **138**, 208 (1994).
[5] B. V. Novikov, A. B. Pavlov, and V. G. Talalaev, Fiz. Tverd. Tela (Leningrad) **23**, 207 (1981) [Sov. Phys. Solid State **23**, 116 (1981)].
[6] A. L. Gurskii, A. N. Gavrilenko, and E. V. Lutsenko, Phys. Status Solidi B **193**, 257 (1996).
[7] J. J. Hopfield and D. G. Thomas, Phys. Rev. **132**, 563 (1963).
[8] V. A. Kiselev, B. V. Novikov, and A. E. Cherednichenko, *Exciton Spectroscopy of the Near-Surface Region of Semiconductors* [in Russian], Izd. LGU, Leningrad (1987).
[9] V. V. Travnikov and V. V. Krivolapchuk, Fiz. Tverd. Tela (Leningrad) **24**, 961 (1982) [Sov. Phys. Solid State **24**, 547 (1982)].
[10] B. V. Novikov, H. Röppischer, and V. G. Talalaev, Fiz. Tverd. Tela (Leningrad) **21**, 817 (1979) [Sov. Phys. Solid State **21**, 478 (1979)].
[11] K. F. Lider and B. V. Novikov, Opt. Spektrosk. **23**, 611 (1967) [Opt. Spectrosc. **23**, 328 (1967)].
[12] R. Garuthara and M. Tomkiewicz, Phys. Rev. B **31**, 7844 (1985).
[13] B. Sermage and M. Voos, Phys. Rev. B **15**, 3935 (1977).
[14] M. S. Brodin, P. S. Kosobutskiĭ, and M. G. Matsko, Ukr. Fiz. Zh. **25**, 1220 (1980).
[15] P. S. Kosobutskiĭ, Ukr. Fiz. Zh. **22**, 980 (1977).
[16] M. S. Brodin and M. G. Matsko, [JETP Lett. **30**, 538 (1979)].
[17] M. S. Brodin and M. G. Matsko, Solid State Commun. **35**, 375 (1980).
[18] Yu. P. Rakovich, G. P. Yablonskii, and A. A. Gladyshchuk, Phys. Status Solidi B **189**, 2247 (1995).
[19] W. C. Tait and R. L. Weiher, Phys. Rev. **178**, 1404 (1969).
[20] V. V. Krivolapchuk, S. A. Permogorov, and V. V. Travnikov, Fiz. Tverd. Tela (Leningrad) **23**, 606 (1981) [Sov. Phys. Solid State **23**, 343 (1981)].
[21] V. M. Agranovich, *Exciton Theory* [in Russian], Nauka, Moscow (1968), 319 pp.
[22] J. Gutovski and A. Hoffmann, Adv. Mater. Opt. Electron. **3**, 15 (1994).
[23] A. D'Andrea and R. Del Sole, Phys. Rev. B **25**, 3714 (1982).
[24] V. A. Sashenko and V. A. Tjagai, Phys. Status Solidi B **88**, 797 (1978).

Translated by P. Shelnitz

Excitons in ZnP_2 crystals in the electric field of a Schottky barrier

S. O. Romanovskiĭ, A. V. Sel'kin, I. G. Stamov, and N. A. Feoktistov

A. F. Ioffe Physicotechnical Institute, Russian Academy of Sciences, 194021 St. Petersburg, Russia
Fiz. Tverd. Tela (St. Petersburg) **40**, 884–886 (May 1998)

A study is made of the effect of electric fields on the exciton states of β-ZnP_2 crystals ($T=77$ K) in structures with Schottky barriers formed by depositing semitransparent electrically-conducting $InSnO_2$ films on the crystal surface. The observed changes in the exciton optical reflection spectra when an electrical potential is applied to a barrier are explained by the shift and broadening of the exciton level caused by the Stark effect. The experimental data are compared with calculations based on a theory of exciton optical reflection from planar spatially nonuniform structures. © *1998 American Institute of Physics.* [S1063-7834(98)03505-9]

With a number of unique physical properties and great importance for numerous practical applications, semiconducting structures with Schottky barriers[1] are also extremely interesting objects for studying the effect of electric fields on the exciton states in crystals.[2] The feasibility of controlling the electric field strength in barrier structures over a wide range and creating high fields makes it possible to study in detail the behavior of excitons under the influence of electric fields up to their complete dissociation, when the field strength reaches a critical (ionization) level.[3–5]

In this paper, the objects of study were structures with Schottky barriers obtained by depositing essentially transparent, electrically conducting films of $InSnO_2$ (ITO) on the surface of β-ZnP_2 crystals. ITO films were deposited on opposite plane-parallel faces of single crystal slabs of ZnP_2, parallel to the optical C_z axis of the crystal (a dipole active transition into the lowest, $n=1$ exciton state is allowed[6] in light polarized with $E\|C_z$), and served as contacts to which an external electrical potential U was applied. Exciton spectra of mirror-reflected light from one of the faces of the sample that had been coated with ITO were measured as a function of the voltage U (for the $E\|C_z$ polarization in a near-normal incidence geometry).

Figure 1a shows reflection spectra for an ITO/ZnP_2 sample ($T=77$ K) in the vicinity of the $n=1$ exciton state for voltages $U\leqslant 0$, corresponding to a reverse bias on the barrier located on the side at which the spectra were taken. As $|U|$ was increased (curves *1–12*), a significant shift of the exciton reflected-light profile to longer wavelengths was observed, accompanied by a gradual flattening of the profile. For $U\approx -260$ V (curve *12*), the spectral structure associated with the exciton contribution has essentially vanished. Here, at the highest voltages $|U|$, the spectrum acquires an antidispersion form, i.e., the main minimum in the reflection coefficient lies on the long-wavelength side and the maximum, on the short-wavelength side.

The shape of the reflection spectrum with reverse bias is strongly affected by supplementary illumination of the reflecting surface of the sample with light in the intrinsic absorption spectral region. Figure 2 shows a comparison of reflection spectra of the test sample obtained without additional illumination ($U=0$ in curve *1* and $U=-250$ V in curve *2*) and spectra taken with supplementary laser illumination for $U=-250$ V (HeNe laser, 0.1 W/cm^2, wavelength $\lambda=632.8$ nm in curve *3*; Ar^+ laser, 5 W/cm^2, wavelength $\lambda=488$ nm in curve *4*).

In order to clarify the mechanism for the formation of the experimental spectra, we analyzed them theoretically in terms of a model[7] of exciton reflection of light from a planar, spatially nonuniform medium, using data[2,8] on the Stark shift and broadening of a hydrogen-like state in an electric field. The basic parameters of the exciton resonance were obtained by analyzing the experimental data of curve *1* in Fig. 1a, which corresponds to the case of no electric field (in the sense of its acting on an exciton).

The parameters (in the notation of Ref. 7) are as follows: exciton resonance frequency $\omega_0=1.5542$ eV, damping constant $\Gamma_0=4.5$ meV, polarizability $\beta_0=6.2\times10^{-3}$, background dielectric permittivity $\varepsilon_b=11.9$, translational exciton mass $M=3.0m_0$ (m_0 is the free electron mass), and thickness of the intrinsic[9] ''dead'' layer $l_{DL}=2.6$ nm. In calculating the spectra, we also included the effect of the ITO film. Its dielectric constant $\varepsilon_{ITO}=3.5+0.7i$ was measured independently using an ellipsometer and the thickness $l_{ITO}=8.5$ nm was obtained as a fit parameter. The spectrum 1 in Fig. 1b was calculated using these values of the parameters and is in good agreement with the experimental curve 1 in Fig. 1a.

In order to describe the influence of an electric field, in the calculations we used the known[6] binding energy of the exciton in ZnP_2 (Ry=46.4 meV) and static dielectric permittivity ($\varepsilon_{st}=11.5$). Here the critical (to ionize an exciton) field E_I is 3.4×10^4 V/cm. The choice of excess shallow donor concentration N_D-N_A took into account the the fact that in the experiment the exciton spectra become sensitive to an applied voltage only at fairly high values of $|U|$.

Figure 1b shows reflection spectra (curves *1–12*) calculated with $N_D-N_A=0.1\times10^{15}$ cm^{-3} for different values of the electric field at the sample surface. (In this case the surface electric field remains essentially uniform over a distance of the order of the exciton mean free path l_{ex}.) A comparison of curves *1–12* with the corresponding experimental curves shows that, in their main features (spectral shift and broadening), the theoretical spectra correctly reproduce the

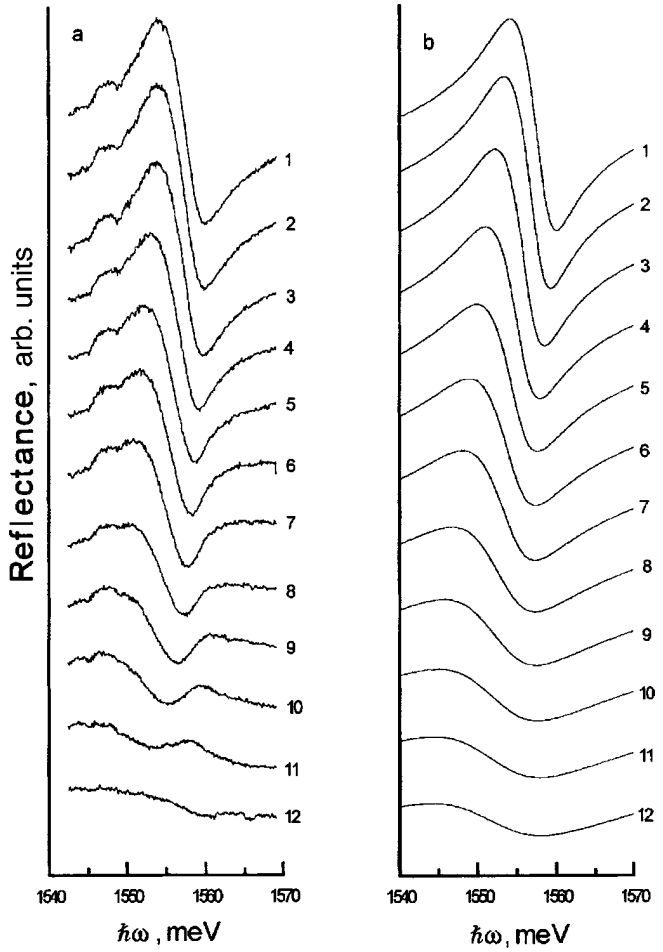

FIG. 1. Exciton optical reflection spectra of ITO/β-ZnP_2 structures ($T=77$ K) as a function of the reverse bias voltage U (*a* experiment; U in Volts) and of the strength E_s of the surface electric field (*b* theory; E_s in relative units $f_s=E_s/E_I$, where E_I is the ionization field): (a) $U=0$ (*1*), 70 (*2*), 110 (*3*), 160 (*4*), 180 (*5*), 190 (*6*), 200 (*7*), 210 (*8*), 220 (*9*), 230 (*10*), 240 (*11*), 260 (*12*); (b) $f_s=0$ (*1*), 0.12 (*2*), 0.17 (*3*), 0.20 (*4*), 0.23 (*5*), 0.26 (*6*), 0.29 (*7*), 0.33 (*8*), 0.37 (*9*), 0.40 (*10*), 0.44 (*11*), 0.47 (*12*).

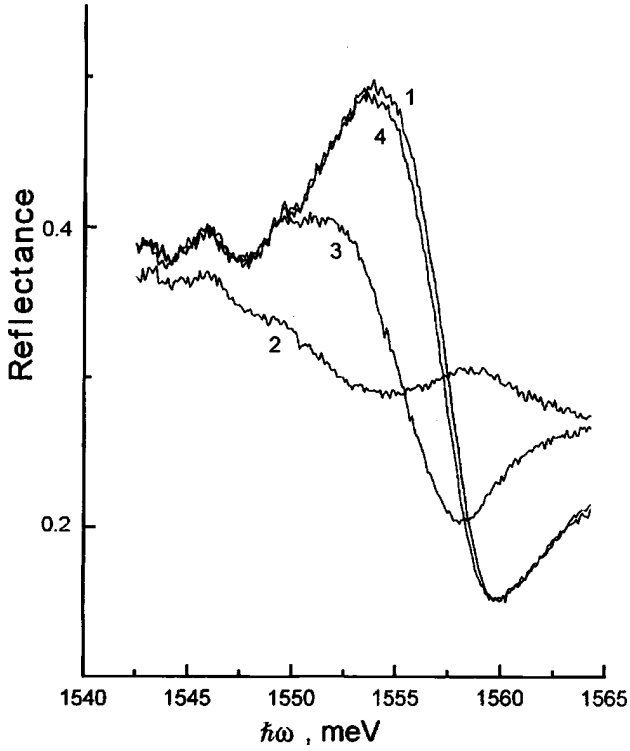

FIG. 2. The effect of supplementary illumination on the exciton optical reflection spectrum of ITO/β-ZnP_2 structures ($T=77$ K) for a reverse bias voltage $U=-250$ V: (*2*) without illumination, (*3*) illumination with an HeNe laser, (*4*) with an Ar^+ laser, (*1*) spectrum without illumination for $U=0$ V.

experimental data. However, the experimentally observed transformation of the spectra from a dispersion to an antidispersion form at high voltages (the ''rotation'' of the exciton optical reflection profile) is not explained by this model.

On the other hand, it is known[2] that ''rotation'' of the exciton optical reflection profile takes place when the electric field distribution near the surface is highly nonuniform. Thus, to explain our experimental data, it must be assumed that, for some reason, at high voltages $|U|$ the surface electric field changes significantly over distances of order l_{ex} from the surface. One such reason might be surface (owing to additional band bending) charge exchange of deep centers,[1] whose concentration is much greater than that of the shallow centers.

The appearance of an exciton structure in the reflection spectrum induced by supplementary illumination of reverse biased samples, which we have observed (Fig. 2), indicates that the surface electric field is greatly reduced by the illumination. This reduction in the field is apparently caused by a drop in the charge of the surface states and an increase in the electrical conductivity of a surface layer with a thickness on the order of the diffusion length l_D ($l_D \gg l_{ex}$) for the photoinduced free charge carriers.

In conclusion, we note that the results presented in this paper open up new prospects for the feasibility of exciton optical reflection spectroscopy for studies of actual semiconducting structures.

This work was conducted in the framework of the State Scientific-Technical Program on the Physics of Solid State Nanostructures (Grant No. 95-1001) and projects supported by the Russian Fund for Fundamental Research (Grants No. 96-02-16933 and No. 97-02-18138).

[1] É. Kh. Roderik, *Metal-semiconductor Contacts* [Russian translation], tr. edited by G. V. Stepanova, Radio i svyaz', Moscow (1982), 208 pp.
[2] V. A. Kiselev, B. V. Novikov, and A. E. Cherednichenko, *Exciton Spectroscopy of Semiconductor Surfaces* [in Russian], Izd-vo. LGU, Leningrad (187), 160 pp.
[3] L. Schultheis, K. Kóhler, and C. W. Tu, Phys. Rev. B **36**, 6609 (1987).
[4] A. B. Novikov, B. V. Novikov, G. Roppisher, A. V. Sel'kin, N. Shtaĭn, and R. B. Yuferev, JETP Lett. **64**, 42 (1996).
[5] M. A. Jacobson, V. D. Kagan, E. V. Kalinina, D. K. Nelson, A. V. Sel'kin, V. A. Dmitriev, K. G. Irvine, and C. H. Carter Jr., in *Proceedings of the 23rd International Conference on the Physics of Semiconductors*, Berlin, Germany (1966), Vol. 1, p. 569.
[6] A. B. Pevtsov, S. A. Permogorov, A. V. Sel'kin, N. N. Syrbu, and A. G. Umanets, Fiz. Tekh. Poluprovodn. **16**, 1399 (1982) [Sov. Phys. Semicond. **16**, 897 (1982)].
[7] A. V. Sel'kin, Vestn. SPbGU. Ser. 4, (2 (11)), 87 (1996).
[8] R. J. Damburg and V. V. Kolosov, J. Phys. B **9**, 3358 (1976).
[9] N. N. Akhmediev, M. I. Sazhin, and A. V. Sel'kin, Zh. Éksp. Teor. Fiz. **96**, 720 (1989) [Sov. Phys. JETP **69**, 408 (1989)].

Translated by D. H. McNeill

Excitons in heteroepitaxial CdSe/CdS structures

D. L. Fedorov and E. P. Denisov

Baltic State Technical University, 198005 St. Petersburg, Russia

L. N. Tenishev and M. B. Chernyshov

A. F. Ioffe Physicotechnical Institute, Russian Academy of Sciences, 194021 St. Petersburg, Russia

P. I. Kuznetsov and G. G. Yakushcheva

Institute of Radio Electronics, Russian Academy of Sciences, 141120 Fryazino, Moscow Region, Russia

Fiz. Tverd. Tela (St. Petersburg) **40**, 887–889 (May 1998)

X-ray diffractometry and low-temperature exciton spectroscopy are used to study heteroepitaxial CdSe/CdS layers grown at temperatures of 350–485 °C by MOCVD. The high-temperature samples are found to display the exciton and x-ray diffraction spectra characteristic of hexagonal Wurtzite (W) structures, while the low-temperature samples display the features characteristic of the cubic structure of sphalerite (ZB). A number of the samples have x-ray spectra characteristic of structures with stacking faults (SF), which represent a separate crystalline phase in the structures studied here. It is found that the individual crystalline phases are spatially separated.
 [S1063-7834(98)03605-3]

The prospects for using CdSe in optoelectronics are closely related to its capacity for sphalerite–wurtzite (ZB–W) type polymorphic transformations, which creates interest in additional structural and optical studies. Here we present results from a study of the diffraction-line profiles obtained from (0001) planes of epitaxial layers of CdSe grown on single-crystal CdS substrates with the same orientation at temperatures of 350–500 °C. (The temperature of the sphalerite-wurtzite phase transition for CdSe is 400–425 °C.) A simultaneous study was made of the low-temperature photoluminescence and exciton reflection from these structures.

This work was performed using equipment at the St. Petersburg Joint Research Center (TsKP). The x-ray structure was studied using Cu Kβ emission on a Rigaku D/max diffractometer. The calculated depth of analysis in the CdSe layer was of the order of 10 μm for normal incidence of the x rays and was proportional to sin θ for other grazing angles θ. The test samples had different, relatively small thicknesses of the CdSe layer (from 1 to 5 μm), so it was also possible to detect x-ray diffraction lines from the CdS substrate at the same time. This made it possible to improve the accuracy in determining the angular position of the profiles from the CdSe layer by using the x-ray diffraction by CdS as reference marks. Part of these profiles are shown in Fig. 1.

The photoluminescence and reflection spectra were measured in a cryostat in a flow of gaseous helium at temperatures of 5–100 K. The photoluminescence was excited by an He–Ne laser with an output wavelength of 632.8 nm. The reflection spectra were measured at angles close to normal. The spectra were detected using a DFS-12 monochromator with a cooled photomultiplier operating in the photon counting mode.

EXPERIMENTAL RESULTS

Diffraction patterns were recorded for all the test samples at angles 2θ ranging from 0.6° to 160° in order to observe and study x-ray diffraction line profiles in all the four possible orders of diffraction peaks from (0002) in the hexagonal phase and, correspondingly, (111) in the cubic phase.

An analysis of the diffraction line profiles reveals the following features:

1. A majority of the profiles are generated by crystallites consisting of thin interlayers with hexagonal and cubic structures. The x-ray spectrum of one of the samples made it possible to determine the angular position of the profiles of the pure cubic and pure hexagonal phases. The inset to Fig. 1 shows its resolution into constituent components.

2. Profiles from different parts of the sample surfaces have quite different width, shape, and position, which indicates that these parts vary in their volume ratios of cubic and hexagonal interlayers and in the thicknesses of these interlayers (Fig. 2).

3. It is clear that, in samples fabricated at a higher temperature, the profiles lie to the left, on average, i.e., closer to the position of the peak from a pure hexagonal structure (arrow *A* in Fig. 1), which indicates that the fraction of hexagonal interlayers is higher in them. This is in good agreement with data from optical studies.

4. A quadratic rise is observed in the physical broadening of the profiles from the CdSe, multiplied by cos θ/λ, as a function of the parameter sin θ/λ, as opposed to the linear dependence of these same parameters for profiles from the CdS substrate. This could be explained by a linear decrease in the local density of dislocations in the CdSe layer with increasing distance from the substrate interface. The forma-

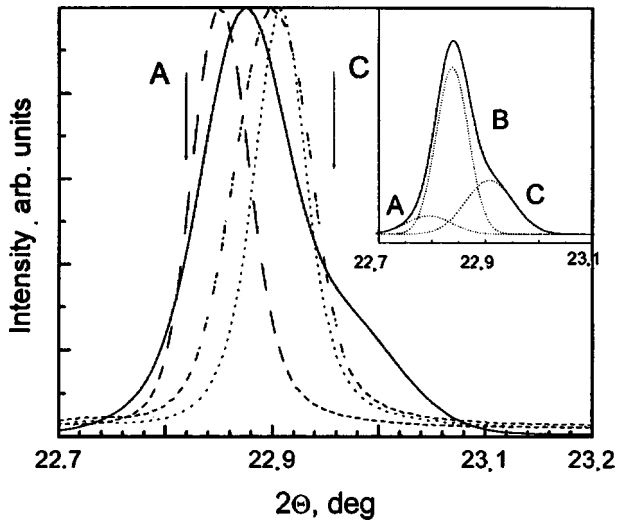

FIG. 1. Profiles of the reflections from the (0001) plane in Cu $K\beta$ radiation for samples with different temperatures of CdSe layer formation (two low-temperature and two high-temperature samples): 485 °C (dot-dashed curve), 450 °C (dashed), 375 °C (smooth), and 350 °C (dotted). The inset in the upper right shows an expansion of the profile for a segment of the 375 °C sample containing crystalline blocks of three phases: pure hexagonal, W (A), pure cubic, ZB (C), and consisting of thin interlayers of hexagonal and cubic structures and containing stacking faults, SF (B).

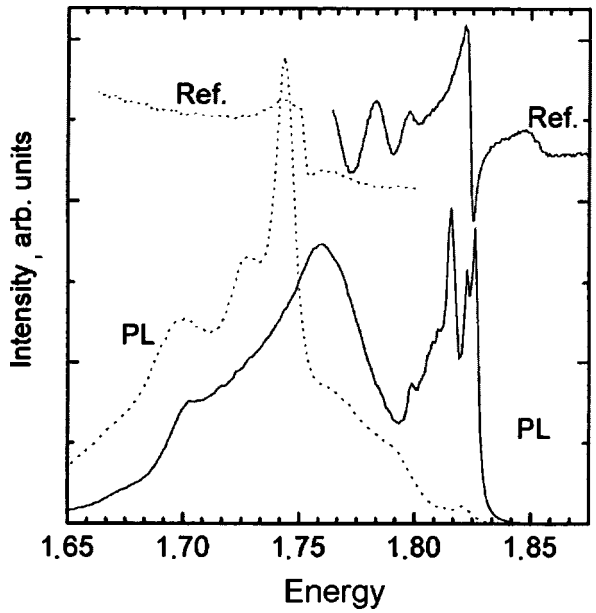

FIG. 3. Exciton reflection (Ref.) and photoluminescence (PL) spectra at $T=5$ K of CdSe/CdS samples grown at temperatures of 350 (dotted curve) (ZB) and 485 °C (smooth curve) (W).

tion of dislocations is explained by a 4% mismatch in the internuclear distances in CdSe and CdS.

5. In some samples, a rapid drop in the intensity of the diffraction lines is observed as the diffraction order increases. This effect is analogous to a rise in the temperature of the sample during the scan. It can be explained by a reduction in the short-range ordering owing to statistically disordered displacements of the atoms from their equilibrium positions in the ideal lattice when a large number of stacking faults, interlayers, and dislocations are present, but the long-range ordering, which is defined and stabilized by the substrate, is retained.

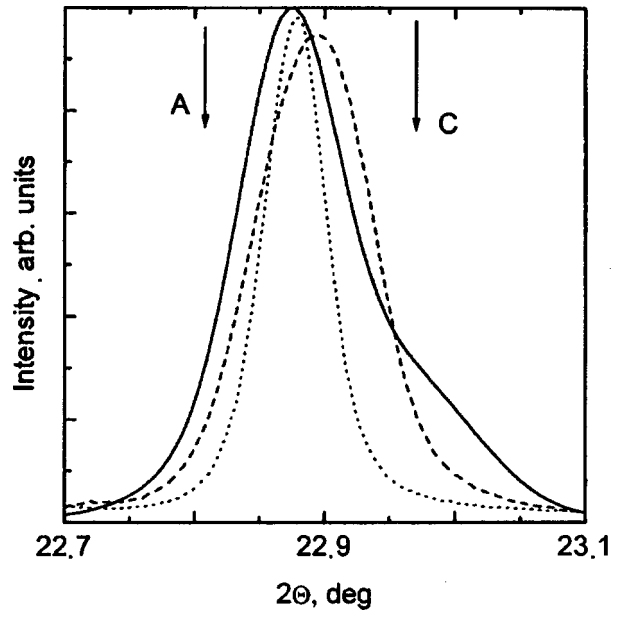

FIG. 2. Profiles of (0001) reflections of the 375 °C sample in CuK_β radiation for three different segments of the surface.

These same samples were studies by exciton spectroscopy. Figure 3 shows photoluminescence and reflection spectra of samples grown at substrate temperatures $T=350$ °C and $T=485$ °C. In the short wavelength part of the photoluminescence spectrum of the sample grown at a high temperature, several narrow lines can be seen, as well as a narrow line in the reflection spectrum, which are characteristic of the exciton spectrum of samples with a hexagonal wurtzite structure.[1] The shortest wavelength line in the luminescence spectrum lies within the confines of the exciton reflection profile and can be attributed to $(\Gamma_9-\Gamma_7)$, 1.826 eV emission from an $n=1$ free exciton. The narrow lines to the left of the free-exciton line can be attributed to emission from bound excitons, $I_1-1.8160$ eV and $I_2-1.8225$ eV.[1] All the samples also have broad lines, shifted by 70–100 meV from the edge of the exciton band, which most likely originate in impurities (defects).

In the samples grown at low temperatures, the sphalerite (ZB–CdSe) structure is stabilized. In the exciton reflection spectrum, a line can be seen that is shifted relative to the $n=1$ line of the spectrum of a film with hexagonal structure by 80 meV to longer wavelengths. This line can be attributed to the $n=1$ ground state $(\Gamma_8-\Gamma_6)$.[2] An intense free-exciton line and its phonon repetitions can be seen in the photoluminescence spectrum.

The luminescence spectrum of the samples grown at a temperature near 375 °C consists of lines of similar intensities belonging to different exciton states.

In some samples grown at intermediate temperatures, it was not possible to observe an exciton reflection spectrum, while the photoluminescence spectrum contained a broad line with a peak in the vicinity of 1.77 eV, which appears to be mainly of impurity origin.

In sum, x-ray and optical studies of samples grown at $T=350$ °C and 485 °C show that they contain cubic and hexagonal phases, respectively. The substrate temperature is the parameter which determines the predominant phase in the grown layer. Essentially all the samples contain stacking faults, as indicated by the presence of the x-ray diffraction *B* line.

The simultaneous observation of resonance luminescence of different exciton states with comparable intensity indicates that the different phases are spatially separated, with a grain size exceeding the diffusion mean free path of an exciton, so there is no energy transport between these phases.

These x-ray studies have shown that the decrease in the local density of dislocations in the CdSe with distance from the substrate interface is linear.

[1] E. F. Gross, B. S. Razbirin, V. P. Fedorov, and Yu. P. Naumov, Phys. Status Solidi **30**, 485 (1968).
[2] S. Ninomiya and S. Adachi, J. Appl. Phys. **78**, 4681 (1995).

Translated by D. H. McNeill

Intrinsic luminescence of amorphous and disordered crystalline systems

A. A. Klochikhin

B. P. Konstantinov Institute of Nuclear Physics, Russian Academy of Sciences, 188350 Gatchina, Leningrad Region, Russia

Fiz. Tverd. Tela (St. Petersburg) **40**, 890–891 (May 1998)

A unified method is developed for describing the steady-state luminescence of exciton fluctuation states for weak excitation in different disordered systems. The phononless luminescence band is found to be formed by ''radiative'' states of the fluctuation tail in the density of states, i.e., by states for which nonradiative states are either nonexistent or have a low probability. The shape of the emission spectra calculated including the phonon interaction is in good agreement with experimental luminescence spectra of α Si:H and of solid solutions of $ZnSe_{(1-c)}Te_c$ and $CdS_{(1-c)}Se_c$. © *1998 American Institute of Physics.* [S1063-7834(98)03705-8]

The intrinsic luminescence of many disordered systems[1] and, in particular, II–VI solid solutions[2–4] is caused by the recombination of excitons localized in the wells of the potential relief. A theoretical description of this process includes the following:

1) Calculating the density of fluctuation states in the vicinity of the localization energies $\omega \geqslant \omega_0$. (The energy is taken relative to the bottom of the virtual crystal band and increases with depth in the band gap.) ω_0 is an upper bound on the energies where the tail states, in the zeroth approximation, can be regarded as localized and isolated from one another. The integrated density of states, $N(\omega_0)$, i.e., the total number of states with a localization energy exceeding ω_0, obeys the inequality $N(\omega_0)a^3 \ll 1$, where a is the radius corresponding to the wave function with a localization energy of the order of ω_0. In calculating the number of states it is assumed that the localized exciton states arise in fluctuations (clusters) with the character of singly connected potential wells.

2) Determining the form of the phononless exciton absorption band on the basis of data on the density of states. In the case of amorphous silicon, it was assumed that the shape of the absorption edge is determined by the density of states in the tail of the valence bands.

3) Finding the form of the phononless luminescence band under conditions such that optical recombination is limited by the lifetime of an exciton relative to radiationless transitions to lower-lying tail states. It is assumed that, for any localized state with energy $\omega_1 \geqslant \omega_0$, we can specify a sphere of radius R_{int}, such that, if within the volume $4\pi R_{\text{int}}^3/3$ of the sphere there is at least one other potential well containing a state with localization energy $\omega_2 \geqslant \omega_1$, then these wells form a complex (supercluster), between whose states a transition involving phonons can take place. The distribution of tail states of interest to us, as they belong to superclusters, is generated using the theory of percolation along overlapping spheres. This approach makes it possible to establish the location of the phononless luminescence bands relative to the peak in the phononless exciton absorption band and the threshold for percolation in the system.

4) Accounting for the interaction of fluctuation states with phonons. The steady-state concentration of populated states in the presence of continuous weak interband excitation is proportional to the density of states for a given energy and their lifetime. The emission probability for the populated states is described by the same optical density as the phononless absorption coefficient $\alpha^0(\omega)$, so that the phononless luminescence band can be written in the form

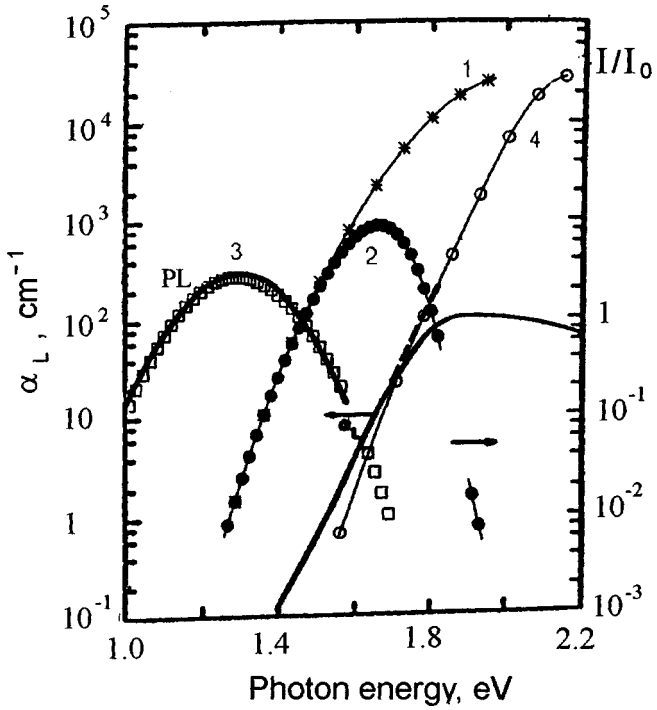

FIG. 1. A comparison of experimental optical spectra[1] with the results of the present calculations. (*1*) The calculated[6] density of states of the valence bands, taken here as an amorphous optical density of states; (*2*) the profile of the band of ''radiative'' states found using Eq. (1); (*3*) the shape of the luminescence band, where the squares are calculated values and the smooth curve is the experimental spectrum in relative units; and, (*4*) the shape of the fundamental absorption band, where the thick dashed curve is the experimental absorption spectrum (left scale) and the thin line with hollow circles is calculated, including the phonon interaction.

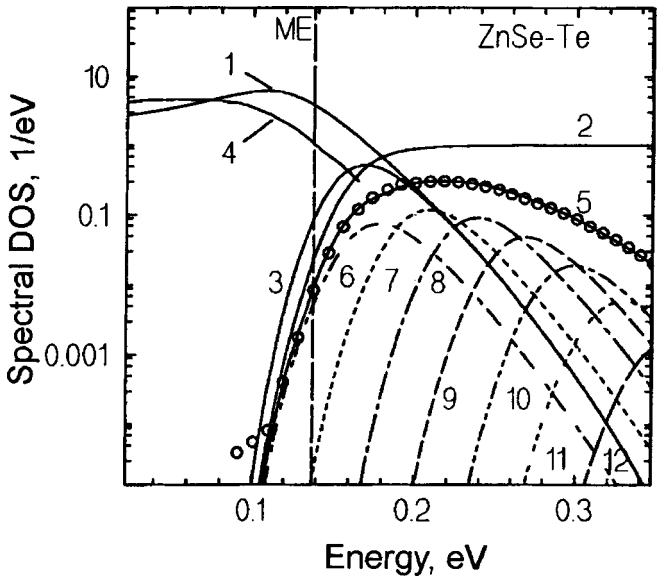

FIG. 2. The luminescence spectrum of $ZnSe_{0.85}Te_{0.15}$ (circles); (*1*) the phononless band of the optical density of the exciton ground state; (*2*) the relative fraction of ''radiating'' states, $P(\omega)$; (*3*) the phononless luminescence band (''radiating'' states); (*4*) the absorption band of the exciton ground state including the interaction with acoustic and optical phonons; (*5*) the calculated profile of the luminescence band; (*6–12*) the profile of the luminescence band including the interaction with acoustic phonons and its repetitions at the frequency of the longitudinal optical phonon. The vertical line denotes the position of the percolation threshold.

$$I^0(\omega)\sim\alpha^0(\omega)P(\omega)\tau_{\rm rad}, \tag{1}$$

where $P(\omega)$ is the overall relative fraction of emitting states with localization energy ω belonging to superclusters of different sizes. The contribution to $P(\omega)$ from isolated wells and the ground states of the pairs can be written as

$$P(\omega)\sim[\exp\{-2\mathcal{P}(\omega)\}+\mathcal{P}(\omega)\exp\{-3.073\mathcal{P}(\omega)\}], \tag{2}$$

where $\mathcal{P}(\omega)=(1/2)[R_{\rm int}/\overline{r(\omega)}]^3$ and $\overline{r(\omega)}=(N^{-1}(\omega)3/4\pi)^{1/3}$. Here $N(\omega)$ is the integrated density of states, while $\mathcal{P}(\omega)$ represents the density of localized excitons in units of the first virial coefficient. In the calculations we used the value $\mathcal{P}(\omega_{\rm ME})=1.40$ for the density of exciton states at the percolation threshold $\omega_{\rm ME}$.[5] In all cases, isolated potential wells and minimally sized superclusters provide the major contributions, while the higher-order terms only provide small corrections.

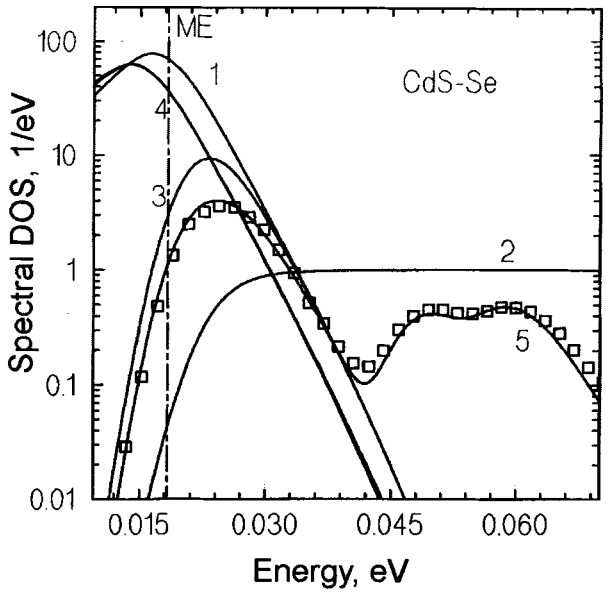

FIG. 3. The luminescence spectrum of $CdS_{0.50}Se_{0.50}$ (squares). (*1–5*) As in Fig. 2.

Figure 1 shows theoretical and experimental[1] luminescence spectra of α Si:H. The density of states of the valence bands was calculated using parameters obtained previously.[6] The interaction with phonons was described using an Einstein model with the phonon energy taken to be 18 meV.

Figures 2 and 3 show luminescence spectra of $ZnSe_{0.85}Te_{0.15}$ and $CdS_{0.50}Se_{0.50}$ solid solutions. In order to attain agreement with the experimental data, we have included the interactions of excitons with both optical and acoustic phonons.[4]

A comparison of the experimental and theoretical data shows that the proposed approach is justified for a broad range of disordered systems.

This work was supported by the INTAS foundation (Grant 94-324) and the Russian Fund for Fundamental Research (Grants 96-02-16933) and 97-02-18138).

[1] R. A. Street, Adv. Phys. **30**, 593 (1981).
[2] S. Permogorov and A. Reznitsky, J. Lumin. **52**, 201 (1992).
[3] E. Cohen and M. Sturge, Phys. Rev. B **25**, 3828 (1982).
[4] A. A. Klochikhin, S. A. Permogorov, and A. N. Reznitskiĭ, Fiz. Tverd. Tela **39**, 1170 (1997) [Phys. Solid State **39**, 1035 (1997)].
[5] S. W. Haan and R. Zwanzig, J. Phys. A: Math. Gen. **10**, 1547 (1977).
[6] A. A. Klochikhin, Phys. Rev. B **53**, 10979 (1995).

Translated by D. H. McNeill

Diffusion of excitons in CdS–Se and ZnSe–Te solid solutions at high excitation levels

A. A. Klochikhin

B. P. Konstantinov Institute of Nuclear Physics, Russian Academy of Sciences, 188350 Gatchina, Leningrad Region, Moscow

S. A. Permogorov and A. N. Reznitskiĭ

A. F. Ioffe Physicotechnical Institute, Russian Academy of Sciences, 194021 St. Petersburg, Russia

T. Breitkopf, R. Westphäling, and C. Klingshirn

Institut für Angewandte Physik, Universität Karlsruhe, 76128 Karlsruhe, Germany

Fiz. Tverd. Tela (St. Petersburg) **40**, 892–893 (May 1998)

It is shown that, with strong pulsed excitation, the intensity of the exciton recombination band in the fluctuation tail of the density of states in the limit of large times in the presence of traps is described by the asymptote of a solution to the diffusion equation. The critical diffusion index corresponds to a ''normal'' process in the CdS–Se solid solution and to ''anomalous'' diffusion in the case of ZnSe–Te. © *1998 American Institute of Physics.* [S1063-7834(98)03805-2]

Under weak excitation, the intrinsic luminescence of solid solutions is produced by ''radiating'' states in the tail of the density of states which have been formed by the localization of excitons at fluctuation isolated clusters of atoms of the narrow-gap component or of the ground states of complexes (superclusters) consisting of small numbers of such clusters.[1,2]

For excitation powers sufficiently high so that the excitons, owing to an interband pumping pulse, are able to fill both the relatively few isolated localized states and the states belong to large superclusters and the percolation cluster, excitations appear in the crystal that are capable of limited or free propagation through the volume. We shall be interested in times $\Delta t \gg \tau_{\rm dec}$, where $\tau_{\rm dec}$ is the time for an exciton to jump into a neighboring well. Under these conditions, a mobile exciton may undergo many jumps over its lifetime. As a consequence, we can assume that (a) after a certain time following the excitation pulse, a quasiequilibrium distribution develops among the excitons, and (b) the time evolution will be determined by the diffusion of excitons to traps, so that under these conditions we can use the well-known asymptote of the solution to the diffusion equation in the limit of large times.[3–7]

The asymptote of the solution of the ''normal'' diffusion equations for the probability of survival of an exciton in a spherical volume of radius R, free from traps, over time t has the form[5]

$$P(R,t) \sim \exp\left\{ -\gamma_d \frac{Dt}{R^2} \right\}, \tag{1}$$

where γ_d is a constant that depends on the dimensionality d of the space and D is the exciton diffusion coefficient. Averaging the probability of survival of mobile excitons over all possible sizes R of the region using an optimization procedure[5] yields a dependence of the form

$$P_{\rm opt} = \exp\left\{ -(1+2/d)\,\gamma_d^{d/(d+2)} \left(\frac{dC_d}{2} \right)^{2/(d+2)} N_{tr}^{2/(d+2)} \times (Dt)^{d/(d+2)} \right\}, \tag{2}$$

where N_{tr} is the average concentration of traps in the crystal and C_d is a dimensionless constant which depends on d. Equation (2) implies, that for normal diffusion, the logarithm of the intensity of the luminescence band depends linearly on a fractional power of t,

$$\ln(I(t)) \sim t^{(d/(d+2))}. \tag{3}$$

If the ''optimal'' dimensions $R_{\rm opt}$ of the diffusion region which make the major contribution to the band intensity are comparable to the correlation length ξ of the percolation cluster ($R_{\rm opt} \leqslant \xi$),[7] then the diffusion becomes anomalous. In this case, the dimensionality d in Eq. (3) has to be replaced by a ''hyperuniversal'' fractal dimensionality,[8,9] i.e., by the spectral dimensionality d_s of the percolation cluster:

$$\ln(I(t)) \sim t^{(d_s/(d_s+2))}. \tag{4}$$

In Eq. (4), $d_s = 2d_f/d_w$, where d_f is the fractal dimensionality (for a three dimensional space,[10] $d_f = \approx 2.51$) and d_w is the index of the fractal dimensionality of the random walk[7] ($d_w \approx 3.8$ for $d=3$). As can be seen from Eq. (4), the diffusion is substantially slower than ''normal.''

The process is slowed down further if diffusion takes place partly over superclusters of finite size. In this case, d should be replaced by the exponent $2d_f/d_w'$ in Eq. (3),[7] where

$$d_w' = d_w/(1-\beta/2\nu), \tag{5}$$

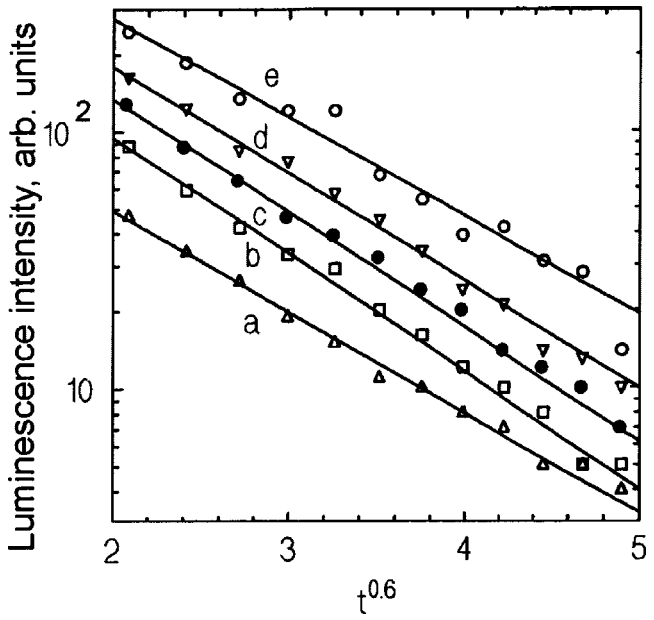

FIG. 1. The damping kinetics of the integrated luminescence intensity of $CdS_{0.93}Se_{0.07}$ over times of 3–16 ns for $T=8$ K and excitation fluxes of 600, 200, 60, 6, and 2 μJ/cm^2 (points on curves *a*–*e*). The smooth curves are the function $I(t)\propto\exp(-t^y)$, with exponents y equal to 0.57, 0.61, 0.61, 0.59, and 0.56, respectively.

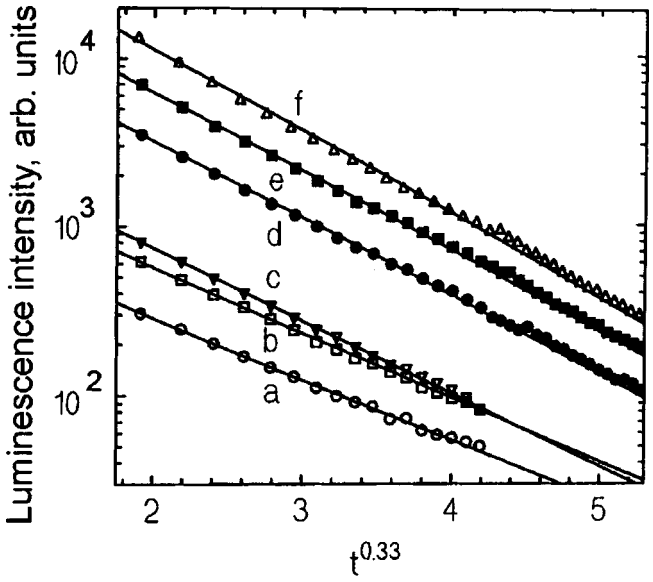

FIG. 2. As in Fig. 1 for a sample of $ZnSe_{0.93}Te_{0.07}$ over 10–160 ns for excitation fluxes of 1000, 300, 100, 30, 10, and 3 μJ/cm^2 (points on curves *a*–*f*). For the smooth curves the exponents on t are 0.35, 0.34, 0.34, 0.33, 0.31, and 0.30, respectively.

while β and ν are the critical indices of the ordering parameter and the correlation length;[10] for $d=3$, we have $d'_w \approx 5.01$.[7]

We have investigated the damping kinetics of the luminescence in CdS–Se and ZnSe–Te solid solutions for high intensities of interband excitation by subnanosecond pulses. The experimental conditions have been described elsewhere.[11]

Figure 1 shows plots of the integrated intensity of the luminescence band of CdS–Se as a function of time, $I(t)$ for different pumping levels. It is clear from the figure that, in all cases, $I(t)$ has a dependence of the form (3), with an asymptotic index close to that for normal diffusion, i.e., $\ln(I(t))\propto t^{-0.6}$.

Figure 2 shows similar curves for the spectrum of the ZnSe–Te solid solution. In distinction from the previous case, here the critical index is roughly equal to 0.33, which agrees well with the value $d_f/(d_f+d'_w)$, as implied by Eq. (3) after d is replaced by $2d_f/d'_w$.

The most probable reason for the different asymptotic behavior of the diffusion is the different amount of traps in these two solid solutions. A direct measurement of the luminescence quantum yield at weak excitation levels for these samples gives roughly 0.7 for CdS–Se and 0.03 for ZnSe–Te. Thus, the condition under which the fractal structure of the percolation cluster becomes significant for diffusion, $R_{\text{opt}}\leqslant\xi$, will be satisfied sooner for a crystal with a large number of traps. A systematic study of the relationship between the damping rate and the luminescence quantum yield is the aim of our next experiments.

This work was assisted by the Deutsche Forschungsgemeinschaft (section SFB 195) and supported by the INTAS foundation (Grant 94-324) and the Russian Fund for Fundamental Research (Grants 96-02-16933 and 97-02-18138).

[1] A. A. Klochikhin, S. A. Permogorov, and A. N. Reznitskiĭ, JETP Lett. **65**, 289 (1997).
[2] A. A. Klochikhin, S. A. Permogorov, and A. N. Reznitskiĭ, Fiz. Tverd. Tela **39**, 1170 (1997) [Phys. Solid State **39**, 1035 (1997)].
[3] B. Ya. Balagurov and V. G. Vaks, Zh. Éksp. Teor. Fiz. **65**, 1939 (1973) [Sov. Phys. JETP **38**, 968 (1973)].
[4] N. D. Donsker and S. R. Varadhan, Commun. Pure Appl. Math. **32**, 721 (1979).
[5] P. Grassberger and I. Procaccia, J. Chem. Phys. **77**, 6281 (1982).
[6] V. Kuzovkov and E. Kotomin, Rep. Prog. Phys. **51**, 1479 (1988).
[7] S. Havlin and A. Bunde, *Percolation II*, in *Fractals and Disordered Systems*, A. Bunde and S. Havlin, Eds., Springer, Berlin (1991), p. 97.
[8] S. Alexander and R. Orbach, J. Physique Lett. **43**, L625 (1982).
[9] T. Nakayama, K. Yakubo, and R. Orbach, Rev. Mod. Phys. **66**, 381 (1994).
[10] A. Bunde and S. Havlin, *Percolation I*, in *Fractals and Disordered Systems*, A. Bunde and S. Havlin, Eds., Springer, Berlin (1991), p. 51.
[11] T. Breitkopf, H. Kalt, C. L. Klingshirn, and A. Reznitsky, J. Opt. Soc. Am. B **13**, 1251 (1996).

Translated by D. H. McNeill

Anisotropy of cubic semimagnetic $Cd_{1-x}Mn_xTe$ solid solutions and excitonic magnetic polaron energy from polarized-luminescence measurements

A. V. Kudinov, Yu. G. Kusraev, and B. P. Zakharchenya

A. F. Ioffe Physicotechnical Institute, Russian Academy of Sciences, 194021 St. Petersburg, Russia

V. N. Yakimovich

Institute of Solid-State and Semiconductor Physics, Academy of Sciences of Belarus, Minsk, Belarus

Fiz. Tverd. Tela (St. Petersburg) **40**, 894–896 (May 1998)

Polarized photoluminescence of $Cd_{1-x}Mn_xTe$ crystals in a weak magnetic field has been studied in Faraday and Voigt geometries. A simple method is proposed to determine the exciton mobility edge and excitonic magnetic-polaron energy. ''Forbidden'' polarization components of the recombination radiation have been experimentally detected. It has been established that the moments of magnetic polarons are oriented predominantly along the {111} axes. © *1998 American Institute of Physics.* [S1063-7834(98)03905-7]

1. Figure 1 presents a typical photoluminescence spectrum of an undoped CdMnTe solid solution. The spectrum is dominated by the inhomogeneously broadened line $L2$, which is due to exciton recombination from magnetic polaron states localized at compositional fluctuations[1]. Also shown is the spectrum of the degree of luminescence circular polarization obtained in a weak longitudinal magnetic field (Faraday geometry). Linear polarization spectra measured in Voigt geometry have a similar shape.

A characteristic feature of such spectra obtained from CdMnTe solid solutions with different compositions is a strong increase of polarization at the short-wavelength edge. The narrow region within which the polarization increases is located differently relative to the maximum of the luminescence line, namely, in the $x=0.08$ sample these features almost coincide, and as x increases, the polarization rise region shifts toward the short-wavelength wing ofthe luminescence spectrum. In the solid solutions studied by us, the distance between the polarization rise threshold and the luminescence line maximum coincided with the magnetic polaron energy.[2] This correlation suggests that the polarization rise threshold is just the exciton mobility edge, starting from which the exciton relaxation in energy can occur only through magnetic polaron formation.[3] This feature could probably provide the simplest possible way to determine the exciton mobility edge and magnetic polaron energy in semimagnetic solid solutions, because the corresponding experiment would require neither time-resolved techniques nor excitation with a tunable laser.

2. We are turning now to the experimental data on cubic anisotropy. Application of a transverse (i.e., parallel to the sample plane) magnetic field **H** produces a signal of linearly polarized luminescence along detection axes one of which is parallel to the field.[4] As seen, however, from Fig. 2a, the degree of polarization can depend strongly on magnetic field orientation with respect to the crystallographic axes. The symmetry of the observed effect reflects that of the (110) cleavage plane, namely, the angular dependence of polarization $\rho_0(\varphi)$ has two deep minima ($\mathbf{H}\|\{100\}$), two more shallow minima ($\mathbf{H}\|\{110\}$), and four maxima (close to $\mathbf{H}\|\{111\}$ directions).

The observed anisotropy should be related to the deviation of local magnetization from the direction of the external magnetic field. This deviation gives rise also to the appearance of linear polarization of radiation along detection axes turned through 45° toward the field direction (ρ_{45}). This alternating polarization whose appearance could not be explained without taking into account the anisotropy has been observed experimentally by us (see Fig. 2b).

In Faraday geometry, we also observed manifestations of cubic anisotropy in polarization. Among them are the appearance, in the presence of a magnetic field, of linear polarization of the luminescence, which is forbidden in spherical

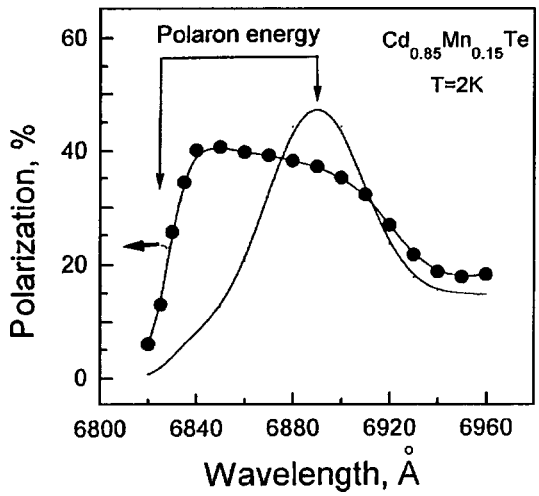

FIG. 1. Spectra of luminescence and of the degree of circular polarization of the luminescence of a (011)$Cd_{0.85}Mn_{0.15}Te$ sample placed in a weak magnetic field (Faraday geometry). $T=2$ K, excitation by the 633-nm line of He–Ne laser. The spectral features indicating the exciton mobility edge and magnetic polaron energy are identified.

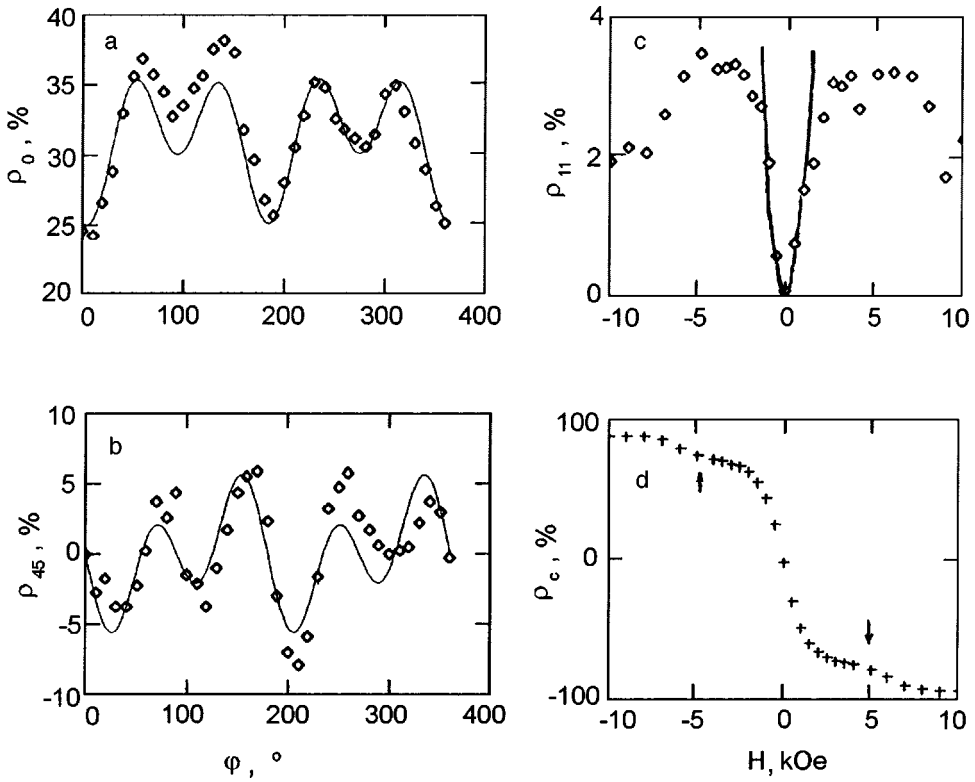

FIG. 2. Manifestation of cubic anisotropy in the (011)$Cd_{0.85}Mn_{0.15}Te$ crystal observed in (a,b) Voigt geometry and (c,d) Faraday geometry: angular dependences of the linear polarization of luminescence, ρ_0 (a) and ρ_{45} (b), field dependences of the degree of linear polarization $\rho_\parallel$ (c) and of degree of circular polarization ρ_c (d). $T=2$ K, excitation by the 633-nm line of He–Ne laser. The curves are calculations.[5]

approximation (Fig. 2c), and of anomalies in the field dependences of the degree of circular polarization ρ_c (Fig. 2d). The degree of linear polarization $\rho_\parallel$ is an even function of the field, and its peaks occur at the same fields as the anomalies in the circular polarization.

The magnitude of the anisotropy effects changes strongly with temperature and magnetic-ion concentration in the solid solution.[5] The general tendencies revealed in these changes can be summed up as follows: the anisotropy increases as one approaches the spin–glass transition[6] both in temperature and manganese content.

3. As evident from Fig. 2a, the degree of polarization ρ_0 reaches a maximum with the magnetic field oriented close to the {111} directions. Therefore, by analogy with the easy axes of magnets we shall call the {111} directions ''easy'' for the polaron magnetic moments. Some of the results can be best understood in terms of the strong-anisotropy model which postulates that the moment of each polaron is oriented along one of the easy axes (i.e., the polaron resides in one of eight possible orientational states), and the luminescence polarization in a magnetic field arises because of a population redistribution among these states.

First of all, the strong-anisotropy model provides a straightforward explanation for the appearance of ''forbidden'' polarizations ρ_{45} and $\rho_\parallel$. The states in which the polaron moment makes the smallest angle with the field possess the lowest energy and, therefore, they are predominantly populated and, thus, determine the characteristics of the radiation. The polarization of the polaron recombination radiation is connected rigidly with the direction of the polaron magnetic moment rather than with that of the external magnetic field. When measuring the angular dependence of ρ_{45}, the analyzer configuration is fixed with respect to the field direction, while the polaron moment deviates from this direction alternately to the closest easy axis, which generates an alternating polarization signal. The appearance of $\rho_\parallel$ in Faraday geometry is connected with the actual selection of the (011) crystal orientation, namely, the degenerate doublet of easy directions closest to the field emits light polarized along $[01\bar{1}]$. Note that the symmetry of a similar experiment in the (100) orientation contains an additional element, rotation through 90° and, therefore, no polarization arises in this case.

The theoretical limit for $\rho_\parallel$ in our case turns out to be 20%, producing strong anisotropy in the model. For the $x=0.15$ samples, however, no saturation occurs, namely, the polarization decreases after passing through a maximum. The decrease of polarization cannot be explained within the strong-anisotropy model, because this decrease is connected with the external field overcoming the anisotropy field. Thus the position of the maximum in the field dependence of $\rho_\parallel$ permits an estimate of the anisotropy field to be made.

4. Thus we have observed and studied manifestations of cubic anisotropy in spectra of polarized luminescence of CdMnTe semimagnetic semiconductors placed in a weak magnetic field. An essentially new result is experimental establishment of the fact that the moments of excitonic magnetic polarons in crystals with a high manganese concentration are oriented along the {111} axes. We have also proposed a simple method for determining the energy of the excitonic magnetic polaron, which is based on measuring the photoluminescence polarization.

The authors are grateful to M. E. Boiko for x-ray diffraction measurements, and to K. V. Kavokin and I. A. Merkulov for fruitful discussions.

Support of the Russian Fund for Fundamental Research (Grant 96-02-16887) is gratefully acknowledged.

[1] A. Golnik, J. Ginter, and J. A. Gaj, J. Phys. C **16**, 6073 (1983).
[2] G. Mackh, W. Ossau, D. R. Yakovlev, A. Waag, G. Landwehr, R. Hellmann, and E. O. Göbel, Phys. Rev. B **49**, 10248 (1994).
[3] B. P. Zakharchenya and Yu. G. Kusraev, JETP Lett. **50**, 225 (1989).
[4] D. Heiman, P. Becla, R. N. Kershaw, D. Ridgely, K. Dwight, A. Wold, and R. R. Galazka, Phys. Rev. B **34**, 3961 (1986).
[5] A. V. Koudinov, Yu. G. Kusrayev, K. V. Kavokin, I. A. Merkulov, and B. P. Zakharchenya, in *Proceedings of the International Conference ''Compound Semiconductors''* (St. Petersburg, 1996), Inst. Phys. Conf. Ser. No. 155 (1997), Ch. 10.
[6] S. Oseroff and P. H. Keesom, in *Diluted Magnetic Semiconductors*, Ser. *Semiconductors and Semimetals* (Academic Press, New York, 1988), Vol. 25, edited by J. Furdyna and J. Kossut.

Translated by G. Skrebtsov

Exciton luminescence of $Cd_{1-x}Fe_xTe$ solid solutions

S. A. Permogorov and L. N. Tenishev

A. F. Ioffe Physicotechnical Institute, Russian Academy of Sciences, 194021 St. Petersburg, Russia

T. P. Surkova

Institute of Metal Physics, Ural Branch of the Russian Academy of Sciences, 620219 Ekaterinburg, Russia

Fiz. Tverd. Tela (St. Petersburg) **40**, 897–899 (May 1998)

Band-edge optical spectra of $Cd_{1-x}Fe_xTe$ solid solutions differ substantially from those of undoped CdTe. The pattern of the change in photoluminescence spectra with increasing Fe concentration is connected with a change in radiative recombination channels. © *1998 American Institute of Physics.* [S1063-7834(98)04005-2]

Iron and other transition metals are ubiquitous residual impurities in wide-gap II–VI semiconductors, and they play an extremely important role in recombination processes. The physical properties of $Cd_{1-x}Fe_xTe$ depend essentially on the position of the Fe^{2+} level relative to the crystal band structure. It is believed that the donor level of the isoelectronic substitutional impurity Fe_{Cd} lies in the gap at $E_c = 1.45$ eV.[1–3] If the Fe concentration is made high enough, this level will coincide in position with the valence-band edge of the solid solution.[4] It appeared of interest to follow the corresponding change in the character of the radiative processes.

The $Cd_{1-x}Fe_xTe$ crystals studied in the work were grown by the Bridgman technique. The photoluminescence (PL) and reflectance measurements were made on samples within the whole interval of Fe solubility, $0 < x < 0.4$, in the 5–250-K temperature range. A He–Ne laser was used as excitation source. The optical spectra were obtained with a DFS-12 monochromator and a PM tube coupled to a photon counting system.

PL and exciton reflectance spectra are shown in Figs. 1 and 2. Table I contains some characteristics of the samples and of optical spectra. As evident from Fig. 1, the PL spectra of $Cd_{1-x}Fe_xTe$ and CdTe differ qualitatively. The undoped CdTe crystal exhibits several radiative recombination channels. Emission of free excitons ($E_x = 1.5964$ eV) and excitons bound to donors (D^0, x) = 1.5931 eV and acceptors (A^0, x) = 1.5899 eV, as well as the donor-acceptor PL, and their LO phonon replicas contribute considerably to the photoluminescence.[5] By contrast, emission spectra of $Cd_{1-x}Fe_xTe$ with a Fe concentration of 3.5×10^{19} cm^{-3} have only one emission band peaking close to the maximum of the exciton reflectance line (Fig. 2). As Fe concentration increases, the total PL intensity decreases, to become undetectable at the highest Fe concentration of 8×10^{20} cm^{-3}. At the same time the exciton reflectance line broadens considerably

TABLE I. Free-exciton line position E_{FE}, exciton reflectance line width $\Delta = (E_{FE}^{\min} - E_{FE}^{\max})$, and activation energy E_{act} of temperature-induced PL quenching of $Cd_{1-x}Fe_xTe$ crystals. E_{FE} and Δ are given for the temperature of 5 K.

Fe concentration	E_{FE}, eV	Δ, meV	E_{act}, meV
0	1.5964	1.0	23.0
1×10^{17}	1.5963	1.53	19.8
3×10^{18}	1.5967	1.96	14.2
3.5×10^{19}	1.5992	3.05	10.6
4×10^{20}	1.6157	7.4	-
8×10^{20}	1.6527	30.0	-

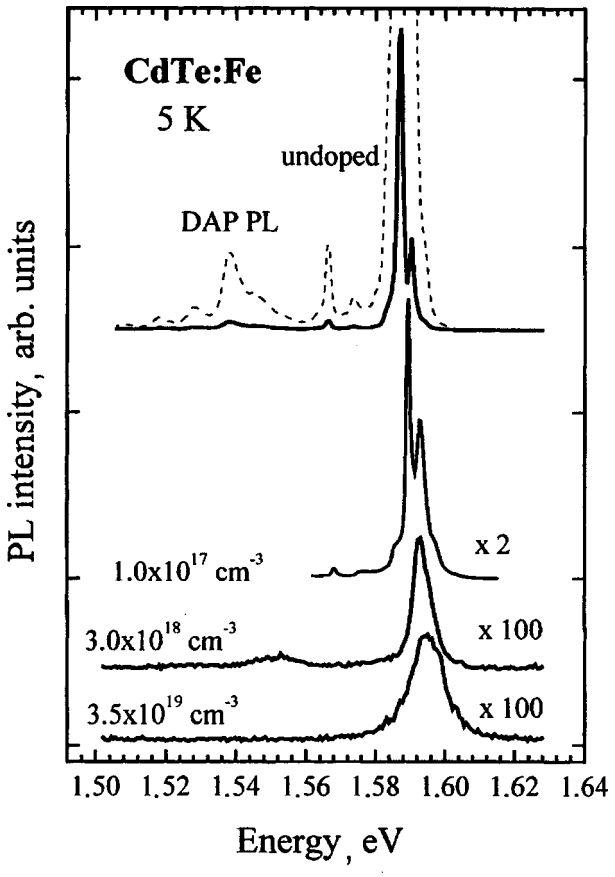

FIG. 1. PL spectra of $Cd_{1-x}Fe_xTe$ crystals with different Fe concentrations. The spectra were obtained at 5 K under He-Ne laser excitation. Dashed line: spectrum of pure CdTe ($\times 10$) exhibiting distinct donor and acceptor PL.

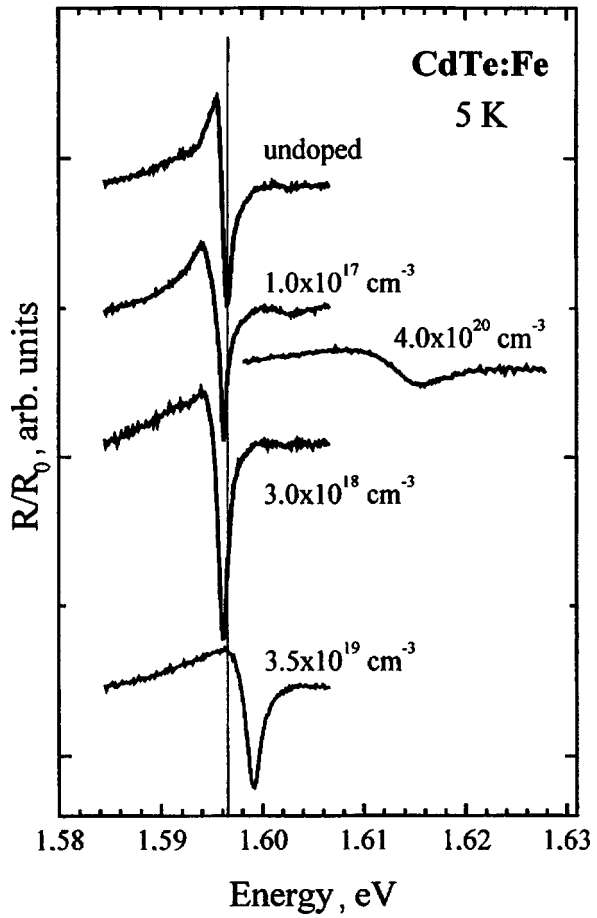

FIG. 2. Exciton reflectance spectra of $Cd_{1-x}Fe_xTe$ crystals with different Fe concentrations. The spectra were obtained at 5 K.

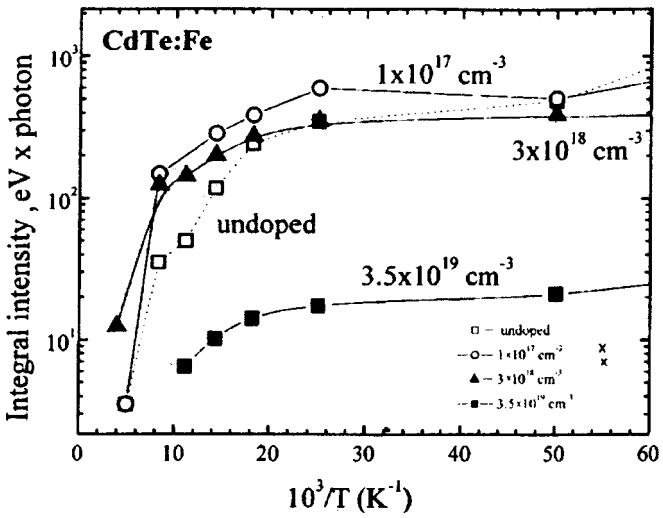

FIG. 3. Temperature-induced quenching of PL in $Cd_{1-x}Fe_xTe$ crystals.

and shifts toward higher energies while remaining fairly narrow.

We may thus conclude that the evolution of PL spectra with increasing Fe concentration is connected with the emission channels changing from predominantly radiation of the acceptor-bound exciton (A^0,x) in undoped CdTe to free-exciton emission in $Cd_{1-x}Fe_xTe$ solid solutions. The observed decrease of the activation energy of temperature-induced quenching of integrated PL intensity (Fig. 3) $E_{\rm act}$ from 23 meV for the bound exciton (A^0,x) in CdTe to 10.6 meV for the free exciton in $Cd_{1-x}Fe_xTe$ supports this conclusion (Table I). We believe that the observed decrease in neutral acceptor concentration is due to Fe ions transferring to another charge state, $2+\rightarrow 3+$.

The character of the variation of PL and reflectance spectra with temperature is similar to that of their variation with Fe concentration. It may be conjectured that both factors affect the free-exciton lifetime, and that the exciton kinetic-energy distribution has a strongly nonequilibrium character. The large difference in width between the exciton reflectance and PL lines indicates that phonons are involved in the recombination process.

In our previous publication[6] we analyzed the shape of the exciton emission line in $Cd_{1-x}Fe_xTe$. We used an expression taking into account both $(A-LO)$ phonon-assisted recombination and resonant exciton emission. The shape of the exciton PL line can be written as

$$I(E)=\frac{[E^{1/2}\exp(-E/kT)+\varphi S(E)](1+\gamma E)}{(E-\omega_{LO})^2+\Gamma^2}, \qquad (1)$$

where E is the exciton kinetic energy, $S(E)$ is the additional nonequilibrium contribution to the distribution function, φ and γ are parameters describing the nonequilibrium/equilibrium distribution and the processes involving conservation/nonconservation of the wave vector, respectively, ω_{LO} is the LO-phonon energy, and Γ is the exciton-state damping evaluated from the exciton reflectance line width. It is assumed that the nonequilibrium part of the free-exciton distribution function reproduces the density of states in the exciton band. The need to take into account the nonequilibrium distribution of excitons originates from the decrease of the exciton lifetime in Fe-doped samples. The partial nonconservation of the wave vector in exciton recombination is due to exciton scattering from the Fe impurity and other defects. The best fit of the calculation to the experimental PL spectrum (Fe concentration 1×10^{17} cm^{-3}, $T=30$ K) was obtained with the parameters $\varphi=0.007$, $\gamma=0.2$, $\Gamma=1.5$ meV. A similar shape analysis of the room-temperature emission line made for undoped CdTe crystals[7] likewise showed the PL to be of excitonic origin and demonstrated the involvement of phonons in the recombination process.

One may thus conclude that formation of a $Cd_{1-x}Fe_xTe$ solid solution results in an increasing gap width with increasing Fe concentration. One observes simultaneously a broadening of exciton reflectance lines and a decrease of integrated PL intensity. We believe that these changes indicate a decrease in the free-exciton lifetime because of strong scattering from radiative and nonradiative recombination centers. As a result, the free-exciton distribution in kinetic energy

becomes strongly nonequilibrium. At low Fe doping levels one observes a decrease in the emission line intensity due to excitons bound to neutral acceptors, which can be attributed to a decrease in their concentration as a result of the change in the iron-ion charge state.

The authors express their gratitude to A. Mycielski for providing the $Cd_{1-x}Fe_xTe$ crystals.

Partial support of the Russian Fund for Fundamental Research (Grant 96-02-16933), INTAS (Grant 93-3657), and State Research&Development Program ''Physics of Solid-State Nanostructures'' (Grant 95-1001) is gratefully acknowledged.

[1] A. Mycielski, J. Appl. Phys. **63**, 3279 (1988).
[2] K. Lishka, G. Brunthauer, and W. Jantsch, J. Cryst. Growth **72**, 355 (1985).
[3] A. J. Szadkowski, J. Phys. Condens. Matter **2**, 9853 (1990).
[4] B. A. Orlowski, B. J. Kowalski, A. Sarem, A. Mycielski, B. Velicky, and V. Chab, in *Proceedings of the 19th International Conference ''Physics of Semiconductors''* (IFPAN, Warsaw, 1988), edited by W. Zawadski, p. 1267.
[5] R. Zanio, in *Cadmium Telluride*, Semiconductors and Semimetals, Vol. 13 (Academic Press, New York, 1978).
[6] S. A. Permogorov, L. N. Tenishev, and T. P. Surkova, Acta Phys. Pol. A **82**, 702 (1992).
[7] J. Lee, N. C. Giles, D. Rajavel, and C. J. Summers, Phys. Rev. B **43**, 1668 (1994).

Translated by G. Skrebtsov

Optical and thermal orientation of localized excitons in solid solutions under resonant excitation in a longitudinal magnetic field

A. N. Reznitskiĭ, A. V. Kornievskiĭ, A. A. Kiselev, S. A. Permogorov, and L. N. Tenishev

A. F. Ioffe Physicotechnical Institute, Russian Academy of Sciences, 194021 St. Petersburg, Russia

A. A. Klochikhin

Nuclear Physics Institute, Russian Academy of Sciences, 188350 St. Petersburg, Russia

S. Yu. Verbin

Physics Scientific-Research Institute, St. Petersburg State University, 198904 St. Petersburg, Russia

H. Gerlach, M. Hetterich, M. Grün, and C. Klingshirn

Institut für Angewandte Physik, Universität Karlsruhe, D-76128 Karlsruhe, Germany

Fiz. Tverd. Tela (St. Petersburg) **40**, 900–902 (May 1998)

A theoretical and experimental study of the effect of a longitudinal magnetic field on optical orientation and magneto-circular polarization of the luminescence of localized excitons in semiconducting solid solutions is reported. It is shown that recombination takes place through two types of emitting states differing substantially in the degree of anisotropy, g factor, and spin relaxation time. Estimates are made of the g factors, anisotropic and exchange splittings, lifetime, and spin relaxation time of localized states in a $CdS_{0.96}Se_{0.04}$/GaAs solid-solution epitaxial layer. © *1998 American Institute of Physics.* [S1063-7834(98)04105-7]

Localized-exciton luminescence produced under resonant excitation by linearly polarized light from the density-of-states tail was found to be linearly polarized predominantly in the direction of pump polarization.[1] Longitudinal magnetic field B causes rotation of the exciton dipole moment, which reduces the degree of linear polarization of the luminescence $\rho_{\rm lin}=(I_{\parallel}-I_{\perp})/(I_{\parallel}+I_{\perp})$, with the $\rho_{\rm lin}(B)$ relation being a Lorentzian with the FWHM determined in a general case by the splitting of the radiative doublet $\hbar\omega_r$ and the relative magnitude of the lifetime (τ_0) and spin relaxation times of electrons (τ_e) and holes (τ_h).

Increase of B also gives rise to the appearance of linear polarization along the X' and Y' axes turned through 45° with respect to the X and Y axes along which the pump polarization is oriented.[2]

An external longitudinal field produces an additional Zeeman splitting $\hbar\Omega=(g_h-g_e)\mu B$, and for B high enough that $\Omega \gg \omega_r$ exciton states $|X\rangle$ and $|Y\rangle$ transform to ''pure'' $|+1\rangle$ and $|-1\rangle$ states, which emit circularly polarized radiation. Excitation with circularly polarized light produces two contributions to circular polarization of radiation $\rho_{\rm circ}$, namely, (1) due to the optical electron-spin orientation $\rho_{\rm opt.or.}$, in which case the sign of the effect depends on the orientation of excitation polarization, and (2) due to thermal orientation of excitons, which is caused by the onset of thermodynamic equilibrium in the system of split emitting states (magneto-circular luminescence polarization ρ_{MCPL}). Because the sign of ρ_{MCPL} is determined by the magnetic field direction, these contributions can be separated, for instance, by comparing the values of $\rho_{\rm circ}$ obtained in oppositely oriented fields. Under stationary excitation by circularly polarized light $\rho_{\rm opt.or.}=[\rho_{\rm circ}(N)+\rho_{\rm circ}(S)]/2$, and $\rho_{MCPL}=[\rho_{\rm circ}(N)-\rho_{\rm circ}(S)]/2$ (where N and S denote the magnetic field directions).

We have also studied the effect of longitudinal magnetic field on the optical and thermal exciton orientation under resonant excitation of localized exciton states in order to estimate the main parameters of the exciton quartet, namely, carrier g factors and the times τ_0, τ_e, and τ_h, as well as the zero-field splittings: the exchange splitting $\hbar\omega_0$ and $\hbar\omega_r$ ($\hbar\omega_{nr}$) splittings for the doublet of radiative (nonradiative) states with moment $J_z=\pm 1(\pm 2)$.

In a similar problem of describing the effect of a longitudinal magnetic field on the optical orientation of excitons, the anisotropically split exciton states were assumed to be oriented along preferred crystallographic directions.[3] Based on the results in Ref. 3 and, after an averaging made to take into account the random distribution of localizing-potential anisotropy in a solid solution, one comes to

$$\rho_{\rm opt.or}\propto \xi(1+\Omega^2T^2)/(1+\Omega^2T^2+\xi\omega_r^2T\overline{T}), \tag{1}$$

$$\rho_{\rm lin}\propto (1+\xi\omega_r^2T\overline{T}/2)/(1+\Omega^2T^2+\xi\omega_r^2T\overline{T}), \tag{2}$$

$$\rho'_{\rm lin}\propto \Omega T/(1+\Omega^2T^2+\xi\omega_r^2T\overline{T}), \tag{3}$$

where $T^{-1}=\tau_0^{-1}+2\tau_+^{-1}$, $\overline{T}^{-1}=\tau_0^{-1}+\tau_+^{-1}$, and $\tau_+^{-1}=(\tau_e^{-1}+\tau_h^{-1})/2$. The dimensionless parameter ξ is determined by the contribution of nonradiative states and grows monotonically with the field while remaining within $1\leqslant\xi\leqslant 4/3$.

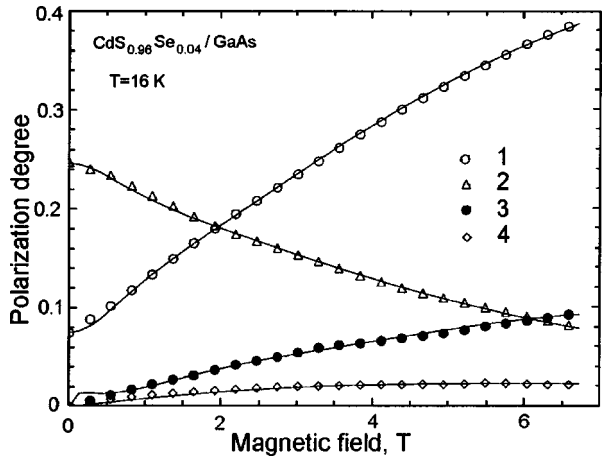

FIG. 1. Magnetic field scan of the degree of polarization of the signals due to optical orientation (open circles), optical alignment (open triangles), $MCPL$ (filled circles), and linear polarization along the X' and Y' axes (open rhombs). Solid curves: fitting with parameters given in Table I.

TABLE I. Characteristics of isotropic and anisotropic localized-exciton states.

	Isotropic (isolated) states	Anisotropic (pair) states
$g_{ex}=g_h-g_e^*$	<0.1	3
$\hbar\omega_0$, meV	0.2	
$\hbar\omega_r$, meV	0.003	0.5
$\hbar\omega_{nr}$, meV	0.08	0.10
ν_e^{**}, meV	0.09	
ν_h^{**}, meV	0.08	0.06
τ_0, ns	0.9	1.0
τ_e, ns	50	
τ_h, ns	0.2	10
β^{***}	0.7	

*The electronic g factor was assumed equal to $g_e=1.7$, i.e., to the weighted mean of the CdS and CdSe g factors.

**ν_e and ν_h are the matrix elements of the perturbation mixing radiative and nonradiative states. 4.

***β is relative concentration of anisotropic and isotropic localized-exciton states.

Figure 1 presents field dependences of the quantities ρ_{lin}, ρ'_{lin} and $\rho_{\text{opt.or.}}$, as well as of ρ_{MCPL} for the case of resonant excitation and detection with a Stokes shift of 2 meV.

It is known[4,5] that in the case of interband excitation of localized-exciton luminescence the $\rho_{MCPL}(B)$ relation has a distinct structure originating from the level crossing of the optically active and inactive state. As evident from Fig. 1, under resonant excitation this structure is practically not seen in the $MCPL$ spectrum. Such a behavior should be expected if population exchange at the level crossover point does not change the intensity of radiative recombination via optically active states. This is possible when the only process placing a limit on the lifetime of $|\pm 2\rangle$ states is spin relaxation to $|\pm 1\rangle$ states, which, in its turn, assumes a small probability of nonradiative recombination of localized states.

A line shape analysis of the $\rho_{\text{lin}}(B)$ dependence presented in Fig. 1 showed that it deviates noticeably from a Lorentzian, but can be described with a very good accuracy by a sumof two Lorentzians. At the same time, as seen from Eq. (2), the theoretical $\rho_{\text{lin}}(B)$ relation practically does not differ from a Lorentzian. The theory can be reconciled with experiment if we assume that, for each energy, there are two sets of localized states differing substantially in properties, primarily in anisotropy. Using the classification proposed in Ref. 6, they can be identified with isolated states (''singles'') and pairs of such states (''twos''). One may expect that there is a small or no anisotropy at all among the singles, whereas the twos are characterized by maximum anisotropy. In this case, the distribution of excitons in anisotropy will have two maxima for any localization energy. Such a distribution pattern will evidently be retained when one takes into account complexes made up of a larger number of potential wells (''threes,'' ''fours'' and so on) possessing intermediate anisotropy.

We carried out a model calculation of the field dependences of the measured quantities ρ_{lin}, ρ'_{lin}, and $\rho_{\text{opt.or.}}$, as well as of ρ_{MCPL}. The results of the fitting are shown in Fig. 1 with solid lines, and the values of the fitting parameters thus obtained are listed in Table I.

We readily see that some characteristics, such as the anisotropic splittings, g factor, and spin relaxation time are substantially different for singles and twos, whereas others, for example, the radiative lifetime are practically equal for these states. It should also be pointed out that the results of fitting turn out to be sensitive primarily to the ratio g_{ex}/ω_r rather than to the quantities g_{ex} and ω_r themselves.

Thus studying the effect of magnetic field on the optical and thermal orientation of excitons yields valuable information both on the fine structure of the energy spectrum and on the dynamic characteristics of localized states. The existing uncertainty in the estimation of some parameters may hopefully be reduced by invoking independent measurements of characteristic parameters. In this respect, direct measurement of the exciton g factor from light scattering spectra with spin flip appears to be most promising of all.

The authors thank with pleasure E. L. Ivchenko for numerous fruitful discussions and for the possibility of learning the results of Ref. 3 before its publication. Partial support of INTAS (Grant 94-324) and of the Russian Fund for Fundamental Research (Grants 96-02-16933 and 97-02-18138) is gratefully acknowledged.

[1] S. Yu. Verbin, S. A. Permogorov, and A. N. Reznitskiĭ, Fiz. Tverd. Tela (Leningrad) **25**, 346 (1983) [Sov. Phys. Solid State **25**, 195 (1983)].
[2] G. E. Pikus and E. L. Ivchenko, in *Excitons*. Modern Problems in Condensed Matter Sciences, Vol. 2, edited by E. I. Rashba and M. D. Sturge (North-Holland, Amsterdam, 1982) [Russ. trans. Nauka, Moscow, 1985], Chap. 6.
[3] R. I. Dzhioev, H. M. Gibbs, E. L. Ivchenko, G. Khitrova, V. L. Korenev, M. N. Tkachuk, and B. P. Zakharchenya, Phys. Rev. B **56**, 13405 (1997).
[4] E. L. Ivchenko and A. Yu. Kaminskiĭ, Fiz. Tverd. Tela (St. Petersburg) **37**, 1418 (1995) [Phys. Solid State **37**, 768 (1995)].
[5] A. Reznitsky, A. Tsekoun, S. Verbin, S. Permogorov, E. L. Ivchenko, and A. Yu. Kaminskii, Mater. Sci. Forum **182-184**, 297 (1995).
[6] A. A. Klochikhin, S. A. Permogorov, and A. N. Reznitskiĭ, Fiz. Tverd. Tela (St. Petersburg) **39**, 1170 (1997) [Phys. Solid State **39**, 1035 (1997)].

Translated by G. Skrebtsov

Lattice rearrangement induced by excitons in cryocrystals

E. V. Savchenko, A. N. Ogurtsov, and O. N. Grigorashchenko

Verkin Institute for Low Temperature Physics and Engineering, 310164 Kharkov, Ukraine

Fiz. Tverd. Tela (St. Petersburg) **40**, 903–906 (May 1998)

Experiments on permanent lattice-defect formation induced by electronic excitation of rare-gas solids are presented. The creation of triplet excitons $\Gamma(3/2)$ is found to be the primary process, followed by the exciton self-trapping. Probable models of defect formation are discussed.
 [S1063-7834(98)04205-1]

The self-trapping of excitons in atomic cryocrystals induces a variety of atomic processes including mass diffusion, and defect formation.[1–4] The basis for the physics of these phenomena is a concentration of the electronic excitation energy within a volume about that of a unit cell. Release of the energy can induce different kinds of lattice rearrangement. The above phenomena have been the subject of numerous experimental and theoretical studies on a variety of insulators.[2,5–7] Atomic cryocrystals with their simple lattice and well defined electronic structure[8] are excellent objects for investigation of exciton induced phenomena. The high quantum yield of these atomic processes caused by small binding energies in conjunction with a strong exciton–phonon interaction makes them especially suitable for experimental study.

A transformation of the initial point defects involving the self-trapped excitons was observed in solid Ne by the transient absorption method.[9] The creation of new lattice defects induced by the self-trapping of excitons in atomic cryocrystals was predicted in Ref. 10. Vacuum ultraviolet spectroscopic study revealed the formation and accumulation of permanent lattice defects generated by excitation with slow electrons in atomic cryocrystals.[4,11–17] It was supposed that the self-trapping of excitons is the stimulating factor. The first direct evidence of the exciton's key role for the creation of radiation-induced defects was obtained in the experiments on selective excitation of solid Xe[18] and Ar[19] to the lowest exciton band $\Gamma(3/2)$, $n=1$. This paper reviews experiments on permanent lattice-defect formation induced by electronic transitions in atomic cryocrystals. As an example, recent results on local lattice rearrangement induced by the excitation of atomic and molecular states of Ar are presented.

EXPERIMENT

Because a manifold of electronic levels can be involved in the phenomena, the optical spectroscopy is the most useful method for such kinds of investigations. The study was performed using cathodoluminescence, photoluminescence, and thermoluminescence. To reveal the effect of irradiation on luminescence spectra, it is necessary to grow the samples with the lowest possible concentration of initial defects and impurities. Suitable transparent samples were grown in special cryogenic cells under isobaric conditions ($P=80$ Pa) at a constant cooling rate of 0.1 K/s. The sample quality was monitored by measuring the luminescence intensity distribution and with the glow-curve analysis. Synchrotron radiation and a beam of electrons with low enough energy to avoid a knock-on defect formation were used for the excitations of the samples. The dose dependence of the luminescence spectra was measured at low temperatures to minimize thermally activated processes. Stable point defects were detected by a sensitized luminescence method. The defect component of the internal structure[12,21] of the well known atomic and molecular bands[1] served as an indicator of lattice rearrangement. Thermoluminescence measurements were a complementary test of defect creation in the samples.

CREATION OF DEFECTS

It is well known[1,3,8] that excitation of atomic cryocrystals from the ground state either by ionizing radiation or by photons results in self-trapping or trapping of excitons into atomic-type (A-STE, A-TE) and molecular-type (M-STE, M-TE) states. These states can be considered as short-lived defects which annihilate via radiative transitions. A part of them can convert to stable long-lived defects in the lattice. Since the energy of electronic excitation is transferred into kinetic energy of atomic motion over a unit cell, formation of three-, two, or one-dimensional defects is ruled out. In this case, only the point radiation defects, viz., Frenkel pairs (interstitials and vacancies) may emerge in the bulk of the crystal.

CONVERSION FROM ATOMIC-TYPE STATES

The analysis of the cathodoluminescence spectra of solid Ne[12] under different crystal-growth conditions as well as under subthreshold and superthreshold excitation made it possible to elucidate an origin of internal structure of the A-STE bands. It was shown that each band of the bulk emission associated with the transitions $^3P_1 \rightarrow {}^1S_0$ and $^1P_1 \rightarrow {}^1S_0$ consists of two components. The high-energy component stems from A-STE in a regular lattice, the low-energy one appears to be associated with structural defects. The emission spectrum of Ar atoms in solid Ne shows a similar structure (Fig. 1). A pronounced increase in the intensity of the defect component during irradiation by subthreshold energy electrons has been observed for both A-STE and A-TE in the Ne lat-

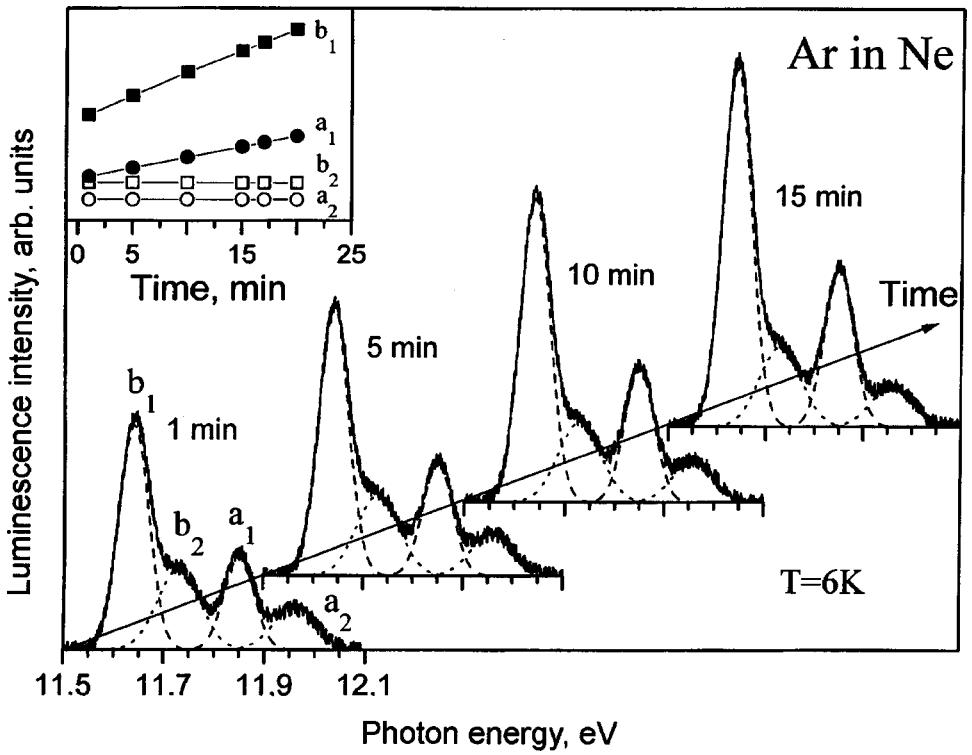

FIG. 1. Modification of the atomic emission with exposure time. The insert shows the dose dependence of the component.

tice. It was interpreted as being an outcome of a accumulation of permanent lattice defects generated during the lifetime of A-STE and A-TE. A current excited state molecular dynamics study[20] supports this interpretation and suggests a microscopic model of the conversion from A-STE to Frenkel pairs. The formation of the A-STE bubble with elastic lattice relaxation has been well studied earlier.[1,2] It is formed due to prevailing repulsive forces because of the negative electron affinity ($E=-1.2$ eV in solid Ne). After the bubble formation the surrounding ground-state atoms appear to have moved to the second shell. It was found that the second-nearest neighboring vacancy-interstitial pairs can create permanent defects which remain in the lattice after the exciton annihilation. The lowest energy bubble with plastic deformation can be considered as the primary STE-bubble accompanied by two non-adjacent vacancies in the first atomic shell and interstitials in the second one. The calculated transition energies from the defect-associated states of A-STE (54–66 meV) and A-TE (105 meV) are in an excellent agreement with the experimental data (63 meV and 100 meV).

CONVERSION FROM MOLECULAR-TYPE STATES

The two-component internal structure of the STE luminescence bands appears to be a general feature of M-STE in atomic cryocrystals formed from heavier rare gases[17,21] as well as for the considered A-STE states. The radiative decay of the self-trapped and trapped excitons in these solids pro-

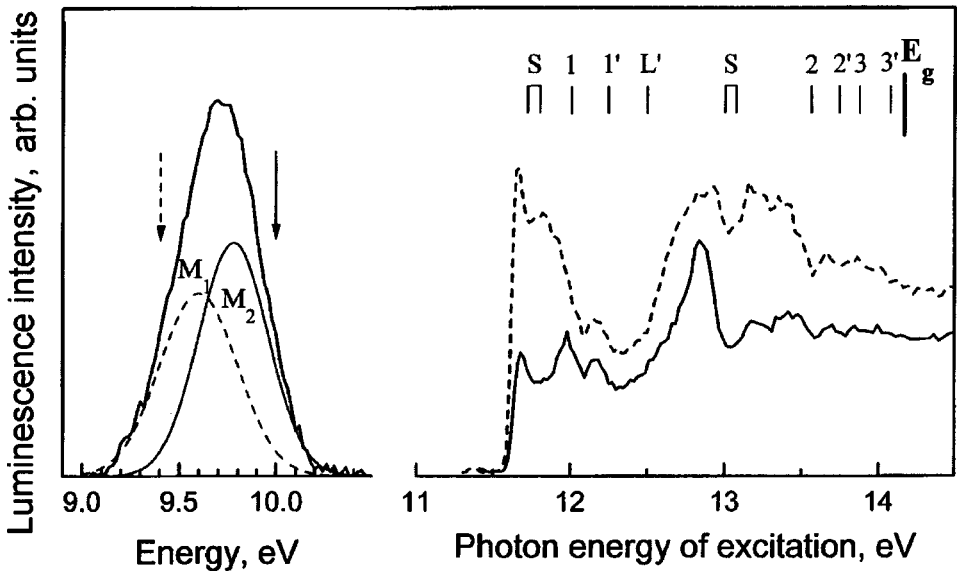

FIG. 2. Internal structure of the molecular luminescence band of solid Ar. The arrows indicate the energies taken at the luminescence yield measurements.[21]

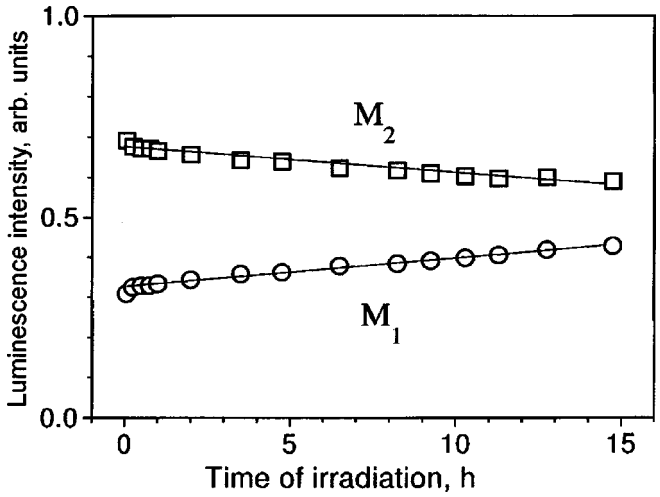

FIG. 3. Dose dependence of the molecular luminescence component measured under selective photoexcitation at $T=7$ K.

duces the well known M bands related to the $^{1,3}\Sigma_u^+ \rightarrow {}^1\Sigma_u^+$ transitions of molecular centers Rg_2^* (Rg stands for a rare gas atom). The high-energy component of the M band is supposed to stem from the exciton self-trapping in a regular lattice. The low-energy component is associated with exciton trapping in lattice imperfections. The internal structure of the M band in solid Ar is shown in Fig. 2. The excitation spectra of the above components measered by the ''red-blue-side'' subband separation method[18] demonstrate that the defect component can be excited below the bottom of the exciton band. An analysis of transformation of the M band during irradiation by low-energy electron[16] has revealed a distinct intensity increase of the defect component with exposure time. The enhancement of the defect component upon a low-temperature irradiation of samples in subthreshold regime can be regarded as a proof of the stable defect formation induced by an excitation of the electron subsystem. An additional support of this conclusion has been inferred from the study of the glow curve (total intensite of the thermoluminescence) variation with exposure time.[22] It was assumed that the stimulating factor of the defect formation is a self-trapping of the triplet excitons into molecular type states.

The use of synchrotron radiation to investigate the defect formation in atomic cryocrystals has the advantage of exciting definite electronic states and reveals the primary states involved in the process. The excitation of solid Ar by photons with the energy in the range of the exciton band $\Gamma(3/2)$ results in an intensity redistribution of the M-band components in favor of the defect one (Fig. 3). The data obtained demonstrate the intrinsic nature of the phenomenon and confirm beyond any doubt the key role of excitons in the creation of radiation induced defects.

The newly-formed defects are thought to be Frenkel pairs. According to theoretical calculations[23] the only stable form of an interstitial atom in atomic cryocrystals is the split $\langle 100 \rangle$ ''dumb-bell'' form. Taking this into account, the model of conversion from M-STE to stable lattice defects was proposed.[4] It was suggested that the defects are created and stabilized within the lifetime of self-trapped excitons. The process is supposed to occur by a displacement of the self-trapped exciton from the centrosymmetric position in the $\langle 110 \rangle$ direction followed by a reorientation to $\langle 100 \rangle$ direction to stabilize the defect. The redistribution of the component intensities associated with the self-trapped excitons in on-center and off-center positions seems to be in line with the assumption. Note that in the starting point of the exciton self-trapping the M-STE center is a system with a strong local vibration. In this case the energy release can proceed in a jumplike process.[24] If this energy release exceeds the energy needed for a local rearrangement of the lattice distorted by an electronic excitation, one can expect generation of defects. However, the further elucidation of the microscopic model requires to theoretical studies of the M-STE conversion to stable point defects.

The authors acknowledge fruitful discussions with Professors I. Ya. Fugol' and G. Zimmerer. We thank Professor K. S. Song for his interest in this work and making his results available prior to publication.

Financial support by the BMFT (Grant 05650 GUB) and PECO-Project is gratefully acknowledged.

[1] I. Ya. Fugol', Adv. Phys. **37**, 1 (1988).
[2] K. S. Song and R. T. Williams, *Self-Trapped Excitons*, 2nd ed. (Springer-Verlag, 1996).
[3] G. Zimmerer, Nucl. Instrum. Methods Phys. Res. B **91**, 601 (1994).
[4] E. V. Savchenko, A. N. Ogurtsov, O. N. Grigorashchenko, and S. A. Gubin, Chem. Phys. **189**, 415 (1994).
[5] N. Itoh and K. Tanimura, J. Phys. Chem. Solids **51**, 717 (1990).
[6] M. A. Elango, *Elementary Inelastic Radiation-induced Processes.* American Institute of Physics, N.Y. (1991).
[7] Ch. B. Lushchik and A. Ch. Lushchik, *Decay of Electronic Excitation with Defect Formation on Solids* (Nauka, Moscow, 1989).
[8] N. Schwentner, E.-E. Koch, and J. Jortner, *Electronic Excitation in Condensed Rare Gases*, Springer Tracts Mod. Phys. **60** (1986).
[9] T. Suemoto and H. Kanzaki, J. Phys. Soc. Jpn. **49**, 1039 (1980).
[10] F. V. Kusmartsev and E. I. Rashba, Czech. J. Phys. **32**, 54 (1982).
[11] E. V. Savchenko, Yu. I. Rybalko, and I. Ya. Fugol', JETP Lett. **42**, 260 (1985).
[12] E. V. Savchenko, Yu. I. Rybalko, and I. Ya. Fugol', Sov. J. Low Temp. Phys. **14**, 220 (1988).
[13] I. Ya. Fugol', A. N. Ogurtsov, O. N. Grigorashchenko, and E. V. Savchenko, Sov. J. Low Temp. Phys. **18**, 27 (1992).
[14] E. V. Savchenko, J. Electron Spectrosc. Relat. Phenom. **79**, 47 (1996).
[15] I. Ya. Fugol, E. V. Savchenko, A. N. Ogurtsov, and O. N. Grigorashchenko, Physica B **190**, 347 (1993).
[16] E. V. Savchenko, A. N. Ogurtsov, O. N. Grigorashchenko, and S. A. Gubin, Low Temp. Phys. **22**, 926 (1996).
[17] E. V. Savchenko, A. N. Ogurtsov, S. A. Gubin, and O. N. Grigorashchenko, J. Lumin. **72–74**, 711 (1997).
[18] D. Varding, J. Becker, L. Frankensten, B. Peters, M. Runne, A. Schröder, and G. Zimmerer, Low Temp. Phys. **19**, 427 (1993).
[19] J. Becker, A. N. Ogurtsov, M. Runne, E. V. Savchenko, and G. Zimmerer, in *HASYLAB Annual Report 1996.* DESY, Hamburg (1997), pp. 251.
[20] Chun-rong Fu and K. S. Song, J. Phys. Condens. Matter (accepted for publication).
[21] A. N. Ogurtsov, E. V. Savchenko, S. A. Gubin, O. N. Grigorashchenko, M. Runne, A. Karl, J. Becker, and G. Zimmerer, in *Excitonic Processes in Condensed Matter*, edited by M. Schreiber, Dresden University Press, Dresden (1996) p. 195.
[22] A. N. Ogurtsov, E. V. Savchenko, O. N. Grigorashchenko, S. A. Gubin, and I. Ya. Fugol', Low Temp. Phys. **22**, 922 (1996).
[23] R. M. J. Cotteril and M. Doyama, Phys. Lett. A **25**, 35 (1967).
[24] V. Hizhnyakov, Phys. Rev. B **53**, 13 981 (1996).

Published in English in the original Russian journal. Reproduced here with stylistic changes by the Translation Editor.

Vibronic charge-transfer excitons: possible nature of the unusual properties of virtual perovskitelike ferroelectrics

V. S. Vikhnin and S. Kapphan

A. F. Ioffe Physicotechnical Institute, Russian Academy of Sciences, 194021 St. Petersburg, Russia

Fiz. Tverd. Tela (St. Petersburg) **40**, 907–909 (May 1998)

A vibronic charge-transfer exciton, which is a pair of Jahn–Teller electron and hole polarons, is considered as a possible cause of the appearance of the Müller phase in the virtual ferroelectric $SrTiO_3$ and the ''green'' luminescence in the virtual ferroelectric $KTaO_3$. The two ''green'' luminescence bands can be associated with emission from two states of a typical intrinsic defect, viz., a vibronic charge-transfer exciton trapped by an oxygen vacancy and an isolated vibronic charge-transfer exciton. In both cases the ''green'' luminescence corresponds to the recombination of the electron and the hole in the vibronic charge-transfer exciton, which is accompanied by the emission of light. The properties of the Müller phase can be attributed to mixing of the normal state and states of the vibronic charge-transfer exciton phase when they interact with polarization in the soft $SrTiO_3$ matrix under the conditions of a pseudo-Jahn–Teller (pseudo-JT) effect on a soft TO mode of the displacement type. In this case the vibronic charge-transfer exciton phase forming the low-lying excited states has ''order–disorder'' degrees of freedom and exists at temperatures significantly below the point of the order–disorder ferroelectric transition in $SrTiO_3$ at $T=T_Q\approx 37$ K. The corresponding lowering of the symmetry of the vibronic charge-transfer exciton phase to polar symmetry leads to the possibility of a long-period incommensurate phase in such excited states, which arises as a result of the appearance of a Lifshitz invariant. The valence-band state making the largest contribution of the pseudo-JT effect corresponds to a wave vector equal to the critical wave vector of the incommensurate vibronic charge-transfer exciton phase. When the temperature is lowered, the pseudo-JT distortion increases down to $\sim T_Q$ and subsequently saturates in accordance with the saturation of the dielectric constant. The basic assumption in the model is that the temperature $T=T_Q$ corresponds to the narrow temperature range for the transition from an intermediate to a strong pseudo-JT effect under the conditions for the realization of polarization tunneling states. The appearance of a significant admixture of states of the modulated ferroelectric vibronic charge-transfer exciton phase to the ground state under the conditions for the realization of polarization tunneling states at low temperatures provides an explanation for the principal properties of the Müller phase.
 [S1063-7834(98)04305-6]

1. Ferroelectric oxides, particularly oxygen-octahedral perovskites, are characterized by considerable charge transfer.[1] As a result, similar systems, including the virtual ferroelectrics $KTaO_3$ (KTO) and $SrTiO_3$ (STO), occupy an intermediate position between ionic and covalent systems. This circumstance, as well as the comparatively great strength of the electron–lattice interaction in d states (particularly for Ti^{3+}, Ta^{4+}, and Nb^{4+} ions), as well as in $2p$ states (for O^- ions), lead to the possibility of the existence of a charge-transfer exciton, whose final state (such as, for example, the Ti^{3+}–O^- state in STO, the Ta^{4+}–O^- state in KTO, and the Nb^{4+}–O^- state in SBN) exhibits enhanced vibronic coupling, which leads to appreciably vibronic lowering of the energy of such a vibronic charge-transfer exciton.[2–4] In addition, there is a polaron electron–hole pair with minimal separation in the lattice, which exists under the conditions of a pairwise pseudo-Jahn–Teller (pseudo-JT) effect on the same lattice distortions. As a result, an electron–hole negative-U effect and additional vibronic lowering of the energy, which is comparable in order of magnitude to the Coulomb attraction, appear in the vibronic charge-transfer exciton. Thus, a vibronic charge-transfer exciton is an electron–hole bipolaron.

This paper presents an analysis of two types of effects in perovskitelike virtual ferroelectrics, whose explanation has run into formidable difficulties until recent times. They are the ''green'' luminescence[5–7] in KTO and the set of low-temperature anomalies[8,9] in STO, which are related to the Müller phase. It is shown that vibronic charge-transfer excitons can play a key role in the formation of these effects.

2. The mechanism of the formation of a vibronic charge-transfer exciton is based on the simultaneous effects of the Coulomb attraction between the electron and the hole and their pairwise vibronic coupling. Achievement of the minimum possible distance between a localized electron and a localized hole in the lattice of oxygen-octahedral perovskite

leads to considerable Coulomb energy lowering. This latter can be estimated on the basis of the results in Ref. 10 for electron–hole Coulomb interactions over short distances and turns out to be $E_c \approx -(0.7-0.9)$ eV for $\varepsilon \gg \varepsilon_\infty$ in the virtual ferroelectrics STO and KTO.

The vibronic contribution to the energy lowering of a vibronic charge-transfer exciton is no less important here. It should be noted at once that the polaron effect on the closely arranged electron and hole considered here, which arises as a result of the interaction of their charges with LO phonons, is weak because of the compensation of the electron and hole contributions. However, in the interaction between a vibronic charge-transfer exciton and the lattice, the dipole–phonon interaction of the equilibrium dipole moments of the ions, on which the electron and hole are localized, with both *LO* and soft *TO* phonons is very significant. This interaction takes place owing to a local-field effect. Another effective interaction observed upon the formation of the electron–hole bipolaron is the modulation of the Coulomb interaction and the charge-transfer effect in the vibronic charge-transfer exciton by the tetragonal strain Q_θ along the charge-transfer axis. The pairwise pseudo-JT effect on an electron and a hole interacting with shear strains plays a very important role here. Finally, the interaction with all the modes considered (both the polar modes and the tetragonal and shear modes) can induce charge transfer in a vibronic charge-transfer exciton and thereby also lower its energy. The corresponding vibronic lowering of the energy of a vibronic charge-transfer exciton can be estimated as $E_V \approx -0.3$ to -0.5 eV with a system of parameters which brings the vibronic charge-transfer exciton close to the situation of a strong pairwise pseudo-JT effect. As a result, the depth of the ground state of the vibronic charge-transfer exciton in the band gap relative to the conduction-band edge is $\Delta \approx 1-1.4$ eV, and the depth relative to the valence-band edge in STO is $\sim 1.9-2.3$ eV, which gives an estimate of the excitation energy of an isolated vibronic charge-transfer exciton. A similar estimate of the excitation energy of an isolated vibronic charge-transfer exciton in KTO gives $\sim 2.2-2.6$ eV. However, when a cluster of vibronic charge-transfer excitons forms, the depth of their energy level increases rapidly with the number of vibronic charge-transfer excitons (N) in the cluster[3,4] due to the exciton–exciton interaction. More specifically, when the radius of the cluster is smaller than the correlation radius in the vibronic charge-transfer exciton phase,[11] the depth of the energy level of such a cluster increases proportionally to N^2. As a result, the position of the energy level of a vibronic charge-transfer exciton cluster can approach the position of the valence-band edge,[4,11] but remains within the band gap. Saturation of this effect appears in a vibronic charge-transfer exciton phase where the vibronic charge-transfer exciton states are at a minimum energy distance from the top of the valence band.

3. The ''green'' luminescence spectrum in nominally pure KTO consists of two lines (with energies $\sim 2.2-2.3$ eV and ~ 2.6 eV), whose intensity ratio depends on the temperature.[5,6] It was shown in Refs. 5 and 6 that the centers responsible for the ''green'' luminescence are intrinsic defects. In addition, they are effective recombination centers for both electrons and holes. Finally, it was discovered in Ref. 7 (see Fig. 1) that the intensity of the ''green'' luminescence increases significantly when the sample is reduced and that it decreases significantly when it is oxidized. The principal properties of the ''green'' luminescence can be understood on the basis of the following model of the active centers. These centers can be typical intrinsic defects, viz., a single vibronic charge-transfer exciton trapped by an oxygen vacancy (a) and an isolated self-trapped vibronic charge-transfer exciton (b). While the luminescence line with the smaller energy can be associated with center (a), the line with the larger photon energy can be associated with center (b). The ''green'' luminescence is a result of the recombination of electron and hole polarons in the centers based on vibronic charge-transfer excitons under discussion. These centers are strong recombination centers for both electrons and holes, and they are intrinsic defects in KTO and have luminescent transition energies which correspond to the values observed within the estimates discussed above. In addition, the concentration of center (a), which plays an important role in shaping the overall contour of the luminescence line, decreases upon oxidation of the sample and increases upon its reduction, in agreement with the experimental data from investigating the dependence of the ''green'' luminescence on the treatment of the sample.[7] To conclude this section we note that an oxygen vacancy in an oxygen-octahedral perovskite can bind not only an intrinsic dipolar defect, i.e., a vibronic charge-transfer exciton, but also an extrinsic dipolar defect, particularly an off-center Li^+ impurity ion in KTO. This results in the appearance of dipolar Li^+–V^{++} complexes, which can serve as the nuclei of polar microdomains. The concentration of the corresponding polar microdomains will increase when the sample is reduced, in agreement with experiment.[12]

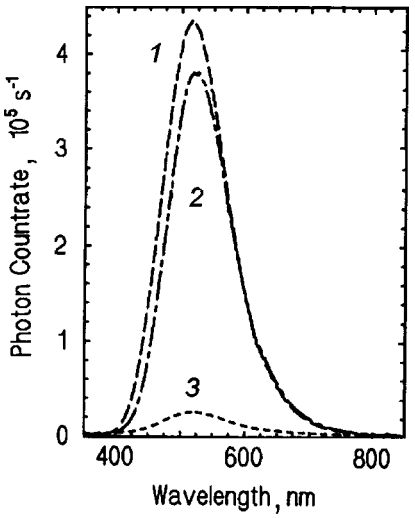

FIG. 1. ''Green'' luminescence spectrum in a nominally pure KTO crystal ($T=80$ K). Influence of reduction (in a vacuum) and oxidation of the sample: *1*—reduction for 2 h, *2*—reduction for 0.5 h, *3*—oxidized sample.

4. As a result of the interaction between individual vibronic charge-transfer excitons in the system under consideration, clusters of vibronic charge-transfer excitons appear along with isolated vibronic charge-transfer excitons,[3,4] and

even a vibronic charge-transfer exciton phase can form. In the latter each unit cell contains a vibronic charge-transfer exciton. Two important factors, which lower the energy of clusters of vibronic charge-transfer excitons and a vibronic charge-transfer exciton phase, are the cooperative negative-U effect and the cooperative lowering of the energy of a covalent nature as a consequence of the covalent $O^- - O^-$ interaction. As a result, the energy levels of a vibronic charge-transfer exciton phase are close to the valence-band edge, although they are within the band gap. This situation can cause strong mixing of the normal state (in the valence band) and states of the vibronic charge-transfer exciton phase. In addition, the vibronic charge-transfer exciton phase has order–disorder degrees of freedom, which are associated both with the orientations of the dipole moments of the electron-hole pairs in the vibronic charge-transfer excitons and with the pseudo-JT degrees of freedom of the electron and the hole. The exciton–exciton interaction in the phase under consideration, which is associated with correlations between degrees of freedom of the former type, is dominant. An estimate shows that the mean fields which can be responsible for the order-disorder ordering in a vibronic charge-transfer exciton phase correspond to energy changes which significantly surpass kT_Q, where T_Q is the characteristic temperature for the transition to the Müller phase. This means that ferroelectric ordering of the dipole moments of the vibronic charge-transfer excitons takes place in the vibronic charge-transfer exciton phase in the temperature range of the Müller phase. This situation has two important consequences: effective dipolar mixing of the normal paraelectric state and the ferroelectric state of the vibronic charge-transfer exciton phase under the effect of the polarization of a soft TO phonon of the ground-state displacement type, as well as the appearance of incommensurate modulation in the vibronic charge-transfer exciton phase due to the appearance of a Lifshitz invariant induced by the field of the ferroelectric order parameter P_z in the vibronic charge-transfer exciton phase, $\sigma(T)(P_j^* \partial P_j/\partial z - P_j \partial P_j^*/\partial z)$. The incommensurate modulation period q_i is specified by the relation $q_i \sim \sigma(T)$. It is important to note that, owing to the soft TO polarization $(q \approx 0)$, the vibronic mixing couples the vibronic states of the incommensurate vibronic charge-transfer exciton phase with electron states in the valence band corresponding to $q \approx q_i$. Thus, we arrive at a pseudo-JT effect on the two states cited and on a soft polarization mode of the displacement type. As a result, the ground state is also incommensurately modulated. In STO this pseudo-JT effect reaches its maximum strength at $T \approx 37$ K, and its parameters remain unchanged at $T \leqslant 37$ K as a consequence of saturation of the frequency of the soft polarization mode. The greatest mixing of the states also occurs in that case. We assume that a transition from an intermediate pseudo-JT effect (in the absence of localization in individual configurations) to a strong pseudo-JT effect with self-trapping in individual configurations and the realization of tunneling states which persist at $T < T_Q$ (although they correspond to tunneling splitting which decreases as T decreases) takes place in STO at $T \approx 37$ K, where saturation of the dielectric constant begins.

The transition to the state just mentioned, which is initiated by the pseudo-JT effect involving the vibronic charge-transfer exciton phase, can account for the set of effects observed, the first being the fact that the coexistence of displacement and order-disorder dynamics leading in particular, to the appearance of a central peak as a consequence of the interaction between the corresponding degrees of freedom, is manifested both outside the Müller phase and even more strongly in the Müller phase. The second is that the Müller phase is characterized by a significantly nonlinear dielectric susceptibility.[13] It is attributed to the interaction of the incommensurate wave of the order parameter with randomly arranged pinning defects, which produces a highly frustrated state.[4] The third is that an additional quasiacoustic A mode is observed in STO at $T < 37$ K,[9] which can be associated with an acoustic TA mode in the incommensurate structure of the vibronic charge-transfer exciton phase.[4] The fourth is that the appearance of polar microdomains, violation of the Lyddane-Sachs-Teller relation, and the strong mixing of modes of different symmetry in the region of the Müller phase can be associated with the appearance here of the highly frustrated spin-glass state just mentioned. Finally, the postulated transition to tunneling states at $T < T_Q$ within the pseudo-JT effect under discussion leads to an increase in the fluctuations near T_Q, which weaken at $T < T_Q$, accounting for the decrease in the crystal field at $T \approx T_Q$ and the results of the pioneering EPR experiment in Refs. 8.

This work was supported by grants from the Russian Fund for Fundamental Research (RFFI Grant 96-02-17972-a and NNIO-RFFI Grant 93-02-00138) and a NATO Scientific Cooperation Grant (HTECH. LG 960540).

[1] W. A. Harrison, *Electronic Structure and the Properties of Solids: The Physics of the Chemical Bond*, W. H. Freeman, San Francisco (1979); Mir, Moscow (1983).
[2] V. S. Vikhnin, Proc. Est. Acad. Sci., Phys. Math. **44** (2/3), 164 (1995).
[3] V. S. Vikhnin, Z. Phys. Chem. (Munich) **201**, 201 (1997).
[4] V. S. Vikhnin, Ferroelectrics (1997) (in press).
[5] E. Yamaichi, K. Watanabe, K. Imamiya, and K. Ohi, J. Phys. Soc. Jpn. **56** (5), 1890 (1987).
[6] E. Yamaichi, K. Watanabe, and K. Ohi, J. Phys. Soc. Jpn. **57**, 2201 (1987).
[7] S. Kapphan and S. Magnien, in *Proceedings of the DFG-Meeting*, Münster, Germany (March 1997).
[8] K.-A. Müller, W. Berlinger, and E. Tosatti, Z. Phys. B: Condens. Matter **84**, 277 (1991).
[9] E. Courtens, G. Coddens, B. Hennion, B. Hehlen, J. Pelous, and R. Vacher, Phys. Scr. T **49**, 430 (1993).
[10] H. Haken, Z. Phys. **146**, 527 (1956); Nuovo Cimento **3**, 1230 (1956).
[11] V. S. Vikhnin, S. Kapphan, and J. Seglins, in *The 9th International Meeting on Ferroelectricity, Seoul, Korea (August, 24–29, 1997)*, Abstr. p. 257. Rep. P-08-TH-287.
[12] S. Magnien, C. auf der Horst, and S. Kapphan, *ibid*., Abstr. p. 166. Rep. O-07-TU-A10.
[13] E. I. Golovenchits, V. A. Sanina, and A. V. Babinskiĭ, JETP Lett. **63**, 674 (1996).

Translated by P. Shelnitz

Structure of the self-trapped exciton luminescence in α-Al_2O_3

B. R. Namozov, M. É. Fominich, and R. I. Zakharchenya

A. F. Ioffe Physicotechnical Institute, Russian Academy of Sciences, 194021 St. Petersburg, Russia

V. V. Myurk

Institute of Physics, EE2400 Tartu, Estonia

Fiz. Tverd. Tela (St. Petersburg) **40**, 910–912 (May 1998)

[S1063-7834(98)04405-0]

Crystals of aluminum oxide, αAl_2O_3 (leucosapphire or sapphire), are characterized by bright self-activated luminescence with an intensity maximum at 7.5 eV (165 nm). It was speculated in Ref. 1 that the luminescence band at 7.5 eV is a result of electron-hole recombination. In Ref. 2 and 3 concerning the luminescence band at 7.5 eV we advanced hypotheses of the luminescence of self-trapped excitons with a single-center hole structure O^-

Investigations of the long-wavelength fundamental absorption edge (see Fig. 1, curves *5–7*) showed that it obeys the familiar Urbach rule with the characteristic parameters $E_0=9.0$ eV, $\alpha_0=10^5$ cm^{-1}, and $\sigma_0=0.64$ (Ref. 3). Figure 1 (curve *8*) presents the luminescence spectrum of sapphire crystals, from which it is seen that the short-wavelength slope of the luminescence band at 7.5 eV intersects the Urbach exciton absorption tail. The short-wavelength portion of this band has a feature in the form of a ''shoulder'' at 9.0 eV, which spectrally coincides with E_0. The band with a maximum at 7.5 eV has a full-width at half-maximum of 0.8 eV, and its intensity at $T\geqslant 45$ K exhibits quenching with an activation energy $E_a\approx 0.025$ eV. The quantum yield of luminescence in the band at 7.5 eV is at least 20% under excitation by 9.0 eV photons.

Kinetic measurements of the luminescence in the band at 7.5 eV (see the inset in Fig. 1) demonstrated the presence of three decay components ($\tau=22$ ns, 230 ns, and $\geqslant 2000$ ns) of the luminescence with insignificant ($\leqslant 100$ meV) spectral differences.[4] Their temperature dependences gave similar values for the activation energies: ~ 25, ~ 20, and ~ 18 meV, respectively. More than half of the integrated intensity is found in the fast (~ 22 ns) luminescence component.

In the temperature range from 4 K to 110 K, the degree of linear polarization of this luminescence varies weakly from 35% to 30% (when it is observed perpendicularly to the optical axis of the crystal) and begins to decrease sharply at crystal temperatures $\geqslant 110$ K. We also note that the intensity of the x-ray luminescence at 7.5 eV in a direction parallel to the C_3 axis is several times larger than the intensity in the direction perpendicular to the C_3 axis.

The luminescence in the band at 7.5 eV is effectively excited at the fundamental absorption edge, i.e., at 8.9–9.25 eV (see Fig. 1, curve *4*). It is seen from the figure that the long-wavelength edge of the excitation spectrum of the band at 7.5 eV coincides with the Urbach tail of the long-wavelength fundamental absorption edge. For comparison, the figure also presents a portion of the exciton absorption spectrum (R) and the luminescence excitation spectrum of Ce^{3+} at 5 K. At room temperature the luminescence excitation spectrum of Ce^{3+} is similar to the excitation spectrum of the band at 7.5 eV. The short-wavelength descending portion of the excitation spectrum of the band at 7.5 eV coincides with the ascending portion of the thermally stimulated luminescence (TSL) spectrum (of electron–hole pairs) at 5 K, as well as the luminescence excitation spectrum of cerium centers (Fig. 1, curve *2*).

Crystals of αAl_2O_3, which have a complex structure (D_{3d}^6-R3c) with 10 atoms in the unit cell, are classified as ionic crystals according to the chemical-bonding type, although the covalency amounts to about 20%. We note that an important feature of this structure is the lower symmetry of the anion (oxygen) sites (C_2) in comparison to the cation (Al^{3+}) sites (C_3). According to the calculations in Ref. 5, the valence band is formed from $2p$ oxygen states, and complete splitting of the p states occurs in a crystal field with a symmetry as low as C_2. When the coordination number

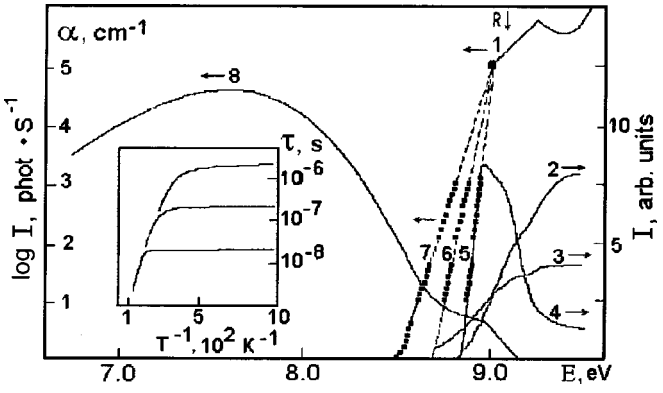

FIG. 1. Optical spectra of αAl_2O_3 at the fundamental absorption edge: *1*—absorption spectrum, *2*—luminescence excitation spectrum of cerium centers at 5 K, *3*—TSL spectrum at 5 K, *4*—luminescence excitation spectrum of the band at 7.5 eV, *5–7*—spectra of the Urbach fundamental absorption edge at 80, 200, and 300 K, respectively, *8*—luminescence spectrum. The temperature dependence of the three components of the decay kinetics of the luminescence band at 7.5 eV is presented in the inset.

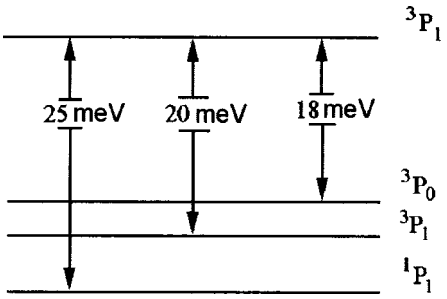

FIG. 2. Energy structure of a self-trapped exciton.

equals 4, one of the oxygen p orbitals is of the nonbonding type, while the other is at a 45° angle to the optical axis, i.e., the C_3 axis.

Comparing the photoconductivity spectra with the reflectance spectrum, Il'mas and Kuznetsov[6] arrived at the conclusion that the reflectance peak at 9.2 eV in sapphire has an excitonic nature. The parameter σ_0 is known to characterize the strength of the electron-phonon interaction.[7] The long-wavelength fundamental absorption edge of sapphire is formed by an exciton state with a strong electron–phonon interaction, which leads to self-trapping, as is evidenced by the small value of $\sigma_0 = 0.64$.

The spectral kinetic data revealed the characteristic features of the broad-band luminescence of sapphire crystals with a maximum at 7.5 eV: 1) a high quantum yield (20%), 2) a large Stokes shift, 3) the absence of selective bands in the transparency region of the crystal, 4) the presence of a component with an exponential decay law in the kinetics, 5) a genetic relationship to the exciton absorption region, 6) the blocking of energy transfer to impurity centers. As we know, the luminescence bands of self-trapped excitons in alkali metal halide crystals have such a set of properties.[8] On the basis of these characteristics we can state that the luminescence band at 7.5 eV is a manifestation of self-trapped excitons in α-Al_2O_3. The feature that we observed at 9.0 eV coincides with the free-exciton state. The absence of a dependence of its intensity on the temperature and the fairly short lifetime (<0.3 nS) point out the ''hot'' character of the luminescence. Therefore, the self-trapping of excitons in sapphire is barrierless.

Runciman[1] postulated that two σ components of the luminescence are oriented parallel to the optic axis and that other σ components and the π component are oriented perpendicularly to the optical axis. Our direct measurements confirmed Runciman's hypothesis that the linear polarization (the π component) of the luminescence is directed perpendicularly to the optic axes. The values for the degree of linear polarization of the luminescence that we determined [$\sim 30\%$($T = 5$ K) and 35%($T = 80$ K)] in the direction perpendicular to the C_3 axis in the crystal indicate that there is also luminescence having a σ character.

The temperature dependences of the integrated intensity and the polarization of the self-trapped exciton luminescence point to the mechanisms which influence the relaxation of electron excitations in the crystal. The temperature quenching of the luminescence intensity at $T \geqslant 45$ K is most probably caused by branching of the electron excitations.[9] The degree of linear polarization of the self-trapped exciton luminescence varies weakly in the temperature range from 5 to 110 K in analogy to the temperature dependence of the fast (22 ns) component of the luminescence. It therefore follows that the component of the self-trapped exciton luminescence with the shortest decay time has a π-type polarization perpendicular to the C_3 axis and, of course, a σ-type parallel to the C_3 axis.

The findings just described confirm the validity of the hypothesis that self-trapped excitons with an O^- hole component form in sapphire crystals. The O^- ion has $^2P_{1/2}$ and $^2P_{3/2}$ terms, which split in the crystal field. An exciton formed from such a hole and an s electron has states with $^3P_2$, $^3P_1$, $^3P_0$, and $^1P_1$ terms. We assume that these terms split completely during the relaxation of a self-trapped exciton. The luminescent transitions are forbidden ($^3P_1$), partially allowed ($^3P_2$,$^3P_0$), or allowed ($^1P_1$), depending on the state of the self-trapped exciton.

An Al_4O quasimolecule, in which each Al^{3+} ion is bonded to the O^{2-} ion, can be identified in the unit cell of sapphire. When an exciton is created in an Al_4O quasimolecule, an electron passes from the O^{2-} ion to one of the four aluminum ions, and it can rotate about the oxygen ion. During relaxation, the hole is displaced from its equilibrium position toward one of the Al–O bonds. An electron, in turn, is also localized near the hole displaced from its equilibrium position. A comparison of the polarization and kinetic parameters of the luminescence allows us to state that the self-trapped exciton annihilates primarily from the $^1P_1$ state in the temperature range $6\text{ K} \leqslant T \leqslant 110$ K. At temperatures below 50 K the $^3P_2$ and $^3P_0$ states are also manifested in the self-trapped exciton luminescence. The forbidden transition from the $^3P_1$ state corresponds to the case in which the hole is localized in a nonbonding orbital of the oxygen ion (Fig. 2).

We thank B. P. Zakharchenya for taking a steady interest in this work.

This work was supported by grants from the Russian Fund for Fundamental Research (No. 95-02-047760a) and the MNTP (No. 5-15).

[1] W. A. Runciman, Solid State Commun. **6**, 537 (1968).
[2] A. I. Kuznetsov, B. R. Namozov, and V. V. Myurk, Fiz. Tverd. Tela (Leningrad) **27**, 3030 (1985) [Sov. Phys. Solid State **27**, 1819 (1985)].
[3] A. I. Kuznetsov, B. R. Namozov, and V. V. Myurk, Izv. Akad. Nauk ESSR, Fiz. Mat. **36**, 193 (1987).
[4] V. V. Myurk and K. M. Ismailov, Fiz. Tverd. Tela (St. Petersburg) **35**, 498 (1993) [Phys. Solid State **35**, 259 (1993)].
[5] I. P. Batra, J. Phys. C.: Solid State Phys. **15**, 5399 (1982).
[6] É. R. Il'mas and A. I. Kuznetsov, Fiz. Tverd. Tela (Leningrad) **14**, 1464 (1972) [Sov. Phys. Solid State **14**, 1255 (1972)].
[7] M. V. Kurik, Phys. Status Solidi **8**, 9 (1971).
[8] Ch. B. Lushchik, ''Free and self-trapped excitons in alkali halides: spectra and dynamics,'' in *Excitons*, E. I. Rashba and M. D. Sturge (Eds.), North-Holland, Amsterdam (1982), p. 505.
[9] V. Murk, B. Namozov, and N. Yaroshevich, Radiat. Meas. **24**, 371 (1995).

Translated by P. Shelnitz

Vacuum-ultraviolet plasma Frenkel excitons: elementary excitations of polymerized fullerene

V. V. Rotkin and R. A. Suris

A. F. Ioffe Physicotechnical Institute, Russian Academy of Sciences, 194021 St. Petersburg, Russia

Fiz. Tverd. Tela (St. Petersburg) **40**, 913–915 (May 1998)

The high-frequency excitations of the molecular insulator C_{60} are investigated theoretically. The model of a quantum well rolled into a sphere is used to calculate the dipole (multipole in the general case) modes of an individual C_{60} cluster. If the spectrum and oscillator strengths of the collective modes of an individual cluster are known, the microscopic continuum approach can be used to calculate the spectrum of delocalized excitations in a cluster crystal. Then the ordinary dielectric constant formalism permits calculation of the optical characteristics of the material in the vacuum ultraviolet region studied. © *1998 American Institute of Physics.* [S1063-7834(98)04505-5]

The molecules in a C_{60} crystal are joined by weak van der Waals forces. As a result, solid-state fullerene is readily soluble in many typical organic solvents. However, it was shown in Ref. 1 that a fullerene surface undergoes a phototransformation during prolonged illumination by incoherent UV radiation or under the action of a high-power low-frequency coherent source. After such treatment, a surface region with a thickness amounting to several C_{60} monolayers becomes practically insoluble. Such a phototransformation has been termed polymerization, in analogy to the process for unsaturated hydrocarbons, whose electronic structure exhibits some similarity to that of fullerene. Apart from photopolymerization, the transformation of fullerene into an insoluble phase at high pressures and temperatures has been reported.[2] X-ray structural investigations of the polymer phase have shown that the formation of linear or two-dimensional structures (apparently chains) of C_{60} clusters bonded to one another and of a united 2D network is typical. The present work examines the elementary excitations in one- and two-dimensional systems of fullerene clusters.

1. HIGH-FREQUENCY DIPOLE MODES OF A C_{60} CLUSTER: SURFACE-PLASMON APPROXIMATION

The foundation for the theory of elementary excitations in molecular insulators was laid in Ref. 3. Application of the ideas advanced by Frenkel to the solution of concrete problems involving calculations of the optical characteristics of insulating crystals has provided explanations for numerous experimental findings based on the model of an exciton of small radius, or a Frenkel exciton. In the case of crystalline C_{60} we are clearly dealing with a typical molecular insulator, whose dipole excitations are localized and migrate through the crystal as a result of dipole-dipole interactions between neighboring clusters.

Despite the fact that C_{60} is similar as a whole to the previously known molecular insulators, the theoretical description of the cluster and the cluster medium is far more difficult. Nevertheless, the high-frequency excitations of the polyatomic electronic structure of fullerene is practically insensitive to the details of its spectrum.

Since the π-electronic system of fullerene is readily polarizable and the total number of valence electrons is high, it turns out that both the analytical quantum-mechanical model of a quantum well rolled into a sphere[4,5] and the simple phenomenological hydrodynamic model of a charged liquid on the surface of a sphere[6,7] can be applied successfully. The high-frequency multipole polarizability of a cluster can be determined from the continuity equation and the equation of motion for the oscillations of a charged liquid on the spherical surface of a cluster:

$$\begin{cases} \dfrac{\partial j}{\partial t} = -\dfrac{ne^2}{m}\nabla\varphi \\ \dfrac{\partial \sigma}{\partial t} + \nabla j = 0 \end{cases}, \tag{1}$$

where $n = 240/4\pi R^2$ is the density of valence electrons on the surface of a spherical cluster of radius R, m and e are the mass and charge of an electron, φ is the effective electric potential, which, by necessity, includes the potential of the charge induced on the cluster itself, σ is the density fluctuation, j is the current density associated with it, and ∇ is the gradient over the surface of the sphere. The solutions of these equations are naturally sought using an expansion in the spherical harmonics $P_L(r)Y_{L,M}(\Omega)$, i.e., a multipole expansion.[8] Then the discontinuity of the field on the cluster surface is related to the amplitude of the multipole fluctuations $\sigma_{L,M}$ according to the Ostrogradsky–Gauss theorem: $(2L+1)\varphi_{L,M}/R = 2\pi\sigma_{L,M}$. Solving these equations together, we obtain the multipole dynamic response function of an individual cluster in the form

$$\alpha_L(\omega) \equiv \frac{-\sigma_{L,M}}{\varphi^{xt}_{L,M}} = \frac{R^3}{(1-\omega^2/\omega_L^2)},$$

where $\varphi^{xt}_{L,M}$ is the spherical harmonic of the external electric potential. When $L=1$, we are dealing with a dipole-moment

excitation in the cluster. The lack of a dependence of α on M is a consequence of the spherical symmetry of the model, and, although C_{60} actually has icosahedral, rather than spherical, symmetry, the dipole polarizability of the cluster remains isotropic. The polarizability has a resonance at the frequency of the collective mode excited in the C_{60} cluster by the external multipole potential:

$$\omega_L=\omega_p\sqrt{\frac{L(L+1)}{2L+1}}=\sqrt{\frac{4\pi ne^2}{m^*R}}\ \sqrt{\frac{L(L+1)}{2L+1}}. \qquad (2)$$

Here ω_p is the characteristic plasma frequency of fullerene. It is the excitation frequency of a surface plasmon in a metallic sphere of radius R with a surface charge density corresponding to the valence electron density of fullerene. We see that collective modes[4,5,7] in the vacuum-ultraviolet region, for example, the dipole mode ($\omega_1\simeq 25$ eV), are excited in C_{60} in a range of frequencies much greater than the frequencies of all the ''single-electron'' modes.

2. EXCITATIONS OF A ONE-DIMENSIONAL CRYSTAL: THE COULOMB PROBLEM

In this section we examine the spectrum of dipole modes of a chain of fullerene clusters neglecting retardation. The Coulomb interaction of the multipole plasma modes of two clusters was previously studied in detail in Refs. 9 and 10. In particular, it was shown there, for a triply degenerate dipole mode of an individual C_{60} cluster, that it is sufficient to take into account the interaction with the dipole mode of the neighboring cluster. Such an axisymmetric perturbation leads to splitting of the state with $L=1$ into longitudinally and transversely polarized modes. In a chain of fullerene molecules the solutions must be sought in the form of plane waves of the same polarizations. Therefore, an anisotropic (axisymmetric) system of C_{60} clusters has transverse modes, i.e., one-dimensional Frenkel excitons, which are formed on the basis of elementary plasma excitations of an individual fullerene cluster. We shall call such excitations ''plasma Frenkel excitons.''

The Fourier transformation

$$\sigma_M(k)=\sum_{n=-N}^{N} e^{-iknH}\sigma_M(x-nH),$$

where $n=-N,\ldots,0,\ldots N$ is the number of the cluster in a chain of length $2N$, k is the wave number of the excitation, and H is the distance between clusters, diagonalizes the problem, and the spectrum takes the form

$$\omega(k)\simeq\omega_1\sqrt{1+\frac{1+3(-1)^M}{2}\left(\frac{R}{H}\right)^3 2\sum_{n=1}^{N}\frac{\cos(kHn)}{n^3}}. \qquad (3)$$

The spectrum is doubly degenerate for $M=\pm 1$. There is natural splitting between the $M=\pm 1$ and $M=0$ states, which describe transversely and longitudinally polarized excitations, respectively. For small $kH\ll 1$ the dispersion of the modes is linear with respect to the wave vector:

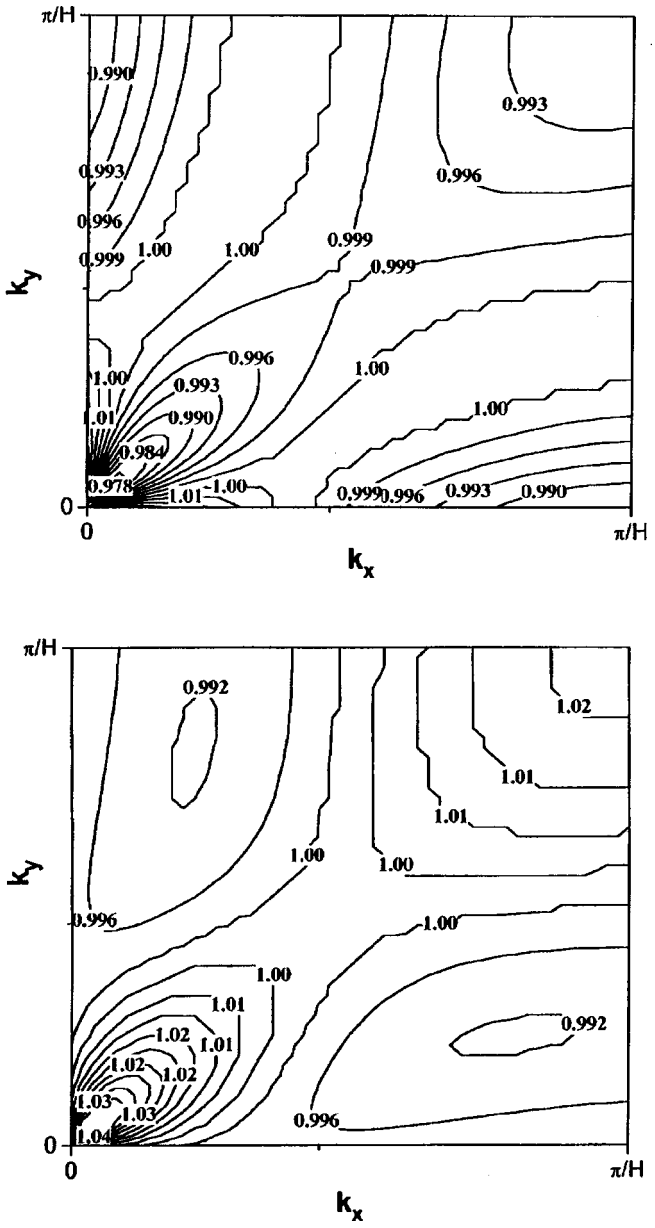

FIG. 1. Spectra of longitudinal ($\parallel$, upper spectrum) and transverse ($\perp$, lower spectrum) two-dimensional plasma Frenkel excitons obtained numerically with consideration of a concrete square lattice of polymerized C_{60}. A quarter of the Brillouin zone is shown: dependence of the normalized frequency $\omega(f)/\omega_1$ of the mode on the wave vectors k_xH and k_yH.

$$\omega(k)\simeq\omega_1\left(1+\frac{1+3(-1)^M}{4}\left(\frac{R}{H}\right)^3\times\left\{2\zeta(3)-(kH)^2\left[\ln\frac{1}{kH}+\frac{3}{2}\right]\right\}\right),$$

where $\zeta(x)$ is a zeta function,[11] which defines the lattice sum for the ground, totally symmetric state of the plasma Frenkel exciton with $k=0$ [$\zeta(3)\simeq 1.202$, compare the results in Ref. 12]. It follows from (3) that the longitudinal–transverse splitting is specified by the ratio $(R/H)^3$ and amounts to 3.9 eV for $k=0$ and -3.1 eV for $k=\pi/H$ when $H\simeq 10$ Å.[1)]

3. TWO-DIMENSIONAL PLASMA FRENKEL EXCITONS

The theory of two-dimensional Frenkel excitons was described in detail in Ref. 13, where there are also references to experimental results in this area. Below we present the results of a microscopic calculation of the spectrum of Coulomb 2D-plasma Frenkel excitons in a monomolecular fullerene film, including results obtained analytically in the continuum approximation.

We choose the directions of the orthogonal polarizations of the eigenmodes of the two-dimensional problem in a natural manner: σ_z is a transverse mode polarized along a normal to the film surface, $\sigma_\perp$ is a second transverse mode (its polarization vector lies in the plane of the film and is perpendicular to the excitation wave vector k), and $\sigma_\parallel$ is a longitudinal mode with polarization along the excitation wave vector. In the continuum approximation, the two-dimensional lattice sum can be replaced by an integral, which is taken in an expansion to the second order in the small parameter of the problem $(R/H)^3 \ll 1/3$ in the approximation of small wave numbers. Neglecting retardation, the frequencies of the Coulomb 2D plasma Frenkel excitons have the form

$$\begin{cases} \omega_\parallel = \omega_1 \sqrt{1+\frac{3}{2}\left(\frac{R}{H}\right)^3\left(\frac{3}{2}-2kH+\frac{5(kH)^2}{16}+o((kH)^4)\right)}, \\ \omega_z = \omega_1 \sqrt{1-\frac{3}{2}\left(\frac{R}{H}\right)^3\left(1-kH+\frac{(kH)^2}{4}+o((kH)^4)\right)}, \\ \omega_\perp = \omega_1 \sqrt{1-\frac{3}{2}\left(\frac{R}{H}\right)^3\left(\frac{1}{2}-kH-\frac{(kH)^2}{16}+o((kH)^4)\right)}. \end{cases} \tag{4}$$

All three branches are clearly linear with respect to the wave number at small kH.

The splitting between the longitudinal and transverse modes at the Γ point is

$$\Delta\omega_{LT} = \omega_1\left(\sqrt{1+\frac{9}{4}\left(\frac{R}{H}\right)^3}-\sqrt{1-\frac{3}{4}\left(\frac{R}{H}\right)^3}\right) \simeq \omega_1\frac{3}{2}\left(\frac{R}{H}\right)^3 \simeq 1.6 \text{ eV}. \tag{5}$$

We also present the spectra of longitudinal and transverse modes obtained by numerical summation for a square lattice of polymerized C_{60} (see Fig. 1).

Thus, the spectra of longitudinal and transverse vacuum-ultraviolet Coulomb excitations in one- and two-dimensional periodic systems of fullerene clusters, which were calculated analytically in the continuum approximation for wave numbers that are small compared with the reciprocal lattice period and numerically in the entire Brillouin zone, have been presented in this paper. The values of the translational-transverse splitting of the elementary excitations near the Γ point, as well as on the Brillouin-zone edge in the one-dimensional case, have been determined.

This work was performed as part of Project No. 94014 of the Russian Scientific-Research Program ''Fullerenes and Atomic Clusters,'' and one of us (V.V.R.) thanks INTAS for a grant arranged through the Center for Fundamental Physics in Moscow, as well as the Russian Fund for Fundamental Research for its partial support (Grant No. 96-02-17926).

[1)] The distance between nearest neighbors in crystalline C_{60}.

[1] A. M. Rao *et al.*, Science **259**, 955 (1993).
[2] V. A. Davydov *et al.*, Mol. Mater. **7**, 285 (1996).
[3] Ya. I. Frenkel, Phys. Rev. **37**, 17 (1931); Phys. Rev. **37**, 1276 (1931).
[4] V. V. Rotkin and R. A. Suris, Mol. Mater. **5**, 87 (1994).
[5] V. V. Rotkin and R. A. Suris, Fiz. Tverd. Tela (St. Petersburg) **36**, 3569 (1994) [Phys. Solid State **36**, 1899 (1994)].
[6] G. Barton and C. Eberlein, J. Chem. Phys. **95**, 1512 (1991).
[7] V. V. Rotkin and R. A. Suris, in *Proceedings of the Symposium on Recent Advances in the Chemistry and Physics of Fullerenes and Related Materials*, K. M. Kadish and R. S. Ruoff (Eds.), Electrochemical Society, Pennington, NJ (1996), pp. 940–959.
[8] L. Robin, *Fonons Spheriques de Legendre*, Gauthier-Villars, Paris (1958).
[9] V. V. Rotkin and R. A. Suris, Solid State Commun. **97(3)**, 183 (1995).
[10] V. V. Rotkin and R. A. Suris, in *Proceedings of the International Symposium ''Nanostructures: Physics and Technology-95,''* St. Petersburg, Russia (26–30 June 1995), pp. 210–213.
[11] M. Abramovitz and I. A. Stegun, *Handbook of Mathematical Functions*, Dover, New York (1964).
[12] A. V. Chaplik, JETP Lett. **31**, 252 (1980).
[13] V. M. Agranovich, *Exciton Theory*, Nauka, Moscow (1968).

Translated by P. Shelnitz

Relaxation and hot luminescence in solid Xe

V. Hizhnyakov, M. Selg, and D. Nevedrov

Institute of Theoretical Physics, Tartu University, EE2400 Tartu, Estonia;
Institute of Physics, EE2400 Tartu, Estonia

Fiz. Tverd. Tela (St. Petersburg) **40**, 916–918 (May 1998)

A theoretical description of multiphonon decay processes of highly excited localized modes is presented. Slowing of the decay rate at large vibration amplitudes and jumps in the relaxation rate at certain critical amplitudes are predicted. Highly excited vibrational states can appear in localized excitons in crystals of noble gases and can also appear in hot luminescence. The observed and calculated spectra of Xe_2^* in a Xe crystal are compared.
 [S1063-7834(98)04605-X]

Processes involving highly excited vibrational states and the mechanisms for redistributing the energy of localized excitations over a crystal lattice are of great interest in modern solid-state physics. The concentration of energy in crystals with impurities, as well as in ideal nonlinear lattices, has been studied in fairly great detail. In the classical description, such excitations are stable, since none of the harmonics of these modes are in resonance with the phonon spectrum. The problem can be solved using quantum-mechanical methods, but since the vibration amplitudes are large, quantum perturbation theory cannot be used due to the lack of a small parameter in the interatomic interaction potential.

The decay of localized excitations bound to defects, as well as of self-trapped solitons in ideal nonlinear lattices,[2] can be described using a previously developed theory.[1] It was discovered that their decay is highly nonexponential. The release of large amounts of vibrational energy into the phonon continuum is observed at certain critical vibration amplitudes. The calculations performed show that this mechanism operates in crystals having a simple cubic lattice[6] and in nonlinear monatomic chains.[3] The critical amplitudes are of the order of 0.3–0.4 Å, which can actually be observed in localized excitons in crystals of noble gases.

In describing the interaction of an excited mode with the phonon continuum, it should be taken into account that the phonon generation and annihilation operators ($\hat{a}^+$ and $\hat{a}$) are altered in the field of a local mode. The new phonon operators equal $\hat{b}=\mu_i(t)\hat{b}_i+\nu_i(t)\hat{a}_i^+$, where $|\mu_i|^2-|\nu_i|^2=1$. As a result, phonons form in the lattice. The decay rate is specified by the expression

$$\frac{dE_L}{dt}=\sum_i \hbar\,\frac{\omega_i d|\nu_i(t)|^2}{dt}, \tag{1}$$

where ω_i is the frequency of phonon i. The problem reduces to a calculation of the correlation function

$$D_i(t;\tau)=\langle 0|\hat{x}_i(t+\tau)\hat{x}_i(t)|0\rangle \simeq \frac{\hbar}{2\omega_i}[|\mu_i(t)|^2 e^{-i\omega_i\tau}+|\nu_i(t)|^2 e^{i\omega_i\tau}], \tag{2}$$

where $t\gg\tau$ (we neglect the rapidly oscillating terms $\sim\exp\pm 2i\omega_i t$).

Let us consider the interaction in the pair-potential approximation with consideration of only the central forces. The $(n+1)$th-order anharmonicity operator is written as

$$\hat{H}_{\rm anh}^{(n+1)}=\frac{2}{n}Q(t)\sum_m V_m^{(n+1)}\hat{q}_m^n, \quad n\geqslant 2, \tag{3}$$

where $Q(t)=A_t\cos\omega_l t$, A_t is the time-dependent amplitude of the mode, the $V_m^{(n+1)}$ are the parameters of the $(n+1)$th-order anharmonic interaction, the $\hat{q}_m=\Sigma_i e_{mi}\hat{x}_i$ are the operators of the coordinates of neighboring atoms, and the $\hat{x}_i$ satisfy the following equation:

$$\hat{x}_i=\hat{x}_i(0)e^{-i\omega_i t}+2A_t\sum_m e_{mi}\omega_i^{-1}V_m^{(n+1)} \times\int_0^t dt_1\,\sin\,\omega_i(t-t_1)\cos\,\omega_L t_1\hat{x}_m^n(t_1). \tag{4}$$

Substituting this equation into the correlation function, with consideration of (1) we obtain

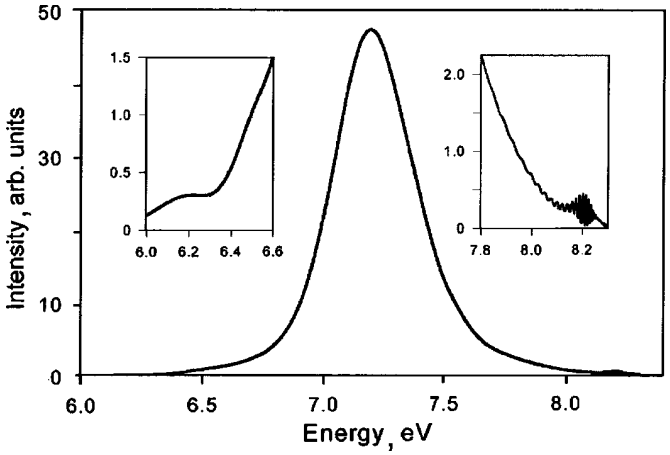

FIG. 1. Calculated hot luminescence spectrum of the Xe_2^+ quasimolecule in solid Xe. Individual portions of the spectrum on magnified scales are presented in the insets.

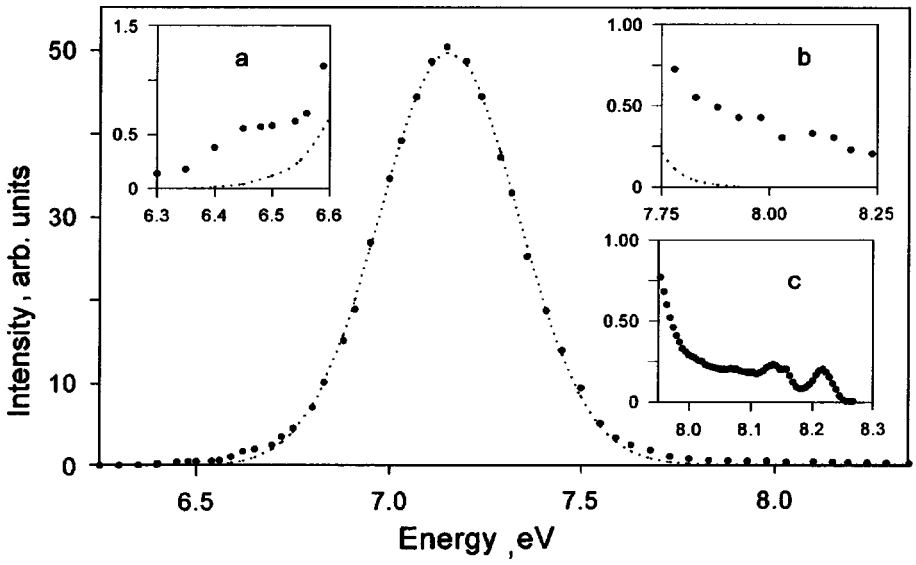

FIG. 2. Experimental luminescence spectrum of a Xe crystal excited by x radiation at $T=20$ K (Ref. 4) (denoted by points). The broken line denotes approximation by a Gaussian curve. a,b—hot luminescence upon excitation by x radiation, c—excitation by an ArF excimer laser (193 nm).

$$\frac{dE_L(t)}{dt} \approx -\hbar A_t^2 (n-1) \times \int_0^{\omega_M} d\omega\ \omega\ \mathrm{Tr}[V^{(n)}\ \mathrm{Im}\ G(\omega_L-\omega)V^{(n)}D^{(n-1)}(t;\omega)], \tag{5}$$

where ω_M is the maximum frequency of the phonon spectrum, $G_{mm'}(t)=\Sigma_i \omega_{mi}^{-1}$ sin $\omega_i t$ is the Fourier transform of the phonon Green's function,

$$D_{mm'}^{(n-1)}(t;\omega)=\int_{-\infty}^{\infty} d\tau e^{i\omega\tau} D_{mm'}^{n-1}(t;\tau),$$

and

$$D_{mm'}(t;\tau)=\Sigma_i e_{mi} e_{m'i} D_i(t;\tau).$$

In the case of two-phonon decay ($n=2$), the equation for $D(t;\omega)$ is linear and can be solved analytically for an arbitrary phonon spectrum. The result is as follows:[1]

$$D(t;\omega) \approx \frac{2}{\pi} |I - A_t^2 G(-\omega) V^{(3)} G(\omega_L-\omega) V^{(3)}|^{-2}\ \mathrm{Im}\ G(\omega). \tag{6}$$

The resolvent has a pole. Consequently, at certain critical amplitudes A_{cr}, the relaxation rate reaches large values leading to abrupt phonon emission.

In the case of $n \geqslant 3$, the equation for $D(t;\omega)$ is nonlinear and can be solved analytically only in some simple cases. However, the following conclusions can be drawn: first, there are no real solutions for very large values of A_t, i.e., the processes of generating three or more phonons are completely suppressed, if the amplitude exceeds a certain value; second, for amplitudes close to the critical value, the rate of the processes for the emission of three or more phonons reaches fairly high values (of the order of a vibrational quantum), but always maintains a finite value; third, the values of $A_{\mathrm{cr}}^{(n)}$ increase with n, while $A_{\mathrm{cr}}^{(n)} \sim 1$ Å.

Hot luminescence appears in the $0_u^+ \rightarrow 0_g^+$ transition in the Xe_2^* quasimolecule. The 0_u^+ excited state is described well by the Morse potential

$$V_1(R)=D_1(e^{-2\alpha_1(R-R_e)}-2e^{-\alpha_1(R-R_e)})-A_1 \tag{7}$$

($D_1=515.53$ meV, $R_e=3.24\pm0.01$ Å, $A_1=35.75$ meV, and $\alpha_1=1.91$ Å^{-1}). The ground state can be approximated by a Morse pseudopotential having a continuous spectrum:

$$V_0(R)=Ae^{-2\alpha R}-\sqrt{A\varepsilon}e^{-\alpha_0 R}-A_0 \tag{8}$$

($A=6.47\times10^5$ eV, $\alpha_0=2.147$ Å^{-1}, $\varepsilon=\hbar^2\alpha_0^2$ a.u., and $A_0=24.3$ meV).

We performed a quantum-mechanical calculation of the Franck-Condon factors for all the levels $n=0-44$, determined their relative weights after solving the corresponding system of kinetic equations, and summed them after obtaining the required hot-luminescence spectrum. The calculated spectrum (Fig. 1) also contains a contribution from the zero-point vibrational level of the 1_u state. Good agreement with the experimental hot-luminescence spectrum[4] was observed for the relaxation jump near $n_{\mathrm{cr}}=23$ (Fig. 2). The oscillating structure of the spectrum ultimately calculated is a purely quantum-mechanical effect. Such a structure was discovered experimentally using a new method for two-phonon excitation of a Xe single crystal by an ArF excimer laser (193 nm) at low temperatures (see inset c in Fig. 1).

This work was supported by the Estonian Science Foundation (Grant 2274).

[1] V. Hizhnyakov, Phys. Rev. B **53**, 13981 (1996).
[2] A. S. Dolgov, Fiz. Tverd. Tela (Leningrad) **28**, 1641 (1986) [Sov. Phys. Solid State **28**, 907 (1986)].
[3] V. Hizhnyakov and D. Nevedrov, Phys. Rev. B **56**, R2809 (1997).
[4] R. Kink, A. Lõhmus, and M. Selg, Phys. Status Solidi B **107**, 479 (1981).
[5] M. Selg, Phys. Scr. **47**, 769 (1993).
[6] V. Hizhnyakov and D. Nevedrov, Pure Appl. Chem. **69**, 1195 (1997).

Translated by P. Shelnitz

Weak localization and nonlinear optical responses of exciton polaritons

E. Hanamura

Department of Applied Physics, University of Tokyo, 7-3-1 Hongo, Bunkyo-ku, Tokyo 113, Japan

Fiz. Tverd. Tela (St. Petersburg) **40**, 919–920 (May 1998)

We discuss novel nonlinear optical responses due to weak localization of exciton-polaritons (EP's): first phase-conjugated signal induced and enhanced by the weak localization of EP's under a single pump and a test beam which are two-photon-resonant to a biexciton. This observation will give us clear evidence of the weak localization. Second, we analyze, in terms of weak localization of EP's, the coherent light emission in the direction normal to the surface under a single beam pumping tilted from the normal to a planar semiconductor microcavity.
 [S1063-7834(98)04705-4]

Since phase-conjugated wave (PCW) generation was shown theoretically to be enhanced by weak localization of exciton or excitonic polaritons (EP's),[1] several theoretical papers[2–5] were published for the effects of weak localization on optical nonlinearities. No experimental observation, however, of these effects has been reported yet. For the case of the conventional phase-conjugation process, three beams are necessary, and forward and and backward pump beams are required to irradiate the front and rear surfaces at the frequency with a finite absorption coefficient. This configuration makes these experiments difficult. On the other hand, we have analyzed, in terms of the weak localization of EP's, coherent light emission in the direction normal to the surface under the tilted pumping in a planar semiconductor microcavity containing quantum wells (QW's).[6,7]

We propose first in the present work how to observe much clearer evidence of weak localization of the excitons of EP's under a single pump and a test beam irradiating a crystal surface and nearly two-photon resonant to a biexciton.[8] The main result is as follows: Let us denote by θ the angle between the pump and test beams. Then it will be shown that for θ larger than the critical angle θ_c, the phase-conjugated wave is induced and enhanced by the weak localization in the direction inverse to the test beam but that no clear enhanced signal is expected for the case $\theta < \theta_c$. The expression of θ_c will be given later. In the latter case, the sharp signal due to the weak localization disappears so that its observation as a function of θ provides us direct evidence.

The EP excited by the forward pump wave is dominantly scattered into the backward direction due to the effect of weak localization of the EP. Here the backward-scattered EP plays the same role as the EP created by the backward pump wave. Without the weak localization, the PCW is missing. Therefore the observation of PCW gives direct evidence of weak localization. This weak localization comes from constructive interference of multiple scattering of the EP and its time reversed process. Multiple scatterings of the EP are composed of the two diagrams, i.e., the ladder-type diagram Γ_l, and the maximally crossed diagram Γ_c, respectively. These effects are summed up into the following forms:[1]

$$\Gamma_l(\mathbf{k}_t-\mathbf{k}_0)=\frac{2(\gamma_0+\gamma)U_0}{2\gamma_0+D(\mathbf{k}_t-\mathbf{k}_0)^2}, \tag{1}$$

$$\Gamma_c(\mathbf{k}_t+\mathbf{k}_0)=\frac{2(\gamma_0+\gamma)U_0}{2\gamma_0+D(\mathbf{k}_t+\mathbf{k})^2}. \tag{2}$$

Here $\mathbf{k}_t$, $\mathbf{k}_0$ and $\mathbf{k}$ are wave vectors, respectively, of EP's excited by the test and pump beams and the signal beam, γ_0 is the inelastic scattering rate of the EP, $\gamma \equiv \pi N(\omega) n_i |V(0)|^2$ with the state density $N(\omega)$ of the EP, n_i is the number density of elastic scatterers and $V(0)$ is the zero-Fourier component of the potential due to the elastic scatterer, $U_0 \equiv n_i |V(0)|^2$ and $D \equiv v_g^2/6(\gamma_0+\gamma)$ is the diffusion constant of the EP with its group velocity v_g.

For the case $\theta < \theta_c$, $|\mathbf{k}_t-\mathbf{k}_0|^2/\mathbf{k}_0^2 \approx \theta^2 < \theta_c^2 \equiv 2\gamma_0/D\mathbf{k}_0^2$ so that we may put $\mathbf{k}_0=\mathbf{k}_t$ in (1). Then the ladder-type contribution Γ_l gives the stronger scattering of the EP into any directions. On the other hand, under such a two-beam pumping as $D(\mathbf{k}_t-\mathbf{k}_0)^2 > 2\gamma_0$, i.e., $\theta > \theta_c$, the ladder-type scatterings Γ_l are negligible in comparison to the maximally crossed ones with $\mathbf{k} \approx -\mathbf{k}_t$. As a result, the backward scattering of the EP excited by the test beam is most effectively brought about and the phase-conjugated signal is observable for $\theta > \theta_c$. While the signal intensity of conventional phase-conjugated wave is proportional to $I_p^2 I_t$, the present signal has the $I_p I_t^2$ dependence. This is understood from the diagram of Fig. 1, where two-photon resonance of biexciton ($\omega_s+\omega_t=\omega_b$: the biexciton frequency) is made of use so that the biexction-photon interaction is used twice and the EP-photon one is once.[8] Here $I_t(I_p)$ and $\omega_t(\omega_p)$ are the intensity and frequency, respectively, of the test (pump) beam. Another interesting point of this process is that, when the biexciton is resonantly excited by the two-photon process $\omega_s+\omega_t=\omega_b$, the phase-conjugated signal is enhanced not only by the resonance effect but also by the giant oscillator strength for the transition between the states of a signal exciton and a biexciton.[8,9] As a conclusion, the observation of PCW as a function of the angle between pump and test beams will give clearer evidence of weak localization.

Second, we will describe the observation by Rhee *et al.* on the coherence transfer between EP's in a system consist-

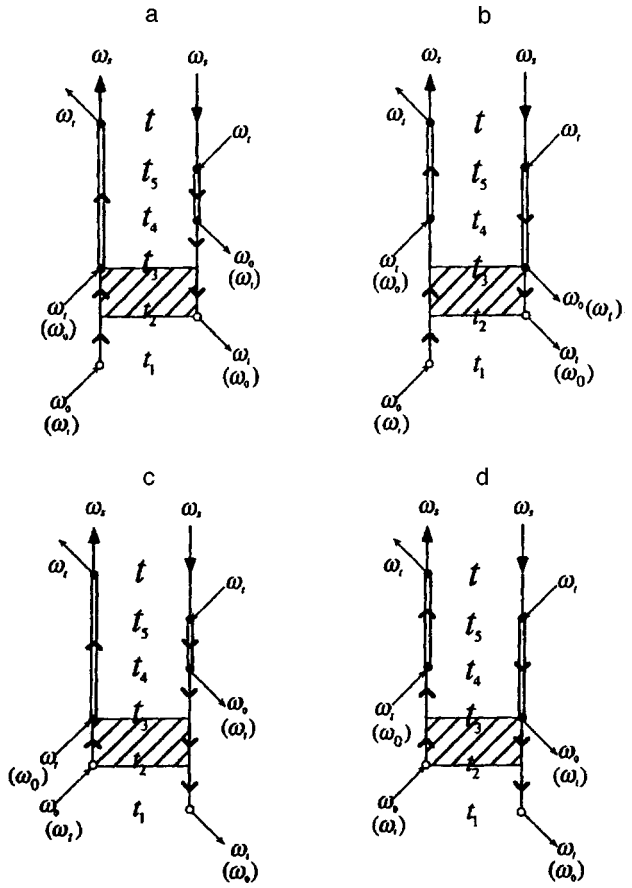

FIG. 1. Diagrams contributing to the generation of phase-conjugated exciton polariton ω_s. Solid line and double solid line describe propagation of an EP and a biexciton, respectively, and thin lines describe the external fields of pump ω_0 and test ω_t beams.

ing of multiple-quantum-well excitons resonantly coupled to a planar Fabry–Pérot microcavity.[6] Specifically, they observed the emission of light in the direction perpendicular to the surface with a small divergence angle, even though the 2D EP states were excited at a much larger angle (3°) from the normal. The emitted light was confirmed to be coherent with the incident pump light by interfering the emission with the pump beam. The emitted light intensity was also observed to increase more strongly than by the second power of pump light intensity. These experimental observations can be accounted for as a consequence of exciton-exciton interactions in a weakly localized system in the following way. The pump excites EP with an initial in-plane wave vector $\mathbf{k}_0$. These EP's may be coherently backscattered due to disorder in the quantum-well confinement potential mainly into states with momentum $-\mathbf{k}$. Collisions between EP's with $\mathbf{k}_0$ and $-\mathbf{k}_0$ result in generation of a population of EP's at exactly $\mathbf{k}=0$, giving rise to coherent emission of light in the normal direction. Note here that the bosonic character is reflected in the scattering and collisional processes, i.e., EP's are most strongly scattered into the most highly populated states $-\mathbf{k}_0$ and $\mathbf{k}=0$.

We assume that the incident laser tilted at an angle θ from the normal excites a coherent state $|\alpha\rangle$ of the EP with an in-plane momentum $\mathbf{k}_0$ in a well. The emission intensity in the normal direction may be considered to be proportional to the number of EP's generated in the single mode per second, and may be evaluated under CW excitation as

$$I_s=\lim_{t\to\infty}\frac{\partial}{\partial t}\langle\langle c_0^+ c_0\rho(t)\rangle\rangle. \tag{3}$$

The double angular brackets in (3) signify both the quantum-mechanical and ensemble average over the distribution of scattering potentials. An irrelevant factor, coming from transmissivity determined by coupling of the EP's at $\mathbf{k}=0$ to the external electric field, has been omitted. The density operator $\rho(t)$ of the total system is

$$\rho(t)=\exp(-iH_T t)\rho_0\ \exp(iH_T t), \tag{4}$$

in terms of the total Hamiltonian H_T. We expand (4) in H' the interaction of EP's with the external electromagnetic field $\mathbf{E}_j$. The lowest-order contribution comes from the fourth-order term, i.e. second-order in the pump and second-order in the signal field. According to the calculations of,[1,3] (3) is evaluated by taking account of multiple scattering of EP by the elastic scattering potential $V_0(\mathbf{q})$, i.e., the effect of maximally crossed Γ_c and ladder-type Γ_l diagrams. Then I_s expressed in the lowest approximation in external fields:

$$I_s=\frac{4AU_0}{\gamma_0^2(\gamma_0+\gamma)}\left[1+\frac{1}{1+D(\mathbf{k}+\mathbf{k}_0)^2/2\gamma_0}\right], \tag{5}$$

$$A=|\langle n_0+1,\alpha|c_0^+ c_0^+ H''|n_0,\alpha\rangle\langle\alpha|c_\alpha^+\boldsymbol{\mu}\cdot\mathbf{E}|\alpha\rangle|^2. \tag{6}$$

Here γ_0 is the inelastic scattering rate, $\gamma\equiv\pi N(\omega)n_i|V_0(0)|^2$ with the EP state density $N(\omega)$ and the number density of scatterers n_i, $U_0\equiv n_i|V_0(0)|^2$, $D\equiv\nu_g^2/6(\gamma_0+\gamma)$ is the diffusion constant of EP with its group velocity ν_g and the transition dipole moment $\boldsymbol{\mu}$ created by $c_\alpha^+\equiv c^+(\mathbf{k}_0)$. From (5) and (6), the signal intensity is proportional to the square of the incident power I_0 in the weak pumping and increases more strongly against I_0. This is because the induced scatterings into $\mathbf{k}=0$ and $-\mathbf{k}$ work, respectively, in the EP-EP collision Hamiltonian H'' and $V_0(\mathbf{q})$ term. There the sharp peak in the normal direction is understood as a combined effect of the weak localization and induced scattering to this mode, which has the longest lifetime in the semiconductor microcavity. The angle of enhancement is within $\theta_c\equiv 2\gamma_0/Dk_0^2=12\gamma_0(\gamma_0+\gamma)/(k_0\nu_g)^2$. Because the EP suffers only from elastic scatterings, the signal light has the same frequency and phase as the incident light within a lifetime $1/2\gamma_0$ and is thus coherent with the pump beam. For times longer than $1/\gamma_0$, the EP suffers from inelastic scattering, so that the interference persists for a time $1/\gamma_0$. These results are consistent with the observation of Rhee *et al.*[6]

[1] E. Hanamura, Phys. Rev. B **39**, 1152 (1989).
[2] V. E. Krabtsov, V. I. Yudson, and V. M. Agranovich, Phys. Rev. B **41**, 2794 (1990).
[3] A. R. McGurn, T. A. Leskova, and V. M. Agranovich, Phys. Rev. B **44**, 11441 (1991).

[4] V. I. Yudson and P. Reineker, Phys. Rev. B **45**, 12470 (1993).
[5] N. Taniguchi and E. Hanamura, Phys. Rev. B **47**, 2073 (1993).
[6] J. K. Rhee *et al.*, in Ultrafast Phenomena OSA (1996). p. 220.
[7] E. Hanamura and T. B. Norris, Phys. Rev. B **54**, R2292 (1996).
[8] E. Hanamura, Phys. Rev. B **54**, 11219 (1996).
[9] E. Hanamura, Solid State Commun. **12**, 951 (1973).

Published in English in the original Russian journal. Reproduced here with stylistic changes by the Translation Editor.

Two-photon photo-voltaic spectroscopy on wannier excitons in Cu_2O

N. Naka, M. Hasuo, and N. Nagasawa

Department of Physics, School of Science, The University of Tokyo, 7-3-1 Hongo, Bunkyo-ku, Tokyo 113, Japan

Fiz. Tverd. Tela (St. Petersburg) **40**, 921–923 (May 1998)

Two-photon excitation spectra of photo-voltaic effects and relevant excitonic emissions of a naturally grown single crystal of Cu_2O have been studied at 77 K and 2 K. The photo-voltaic effects have been detected under local excitation at a macroscopical distance apart from the electrodes. The participation of the yellow series excitons in the generation of the photo-voltaic signal has been discussed. © *1998 American Institute of Physics.* [S1063-7834(98)04805-9]

The correlation between photo-electric effects and relevant optical absorption in semiconductors had been a central interest of Prof. E. F. Gross and his colleague since the beginning of 1950s.[1,2] They found hydrogenic absorption lines of excitons in Cu_2O and verified the concept of Wannier excitons experimentally.

Application of laser technology to solid-state spectroscopy triggered new progress in exciton physics. A pioneering challenge to observe the two-photon absorption spectrum of the excitons in Cu_2O was the milestone,[3] and the clear demonstration was established later on.[4] It was demonstrated there that the *s* and *d* excitons in the yellow series are excited selectively by two-photon processes. Corresponding *p* excitons are excited by one-photon transitions as is widely known.

The participation of excitons in photoconduction and photo-voltaic effects has been discussed in Refs. 5 and 6. These phenomena have been utilized to detect the ballistic propagation of the excitons, that has been interpreted as a manifestation of the superfluid phase of paraexcitons.[7]

The aim of our experiments is to develop a new method to study the dynamical aspect of the excitons. The principle of the method is a simple application of linear photo-voltaic spectroscopy to the two-photon excitation regime. Simultaneously the excitation spectra of relevant exitonic emissions is also observed.

1. EXPERIMENTS

A naturally grown single crystal was used as a sample. A rectangular plate of $6\times2.6\ mm^2$ on side of a [100] plane and of about 1 mm thickness was used. One electrode of $2.5\times2.5\ mm^2$ size was set at one side of the sample and the other electrode of similar size was located at the opposite side. Electrodag was used to from the contacts. The sample was immersed in liquid N_2 or superfluid He.

A color-center laser (Solar CF-151M) pumped by a *Q*-switched Nd:YAG laser was used as a light source for the two-photon excitation. The pulse width and the repetition were ~50 ns and ~400 Hz, respectively. One-photon excitation was performed by monochromatized light from a Xe lamp. Emissions from the sample were observed by a standard system for spectroscopy. Photo-voltaic signal was measured by a digital voltmeter (Advantest R6452). Optical and electric signals were recorded simultaneously by a computer.

2. RESULTS AND DISCUSSION

Figure 1 shows examples of photo-voltaic spectra obtained by one-photon excitation at 77 K (a) and 2 K (b). General shapes of the spectra were consistent with the photoconduction spectra[2] and the photo-voltaic spectra.[8] Relevant energies of the excitonic structures are shown in the figure.

It should be noticed that voltaic effects reaching ~2 V in the dark are present at 2 K. Large amount of the dark-voltaic signal quickly diminished to the level shown in Fig. 1b when the sample was irradiated by light. A striking phenomenon observed characteristically at 2 K was a very slow recovery of the signal after interrupting the light irradiation.

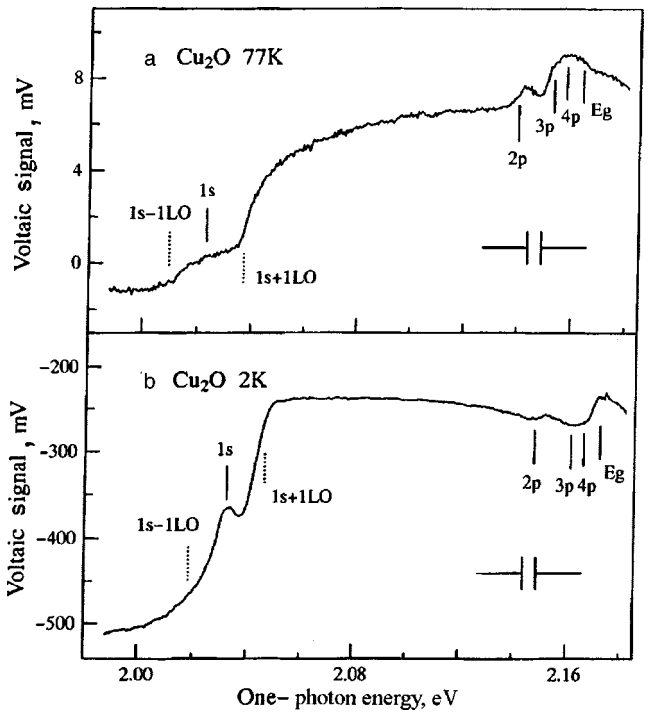

FIG. 1. Photo-voltaic spectra at of Cu_2O 77 K (a) and 2 K (b).

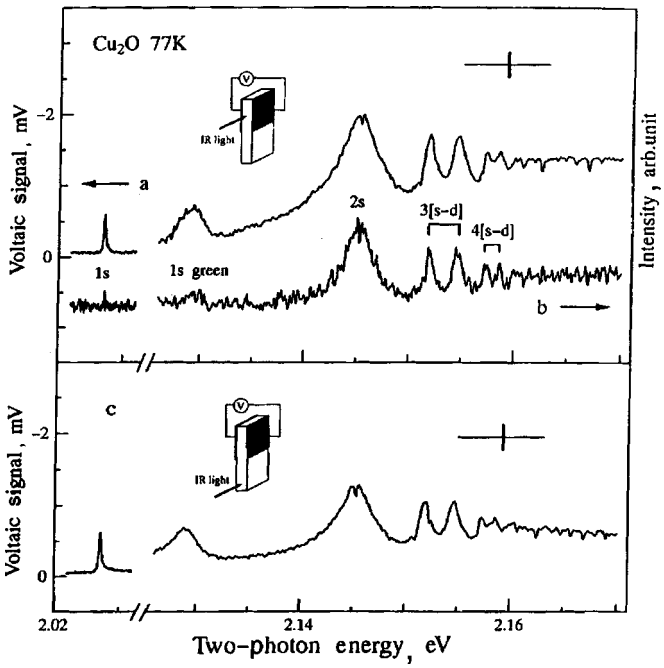

FIG. 2. Photo-voltaic spectra (a), (c), and excitation spectrum of $X_0-\Gamma_3^-$ band (b) at 77 K. The insets show respective configurations of light irradiation.

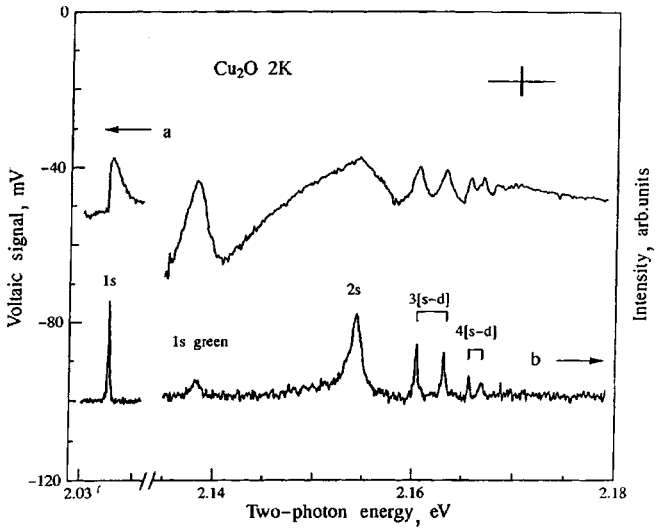

FIG. 3. Photo-voltaic spectra (a), (c), and excitation spectrum of X_0 (b) at 2 K.

Recently, it was found that $I-V$ character and relevant electroluminescence of the sample used here are strongly influenced by the irradiation of light.[9] The origin of the photo-induced diminution of the dark voltaic effects should be correlatively clarified revering researches on transport phenomena of carriers in low temperature.[10]

Figure 2a shows an example of two-photon photo-voltaic spectra at 77 K when the incident laser beam of ~ 0.3 mm diameter passes through a central region of the crystal sandwiched by the electrodes. The excitation density was ~ 500 kW/cm^2 at the maximum. Fig 2b shows an excitation spectrum of the 1 LO phonon-assisted 1 s ortho-exciton emission ($X_0-\Gamma_3^-$). The excitonic structures are clearly resolved. The energy of each structure in the spectra corresponds to relevant $[s-d]$-exciton energy as labeled in the figure.[1)] These facts show that the excitons participate in the generation of the photo-voltaic signal.

Figure 2c shows a similar photo-voltaic spectrum when the location of the laser beam was shifted ~ 3 mm apart from the edge of the electrodes as shown in the inset of the figure. Almost similar spectrum with similar intensity was obtained. This fact shows that the remote generation of the excitons gives clear effects of the generation to photo-voltaic signal.

The participation of the ortho-excitons in such phenomenon should be ruled out except for their polaritonic propagation, because their lifetime is observed to be in order of nsec.[13] The contribution of diffusive propagation of the para-excitons may be also ruled out taking account of their diffusion length at 77 K.[14] One possibility is free carrier generation at local centers influenced by the excitons as implied from the fact obtained by the excitation spectrum of free holes.[15] However, the diffusion length of free holes is roughly estimated to be only $\sim 100\ \mu$m at 77 K from the hole mobility with appropriate lifetime.[16] It is worth investigating the mechanism of this long-range effect comparing with that of the ballistic propagation.[7]

Figure 3a is an example of two-photon photo-voltaic spectra under the remote excitation at 2 K. Fig. 3b is the excitation spectrum of the resonance emission of the ortho-excitons (X_0). Each excitonic structure in Fig. 3a corresponds with relevant structures in Fig. 3b. In this case, the excitonic effects appear as the diminution of the signals as seen in the case of 1s exciton generation by one-photon excitation.

Finally, a few comments are given for the two-photon photovoltaic spectrum around the 1s yellow exciton resonance at 2 K. As witnessed in Fig. 3, the photo-voltaic spectrum shows broadening toward high energy side comparing with the sharp structure of the excitation spectrum of the emission. The fact clearly suggests that the mechanism of the generation of photo-voltaic signal is different from that of emissions. The high-energy wing may be due to the ortho-excitons of large kinetic energy actually produced by coherent scattering of acoustic phonons. They may not contribute to the X_0 emissions before relaxation. On the other hand, the coherent excitation of the ortho-excitons makes coherent resonance scattering dominant[17] and carrier generation suppressed.

3. CONCLUSION

We have demonstrated two-photon photo-voltaic spectroscopy to study the photo-carrier generation mediated by the yellow series excitons in Cu_2O. With the simultaneous observation of the excitonic emissions, it is revealed that excitons participate in giving rise to the photo-voltaic effects. Remarkable photo-voltaic signal is observed even under remote generation of excitons. The dark-voltaic effect is present at 2 K and is found to be remarkably influenced by light irradiation. The present method is promising to investigate exciton-mediated generation of free carriers and their dynamical feature.

One of the authors (N. Nagasawa) is deeply grateful to Prof. M. Kikuchi (Tokai Univ.) for his encouraging discussions. Authors thank Mr. H. Okagawa (Fujitsu Co.) for his basic studies on photo-electric effects of this material. This work is partially supported by The Grant-in-Aid for Scientific Research from The Ministry of E.S.C. in Japan.

[1)]The assignements for the excitonic structures are different in literature.[4,11] The structure of the highest energy in a family of the same principal quantum number showed the largest diamagnetic shift suggesting the *s*-dominant nature.[12]

[1] E. F. Gross, Nuovo Cimento **3**, Suppl., 672 (1956).
[2] E. F. Gross and I. Pastrnyak, Sov. J. Sol. Stat. Phys. 1, 837 (1959).
[3] F. Pradère, A. Mysyrowicz, and K. C. Rustagi, Phys. Rev. B **4**, 3570 (1971).
[4] D. Fröhlich, R. Kenklies, Ch. Uihlein, and C. Schwab, Phys. Rev. Lett. **43**, 1260 (1979).
[5] J. H. Apfel and A. M. Portis, J. Phys. Chem. Solids **15**, 33 (1960).
[6] E. F. Gross, and B. V. Novikov, J. Phys. Chem. Solids **22**, 87 (1961).
[7] E. Fortin, S. Fafard, and A. Mysyrowicz, Phys. Rev. Lett. **75**, 3951 (1993).
[8] E. Tselepis, E. Fortin, and A. Mysyrowicz, Phys. Rev. Lett. **59**, 2107 (1987).
[9] H. Okagawa, Master thesis. The Univ. of Tokyo (1996).
[10] T. Masumi and H. Shimada, J. Phys. Soc. Jpn. **60**, 3633 (1991).
[11] V. T. Agekyan, B. S. Monozon, and I. P. Shiryapov, Phys. Status Solidi B **66**, 359 (1974).
[12] H. Matsumoto, Master thesis. The Univ. of Tokyo (1995).
[13] A. Mysyrowicz, D. Hulin, and A. Antonetti, Phys. Rev. Lett. **43**, 1123 (1979).
[14] D. P. Trauernicht and J. P. Wolfe, Phys. Rev. B **33**, 8506 (1986).
[15] S. V. Gastev, A. A. Kaplyanskii, and N. S. Sokolov, Solid State Commun. **42**, 389 (1982).
[16] H. Shimada and T. Masumi, J. Phys. Soc. Jpn. **58**, 1717 (1989).
[17] N. Naka, M. Hasuo, S. Kono, and N. Nagasawa, in *Proceedings of the 23rd International Conference ''Physics of Semiconductors''* (1996), p. 273.

Published in English in the original Russian journal. Reproduced here with stylistic changes by the Translation Editor.

Exciton absorption and optical-gain bands in the presence of laser radiation

S. A. Moskalenko, V. G. Pavlov, and V. R. Mis'ko

Institute of Applied Physics, Moldovan Academy of Sciences, MD-2028 Kishinev, Moldova

Fiz. Tverd. Tela (St. Petersburg) **40**, 924–927 (May 1998)

The absorption and gain bands of a weak probe signal in the presence of the Bose–Einstein condensation of excitons, which appears under nonequilibrium conditions in a field of coherent laser radiation, are considered. It is shown that the absorption of light is caused by a quantum transition from the ground state of the crystal to the quasiexciton branch of the spectrum. Amplification of the signal occurs as a result of transitions from the quasiexciton branch of the spectrum to the ground state of the crystal. © *1998 American Institute of Physics.* [S1063-7834(98)04905-3]

The optical Stark effect in the exciton region of the spectrum has been studied in numerous experimental and theoretical investigations.[1–6] The interpretation of the observed phenomenon proposed by Schmitt-Rink, Chemla, and Haug[3,4] is based on the idea of the stimulated Bose–Einstein condensation of excitons induced by external coherent laser radiation. In contrast to Keldysh and Kozlov's work, which was devoted to the spontaneous Bose–Einstein condensation of excitons in an electron-hole description,[7] the frequency of the laser radiation plays the role of the chemical potential. Stimulated Bose–Einstein condensation can be real, but nonequilibrium[8] when the coherent laser photons excite resonant excitons in a band with the same wave vector value, or it can be virtual when the frequency of the laser radiation differs significantly from the frequency of the excitonic transition.[3–6] Just this variant was realized experimentally in Refs. 1 and 2, where the photon energy was smaller than the energy of the low-lying exciton level. Displacement of the exciton level was observed experimentally after the onset of an ultrashort laser pulse, and its return to the original position was observed after completion of the pulse.

Below we shall examine the probability of the absorption and amplification of a weak optical probe signal upon transitions from the ground state of a crystal to an exciton state when the crystal is in a field of intense coherent laser radiation that causes coherent macroscopic polarization of the medium. The issue here is the transition probability under conditions where one more exciton is created in the presence of a large number of real or virtual excitons generated under fixed conditions by coherent laser radiation. The presence of laser radiation and coherent polarization of the medium is the important factor, which leads to the possibility of the amplification of a weak signal and distinguishes this type of exciton absorption from the type previously studied in unexcited crystals.

1. NET ABSORPTION PROBABILITY

The probability of the absorption of light minus the probability of its emission gives the net absorption probability. After replacing the δ functions by Lorentzians, we found the probability sought at $T=0$ in the form

$$P_{\text{net absorb}}(\mathbf{Q}) = \frac{2|\lambda_{\mathbf{k}_0+\mathbf{Q}}|^2}{\hbar}\left[\frac{1}{|1-|A_Q|^2|} \times \frac{\Gamma(\mathbf{Q})}{(\hbar c|\mathbf{k}_0+\mathbf{Q}|-\hbar\omega_L-E_1(\mathbf{Q}))^2+\Gamma^2(\mathbf{Q})} - \frac{|A_Q|^2}{|1-|A_Q|^2|} \times \frac{\Gamma(-\mathbf{Q})}{(\hbar c|\mathbf{k}_0+\mathbf{Q}|-\hbar\omega_L+E_1(-\mathbf{Q}))^2+\Gamma^2(-\mathbf{Q})}\right]. \quad (1)$$

The coefficients A_k of the unitary Bogolyubov transformation,[9] which was used to diagonalize the quadratic part of the Hamiltonian of excitons interacting with light, depend on the detuning $\tilde{\Delta}$, the kinetic energy of the exciton T_k, the displacement of the exciton level L_k, and $\mathcal{E}(k)$ in the following manner:

$$A_k=\frac{\tilde{\Delta}+T_k+L_k-\mathcal{E}(k)}{L_k}. \quad (2)$$

Here we have introduced the notation

$$\tilde{\Delta}=\hbar\omega_{\text{ex}}(\mathbf{k}_0)-\hbar\omega_L+L_0, \quad T_k=\frac{\hbar^2k^2}{2m_{\text{ex}}},$$

$$L_k=\nu(k)\frac{N_{\mathbf{k}_0}}{V},$$

$$\mathcal{E}(k)=\sqrt{(\tilde{\Delta}+L_k+T_k)^2-L_k^2}. \quad (3)$$

The detuning $\tilde{\Delta}$ is specified by the difference between the energy of the renormalized exciton level $\hbar\omega_{\text{ex}}(\mathbf{k}_0)+L_0$ and the energy of a laser photon having the frequency ω_L and the wave vector $\mathbf{k}_0$; $\nu(k)$ is the exciton-exciton interaction constant, and $n_{\mathbf{k}_0}=N_{\mathbf{k}_0}/V$ is the exciton density in the condensate. The expression

$$\mathcal{E}(k)=\sqrt{(\tilde{\Delta}+L_k+T_k)^2-L_k^2} \quad (4)$$

is a component part of the total energy of an elementary excitation $E(\mathbf{k})$,

$$E(\mathbf{k})=\mathcal{E}(\mathbf{k})+\hbar\mathbf{V}_s\cdot\mathbf{k};\quad \mathbf{V}_s=\frac{\hbar\mathbf{k}_0}{m_{\rm ex}},\tag{5}$$

which depends on the velocity $\mathbf{V}_s$ of the induced condensate. This rate is determined by the laser photon momentum $\hbar\mathbf{k}_0$ and the exciton translational mass $m_{\rm ex}$. In order that the A_k satisfy the condition

$$|A_k|\leqslant 1\tag{6}$$

over the entire region of $\mathbf{k}$-space, the sign in front of the square root in (11) must be chosen to coincide with the sign of the expression $(\tilde{\Delta}+T_k+L_k)$. We use $\mathcal{E}_1(k)$ to denote this solution and define it by the rule

$$\text{sgn}\ \mathcal{E}_1(k)=(\tilde{\Delta}+T_k+L_k).\tag{7}$$

Net absorption takes place at values of $\hbar\omega=\hbar c|\mathbf{k}_0+\mathbf{Q}|$ where the difference (1) is positive, and net optical emission or amplification occurs at values where it is possible.

2. ANISOTROPY OF EXCITON ABSORPTION AND EMISSION BANDS IN A COHERENTLY POLARIZED CRYSTAL

The function $\mathcal{E}(k)$ was previously obtained in Ref. 6. However, the coefficients A_k and the quantum transition probabilities were not investigated. The analogous expressions in the form of functions of $|\mathbf{q}-\mathbf{k}_0|$ depend on the orientation of the vector $\mathbf{q}$ of the probe radiation relative to the vector $\mathbf{k}_0$ of the laser radiation inducing the coherent macroscopic polarization of the medium. Three possible geometries for observing the absorption coefficient are of interest. They are $\mathbf{q}\uparrow\uparrow\mathbf{k}_0$, $\mathbf{q}\perp\mathbf{k}_0$, and $\mathbf{q}\downarrow\uparrow\mathbf{k}_0$, in which the probe radiation propagates along the direction of the laser radiation, perpendicularly to it, or antiparallel to it.

The absolute value $|(\mathbf{q}-\mathbf{k}_0)/k_0|$ takes different values for the same absolute value of $q=xk_0$, where $\infty>x>0$, depending on the orientation of $\mathbf{q}$ relative to $\mathbf{k}_0$. They equal $|x-1|$, $\sqrt{x^2+1}$, and $(x+1)$, respectively.

For this reason, the energy spectrum $\mathcal{E}_1(\mathbf{q}-\mathbf{k}_0)$, the coefficients $|A_{\mathbf{q}-\mathbf{k}_0}|$, and the multiplier $(1-|A_{\mathbf{q}-\mathbf{k}_0}|^2)^{-1}$ are found as functions of x for the three orientations of $\mathbf{q}$ relative to $\mathbf{k}_0$. The dependences on x simultaneously convey the dependences on the frequency of the light absorbed, since $\hbar\omega=\hbar cq=x\hbar ck_0=x\hbar\omega_L$, where $x>0$. These dependences were found for a specific value of the detuning $\tilde{\Delta}$ and contain the frequency dependences of $\mathcal{E}_1(x)$, $|A(x)|$, and $(1-|A(x)|^2)^{-1}$ for the three observation geometries.

The dependence of $(1-|A(x)|^2)^{-1}$ has pronounced anisotropy. The latter is manifested at positive values of $\tilde{\Delta}=L_0$ and amounts to 2%. At large positive values of $\tilde{\Delta}$ the anisotropy becomes vanishingly small, i.e., the coefficients $|A_{\mathbf{k}}|$ for the quasiexciton branch of the spectrum become much smaller than unity. When $\tilde{\Delta}=0$, a real, but nonequilibrium induced Bose condensate of excitons with the wave vector $\mathbf{k}_0$ is observed. The exciton occupation number $n^{\rm ex}_{\mathbf{k}_0+\mathbf{k}}$ becomes infinitely large as $k\to 0$, as follows from the Bose–Einstein distribution function with a chemical potential equal to zero. A sharp difference appears between the occupation numbers

$$n^{\rm ex}_{\mathbf{k}_0+\mathbf{k}}=n^{\rm ex}_q=\frac{|A_{\mathbf{q}-\mathbf{k}_0}|^2}{1-|A_{\mathbf{q}-\mathbf{k}_0}|^2};\quad \mathbf{q}=\mathbf{k}_0+\mathbf{k}\tag{8}$$

for the cases in which $\mathbf{q}$ tends toward $\mathbf{k}_0$ or $-\mathbf{k}_0$. Since the optical absorption coefficients are proportional to $(1+n^{\rm ex}_q)$, sharp anisotropy of the absorption of light hence appears.

Instabilities appear in the spectrum when $\tilde{\Delta}$ is negative. They were discussed above. At wave vectors which produce instabilities the coefficients $|A_{\mathbf{k}}|^2=1$, and the corresponding occupation numbers go to infinity. These singularities can be

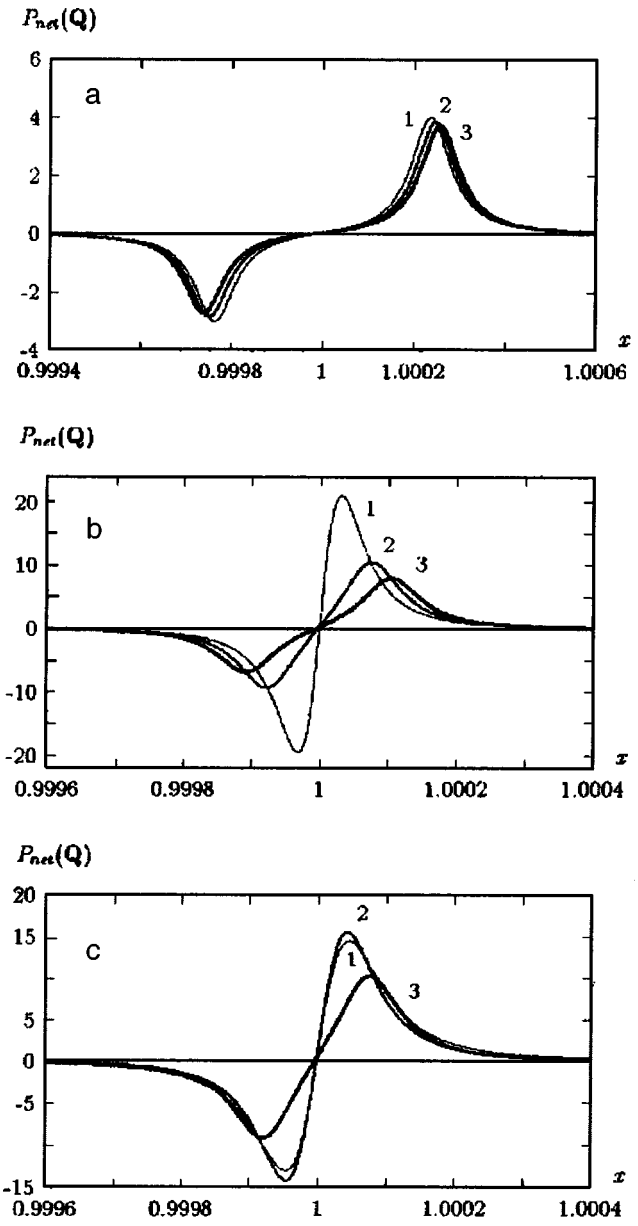

FIG. 1. The frequency dependence $P_{\rm net}(\mathbf{Q})$ for three orientations of the wave vector $\mathbf{q}$ of the probe radiation relative to the wave vector $\mathbf{k}_0$ of the laser radiation. *1*—$\mathbf{q}\uparrow\uparrow\mathbf{k}_0$, *2*—$\mathbf{q}\perp\mathbf{k}_0$, *3*—$\mathbf{q}\downarrow\uparrow\mathbf{k}_0$ for various values of the detuning: a) $\tilde{\Delta}=0.01L_0$; b) $\tilde{\Delta}=0$, c) $\tilde{\Delta}=-0.001L_0$.

eliminated, if the damping of excitons in the band due to scattering by other excitons or by phonons is introduced phenomenologically.

The generation of new waves and the stimulated scattering of excitons take place in these regions. The latter process is threshold-free as long as the damping of the energy spectrum of the seed excitons is disregarded. Since the number of nonequilibrium excitons becomes anomalously large in the vicinity of these regions in **k** space, the absorption coefficient becomes anomalously large. It is noteworthy that the region where anomalous absorption is possible also shifts along the energy scale as a function of the observation geometry. Besides $(1-|A(x)|^2)^{-1}$, the net absorption probability (1) contains a second multiplier, which has the form of a Lorentzian. The latter can also exhibit different frequency dependences for different orientations of $\mathbf{q}$ and $\mathbf{k}_0$. However, it depends on the small difference between quantities such as $\hbar\omega$ and $\hbar\omega_L$, each of which is large in comparison with the spectrum of elementary excitations $E_1(\mathbf{q}-\mathbf{k}_0)=\mathcal{E}_1(\mathbf{q}-\mathbf{k}_0)+\hbar\mathbf{V}_s\cdot(\mathbf{q}-\mathbf{k}_0)$. Therefore, the anisotropy is more clearly displayed through the multiplier $(1-|A_{\mathbf{q}-\mathbf{k}_0}|^2)^{-1}$. In addition, if the arguments in the corresponding Lorentzians coincide exactly, the anisotropy discussed above vanishes. In this case the regions where pure absorption and pure emission take place are superimposed on one another, and their anisotropies are compensated exactly.

Similarly, the anisotropy becomes inappreciable, if the Lorentzians have a half-width larger than the width of $2|\mathcal{E}_1(\mathbf{Q})|$. The most favorable conditions for observing anisotropy of the absorption and luminescence bands correspond to the case of $\Gamma(\mathbf{Q})<|\mathcal{E}_1(\mathbf{Q})|$ and to small values of the detuning $\tilde{\Delta}$, where the $|A_{\mathbf{q}}|^2$ are close to unity.

The forms of the absorption and gain bands are presented in Fig. 1 for three values of the detuning: $\tilde{\Delta}=0.01L_0$, $\tilde{\Delta}=0$, and $\tilde{\Delta}=-0.001L_0$. The gain bands are located on the long-wavelength side of the laser radiation frequency while absorption bands are located on the short-wavelength side. They shift relative to one another as a function of the orientation of the wave vectors of the probe radiation $\mathbf{q}=\mathbf{k}_0+\mathbf{Q}$ and $\mathbf{k}_0$.

This work was performed as part of an INTAS project (Grant 94-324).

[1] A. Mysyrovicz, D. Hulin, A. Antonetti *et al.*, Phys. Rev. Lett. **56**, 2748 (1986).
[2] A. von Lehmen, D. S. Chemla, J. E. Zucker, and J. P. Heritage, Opt. Lett. **11**, 609 (1986).
[3] S. Schmitt-Rink and D. Chemla, Phys. Rev. Lett. **57**, 2752 (1986).
[4] S. Schmitt-Rink, D. S. Chemla, and H. Haug, Phys. Rev. B **37**, 941 (1988).
[5] V. R. Mis'ko, S. A. Moskalenko, and M. I. Shmiglyuk, Fiz. Tverd. Tela (St. Petersburg) **35**, 3213 (1993) [Phys. Solid State **35**, 1580 (1993)].
[6] S. A. Moskalenko and V. R. Mis'ko, Ukr. Fiz. Zh. **37**, 1812 (1992).
[7] L. V. Keldysh and A. N. Kozlov, Zh. Éksp. Teor. Fiz. **54**, 978 (1968) [Sov. Phys. JETP **27**, 521 (1969)].
[8] S. A. Moskalenko, Fiz. Tverd. Tela (Leningrad) **4**, 276 (1962) [Sov. Phys. Solid State **4**, 199 (1962)].
[9] N. N. Bogolyubov, *Collected Scientific Works, Vols. 1–3* [in Russian], Naukova Dumka, Kiev (1971).

Translated by P. Shelnitz

Features of the optical bistability in an exciton-biexciton system

O. F. Pasechnik and P. I. Khadzhi

Institute of Applied Physics, Moldovan Academy of Sciences, MD-2028 Kishinev, Moldova

Fiz. Tverd. Tela (St. Petersburg) **40**, 927–928 (May 1998)

The role of exciton-exciton, exciton-biexciton, and biexciton-biexciton interactions in the nonlinear transmission function of a ring cavity is studied. It is shown that transmission functions both without hysteresis and with one or two hysteresis loops can be obtained by taking into account the elastic interparticle interactions in the exciton-biexciton system. © *1998 American Institute of Physics.* [S1063-7834(98)05005-9]

This paper presents the results of a theoretical investigation of optical bistability in the region of the M luminescence band of semiconductors, which is caused by the optical conversion of excitons into biexcitons. Such a system is completely analogous to the ordinary two-level model.[1] However, elastic exciton-exciton, exciton-biexciton, and biexciton-biexciton interactions take place at high excitation levels. Here emphasis is placed on ascertaining the role of these interactions in the nonlinear transmission function of a ring cavity.

The starting point for a theoretical treatment of optical bistability in an exciton-biexciton system is the interaction Hamiltonian in the second quantization representation:

$$\frac{H}{\hbar}=-\sigma g(a^+bE^-+b^+E^+a)+\frac{\nu_1}{2}a^+a^+aa + \frac{\nu_2}{2}b^+b^+bb+\frac{\nu}{2}a^+b^+ba, \tag{1}$$

where the field amplitude E is a sum of the positive- and negative-frequency components, i.e., $E=E^++E^-$, a (b) is the amplitude of the exciton (biexciton) wave, σg is the constant of the interaction of excitons and biexcitons with the field, and ν_1, ν_2, and ν are the elastic exciton-exciton, exciton-biexciton, and biexciton-biexciton interaction constants, respectively.

Only one macroscopically filled mode of coherent excitons, biexcitons, and phonons is considered (the index characterizing this mode is omitted). The problem is solved semiclassically using the Heisenberg equations of motion for the amplitudes of the exciton and biexciton waves and the wave equation for the field.

In this paper optical bistability is studied in the geometry of a ring cavity (Fig. 1). A sample of length L is placed between the entrance and exit mirrors of the cavity, which are characterized by the same transmission coefficient T. As in Ref. 1, we use the boundary conditions for the field amplitudes at the points 0 and L of the crystal in the form

$$E(L)=\frac{E_t}{T}, \quad E(0)=\sqrt{T}E_i+RE(L), \tag{2}$$

where E_i and E_t are the field amplitudes of the incident and transmitted waves, respectively, and $R+T=1$. We introduce the normalized amplitudes using the formulas

$$x=\frac{E_t}{E_s\sqrt{T}}, \quad y=\frac{E_i}{E_s\sqrt{T}}, \tag{3}$$

where $E_s=\hbar/(\mu T_1T_2)^{-1/2}$, $\mu=\hbar\sigma g$, and T_1 and T_2 are the longitudinal and transverse relaxation times.

It is assumed that the incident wave is coherent and monochromatic. In the approximation of a slowly varying envelope, the function $E(x)$ varies weakly over distances of the order of the optical wavelength. We consider the case of exact resonance $\Delta=\omega-\omega_m=0$, where ω_m is the frequency of the exciton-biexciton transition. With consideration of the foregoing, in the mean-field approximation, we obtain the equation of state of an exciton-biexciton system, which relates the amplitudes of the transmitted (x) and incident (y) fields, in the form

$$y=x+\frac{2Cx}{1+x^2+w^2(\alpha+\beta z)^2}, \tag{4}$$

where $w=\nu_1(N+n)T_2/2$, $\alpha=1+\nu_2/\nu_1-2\nu/\nu_1$, $\beta=\nu_2/\nu_1-1$, and N and n are the occupation numbers of the biexcitons and excitons. The bistability parameter C is expressed by the formula $C=\alpha L/4T$.[1] Equation (4) is a generalization of the results in Ref. 1 for the case taking into account the elastic interparticle interactions in a system of excitons and biexcitons. It contains not only the bistability

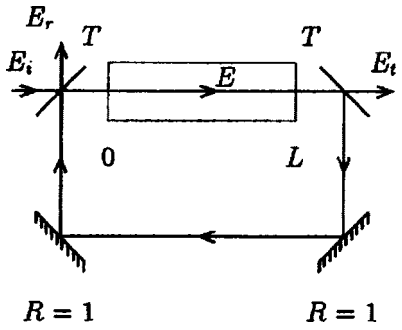

FIG. 1. Schematic representation of a ring cavity.

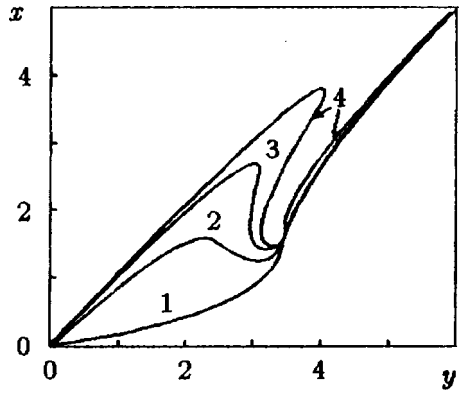

FIG. 2. Transmission function for the case of $C=2$ and various values of w: *1*—0, *2*—2, *3*—3.5, *4*—5.

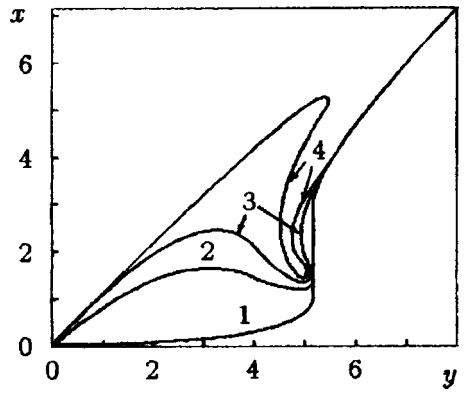

FIG. 3. Transmission function for the case of $C=4$ and various values of w: *1*—0, *2*—2, *3*—3, *4*—7.

parameter C, but also the additional parameters w, α, and β, which specify the behavior of the transmission function.

Let us ascertain the dynamics of the variation of $x(y)$ for different values of w and C. Figure 2 presents the transmission function for the case of $C=2$ and various values of w. As w increases, a hump appears on the left-hand side of the figure, and then its height and steepness increase. At a certain value of w, this hump deforms so much that a hysteresis loop appears (for example, at $w=3.5$). This is caused by the strong influence of the interparticle interactions, which are specified mainly by the behavior of the third term in the denominator of the transmission function (4). Thus, it is seen that optical bistability also appears in an exciton-biexciton system when $C<4$ (in contrast to the results in Ref. 1), but in this case w must exceed the critical value ($w_c=0.9$).

Figure 3 shows the $x(y)$ curves for $C=4$ and various values of the bistability parameter w. It is seen that we obtain the results described in Ref. 1 when $w=0$. As w is increased, strong deformation of the initial portions of the curves takes place with the formation of a hump on the transmission function, whose position and shape are specified by the value of w. At a certain value of w, a segment of differential amplification appears on the right-hand slope of the hump and then quickly transforms into a bistable segment. A further increase in w leads to expansion of the bistability region and even to a change in the number of upward and downward switchings during cyclic variation of the incident light intensity. For example, for the case of $w=7$ there are two downward switchings and only one upward switching.

When $C=8$, two hysteresis loops also appear. As follows from Ref. 1, the first loop exists already for $w=0$. It is quite pronounced, in contrast to the preceding case, and remains practically unchanged as w is increased. The appearance of the second hysteresis loop is caused by deformation of the hump, whose existence is associated with nonlinear effects in the exciton-exciton, exciton-biexciton, and biexciton-biexciton interactions.

Thus, it is seen that the existence of transmission functions with two hysteresis loops is possible in a system of excitons and biexcitons when the elastic interparticle interactions are taken into account. The first hysteresis loop is caused by the existence of internal feedback and can appear in transmission even without the ring cavity. The second hysteresis loop is caused by external feedback and appears only in the presence of the ring cavity. In such a system not only the bistability parameter C, but also w, α, and β can be bifurcation parameters. A transmission function without hysteresis, a transmission function with one hysteresis loop, or a transmission function with two hysteresis loops can be obtained, depending on the relation between these parameters. In addition, variation of the number of upward and downward switchings during cyclic variation of the intensity of the incident radiation is possible for certain values of these parameters.

[1] R. Bonifacio and L. A. Lugiato, Lett. Nuovo Cimento **21**, 505 (1978).

Translated by P. Shelnitz

Exciton molecules and exciton liquids in semiconductors

A. A. Rogachev

A. F. Ioffe Physicotechnical Institute, Russian Academy of Sciences, 194021 St. Petersburg, Russia

Fiz. Tverd. Tela (St. Petersburg) **40**, 929–931 (May 1998)

Excitons in many-valley semiconductors form molecules consisting of four and more excitons. The degeneracy factor g of the conduction band in germanium is 8, and in silicon $g=12$. As in acceptors, the hole ground state in excitons is fourfold degenerate. The same is valid for exciton molecules, because they are quantum objects with spherical symmetry. The exciton binding energy in molecules is close to that in exciton-liquid droplets. Experimental evidence is considered for the existence, besides biexcitons, of stable exciton molecules consisting of three and four, and, possibly, 11 and 12 excitons. Molecules containing from five to ten excitons are apparently unstable. © *1998 American Institute of Physics.* [S1063-7834(98)05105-3]

The existence of exciton molecules and of the exciton liquid was predicted more than 30 years ago.[1,2] The authors proceeded from an analogy between the exciton and the hydrogen atom or positronium. The exciton molecule would thus consist of two excitons, and the existence of the exciton liquid follows from the theorem of statistical physics which states that, if molecules or atoms are subject to attraction, no matter how weak, a condensate must form provided the temperature is low enough. The question of whether the condensed state should be an insulator or a metal has been awaiting an answer for a long time. If we consider the exciton as an analog of positronium, the exciton liquid should be an insulator. Keldysh and Kopaev[3] proved theoretically that at very high densities (substantially in excess of that derived from Mott's criterion for the metal–insulator transition), the exciton gas is an insulator. In the region of ''metallic'' densities the exciton gas is also found to be an insulator.[4] The problem of superfluidity of the exciton liquid was considered by Keldysh.[5] While no experiment with an insulating exciton liquid has been carried out thus far, the validity of the above theoretical considerations in not doubted.

The first experiment offering information on the electrical conductivity of an exciton liquid was performed on germanium single crystals and showed that the electron–hole plasma of sufficiently high density is metallic.[6,7] Subsequent theoretical and experimental studies showed that the very strong differences between the properties of the exciton liquid in such semiconductors as germanium and silicon, on the one hand, and many other semiconductors is due to the many-valley character of the former.[8] In pure silicon, luminescence spectra of free-exciton molecules exhibit six lines.[9] Six lines were found also in the luminescence of exciton complexes (molecules) bound to shallow donors in silicon. The existence of two additional lines was initially ascribed to a contribution of the spin–orbit split band, whose symmetry is Γ_7^+.[10] This band, however, is too far away. Another explanation suggests that these lines have the following nature. In a molecule containing five or six excitons, the hole shell with the principal quantum number $n=1$ (four holes) is completely filled, with one or two holes residing in the shell with the principal quantum number $n=2$. The luminescence involves an electron (the $n=1$ electron shell contains 12 states and, hence, is not filled) and a hole from the filled $n=1$ shell. Recombination leaves the molecule in an excited state. In order for the molecule to transfer to ground state, a hole from the $n=2$ shell has to drop to the empty state in the $n=1$ shell. There is, however, a serious argument against this explanation as well. The lifetime of an empty valence-band state in the $n=1$ shell, with holes present in the $n=2$ shell, is of order $\tau=\hbar/E_z$, where E_z is the exciton binding energy in the molecule. These luminescence lines should have then about the same width as the exciton-liquid lines, a prediction that has not received experimental support.

The nature of the next two lines presently raises much controversy.[9,11,12] All the six lines exist in spectra of both free- and of donor-bound-exciton molecules.[10] The present author is of the opinion that these molecule produce two lines of each in the luminescence spectrum two lines each. One of the lines is due to radiative recombination, i.e., annihilation of an $n=2$ hole with an $n=1$ electron. Thus this recombination leaves the molecule in the ground state and generates a narrow line. The second line is actually the long-wavelength tail of the luminescence line discussed earlier. The width of this line is determined by the lifetime of the empty state in the $n=1$ hole shell.

The position of the E_z line in luminescence spectra, which we shall reckon from the free-exciton line, is connected with the exciton free energy F_z through a simple relation

$$F_z=\frac{1}{z}\sum_{z'=2}^{z'=z} E_{z'}, \tag{1}$$

where z is the number of excitons in the molecule.

The experimental values of E_z are (in meV): $E_2=-2.0$, $E_3=-4.9$, $E_4=-7.0$, and for the last two lines E_z is -8.6 and -10 meV. The exciton-gas–exciton-liquid phase diagram for the case where the gas consists of exci-

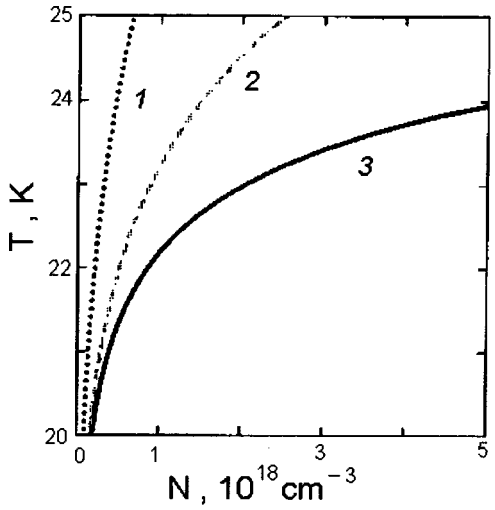

FIG. 1. The gas part of the exciton-gas–exciton-droplets phase diagram for silicon. *1* — boundary between the gas and the phase containing exciton droplets, with free electrons and holes, excitons, biexcitons, and trions taken into account; *2* — same with inclusion of exciton molecules containing 2, 3, and 4 excitons; *3* — same with inclusion of exciton molecules containing from two to 12 excitons.

tons, free electrons and holes, trions, and biexcitons is presented in Fig. 1. The other two lines take into account also the existence of molecules with $z=3-4$ and $x=3-12$. For unstable molecules ($z=5-10$) E_z was estimated using the data presented in Fig. 2.

To calculate the degeneracy factor $g(z)$ needed for thermodynamic determination of the boundary of the gas–liquid phase diagram, some simplifications should be introduced into the gas-phase model. First, we assume the ground state of holes in the molecule to be fourfold degenerate. Second, we assume the $2s$ and $2p$ states of holes to have approximately the same energy, which is valid only for sufficiently high temperatures. Since the triple point in silicon is expected to be at $T\approx 20$ K,[12] this assumption may be considered justified. This assumption is also argued for by the fact that the $2p$ state lies deeper than $2s$, and that the $2s$ states are only fourfold degenerate.

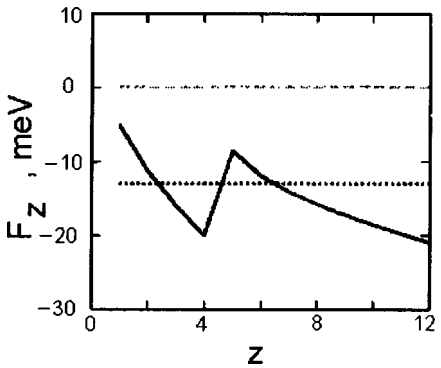

FIG. 2. Solid line — positions of spectral lines of excitonic molecules containing different numbers of excitons, calculated using Eq. (7). The number of excitons in a molecule is plotted along the X axis. The dashed and dotted lines identify the positions of the levels of free $e-h$ pairs and free excitons, respectively.

The boundary separating the gas phase from the gas–liquid-droplets mixed phase is determined by the equation

$$N=n_{ex}+\sum_{z'=2}^{z'=z} n_{ex}^{z}\left(\frac{2\pi\hbar^2}{kTm_{ex}}\right)^{\frac{3(z-1)}{2}} z^{\frac{3}{2}}\frac{g(z)}{g_{ex}^{z}}\exp\left(\frac{zF_z}{kT}\right), \quad (2)$$

where

$$n_{ex}=g_{ex}\left(\frac{m_{ex}kT}{2\pi\hbar^2}\right)^{\frac{3}{2}}\exp\left(-\frac{E_d}{kT}\right),$$

E_d is the exciton binding energy in the liquid, and N is the total concentration of electron–hole pairs. For $z\leqslant 4$, factor $g(z)$ is given by the expression

$$g(z)=\frac{12!}{(12-z)!n!}\,\frac{4!}{(4-z)!z!}, \quad (3)$$

and for $z>4$:

$$g(z)=\frac{12!}{(12-z)!n!}\,\frac{16!}{(16-(z-4))!(n-4)!}. \quad (4)$$

Thus by filling four $1s$ states in the valence band one can obtain a molecule made up of four excitons. This will be a strongly bound molecule. In the case of $2p$ and $2s$ hole states, the states that will be filled are those with a considerably lower binding energy. The $1s$ states for electrons are filled when the number of electrons reaches 12. As a result of an increasing number of electron–hole pairs in the molecule, one may expect the rise in the hole kinetic energy to be compensated by a growth in Coulomb energy.

Consider a simple model of the exciton molecule in a many-valley semiconductor. We assume the size of molecules to be determined by the electron and hole wave function, which can have the form of a hydrogen-like function $\Psi'(R)=\sqrt{1/\pi R^{-3}}\,e^{-R/r}$, where r is the effective radius of the molecule. For the kinetic energy of electrons we shall then have $E_{ke}=\hbar^2/(2m_e r^2)$, and for that of holes, $E_{kh}=\hbar^2/(2m_h r^2)$. For a $2s$ or $2p$ hole, $E_{kh}=2\hbar^2/(m_h r^2)$.

The potential energy per one electron–hole pair (exciton) is $e^2/\varepsilon L$, where $L=\sqrt{(\varepsilon E_k)/(6\pi e^2 n_{ex})}$, the effective $e-h$ pair density is $n_{ex}=(2\pi/9)Azr^{-3}$, parameter A is approximately one, and E_k is the average kinetic energy, which is the sum $E_{ke}+E_{kh}$. If more than one hole are in the $n=2$ state, then

$$E_k=\frac{\hbar^2}{2r^2}\left(\frac{1}{m_e}+\frac{4}{zm_h}+\frac{(z-4)}{z}\,\frac{4}{m_h}\right). \quad (5)$$

The free energy per exciton can then be written

$$F_z=-\frac{e^2}{\varepsilon L}+E_k. \quad (6)$$

The radius of the exciton molecule is found from the condition $dF_z/dr=0$:

$$F_z=0.94\,\frac{\varepsilon^2(Az)^{2/3}}{2e^4\hbar^2}\,\frac{m_e m_h}{m_e+m_h}. \quad (7)$$

If $z>4$, then

$$F_z = 0.94 \frac{\varepsilon^2 (Az)^{2/3}}{2e^4\hbar^2} \frac{1}{\dfrac{1}{m_e} + \dfrac{4}{zm_h} + \dfrac{(z-4)}{z}\dfrac{4}{m_h}}.$$

The position of the line in the spectrum (i.e. the distance between the exciton line and the line of the molecule) is

$$E_z = zF_z - (z-1)F_{z-1}. \tag{8}$$

Figure 2 shows the results of a calculation where it is assumed that $m_e/m_h = 0.7$, and parameter A is chosen so that the theoretical value of E_4 is equal to the experimental value of 7 meV. It was found that stable molecules are those that contain 2, 3, 4, 11, and 12 excitons. Molecules containing two and four excitons contribute also to luminescence spectra long-wavelength tails due to recombination of 1*s* electrons with 1*s* holes, which leaves the molecule in excited state. These spectra resemble very much those of the exciton liquid.

We note in conclusion that the largest contribution to the gas-liquid phase diagram comes from exciton molecules containing two, three, and four excitons, as well as from the two molecules made up of 11 and 12 excitons.

Support of the ''Integration'' Project (Grant 326.37) is gratefully acknowledged.

[1] S. A. Moskalenko, Opt. Spektrosk. **5**, 147 (1958).
[2] M. A. Lampert, Phys. Rev. Lett. **1**, 450 (1958).
[3] L. V. Keldysh and Yu. V. Kopaev, Fiz. Tverd. Tela (Leningrad) **6**, 2791 (1964) [Sov. Phys. Solid State **6**, 2219 (1964)].
[4] L. V. Keldysh and A. N. Kozlov, Zh. Éksp. Teor. Fiz. **54**, 978 (1968) [Sov. Phys. JETP **27**, 521 (1968)].
[5] L. V. Keldysh, in *Problems in Theoretical Physics (In Memoriam I. E. Tamm)*, p. 433.
[6] A. A. Rogachev, Prog. Quantum Electron. **6**, 141 (1980).
[7] A. A. Rogachev, *Handbook on Semiconductors*, Vol. 1, edited by P. T. Landsberg (Elsevier, Amsterdam, 1992), p. 449.
[8] V. S. Bagaev, T. I. Galkina, O. V. Gogolin, and L. V. Keldysh, JETP Lett. **10**, 195 (1969).
[9] M. L. W. Thewalt, V. A. Karasyuk, D. A. Harrison, and D. A. Huber, in *Proceedings of the 23rd International Conference on the Physics of Semiconductors* (Berlin, 1996), edited by M. Scheffler and R. Zimmermann (World Scientific, Singapore, 1996), Vol. 1, p. 341.
[10] P. D. Altukhov, K. N. El'tsov, G. E. Pikus, and A. A. Rogachev, Fiz. Tverd. Tela (Leningrad) **22**, 239 (1980) [Sov. Phys. Solid State **22**, 140 (1980)].
[11] A. A. Rogachev, in *Proceedings of the International Conference Symposium Nanostructures: Physics and Technology* (St. Petersburg, Russia, 1997), p. 126.
[12] A. A. Rogachev, in *Proceedings of the 23rd International Conference on the Physics of Semiconductors*, Berlin, 1996), edited by M. Scheffler and R. Zimmermann (World Scientific, Singapore, 1996), Vol. 1, p. 173.

Translated by G. Skrebtsov

Cavityless optical bistability in a thin semiconductor film upon the resonant excitation of excitons and biexcitons

P. I. Khadzhi and S. L. Gaĭvan

Institute of Applied Physics, Moldovan Academy of Sciences, MD-2028 Kishinev, Moldova

Fiz. Tverd. Tela (St. Petersburg) **40**, 932–933 (May 1998)

The bistable properties of a thin semiconductor film under conditions of resonant excitation of coherent excitons and biexcitons by photons in one or two different pulses are studied theoretically. [S1063-7834(98)05205-8]

Let us consider the steady-state transmission of a thin semiconductor film of thickness L, which is considerably smaller than the wavelength of the exciting radiation in the exciton region of the spectrum. We shall simultaneously take into account two quantum transitions, one in the region of an exciton resonance and one in the region of the M luminescence band. The giant oscillator strength for optical exciton-biexciton conversion[1] can promote the appearance of optical bistability even at moderate excitation levels of the crystal; therefore, we shall not take into account the effects of interparticle interactions.

SINGLE-PULSE EXCITATION

In crystals of such materials as CdS, CdSe, etc., in which the biexciton binding energy is small (<3 meV), the photons of one pulse can induce stepwise transitions from the ground state of the crystal to an exciton state and from the latter to a biexciton state. The temporal evolution of the macroscopically filled amplitudes of the exciton (a) and biexciton (b) waves under the action of a field E is specified by the Heisenberg equations:[2]

$$i\dot{a}=\omega_0 a-i\gamma_e a-gE^+-\sigma bE^-, \tag{1}$$

$$i\dot{b}=\Omega_0 b-i\gamma_m b-\sigma aE^+, \tag{2}$$

where ω_0 and Ω_0 are the eigenfrequencies of the exciton and biexciton states, respectively, γ_e and γ_m are the phenomenologically introduced damping constants, g is the constant of the interaction of the excitons with the field, and σ is the optical exciton-biexciton conversion constant.

Assuming that a pulse with an electric field amplitude E_0 and a frequency $\omega=\omega_0=\Omega_0-\omega_0$ impinges on a thin semiconductor film located in a vacuum, from the continuity conditions of the tangential field components we obtain an electrodynamic expression, which relates the field and quasiparticle amplitudes,

$$E^+=E_0^++i\alpha(ga+\sigma a^+b), \tag{3}$$

where $\alpha=2\pi\hbar\omega L/c$. When (3) is taken into account, we can easily obtain the following steady-state equation of state for the normalized amplitudes of the incident ($X=\sigma E_0(\gamma_e\gamma_m)^{-1/2}$) and transmitted ($Y=\sigma|E|(\gamma_e\gamma_m)^{-1/2}$) pulses from (1) and (2):

$$X=Y\left[1+C\frac{1+2Y^2}{(1+Y^2)^2}\right], \tag{4}$$

where the bistability parameter $C=\alpha g^2/\gamma_e$. An investigation of the function $Y(X)$ reveals that the criterion for the existence of cavityless optical bistability is the inequality $C>C_{\rm cr}=108/17\approx 6.35$. When $C<C_{\rm cr}$, the system of equations (1)–(3) has one stable steady-state solution, and when $C>C_{\rm cr}$, it has three such solutions, two of which are stable. It follows from (4) that Y as a function of X has different types of asymptotic behavior at small and large values of X: $Y\approx X/(1+C)$ at $X\ll 1$ and $Y\approx X$ at $X\gg 1$. When $C>C_{\rm cr}$, switching from one branch of the hysteresis dependence to the other occurs at definite values of the pump amplitude.

To clarify the physical meaning of this finding, let us also consider the steady-state dependences of the exciton density n and the biexciton density N on the amplitude of the incident pulse. We obtain the following relations directly from (2) and (3):

$$n=\frac{\gamma_m}{\gamma_e}\frac{Y^2}{(1+Y^2)^2},\quad N=\frac{Y^4}{(1+Y^2)^2}, \tag{5}$$

where $n=(\sigma/g)^2|a|^2$ and $N=(\sigma/g)^2|b|^2$ are the normalized densities of the coherent excitons and biexcitons, respectively. An analysis of (5) shows that the exciton density in the film increases more rapidly at low excitation levels than does the biexciton density and that it reaches its maximum possible value fairly quickly. As the pump amplitude is increased further, the exciton density begins to decrease rapidly and, at a certain critical value of X, it drops abruptly to zero, while the biexciton density increases to g^2/σ^2. This means that saturation of the excitonic transition is achieved and that all the excitons formed in the film thereafter transform at once into biexcitons. At that moment, the medium becomes practically transparent, i.e., $Y\approx X$.

The time for switching from one branch of the hysteresis dependence is of the same order as the parameter $\tau_0=\alpha g^2$, which is of the order of 10^{-13} s for a CdS film with a thickness $L\sim 40$ nm. Since $\gamma_e\sim 10^{11}$ s^{-1},[3] the parameter C must exceed the critical value $C_{\rm cr}$. The intensity of the incident radiation $I=cE_0^2/8\pi$ corresponding to the value of the normalized pump amplitude $X=10$ must be of the order of $c\gamma_e\gamma_m X^2/8\pi\sigma^2\sim 1$ kW/cm^2.

TWO-PULSE EXCITATION

In crystals of the CuCl type, the biexciton binding energy is of the order of 30 meV; therefore, the transition within the M band is characterized by considerable detuning relative to the transition at the exciton resonance. It is assumed that the excitons and biexcitons in a thin semiconductor film are excited by two pulses of laser radiation with the peak electric field strengths E_{01} and E_{02} and the photon frequencies ω_1 and ω_2, respectively. We shall assume that the photons of one of the pulses are in resonance with the frequency of the excitonic transition and that the photons of the other pulse are in resonance with the frequency of the transition within the M band.

The Heisenberg (material) equations for the amplitudes a and b in this case have the form

$$i\dot{a}=\omega_0 a-i\gamma_e a-gE_1^+-\sigma bE_2^-, \tag{6}$$

$$i\dot{b}=\Omega_0 b-i\gamma_m b-\sigma aE_2^+, \tag{7}$$

and the analogs of (3) are now

$$E_1^+=E_{01}^+ +i\alpha_1 ga, \quad E_2^+=E_{02}^+ +i\alpha_2\sigma a^+ b. \tag{8}$$

Setting the derivatives $\dot{a}$ and $\dot{b}$ equal to zero, we have the steady-state equations of state:

$$X_1^2=n\left[1+C_1+\frac{X_2^2}{(1+C_2n)^2}\right]^2, \quad N=\frac{X_2^2}{(1+C_2n)^2}n, \tag{9}$$

$$X_1=X_1\left(1+\frac{C_1}{1+Y_2^2}\right), \quad X_2=X_2\left(1+\frac{C_2Y_1^2}{(1+Y_2^2)^2}\right), \tag{10}$$

where $C_1=\alpha_1\hbar g^2/\gamma_e$ and $C_2=\alpha_2\hbar g^2/\gamma_e$ are the bistability parameters.

Let us determine the region of values of the pump amplitudes X_1 and X_2 in which the exciton density n and the biexciton density N, as well as the output amplitudes Y_1 and Y_2, can be multivalued functions of X_1 and X_2. The boundary of the saddle-type critical points in the parametric space (X_1,X_2) is specified by the system of parametric equations

$$X_1^2=n\left[\frac{4C_2n(1+C_1)}{3C_2n-1}\right]^2, \tag{11}$$

$$X_2^2=\frac{(1-C_1)(1+C_2n)^3}{3C_2n-1}. \tag{12}$$

In the region bounded by this curve the system of equations (6)–(8) has three steady states. Let us next investigate the stability of the steady-state solutions obtained. The system of parametric equations

$$X_1^2=n\left[\frac{(2+C_1)(1+C_2n)}{C_2n}\right]^2, \tag{13}$$

$$X_2^2=\frac{(2+C_1+C_2n)(1+C_2n)^2}{C_2n} \tag{14}$$

defines the stability boundary of the nonsaddle-type critical points. The bifurcation curves obtained divide the parametric space (X_1,X_2) into three regions. In region I the system of equations (6)–(8) has one critical point, viz., a stable focal point, in region II it has three critical points, of which one is stable and two are unstable, and, finally, in region III it has two stable focal points and a saddle-type critical point. The apex of the peak has the coordinates $X_{1c}=2(1+C_1)/\sqrt{C_2}$, $X_{2c}=2\sqrt{1+C_1}$.

Thus, for the resonant excitation of excitons and biexcitons there are hysteretic dependences of the amplitudes of the outgoing fields and quasiparticle concentrations on the pump amplitudes. An important circumstance is that, besides the constants C_1 and C_2, the amplitudes of the incident pulses X_1 and X_2 are bistability parameters. When the value of the pump amplitude in one channel is fixed, the nonlinear transmission in both channels can be controlled by varying the pump amplitude in the other channel. Thus, there is a possibility for controlling the bistable behavior of one beam by means of the other.

To estimate the corresponding parameters we use the values $\gamma\sim 10^{11}$ s^{-1}, $g=5\times 10^{19}$ esu, $\sigma=5\times 10^{10}$ esu, and $\hbar\omega_1\approx\hbar\omega_2=5\times 10^{-12}$ erg.[4,5] Then for $L=10^{-6}$ cm we find $C_1\approx C_2\sim 10$. These values of C_1 and C_2 correspond to the critical values of the normalized amplitudes $X_{1c}\approx X_{2c}\approx X_{\rm cr}=7$. The pump intensities at which cavityless optical bistability is possible should be of the order of $I=c\gamma X_{\rm cr}^2/8\pi\sigma^2\sim 20$ kW/cm^2.

It can be concluded from the foregoing that a thin semiconductor film can function effectively as a bistable switching element for integrated optics when the excitons in it are subjected to resonant excitation and simultaneously converted into biexcitons by the photons of one or two different pulses.

[1] A. A. Gogolin and É. I. Rashba, JETP Lett. **17**, 478 (1973).
[2] P. I. Khadzhi, *Kinetics of the Recombination Luminescence of Excitons and Biexcitons in Semiconductors* [in Russian], Shtiintsa, Kishinev (1977).
[3] J. M. Hvam, C. Dörnfeld, and H. Schwab, Phys. Status Solidi B **150**, 387 (1988).
[4] Vu Duy Phach, A. Bivas, B. Hönerlage, and J. B. Grun, Phys. Status Solidi B **84**, 731 (1977).
[5] R. Levy, B. Hönerlage, and J. B. Grun, Phys. Status Solidi B **150**, 825 (1988).

Translated by P. Shelnitz

Exciton susceptibility of semiconductors at high laser-excitation levels

P. I. Khadzhi and D. V. Tkachenko

Pridnestr State University, 3300 Tiraspol', Moldava

Fiz. Tverd. Tela (St. Petersburg) **40**, 934–935 (May 1998)

The hysteresis behavior of the real and imaginary parts of the susceptibility of a semiconductor in the exciton region of the spectrum is investigated with consideration of the exciton–phonon and elastic exciton–exciton interactions in the pump-probe regime as a function of the intensity and frequency of the strong laser pulse and the frequency of the probe pulse. The conditions for the appearance of suppression of the damping and amplification of the probe pulse are determined. Abrupt red and blue shifts of the spectral position of the exciton absorption band as a function of the pump pulse intensity are predicted. © *1998 American Institute of Physics.* [S1063-7834(98)05305-2]

The pump-probe technique has been used widely in recent years to investigate the optical properties of semiconductors at high laser-excitation levels. Under this method the semiconductor is excited by high-power laser radiation to produce changes in the properties of the crystal, which are subsequently probed by weak radiation. The theoretical basis for this method has been developed for a system of two-level atoms.

Below we present the results of a theoretical analysis of the bistable and spectral features of the behavior of the real (χ') and imaginary (χ'') parts of the dielectric susceptibility of a semiconductor in the exciton region of the spectrum during stationary excitation by high-power laser radiation with a frequency ω_e and an electric field amplitude E_0 of the wave. This pulse is followed by the generation of excitons in a high concentration, whose interaction with one another leads to renormalization of the energy spectrum of the crystal, causing significant changes in its optical properties. These changes are probed by weak laser radiation with a frequency ω and a field amplitude E.

The Hamiltonian of a system of coherent excitons interacting with external electromagnetic fields in the approximation of a rotating wave with the frequency ω_e of the strong pump field has the form

$$H=\hbar\Delta\alpha^+\alpha+\hbar\nu\alpha^+\alpha^+\alpha\alpha/2+\hbar g(E_0^+\alpha^++\alpha E_0) -\hbar g(\alpha^+E^+e^{-i\delta t}+\alpha Ee^{i\delta t}), \quad (1)$$

where $\Delta=\omega_e-\omega_0$, $\delta=\omega-\omega_e$ is the mismatch between the frequencies of the strong (ω_e) and weak (ω) fields, ω_0 is the frequency of the excitonic transition, α is the amplitude of the exciton wave, ν is the elastic exciton–exciton interaction constant, and g is the exciton–photon coupling constant. In accordance with (1) it is easy to obtain the (material) equation for the variation of the amplitude of the exciton wave. Calculating the steady-state response of the system of excitons in all orders of perturbation theory with respect to the strong field E_0, and in first-order perturbation theory with respect to the weak field E, we obtain the following expressions for the dispersion (χ') and absorption (χ'') components of the susceptibility of the crystal:

$$\chi'/\chi_0=\left[\delta_0+\Delta_0-2z+z^2\frac{(\delta_0-\Delta_0+2z)}{1+(\delta_0-\Delta_0+2z)^2}\right]F^{-1}, \quad (2)$$

$$\chi''/\chi_0=\left[1-\frac{z^2}{1+(\delta_0-\Delta_0+2z)^2}\right]F^{-1}, \quad (3)$$

where

$$F=\left[1-\frac{z^2}{1+(\delta_0-\Delta_0+2z)^2}\right]^2 +\left[\delta_0+\Delta_0-2z+z^2\frac{\delta_0-\Delta_0+2z}{1+(\delta_0-\Delta_0+2z)^2}\right]^2, \quad (4)$$

$\chi_0=\hbar g^2/\gamma$, $\Delta_0=\Delta/\gamma$, $\delta_0=\delta/\gamma$, $x=\Delta_0+\delta_0=(\omega-\omega_0)/\gamma$, $z=\nu n_0/\gamma$, γ is the phenomenological exciton damping constant, and n_0 is the concentration of coherent excitons excited by the field of the high-power laser pulse, which can be determined from the nonlinear equation

$$z[(z-\Delta_0)^3+1]=j^2. \quad (5)$$

Here $f=E_0/E_s$ is the normalized amplitude of the pump field, and $E_s^2=\gamma^3/\nu g^2$.

It follows from Eqs. (2)–(5) that χ' and χ'' are complicated functions of the pump field amplitude f and the detunings of the strong (Δ_0) and weak (x) fields relative to the excitonic transition frequency. Because the normalized exciton density z is a multivalued function of f when $\Delta_0>3^{1/2}$, χ' and χ'' are also multivalued functions of f, i.e., they display hysteresis as a function of the pump field amplitude.

Figure 1 presents the spectral form of the absorption band of the weak (probe) radiation χ''/χ_0 for the fixed value of the detuning (with respect to the high-power pulse) $\Delta_0=3$ and several values of the pump field amplitude, i.e., under the conditions of developed bistability for the function $z(f)$. The position and shape of the absorption band depend significantly not only on f and Δ_0, but also on whether the pump amplitude increases or decreases as it varies. The ab-

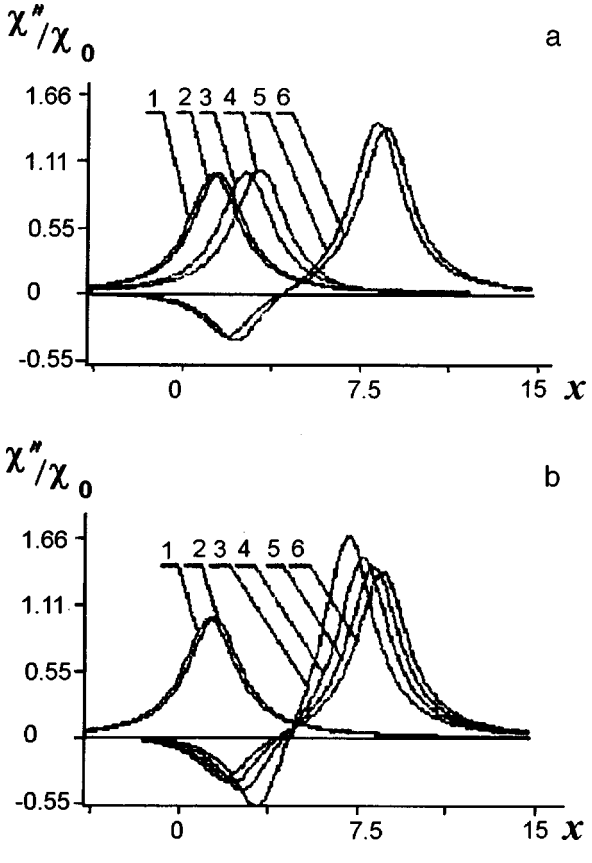

FIG. 1. Normalized absorption part of the susceptibility χ''/χ_0 as a function of the normalized detuning x for the pump detuning $\Delta_0=3$ in the case of increases (a) and decreases (b) in the pump amplitude f. $f_{cr}=2.25$ (a) and 1.71 (b). Curves *1–6* correspond to $f=0$, 0.85, 1.89, 2.07, 2.25, and 2.44.

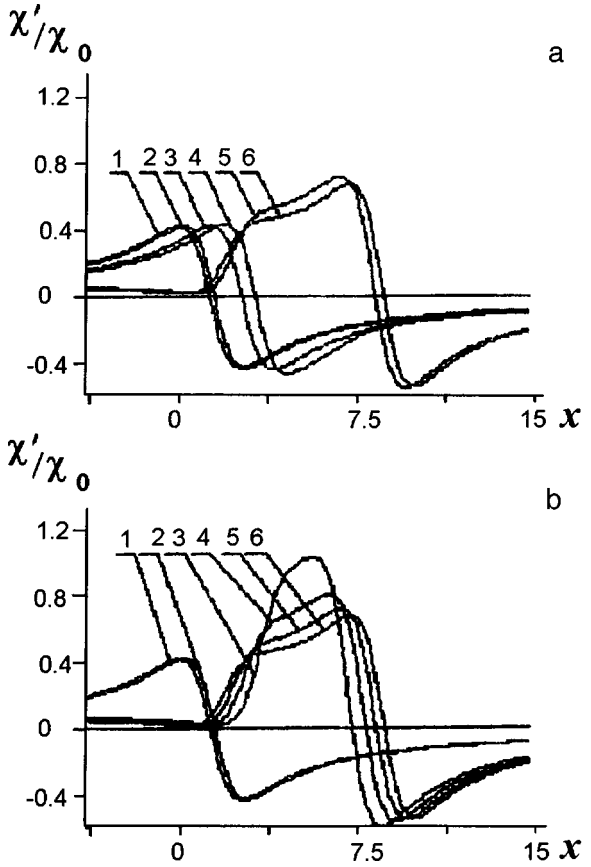

FIG. 2. Normalized dispersion part of the susceptibility χ'/χ_0 as a function of the normalized detuning x for the pump detuning $\Delta_0=3$ in the case of increases (a) and decreases (b) in the pump amplitude f. $f_{cr}=2.25$ (a) and 1.71 (b). Curves *1–6* correspond to the same values of f as in Fig. 1.

sorption band of the probe radiation gradually shifts toward shorter wavelengths as the pump amplitude f is increased from 0 to f_{cr} (Fig. 1a). Upon passage through the value $f=f_{cr}$ the absorption band peak undergoes an abrupt blue shift, and a region of negative absorption simultaneously appears, i.e., amplification of the probe radiation occurs, on the long-wavelength tail. As $f>f_{cr}$ is increased further, only monotonic blue displacement of both the absorption band and the gain band is observed. The appearance of the gain band is caused by the pairwise escape of excitons from the coherent state generated by the pumping and their passage into the long-wavelength and short-wavelength regions of both polariton branches in accordance with the energy and momentum conservation laws. The radiative recombination of these excitons also leads to amplification of the probe pulse.

As the pump amplitude is lowered (Fig. 1b) from $f>f_-$ down to $f=f_+<f_-$, at first the peaks of the absorption and gain bands shift monotonically toward longer wavelengths, and the gain band vanishes. A further decrease in f leads to further monotonic displacement of the absorption band peak toward longer wavelengths. Here $f_\pm$ is determined only by the detuning Δ_0.

As is seen from Fig. 2, similar features are also characteristic of the real part of the susceptibility χ'.

Translated by P. Shelnitz

Influence of an electric field and a high excitation density on the luminescence of epitaxial GaN films

M. A. Yakobson, D. K. Nel'son, and E. V. Kalinina

A. F. Ioffe Physicotechnical Institute, Russian Academy of Sciences, 194021 St. Petersburg, Russia

Fiz. Tverd. Tela (St. Petersburg) **40**, 936–937 (May 1998)

The influence on the recombination luminescence spectra of a field applied to the Schottky barrier and a high excitation density GaN epitaxial films grown by metalorganic chemical-vapor deposition (MOCVD) is investigated. It is discovered that quenching of the luminescence takes place under a reverse bias, while an increase in its intensity occurs under a forward bias. The effect observed is attributed to thickness variation of the space-charge layer under the effects of the applied voltage. The appearance of a new band caused by exciton–exciton collisions is observed under the conditions of a high excitation density. © *1998 American Institute of Physics.* [S1063-7834(98)05405-7]

There has been recently heightened interest around the world in the investigation of nitrides of group III elements. It is due to the prospect of using these wide-gap semiconductor materials to create laser structures that operate in the blue and ultraviolet regions of the spectrum. In the present work we investigated the low-temperature ($T=6-80$ K) photoluminescence of GaN films grown by metalorganic chemical-vapor deposition (MOCVD) on 6*H*-SiC and Al_2O_3 substrates. The influence of the field applied to the Schottky barrier on the luminescence of GaN was investigated. The photoluminescence of GaN films under the conditions of a high excitation density was also investigated. In this case the luminescence was excited by a pulsed nitrogen laser ($\lambda=337.1$ nm). The excitation density was varied from 10 to 1000 kW/cm^2.

At $T=6$ K the dominant feature in the photoluminescence spectrum of GaN is the intense line of an exciton bound to a neutral donor in the region of the $A_{n=1}$ exciton resonance ($h\nu=3.468$ eV).[1] At $T=80$ K a series of lines caused by donor–acceptor recombination is clearly observed in the spectral region below the exciton resonance ($h\nu=2.80-3.30$ eV). We studied the behavior of these lines when an external voltage was applied to the Schottky barrier. The dependence of the intensity of the bound exciton line on the magnitude of the applied voltage for three GaN samples, as well as the dependence of the intensity of the donor–acceptor recombination line for sample 3, are presented in Fig. 1. As a whole, the influence of the electric field on the luminescence intensity can be described as follows. Under a forward bias the intensity at first increases, and then saturation is observed. Under a reverse bias quenching of the luminescence is observed. At the same time, the influences of the applied voltage on the luminescence intensity differed somewhat for the different samples. For example, for Sample 1 only quenching of the luminescence was observed, while the increase in intensity under a forward bias was absent. Sample 2 exhibited both quenching under a reverse bias and an increase in intensity followed by saturation under a forward bias. Sample 3 displayed an increase in the intensity of the bound exciton line under a forward bias, as well as quenching under a reverse bias, but it was very weak. Strong quenching and a relatively weak increase in intensity were observed for the donor–acceptor recombination line.

The effect observed is described well within the model in Ref. 2. According to that model, luminescence is excited only outside the region of the space charge *W*, and its intensity is determined by the absorption of the exciting light, which decreases exponentially as we move into the sample.

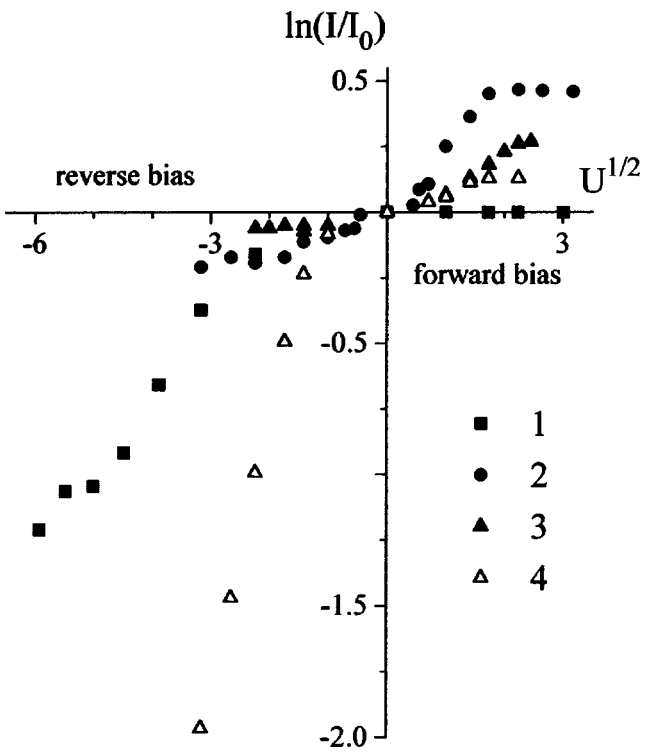

FIG. 1. Dependence of the relative intensity of the luminescence lines of GaN on the applied voltage: *1–3*—bound exciton line for samples 1, 2, and 3, respectively ($T=6$ K), *4*—donor–acceptor recombination line for sample 3 ($T=80$ K).

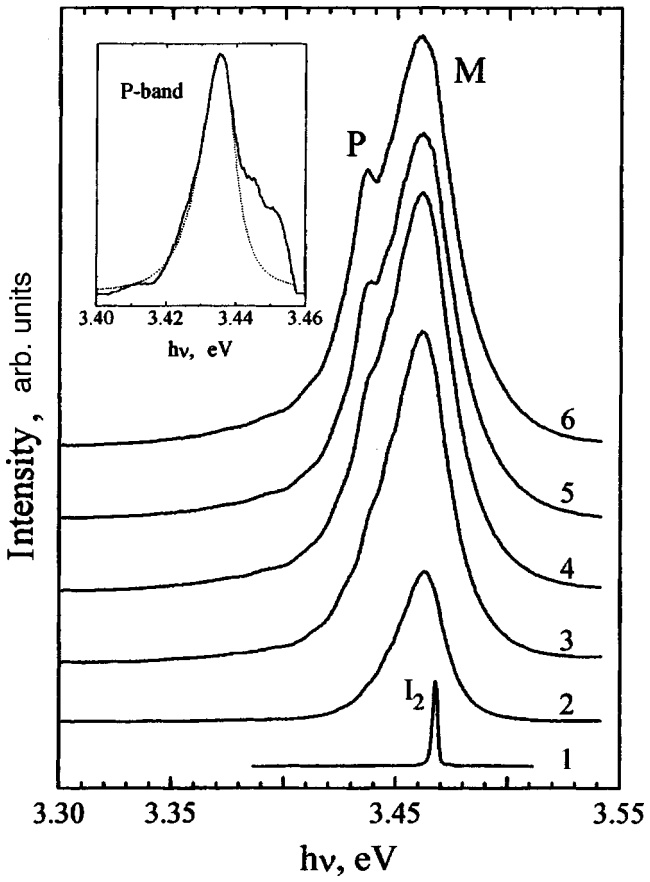

FIG. 2. Luminescence spectra of GaN for various excitation intensities. $T=6$ K. Excitation: *1*—mercury lamp, *2*—200 kW/cm^2, *3*—500 kW/cm^2, *4*—900 kW/cm^2, *6*—1000 kW/cm^2. Inset—analysis of the shape of the *P* band. Solid line—experiment, dotted line—calculation.

In this case the exciton (or carrier) density is small near the surface of the sample, in the region of the strong nonuniform electric field. The relative luminescence intensity is described by the expression

$$I/I_0=\exp[-\alpha(\lambda_{\text{exc}})W],$$

where I and I_0 are the luminescence intensity in the presence and in the absence of a voltage U, and $\alpha(\lambda_{\text{exc}})$ is the absorption coefficient at the wavelength of the exciting light. The variation of W with U leads to corresponding variation of the luminescence intensity. Taking into account that $W\sim U^{1/2}$, we have

$$\ln(I/I_0)\sim U^{1/2}.$$

The achievement of saturation under a forward bias can be associated with straightening of the bands. The differences in the behavior of the different samples is due, in our opinion, to differences in their properties, such as the thickness of space-charge layer, the concentration of electrically active impurities, etc.

Figure 2 presents the luminescence spectra of GaN obtained with different excitation densities. Under weak excitation the spectrum displays the I_2 bound exciton line. When the excitation density is increased, this line transforms into an *M* band. When the excitation level is increased further, a new *P* band appears on the long-wavelength wing of the *M* band. The intensity of the *P* band increases superlinearly as the excitation density is increased.

The nature of the *M* band is apparently complex, and several processes are responsible for it. In the present work we shall discuss only the *P* band. Two processes can be responsible for the appearance of the *P* band: inelastic collisions of free excitons and radiative decay of an excitonic molecule. In both cases the shape of the *P* band should be the inverse of a Maxwellian line shape and should be described by the expression

$$I(h\nu)=\int_0^\infty \sqrt{E}\,\exp(-E/kT_{\text{exc}})\frac{\Gamma}{[E-(h\nu_0-h\nu)]^2+\Gamma^2}dE,$$

where Γ is the total damping of the initial and final states, and T_{exc} is the temperature of the exciton gas. The inset in Fig. 2 presents an analysis of the shape of the *P* band. The best fit between the calculated and experimental curves is obtained for the following values of the parameters: $T_{\text{exc}}=40$ K, $\Gamma=3.5$ meV, and $h\nu_0=3.439$ eV. As we see, the temperature of the exciton gas is significantly higher than the temperature of the bath. Such excessive heating can be caused, first, by the excess energy of the exciting quantum and, second, by Auger processes, which can be very effective in crystals with a large donor concentration.[3] Investigations of the temperature dependence of the luminescence spectra showed that no changes in the spectrum occur in the temperature range from 6 to 60 K. Therefore, the *P* band cannot be caused by the annihilation of a biexciton as a consequence of its small binding energy. Thus, taking into account the entire set of properties of the *P* band just mentioned, we can conclude that it is caused by inelastic exciton–exciton collisions. During a collision one exciton annihilates radiatively, while the other exciton passes into an excited state.

[1] D. K. Nel'son, Yu. V. Mel'nik, A. V. Sel'kin, M. A. Yakobson, V. A. Dmitriev, K. J. Irvine, and C. H. Carter, Jr., Fiz. Tverd. Tela (St. Petersburg) **38**, 822 (1996) [Phys. Solid State **38**, 455 (1996)].
[2] R. E. Hetrick, and K. F. Yeung, J. Appl. Phys. **42**, 2882 (1971).
[3] G. V. Mikhaĭlov, D. K. Nel'son, B. S. Razbirin, and V. A. Kharchenko, Fiz. Tverd. Tela (Leningrad) **31**, 160 (1989) [Phys. Solid State **31**, 2116 (1989)].

Translated by P. Shelnitz

Resonant Mandelstam–Brillouin light scattering and Raman scattering in semiconductors with intermediate exciton states belonging to discrete exciton bands and the continuous spectrum

B. Kh. Baĭramov, A. V. Gol'tsev, and V. V. Toporov

A. F. Ioffe Physicotechnical Institute, Russian Academy of Sciences, 194021 St. Petersburg, Russia

R. T. Phillips

Department of Physics, Cavendish Laboratory, Cambridge University, Cambridge CB3 0HE, United Kingdom

R. Laĭho

Wihuri Physical Laboratory, University of Turku, 20500 Turku, Finland

K. Dettmer

Institut für Halbleiterphysik und Optik, Technische Universität Braunschweig, D-38106 Braunschweig, Germany

Fiz. Tverd. Tela (St. Petersburg) **40**, 938–940 (May 1998)

The results of a theoretical and experimental investigation of resonant Mandelstam–Brillouin light scattering by thermal acoustic phonons with $\mathbf{k}=0$ near the direct absorption edge (in the case of ZnSe crystals) are analyzed. The appearance of a new type of resonant increase in the intensity of Raman scattering by optical phonons with $\mathbf{k}\neq 0$, which corresponds to resonance with the scattered light in the output channel, near the indirect absorption edge (in the case of semi-insulating GaP:N crystals) is also reported. The resonant gain reaches $\sim 4\times 10^3$ at frequencies corresponding to overtone scattering assisted by $LO(X)$ and $LO(L)$ phonons. Exciton states belonging to both discrete exciton bands and to the continuous spectrum are considered as the intermediate states involved in the scattering processes in calculations of the resonant scattering tensors. In addition, all the intraband transitions, as well as the interband transitions between the conduction band, the valence bands, and the spin–orbit split-off band are taken into account, and good agreement with the experimental results is obtained.
 [S1063-7834(98)05505-1]

The inclusion of excitons as virtual intermediate states in an analysis of the quantitative laws governing the resonant increase in the intensity of inelastic light scattering in semiconductors is known to permit more exact reproduction of experimental results. A theory of single-phonon resonant Raman scattering that takes into account excitonic effects was first given by Loudon.[1] An expression for the resonant Raman scattering tensor with consideration of the weak exciton–photon coupling was obtained in Ref. 2 within the strain potential and Fröhlich electron–phonon coupling mechanisms. Similar calculations were performed in Ref. 3 using Green's functions, and it was assumed in Ref. 4 that the exciton states are hydrogenic. In this case scattering through only one valence band and the conduction band was taken into account. The consideration of only one valence band turned out to be insufficient for a quantitative interpretation of the experimental results for the scattering of light by acoustic and optical phonons in crystals having diamond and zinc blende structures that were not specially doped. To overcome the contradictions that arose, a theory of resonant Mandelstam–Brillouin light scattering was developed in Refs. 4–6, and a theory of resonant Raman scattering with consideration of the exciton correlations in both the intraband transitions and the interband transitions between the conduction band, quadruply degenerate valence bands, and a doubly degenerate spin–orbit split-off band was derived in Refs. 6–10. Here exciton states belonging to both discrete exciton bands and to the continuous spectrum were considered as intermediate states involved in the scattering processes.

This paper presents an analysis of results which attest to the appearance of significant resonant increase in the intensity of resonant Mandelstam–Brillouin light scattering by thermal acoustic phonons with $\mathbf{k}=0$ in semi-insulating ZnSe crystals without special doping near the direct absorption edge, and Raman scattering by optical phonons with $\mathbf{k}\neq 0$ near the indirect absorption edge in doped semi-insulating GaP:N (si-GaP:N) crystals.

Figure 1 presents the dependence of the intensity of resonant Mandelstam–Brillouin light scattering by acoustic phonons on the quantum energy of the exciting radiation in ZnSe crystals.

If the Coulomb interaction between electrons and holes, in which the intermediate states are exciton states belonging

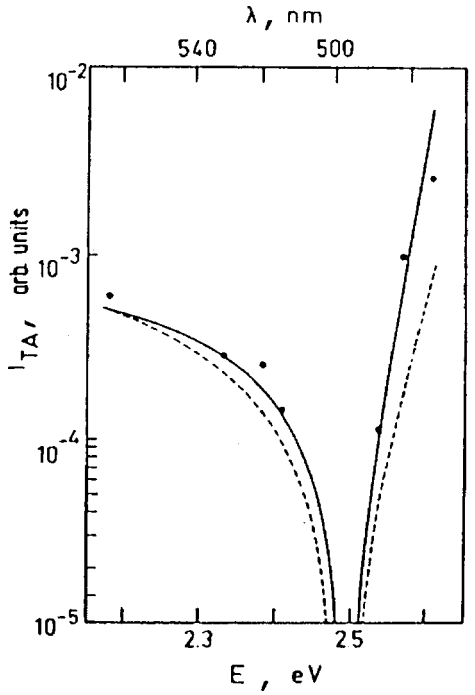

FIG. 1. Dependence of the light scattering cross section for *TA* phonons in ZnSe on the quantum energy of the exciting radiation in the $y(xy)\bar{z}$ scattering geometry. The axes are oriented as follows: $x\|[100]$, $y\|[01\bar{1}]$, and $z\|[011]$. $T=296$ K. Points—experimental data. Solid lines—calculation with consideration of the Coulomb interaction, i.e., Eq. (1). Dotted lines—calculation within Loudon's theory.[1]

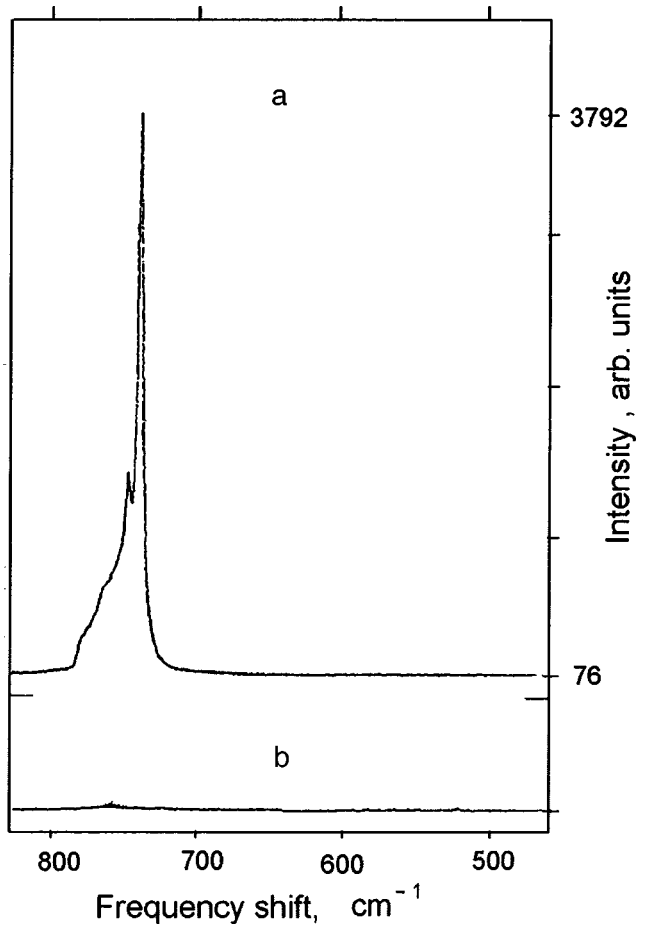

FIG. 2. Raman scattering spectra of si-GaP:N crystals (a, b) obtained with excitation by the output of an argon laser with the wavelength $\lambda_i=514.536$ nm in the $z(y,x)\bar{z}$ geometry for backscattering from the (001) plane at $T=5$ K. The spectral slit width $R=1.8$ cm^{-1}.

to both the discrete bands and the continuous spectrum, is taken into account, the following expression for the inelastic resonant light scattering tensor can be obtained[6,7]

$$R_{is}=\sum_{\alpha,\beta}\frac{p_{\beta 0}H_{\beta,\alpha}p_{\alpha 0}}{\omega_{g\beta}\omega_{g\alpha}+\omega_1}\left\{\frac{1}{2\pi a_0^3}\sum_{n=1}^{\infty}\frac{1}{n^3}\left[\frac{1}{\omega_{g\alpha}-\omega_i-R/n^2}-\frac{1}{\omega_{g\beta}-\omega_i-R/n^2}\right]+\frac{1}{4\pi}\left[\frac{2\mu}{\hbar}\right]^{3/2}\times R^{1/2}\ln\frac{\omega_{g\beta}-\omega_s}{\omega_{g\alpha}-\omega_s}+\frac{1}{4}\left[\frac{2\mu}{\hbar}\right]^{3/2}R^{1/2}\left[\cot\left[\frac{\pi^2R}{\omega_{g\beta}-\omega_s}\right]^{1/2}-\cot\left[\frac{\pi^2R}{\omega_{g\alpha}-\omega_s}\right]^{1/2}\right]\right\}, \quad (1)$$

where $a_0=\varepsilon\hbar^2/\mu^2$ is the Bohr radius for an exciton, and $R=\mu e^4/2\hbar^2\varepsilon^2$ is the exciton Rydberg constant. All the intraband transitions and interband transitions between the Γ_6 conduction band, the quadruply degenerate Γ_8 valence bands, and the doubly degenerate Γ_7 spin–orbit split-off band are systematically taken into account. The first term in the curly brackets in (1) represents the contribution of the scattering processes through exciton states of the discrete spectrum, while the last two terms represent the contribution of the continuous exciton spectrum.

The results of a theoretical calculation using Eq. (1) are presented as solid lines in Fig. 1 and exhibit good agreement with the observed data.

In contrast to such resonance with discrete exciton bands and the continuous spectrum near the direct absorption edge E_0 (Refs. 4–10) (for ZnSe $E_0=2.67$ eV at $T=300$ K), Fig. 2 presents results which attest to the appearance of a new type of resonant increase in the intensity of Raman scattering by optical phonons with $\mathbf{k}\neq 0$ near the indirect absorption edge in doped si-GaP:N crystals.

The spectra shown in Fig. 2 were obtained under identical experimental conditions for two si-GaP:N crystals with excitation by the output of an argon laser with the wavelength $\lambda_1=514.536$ nm. They were normalized with respect to the intensity of the line of the $TO(\Gamma)$ phonons.

It is known that the $1s$ state of excitons bound to isoelectronic nitrogen impurities in si-GaP:N crystals is split as a consequence of an electron-hole interaction into two states with the orbital quantum numbers $J=1$ and $J=2$. The corresponding energy in the low-temperature luminescence spectra of this sample at $T=5$ K for excitons with $J=1$ was equal to 2.3174 eV. The proximity of this value to the quantum energy of the exciting light $E_i=2.4092$ eV points out the possibility of resonance with light scattered on two optical phonons. The spectra for si-GaP:N exhibit a considerable ($\sim 4\times 10^4$ fold at $\nu=736.3$ cm^{-1}) resonant increase of the intensity of two-phonon light scattering by $LO(X)$ and

$LO(L)$ phonons. We assume that the resonance observed is caused by a scattering process with resonant excitation of intermediate exciton states formed by electron states at the X and L points of gallium phosphide Brillouin zone. The exciton states are excited as a result of the indirect absorption of a photon of incident light with a frequency ω_i with the simultaneous emission of two LO phonons at the X and L points ($\omega_{LO(X,L)}$). In the last step, the electron and hole bound in the exciton annihilate. Photons of scattered light with the frequencies $\omega_s=\omega_i-2\omega_{LO(X)}$ and $\omega_s=\omega_i-2\omega_{LO(x)}$ are emitted as a result. The large value of the cross section is specified by the presence of a small energy denominator in the scattering cross section:

$$\sigma\propto 1/(\hbar\omega_i-2\hbar\omega_{LO(X,L)}-E_{\mathrm{ex}})^2=1/(\hbar\omega_s-E_{\mathrm{ex}})^2, \qquad (2)$$

where E_{ex} is the energy of the excited excitons.

[1] R. Loudon, Proc. R. Soc. London, Ser. A **275**, 218 (1963).
[2] A. K. Ganguly and J. L. Birman, Phys. Rev. **162**, 806 (1967).
[3] R. Zeyher, Ting Chiu-Sen, and J. L. Birman, Phys. Rev. B **4**, 1725 (1974).
[4] B. Kh. Baĭramov, A. V. Gol'tsev, E. Karajamaki, R. Laiho, T. Levola, and V. V. Toporov, Fiz. Tverd. Tela (Leningrad) **25**, 1286 (1983) [Sov. Phys. Solid State **25**, 739 (1983)].
[5] E. Karajamaki, R. Laiho, T. Levola, B. H. Bairamov, A. V. Gol'tsev, and V. V. Toporov, Phys. Rev. B **29**, 4508 (1984).
[6] B. Kh. Baĭramov, N. V. Lichkova, A. V. Gol'tsev, V. D. Timofeev, and V. V. Toporov, Fiz. Tverd. Tela (Leningrad) **29**, 244 (1987) [Sov. Phys. Solid State **29**, 138 (1987)].
[7] B. H. Bairamov, A. V. Gol'tsev, V. V. Toporov, R. Laiho, and T. Levola in *Proceedings of the 18th International Conference on the Physics of Semiconductors*, O. Engstrom (Ed.), World Scientific, Singapore (1987), p. 1721.
[8] A. Cantarero, C. Trallero-Giner, and M. Cardona, Phys. Rev. B **39**, 8388 (1989).
[9] C. Trallero-Giner, A. Cantarero, and M. Cardona, Phys. Rev. B **40**, 4030 (1989).
[10] A. Cantarero, C. Trallero-Giner, and M. Cardona, Phys. Rev. B **40**, 12290 (1989).

Translated by P. Shelnitz

Investigation of the excitonic structure in the photoconductivity spectra of CdS crystals

A. S. Batyrev, O. É. Botov, N. V. Karasenko, and E. V. Sum'yanova

Kalmyk State University, 358000 Élista, Russia

R. A. Bisengaliev and B. V. Novikov

Scientific-Research Institute of Physics, St. Petersburg State University, 198904 Petrodvorets, Russia
Fiz. Tverd. Tela (St. Petersburg) **40**, 941–943 (May 1998)

The changes in the low-temperature photoconductivity spectra of CdS crystals under the action of external influences are investigated. The high sensitivity of the fine (excitonic) structure of the spectra to changes in the conditions for the recombination of nonequilibrium carriers near the surface and in the bulk of the semiconductor is demonstrated. © *1998 American Institute of Physics.* [S1063-7834(98)05605-6]

A fine structure caused by excitons in the form of maxima (type 1) or minima (type 2) can be observed in the photoconductivity spectra of semiconductors in the region of the fundamental absorption edge at low temperatures. The presence of this fine structure is due to the difference between the lifetimes of the nonequilibrium majority carriers in the near-surface layer (τ_s) and in the bulk of the semiconductor (τ_v).[1] The type of fine structure is determined by the relationship between these times: in the case of a type-1 fine structure $\tau_s > \tau_v$, in the case of a type-2 fine structure $\tau_s < \tau_v$, and the photoconductivity spectra should have a structureless (smooth) form when $\tau_s = \tau_v$. The relationship between τ_s and τ_v and, consequently, the type of fine structure can be altered by treating the semiconductor in various ways, and the type of fine structure can serve as an indicator of changes in the photosensitivity of the near-surface region and/or the bulk of the semiconductor.

In the present work the low-temperature ($T = 4 - 77$ K) photoconductivity spectra of CdS crystals as a function of the electric field applied to the semiconductor were investigated using the field effect, preliminary photoexcitation by intrinsic light, IR illumination, and increases in the drift field. Characteristic changes in the fine structure of the spectra and in the photosensitivity were discovered in the intrinsic and impurity regions of the spectrum.

The application of an electric field which creates a depletion layer near the surface of the semiconductor leads to reversible transformation of the fine structure from type 1 to type 2, as the field strength is increased (Fig. 1, curves *1–3*). In the intermediate stage of this transformation, the spectral photoconductivity curve acquires a smooth appearance (curve *2*). At values of the potential on the field electrode corresponding to an accumulation layer near the surface, the type of fine structure remains unchanged (curve *4*).

Reversible transformation of the fine structure from type 1 to type 2 is also caused by preliminary illumination of the crystal by intrinsic light.[1)]

Reversible transformation of the fine structure from type 2 to type 1 was observed in several crystals during intense infrared (IR) illumination. There were samples in which the transition from a type-2 fine structure to a type-1 fine structure took place in response to increases in the drift field (Fig. 2). We note a detail which is significant for later on: the inversion of the type of fine structure in response to increases in the drift field was observed in samples with linear dimensions ~ 1 mm.

The main qualitative features of the changes in the photoconductivity spectra in the intrinsic and extrinsic regions of the spectrum are as follows.

In the case of the conversion of a type-1 fine structure into a type-2 fine structure, the photosensitivity in the intrinsic region of the spectrum decreases dramatically, while the changes in the impurity region at the AM_1 and AM_2 maxima are relatively weak. As a result, the photoconductivity spectra acquire the form of a curve with a dominant long-wavelength maximum in the impurity region of the spectrum, which is characteristic of crystals with a type-2 fine structure (Fig. 1, curves *1–3*) (see also Ref. 3).

In the case of inversion of the type of fine structure during IR illumination, overall quenching of the photosensitivity takes place, but it is significantly greater in the spectral region of the additional AM_1 and AM_2 maxima. In the case of inversion of the type of fine structure in response to increases in the drift field, the photosensitivity remains practically unchanged at the AM_1 and AM_2 maxima, while it increases significantly in the intrinsic portion of the spectrum (Fig. 2). In both cases the photosensitivity is lower at the AM_1 and AM_2 maxima than in the intrinsic region, and the general form of the spectral photoconductivity curves acquires features which are characteristic of crystals with a type-1 fine structure.

The transformation of the photoconductivity spectra observed as the depleted layer near the surface increases (Fig. 1, curves *1–3*) is attributed to a decreases in τ_s due to an increase in the recombination rate in the space-charge region as the transition from weak accumulation-inducing near-surface band bending to depletion-inducing band bending proceeds.[1] The influence of preliminary illumination by intrinsic light on the photoconductivity spectra can be explained in a similar manner, since illumination can result in changes in the charge of surface states due to filling by electrons. The formation of a depletion layer near the surface of

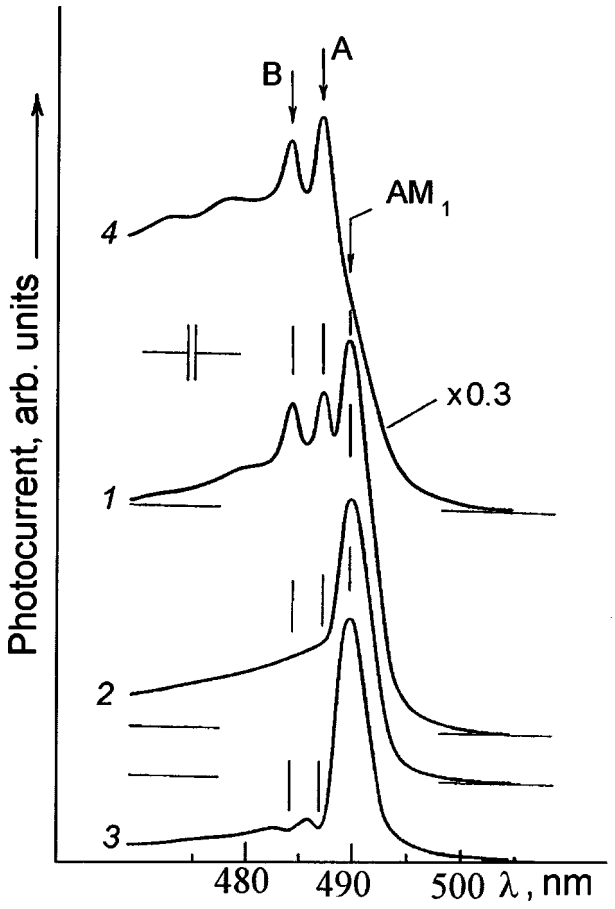

FIG. 1. Photoconductivity spectra of a CdS crystal at $T=77$ K for $E \perp C$ and various values of the potential φ on the field electrode relative to the sample; $\varphi=0$, -50, -300, and 50 V for curves *1–4*, respectively.

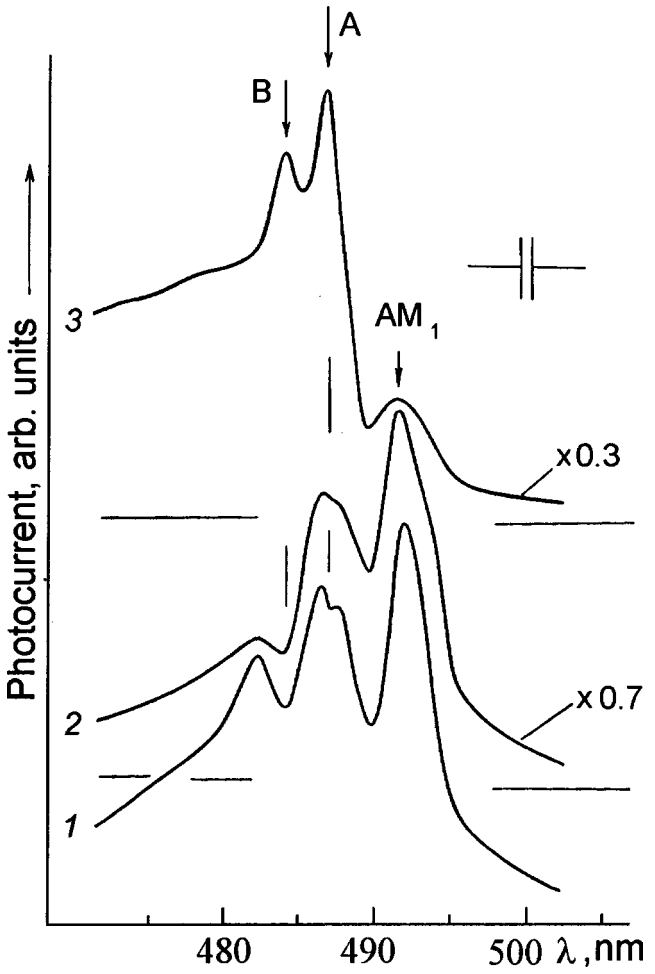

FIG. 2. Photoconductivity spectra of a CdS crystal at $T=77$ K for $E \perp C$ and various values of the drift voltage U; $U=20$, 25, and 35 V for curves *1–3*, respectively.

CdS crystals with a type-1 fine structure due to the ''sticking'' of photoelectrons to surface states was detected in Ref. 4 by photoreflectance spectroscopy at exciton resonances.[2)]

The character of the effect of IR illumination on the fine structure of the photoconductivity spectra indicates reversal of the inequality $\tau_s < \tau_v$ under its influence. At the same time, the significant decrease in the photocurrent in the intrinsic region of the spectrum during IR illumination indicates a corresponding decrease in τ_s. Therefore, the inequality $\tau_s > \tau_v$ can be achieved during IR illumination only in the case of a greater decrease in τ_v. This is, in fact, observed experimentally in the form of predominant IR quenching of the photocurrent in the impurity region at the AM_1 and AM_2 maxima.

On the one hand, the selective character of the IR quenching of the photoconductivity accounts for the transformation of the fine structure upon IR illumination, and, on the other hand, it points out the bulk origin of the AM_1 and AM_2 maxima (the latter is also indicated by their weak sensitivity to band bending at the surface).

In our opinion, the IR quenching of the AM_1 and AM_2 maxima is due to the ionization of the activating r centers, with which the centers corresponding to these maxima interact directly, by IR radiation. It is possible that the r centers are a component part of the latter centers. It has also not been ruled out that the centers forming the AM_1 and AM_2 maxima are doubly ionized intrinsic acceptor defects, which are isolated[2] (AM_2) or are perturbed by other charged centers (AM_1).

The influence of the drift field on the fine structure seems to us to be of significance. As in the case of IR illumination, the transformation of the fine structure indicates reversal of the inequality $\tau_s < \tau_v$ as the strength of the drift field is increased. However, in this case such reversal is associated with an increase in τ_s and a simultaneous decrease in τ_v, as follows from the superlinear increase in the photocurrent with increasing strength of the drift field in the intrinsic region and from the sublinear increase in the impurity region (Fig. 2). Such changes in τ_s and τ_v in response to increases in the drift field can be associated with the injection of holes from the contact (anode) in strong fields, which are easily achieved in CdS samples with small dimensions.[5] The injection of holes can lead to the shortening of τ_v due of the trapping of injected holes by r centers and an increase in the bulk recombination rate of free electrons with holes trapped in shallow acceptor centers. The increase in τ_s with increasing strength of the drift field can be caused by a decrease in the depletion-inducing band bending near the sur-

face as a result of the trapping of some of the injected holes by a near-surface hole ''pocket.''

[1)]We observed this effect only in crystals which displayed one or both of the additional long-wavelength AM_1 and AM_2 maxima in their photoconductivity spectra[2] [these maxima were designated as $I_1(AM_1)$ and $I_x(AM_2)$ in Ref. 3]. Such crystals comprised the majority in the batch of samples that we investigated.

[2)]A correlation between the type of fine structure in the photoconductivity spectra and the type of photoreflectance spectra was also established in Ref. 4, pointing out the important role of surface states in forming the finestructure of the photoconductivity spectra.

[1] V. A. Kiselev, B. V. Novikov, and A. E. Cherednichenko, *Exciton Spectroscopy of the Near-Surface Region of Semiconductors* [in Russian], LGU, Leningrad (1987), p. 162.
[2] A. S. Batyrev, N. V. Karasenko, and B. V. Novikov, Vestn. St. Petersb. Univ. **4** (1(4)), 28 (1994).
[3] J. A. Bragagnolo, G. M. Storti, and K. W. Boer, Phys. Status Solidi A **22**, 639 (1974).
[4] R. A. Bisengaliev, E. D. Batyrev, B. V. Novikov, and A. V. Sel'kin, in *Abstracts of the International Conference ''Optics of Excitons in Condensed Matter,''* St. Petersburg (1997), p. 68.
[5] R. W. Smith, Phys. Rev. **105**, 900 (1957).

Translated by P. Shelnitz

Influence of the formation of hot excitons on the quantum efficiency of short-wavelength photoelectric conversion in III–V semiconductors

Yu. A. Gol'dberg, O. V. Konstantinov, O. I. Obolenskiĭ, and E. A. Posse

A. F. Ioffe Physicotechnical Institute, Russian Academy of Sciences, 194021 St. Petersburg, Russia

Fiz. Tverd. Tela (St. Petersburg) **40**, 944–945 (May 1998)

A new excitonic mechanism for decreasing the quantum efficiency of the photoelectric conversion process in surface-barrier structures is considered. This mechanism involves the formation of hot excitons which have a large ionization energy and are not subject to the influence of the barrier electric field. The spectral dependence of the hot photocarrier losses is derived in an explicit form from experimental data on the basis of a previously proposed model and is analyzed. This dependence has two segments with abrupt increases, which are caused by the formation of excitons in the L and X valleys of the semiconductor. © *1998 American Institute of Physics.* [S1063-7834(98)05705-0]

Surface-barrier structures based on III–V semiconductors are employed as detectors of infrared, visible, and ultraviolet light. However, their sensitivity decreases markedly as the energy of the photon being detected increases[1] (see also Fig. 1). This drop in sensitivity has usually been associated in the literature with the influence of surface recombination and/or thermionic emission (see, for example, Ref. 2).

In this communication we propose a new mechanism for lowering the photosensitivity of surface-barrier structures, i.e., for lowering the quantum efficiency of the photoelectric conversion process.

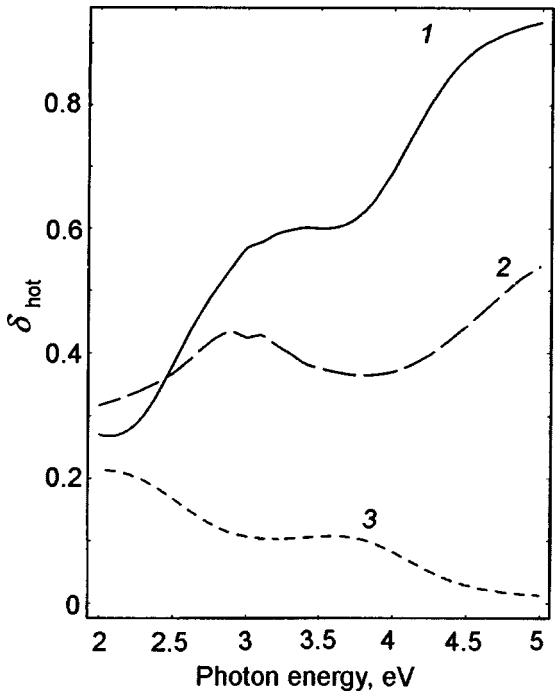

FIG. 1. Dependence of the hot-carrier loss coefficient δ_{hot} on the photon energy $h\nu$ in a Ni–n-GaAs structure (*1*). The spectral dependences of the photoelectric-conversion quantum efficiency γ (*3*) and the reflectivity R (*2*) are also presented.

Our treatment is based on separating the losses of thermalized and hot photocarriers. Using measurements of the temperature, field, and spectral dependences of the photoelectric-conversion quantum efficiency and the fluctuational-trap model,[3,4] we can isolate the hot-photocarrier loss in an explicit form. Figure 1 presents the dependence of the hot-photocarrier loss coefficient on the photon energy for a Ni–n-GaAs structure. This dependence has a stepwise character and contains two segments with abrupt increases. We assume that these features are a consequence of the formation of hot excitons in the space-charge layer of the structure. In k space there are two large regions where the bottom of the conduction band and the top of the valence band are almost parallel to each other (Fig. 2). These regions are responsible for the presence of the two broad absorption peaks of gallium arsenide. Since the conduction band and the valence band are parallel, the electron and hole created upon the absorption of a photon move in space in the same direction and can consequently easily bind to form a hot exciton. A comparison of Figs. 1 and 2 allows us to estimate the ionization energy of such an exciton at several hundred millielectron volts. Such a tightly bound exciton has a large mean free path and scarcely dissociates in the barrier electric field. Thus, a hot exciton is

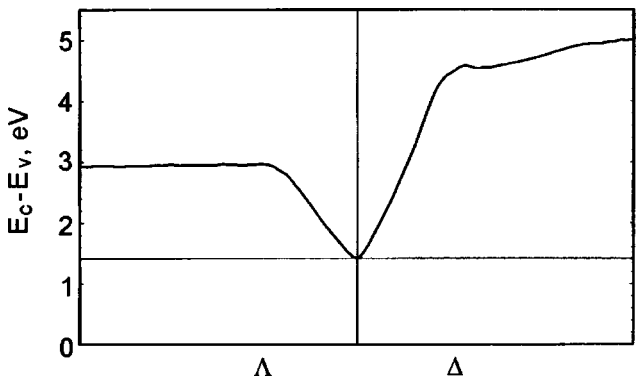

FIG. 2. Gap width of gallium arsenide as a function of the quasiwave vector **k** in the Λ and Δ directions.

capable of escaping into the metal or the quasineutral bulk of the semiconductor and recombining there without making a contribution to the photocurrent.

The loss of hot photocarriers can be isolated on the basis of the fluctuational-trap model.[3] The photoelectric-conversion quantum efficiency γ is represented as the product of three cofactors:

$$\gamma=(1-R)(1-\delta_{\text{hot}})(1-\delta_{\text{therm}}), \tag{1}$$

where R is the reflectivity, and δ_{hot} and δ_{therm} are the hot- and thermalized-carrier loss coefficients, respectively. Each of the cofactors in (1) is correlated with one of the three main stages of the photoelectric conversion process. The probability that a photon will be absorbed in the semiconductor equals $(1-R)$; the probability that the electron–hole pair created will thermalize in the space-charge layer, i.e., will become subject to the action of the barrier electric field, equals $(1-\delta_{\text{hot}})$, and the probability that a pair consisting of a thermalized electron and a thermalized hole will be separated by the barrier field and make a contribution to the photocurrent equals $1-\delta_{\text{therm}}$.

It is assumed in the fluctuational-trap model that there are fluctuations of the bottom of the conduction band and the top of the valence band in the space-charge layer of the structure, which simultaneously serve as traps for thermalized electrons and holes. The photocarriers captured in the traps quickly recombine without making a contribution to the photocurrent.

In the case of Boltzmann statistics

$$1-\delta_{\text{therm}}=e^{-E(\varepsilon)/kT}, \tag{2}$$

and

$$\gamma=(1-R)(1-\delta_{\text{hot}})e^{-E(\varepsilon)/kT}. \tag{3}$$

The dependence of the localization energy E of the carriers in a trap on the barrier field $\mathcal{E}$ can be written in the form

$$E(\mathcal{E})=E_0-[W(\mathcal{E})-W(\mathcal{E}_0)]. \tag{4}$$

Here $E_0=22$ meV is the localization energy in the absence of a bias on the structure when the barrier electric field $\mathcal{E}_0=15$ kV/cm, the value of E_0 being determined from the temperature dependence of the photoelectric conversion quantum efficiency, and $W(\mathcal{E})$ is the level of the charge carrier in the trap measured from the bottom of the trap. To find $W(\mathcal{E})$ we used the rough approximation of a triangular potential well:

$$W(\mathcal{E})=\xi_1\left(\frac{\hbar^2e^2}{2m}\,\mathcal{E}^2\right)^{1/3}, \tag{5}$$

where $\xi_1\approx 2.34$ is the first root of the Airy function.

A comparison with experiment shows that the fluctuational trap model is capable of faithfully describing the temperature and field dependences of the photoelectric-conversion quantum efficiency, despite its simplicity. A combination of this model with the representation of the formation of hot excitons in the space-charge layer makes it possible to completely account for the available experimental data.

[1] ''Photodiodes,'' Hamamatsu Photonics K. K. Catalog (1996), p. 34.
[2] B. I. Reznikov and G. V. Tsarenkov, Fiz. Tekh. Poluprovodn. **25**, 1922 (1991) [Sov. Phys. Semicond. **25**, 1158 (1991)].
[3] Yu. A. Gol'dberg, O. V. Konstantinov, O. I. Obolenskiĭ, E. A. Posse, and B. V. Tsarenkov, Fiz. Tekh. Poluprovodn. **31**, 563 (1997) [Semiconductors **31**, 473 (1997)].
[4] T. A. Blank, Yu. A. Gol'dberg, O. V. Konstantinov, O. I. Obolenskiĭ, and E. A. Posse, Fiz. Tekh. Poluprovodn. **31**, 1225 (1997) [Semiconductors **31**, 1053 (1997)].

Translated by P. Shelnitz

Spatial dispersion phenomena in magneto-optics

V. N. Gridnev, B. B. Krichevtsov, V. V. Pavlov, R. V. Pisarev, and A. A. Rzhevskiĭ

A. F. Ioffe Physicotechnical Institute, Russian Academy of Sciences, 194021 St. Petersburg, Russia

Fiz. Tverd. Tela (St. Petersburg) **40**, 946–948 (May 1998)

An experimental study of nonreciprocal spatial-dispersion effects in para-($Cd_{1-x}Mn_xTe$), ferro-($LiFe_5O_8$), and antiferromagnetic (Cr_2O_3) crystals caused by an external magnetic field or magnetic order is reported. © *1998 American Institute of Physics.* [S1063-7834(98)05805-5]

Compounds whose symmetry group does not contain time and space inversion operations may exhibit optical phenomena forbidden in centrosymmetric or nonmagnetic media. Such phenomena were first observed in Refs. 1, 2 and, later, in Refs. 3 and 4, in the exciton spectral region. These effects can be described in a general form by the corresponding terms of an expansion of the dielectric permittivity tensor ε_{ij} in components of the light-wave vector **k** and of the vector **G**, which is odd under time reversal and determines the magnetic state of the crystal[5]

$$\Delta\varepsilon_{ij}(\omega,\mathbf{k},\mathbf{G})=\gamma_{ijkl}k_kG_l. \tag{1}$$

Vector **G** may denote here external magnetic field **B** or a magnetic order parameter, for example, spontaneous magnetization **M** or antiferromagnetic vector **L**. The terms of Eq. (1) are responsible for the appearance of magneto-optical effects in light transmission or reflection in the cases where traditional magneto-optical phenomena are forbidden, thus opening new possibilities for probing electronic states in crystals.

Viewed from the standpoint of microscopic theory, the existence of terms (1) is determined by different mechanisms. The absence of space inversion and time reversal operations results in a change of the ground- and excited-state wave functions and the appearance of nonzero combinations of matrix elements of the type $\mathrm{Re}\, d_{kn}m_{nk}$ and $\mathrm{Re}\, d_{kn}Q_{nk}$, where **d**, **m**, and **Q** are operators of electric, magnetic, and quadrupole moments, respectively, The combination $\mathrm{Re}\, d_{kn}m_{nk}$ is responsible for magneto-electric susceptibility α_{ij} at optical frequencies, which, when included in the constitutive relations[6]

$$D_i=\varepsilon_{ij}E_j+\alpha_{ij}H_j,\quad B_i=\mu_{ij}H_j+\alpha_{ij}E_j \tag{2}$$

provides a contribution to components $\Delta\varepsilon_{ij}$ and can manifest itself in crystals exhibiting spontaneous magneto-electric effect. As for $\mathrm{Re}\, d_{kn}Q_{nk}$, it determines the quadrupole contribution to $\Delta\varepsilon_{ij}$. Another conceivable mechanism for the appearance of terms (1) could be the linear dependence of resonant optical-transition frequencies on **k** and **G** for excitonic and interband transitions in semiconductors. This work reports on a spectral study of magneto-optical spatial-dispersion effects in para- (**G**=**B**), ferro-(**G**=**M**), and antiferromagnetic (**G**=**L**) crystals.

In the transparency region of acentric para- or diamagnets, terms (1) are responsible for nonreciprocal birefringence linear in **B** and **k**, which in cubic crystals (T_d) are described by two parameters, A and g, determining the diagonal and nondiagonal components of tensor $\Delta\varepsilon_{ij}$. Birefringence of the **kB** type was observed to exist in $Cd_{1-x}Mn_xTe$ semimagnetic semiconductors ($x=0$, 0.25, 0.35, 0.42, 0.52) in $\mathbf{k}\parallel[110]$ and $\mathbf{k}\parallel[111]$ geometries. The effect exhibits a strong anisotropy relative to the B direction and is described by first- and third-order harmonics. Figure 1 displays the reduced parameters A/x and g/x vs E_g-E, where E_g is the gap width, and E is the photon energy. Also shown is the behavior of the reduced Faraday effect FR/x and magnetic linear birefringence VB/x^2. The **kB** birefringence depends linearly on x, which implies the dominant role of $sp-d$ exchange in the phenomenon. The diagonal component γ_{ijkl} follows a resonance-type dependence $A/x=d+c/(E_g-E)^{1.4}$ near the band edge. The nondiagonal component g/x is small near the edge and does not exhibit a resonant character. Such a behavior is in agreement with

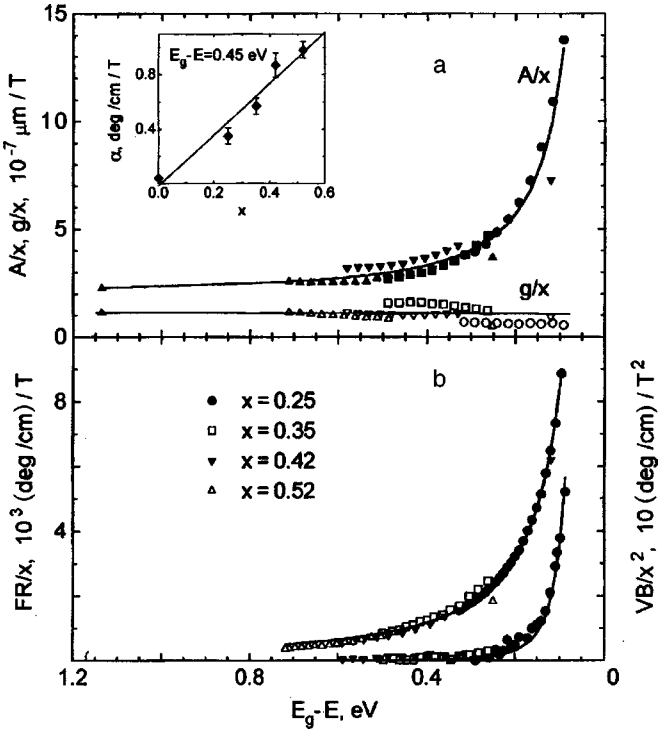

FIG. 1. (a) A/x and g/x, (b) Faraday effect FR/x and magnetic linear birefringence VB/x^2 vs E_g-E for $Cd_{1-x}Mn_xTe$ crystals.

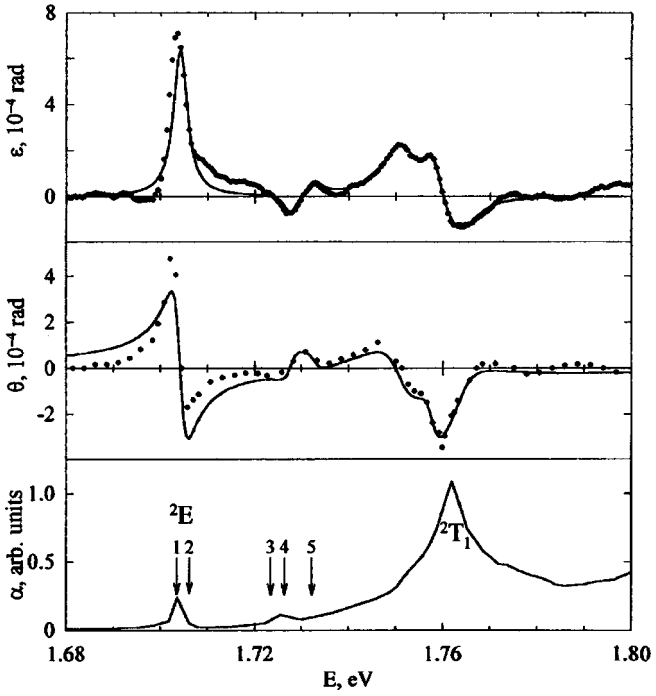

FIG. 2. Nonreciprocal ellipticity ε and rotation of the plane of polarization θ in light reflection from the basal plane of Cr_2O_3 obtained at $T=90$ K in the region of spin-forbidden $^4A_2 \rightarrow {}^2E$, $^4A_2 \rightarrow {}^2T_1$ transitions. Shown below is the absorption spectrum. ($T=77$ K.)

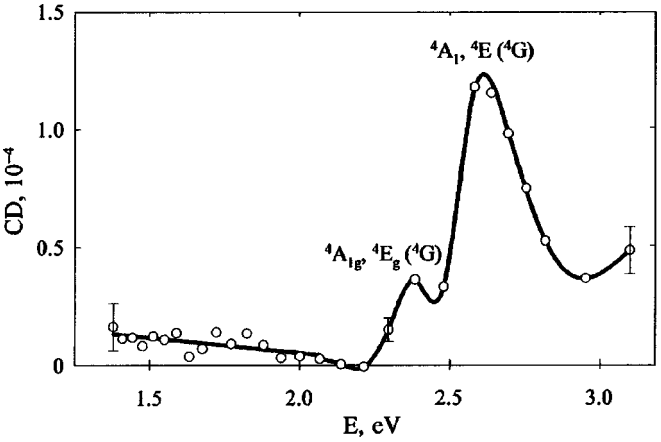

FIG. 3. Spectral behavior of circular dichroism in light reflection from a (111)-type plane obtained under normal incidence and transverse magnetization in $LiFe_5O_8$.

microscopic theory, within which the **kB** effect is related to interband transitions, the inclusion of hole energy dispersion linear in **k**, and dependence of the exchange coupling parameter on electron wave vector.

Figure 2 plots spectral dependences of the nonreciprocal rotation of the plane of polarization θ and of ellipticity ε in light reflection from the basal plane of the Cr_2O_3 antiferromagnet $[D_{3d}(D_3)]$ in the region of the $^4A_2 \rightarrow {}^2E$, $^2T_1$ excitonic transitions.[7,8] The violation of space and time inversion operations in Cr_2O_3 is caused by the onset of antiferromagnetic order ($\mathbf{L} \parallel C_3$). The nonreciprocal effects linear in **L** are due to magneto-electric susceptibility $\alpha_\perp$ at optical frequencies: $\theta + i\varepsilon = 2\alpha_\perp(1+n)/(1-n)$, where n is the refractive index. Microscopic theory of magneto-electric susceptibility in the optical range for Cr_2O_3 was developed in Ref. 9.

Figure 3 presents the spectral dependence of nonreciprocal circular dichroism (CD) observed in light reflection from a (111)-type plane of the offcentrosymmetric cubic O^6 ferrimagnet $LiFe_5O_8$ in the region of the $^6A_1 \rightarrow {}^4A_1$, $^2E(^4G)$ transitions in the Fe^{3+} ion occupying octahedral and tetrahedral positions. The spectra were taken at normal incidence and perpendicular magnetization of the crystal in the (111) plane, $\mathbf{M} \perp C_3$. The observed spectra can be related to magneto-electric susceptibility in the optical range and to Kerr effect cubic in **M**. A phenomenological analysis showed the magneto-electric mechanism to provide a dominant contribution to the effect.[10]

Support of the Russian Fund for Fundamental Research and of the ''Fundamental Spectroscopy'' program is gratefully acknowledged.

[1] E. F. Gross, B. P. Zakharchenya, and O. V. Konstantinov, Fiz. Tverd. Tela (Leningrad) **3**, 305 (1961) [Sov. Phys. Solid State **3**, 221 (1961)].
[2] J. J. Hopfield and D. G. Thomas, Phys. Rev. Lett. **4**, 357 (1960).
[3] E. L. Ivchenko, V. P. Kochereshko, G. V. Mikhaĭlov, and I. N. Ural'tsev, JETP Lett. **37**, 164 (1983).
[4] O. V. Gogolin, V. A. Tsvetkov, and E. G. Tsitsishvili, Zh. Éksp. Teor. Fiz. **87**, 1038 (1984) [Sov. Phys. JETP **60**, 593 (1984)].
[5] V. M. Agranovich and V. L. Ginzburg, *Spatial Dispersion in Crystal Optics and the Theory of Excitons* (Wiley, New York, 1967) [Russ. original, Nauka, Moscow, 1979].
[6] R. M. Hornreich and S. Shtrikman, Phys. Rev. **171**, 1065 (1968).
[7] B. B. Krichevtsov, V. V. Pavlov, R. V. Pisarev, and V. N. Gridnev, Phys. Rev. Lett. **76**, 4628 (1996).
[8] B. B. Krichevtsov, V. V. Pavlov, R. V. Pisarev, and V. N. Gridnev, Zh. Éksp. Teor. Fiz. **110**, 1505 (1996) [JETP **83**, 834 (1996)].
[9] E. Hanamura, Y. Tanabe, T. Iizuka-Sakano, and M. Muto, in *Proceedings of International Conference DCP-97*.
[10] V. N. Gridnev, B. B. Krichevtsov, V. V. Pavlov, and R. V. Pisarev, JETP Lett. **65**, 68 (1997).

Translated by G. Skrebtsov